# Probing the Organisation, Interaction and Dynamics of Membrane Supramolecular Complexes using Atomic Force Microscopy

Thesis is submitted in accordance with the requirements of the University of Liverpool for degree of Doctor in Philosophy by Leanne Miller

July 2020


UNIVERSITY OF LIVERPOOL

The University of Liverpool
Institute of Systems, Molecular and Integrative Biology

# Declaration

I declare that this thesis is the result of my own work, the only work included which is the outcome of work done in collaboration has been declared in the contributions section below and specified in the text. It is not substantially the same as any that I have submitted, or is being concurrently submitted for a degree or diploma or other qualification at the University of Liverpool or any other University or similar institution, except as declared in the contributions section and specified in the text. I further state that no substantial part of my thesis has already been submitted, or is being concurrently submitted for any such degree, diploma or other qualification at the University of Liverpool or any other University or similar institution except as declared in the contributions section below and specified in the text. This Thesis does not exceed the prescribed word limit of 100,000 words.

Leanne Miller

# Publications and Author's Contributions

Chapter I of this thesis makes up the chapter of a textbook:

- **Miller L.C**., Martin D.S., Liu LN., Canniffe D.P. (2020) Composition, Organisation and Function of Purple Photosynthetic Machinery. In: Wang Q. (eds) Microbial Photosynthesis. Springer, Singapore.

The content of chapter IV is based on a recently published article, of which I was the first author:

- **Miller L.C.**, Zhao L., Canniffe D.P., Martin D., Liu LN. (2020) Unfolding pathway and intermolecular interactions of the cytochrome subunit in the bacterial photosynthetic reaction center [published online ahead of print, 2020 Apr 17]. Biochim Biophys Acta Bioenerg. 1861(8):148204.

The work in chapters V and VI are unpublished.

I acknowledge the following collaborator contributions to the results described in this thesis; unless specified below, all work was completed by the author.

| | |
|---|---|
| Professor Luning Liu<br>**University of Liverpool** | High resolution AFM imaging of *Blc. viridis* intracellular membrane |
| Dr Longshen Zhao<br>**University of Liverpool** | Assistance with high-speed AFM imaging of *Blc. viridis* |
| Gregory Dykes<br>**University of Liverpool** | Thin-section electron microscope imaging of purple bacteria |

| | |
|---|---|
| Laura Bracun<br>**University of Liverpool** | Comparative sucrose gradients *Rba. sphaeroides* wild-type and mutant intracellular membranes |
| Dr Daniel Canniffe<br>**University of Liverpool** | Assistance with *Blc. viridis* cloning |
| Dowrung Namoon<br>**University of Liverpool** | Conjugation of pBBRBB-*pufBA*-pufγ into *Blc. viridis* |

Other publications produced during my PhD studies but not included in my thesis include:

- Davies H.A., Lee C.F., **Miller L.**, Liu LN., Madine J. (2018) Insights into the Origin of Distinct Medin Fibril Morphologies Induced by Incubation Conditions and Seeding. Int J Mol Sci. 19(5):1357. Published 2018 May 3. doi:10.3390/ijms19051357.

In this manuscript I contributed the AFM imaging of the fibrils and subsequent data analysis.

## Acknowledgements

I would like to start this thesis by warmly acknowledging all the people who have helped and contributed to the success of my work. Firstly, I would like to thank Professor Lu-Ning Liu for his supervision, help, advice and support, as well as my second supervisor Dr David Martin. I would also like to thank everyone else in the Liu Lab for their help, support and inspiring discussions over the past four years, including members who have now left. Notably, I would like to thank Greg Dykes for the EM imaging and Dr Jorge Rodrigues-Ramos, Dr Matthew Faulkner and Dr Longsheng Zhao for their AFM guidance, image processing advice and physics discussions. I would also like to thank Dr Daniel Canniffe for all his help and advice with the growth and genetic manipulation/cloning work of purple photosynthetic bacterial strains. I would like to thank everyone in lab G for making it an enjoyable place to work, and especially Paul Loughane for his technical help. I extend my thanks to all the CCI staff for their help with the use of the Bio-AFM over the years. Last but by no means least, I would like to extend my gratitude to my friends and family for their constant support and encouragement of my studies when it was most needed; I truly could not have successfully completed this work without you. It is impossible to recall every single person who has helped me through these studies, but I thank each one for their help, support and advice over these four years.

# Abstract

Photosynthesis, one of the most globally important, fundamental biological processes, provides the energy for almost all life on Earth by the conversion of sunlight into chemical energy. This exceedingly efficient process relies on a set of highly ordered multicomponent assemblies of pigment-protein complexes located within specialised photosynthetic membranes. Purple photosynthetic bacteria utilise cyclic electron transport to efficiently carry out photosynthesis. Light-harvesting (LH) antenna complexes absorb light energy, which is then transferred through a network of pigment-protein complexes, eventually promoting charge separation in the reaction centre (RC), ultimately resulting in the formation of a proton motive force used to drive ATP synthesis; these complexes are housed in the intracytoplasmic membrane (ICM). The assembly, organisation and interactions of these complexes differs among species and are paramount to high-efficiency light-harvesting and energy conversion. In this thesis, we use atomic force microscopy (AFM) and single-molecule force spectroscopy (SMFS) to probe the long-range organization of the photosynthetic apparatus from *Blc. viridis* and the unfolding pathway of the 4Hcyt subunit in its native supramolecular assembly with its functional partners. AFM images reveal that the RC-LH1 complexes are densely organized in the photosynthetic membranes, with restricted lateral protein diffusion. Unfolding of the 4Hcyt subunit represents a multi-step process and the unfolding forces of the 4Hcyt α-helices are approximately 121 picoNewtons. Pulling of 4Hcyt could also result in the unfolding of the RC L subunit that binds with the N-terminus of 4Hcyt, suggesting strong interactions (>150 pN) between RC subunits. This study provides new insights into the protein folding and interactions of photosynthetic multicomponent complexes, which are essential for their structural and functional integrity to conduct photosynthetic electron flow. We demonstrate, using AFM and transmission electron microscopy (TEM), that in the PufX of *Rba. Veldkampii* alters the composition of not only the *Rba. sphaeroides* RC-LH1 complex, but also the organisation of the ICM and the architecture of the ICM vesicles. Finally, we made progress towards the re-engineering of the *Blc. viridis* photosynthetic membrane.

# Table of Contents

# List of Figures

# List of Tables

# Appendices

# Abbreviations

| | |
|---|---|
| 3-PGA | 3-phosphoglyceric acid |
| 4Hcyt | tetrahaem cytochrome subunit |
| AAP | aerobic anoxygenic phototroph |
| AFM | atomic force microscopy |
| ATP | adenosine triphosphate |
| ATPase | ATP synthase |
| BChl | bacteriochlorophyll |
| bp | base pair |
| BPhe | bacteriopheophytin |
| BR | bacteriorhodopsin |
| CBB | Calvin-Benson-Bassham |
| Cyt | cytochrome |
| EM | electron microscopy |
| F-D | force-distance |
| HF | high-fidelity |
| ICM | intracytoplasmic membrane |
| kb | kilobase pairs |
| kDa | kilo Dalton |
| LB | Lysogeny Broth |
| LH | light-harvesting |
| $M22^+$ | Medium $22^+$ |
| M27 | Medium 27 |
| Mob | mobility genes |
| MQ | menaquinone |

| | |
|---|---|
| MW | molecular weight |
| NADPH | nicotinamide adenine dinucleotide phosphate |
| PAGE | polyacrylamide gel electrophoresis |
| PCF | pair correlation function |
| PCR | polymerase chain reaction |
| PDB | protein data bank |
| PGC | photosynthesis gene cluster |
| PIC | protease inhibitor cocktail |
| Pmf | proton motive force |
| pN | pico Newton |
| Q | quinone |
| $QH_2$ | quinol |
| RC | reaction centre |
| Rpm | rounds per minute |
| RuBisCO | ribulose-biphosphate carboxylase/oxygenase |
| RuBP | ribulose-1,5-bisphosphate |
| SDS | sodium dodecyl sulphate |
| SEM | standard error of the mean |
| SMFS | single-molecule force spectroscopy |
| SP | special pair |
| TEM | transmission electron microscope |
| UQ | ubiquinone |
| WLC | worm-like chain |
| WT | wild-type |

# CHAPTER I
# General Introduction

# 1 General Introduction

This thesis is concerned with the fundamental understanding of the organisation, interactions and dynamics of purple bacterial photosynthesis. The mechanisms underlying photosynthesis are well studied, as well as the structures of various photosynthetic components; however, there are many questions left unanswered, including the forces and interactions underlying this process, and the functional and organisational properties of specific components. The aim of this introductory chapter is to describe the current knowledge outlined in the scientific literature surrounding purple bacterial photosynthesis, highlighting the gaps in our understanding.

## 1.1 Purple bacterial photosynthesis

Photosynthesis is a globally important, fundamental process by which plants, algae and some bacteria convert sunlight into chemical energy. The process relies on a set of highly ordered multicomponent assemblies of pigment-protein complexes, located within invaginated membranes; the organisation and dynamics of these complexes is vital for efficient photosynthesis. Although the overall objective of photosynthesis, the production of metabolites for the cell, across different organisms is similar, the multiprotein assemblies and compartments that perform this differ among different organisms.

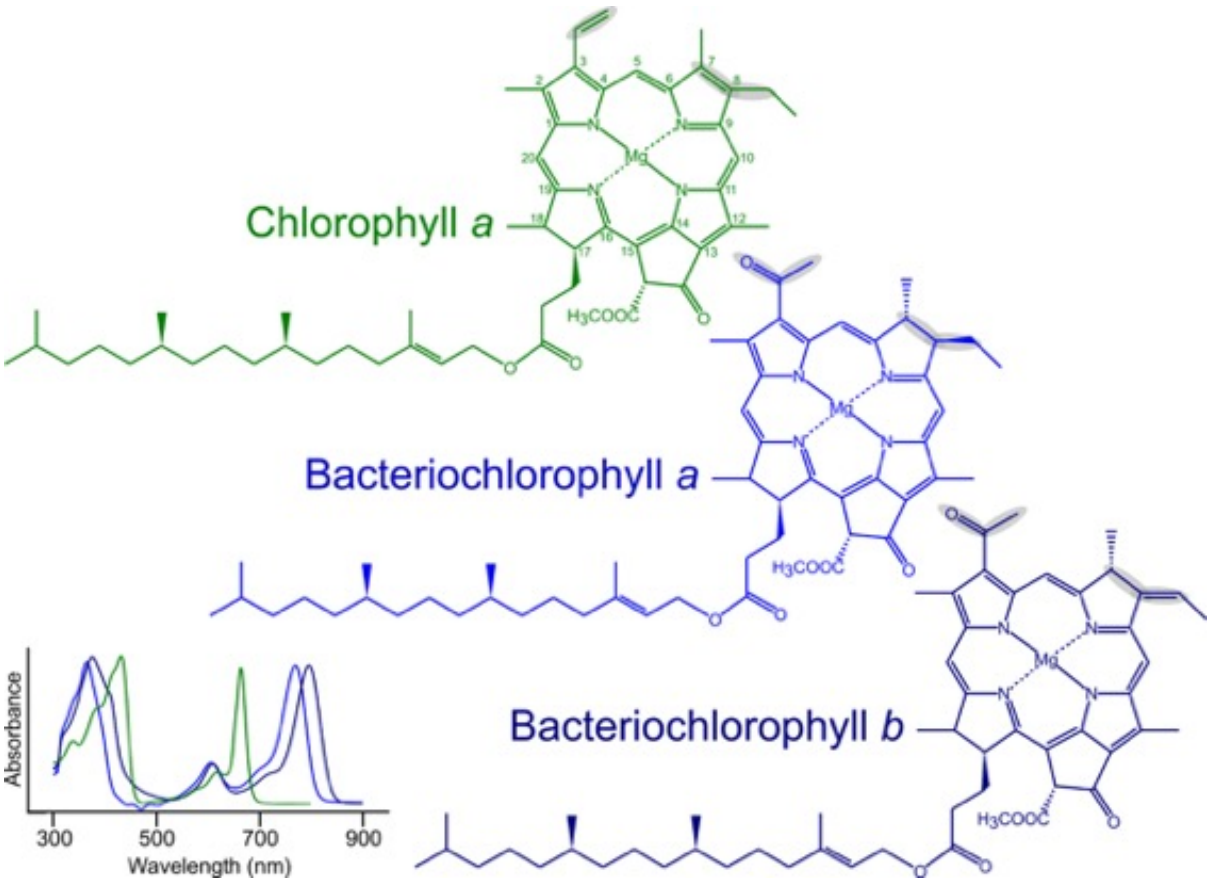


**Figure 1.1. Structures of (bacterio)chlorophylls.** Chemical structures of common (bacterio)chlorophylls. The carbon numbering system displayed on chlorophyll a is that approved by the International Union of Pure and Applied Chemistry (IUPAC). Structural differences between these pigments are highlighted in gray. Absorption spectra of these pigments in methanol are displayed (inset).

Unlike the chlorophyll-containing plants, algae and cyanobacteria that perform oxygenic photosynthesis, purple bacteria are anoxygenic phototrophs that use bacteriochlorophyll (BChl) *a* or *b* (Fig. 1.1), as well as carotenoid pigments that are ubiquitous in photosynthesis. The differences in structure between the bacteriochlorophyll and chlorophyll pigments results in varied absorption properties of phototrophic organisms (Fig 1.1). Purple phototrophic bacteria are proteobacteria, the

most metabolically versatile of the seven phyla of photosynthetic prokaryotes: Chlorobi, Acidobacteria, Firmicutes, cyanobacteria, proteobacteria, Chloroflexi and Gemmatimonadetes (Gupta and Khadka, 2016). Purple bacteria display a wide range of metabolic lifestyles with the capability to be photoautotrophic, photoheterotrophic, chemoautotrophic, mixotrophic, capable of fermentation and aerobic or anaerobic respiration, along with many different metabolic pathways for energy generation and carbon and sulfur metabolism (Imhoff *et al.*, 2005). This is reflected in the diverse habitats in which they grow, including lakes, ponds, estuaries, marine environments, microbial mats, sewage and waste lagoons, as well as extreme environments including hot, cold, acidic, alkaline, and hypersaline environments (Madigan, 2003). Purple bacteria include both purple sulfur and purple non-sulfur bacteria, classically dependent on their ability to metabolise and assimilate sulfur compounds (Frigaard and Dahl, 2008), although more contemporary studies have demonstrated that all purple bacteria are capable of sulfur metabolism to an extent (Hansen and Gemerden, 1972). They can use a variety of reductants as electron donors, including $H_2S$, other sulfur-containing compounds (such as cyst(e)ine and thiosulfate) or $H_2$ (Truper and Fischer, 1982; Brune, 2004); some species can use $Fe^{2+}$ iron as an electron donor (Ehrenreich and Widdel, 1994). Table 1.1 shows the basic characteristics of various species of purple bacteria.

**Table 1.1.1. Basic characteristics of various model purple bacterial photosynthetic organisms.** AAP – aerobic anoxygenic phototroph; BChl – bacteriochlorophyll.

| Taxonomy | Phylogeny/Class | Family | Genus | Abbreviation | AAP | BChl | Morphology |
|---|---|---|---|---|---|---|---|
| Purple nonsulfur bacteria | Alphaproteobacteria | Rhodobacteraceae | *Rhodobacter* | *Rba.* | - | *a* | Rods |
| | | Bradyrhizobiaceae | *Rhodoblastus* | *Rbl.* | - | *a* | Budding rods |
| | | | *Rhodopseudomonas* | *Rps.* | - | *a* | Budding rods |
| | | Rhodospirillaceae | *Rhodospirillum* | *Rsp.* | - | *a* | Spirilla |
| | | | *Phaeospirillum* | *Phs.* | - | *a* | Spirilla |
| | | Hyphomicrobiaceae | *Blastochloris* | *Blc.* | - | *b* | Budding rods |
| | | Acetobacteraceae | *Roseococcus* | *Rsc.* | ✓ | *a* | Cocci |
| | | | *Acidiphilium* | *Acp.* | ✓ | *a* | Rods |
| | | Sphingomonadales | *Erythromicrobium* | *Erm.* | ✓ | *a* | Rods, branched |
| | | | *Erythromonas* | *Emn.* | ✓ | *a* | Ovoid |
| | Betaproteobacteria | Burkholderiales | *Rubrivivax* | *Rbv.* | - | *a* | Rods,curved rods |
| Purple Sulfur Bacteria | Gammaproteobacteria | Chromatiaceae | *Allochromatium* | *Alc.* | - | *a* | Rods |
| | | | *Thermochromatium* | *Tch.* | - | *a* | Rods |

Anoxygenic photosynthesis is a simpler form of the process carried out by oxygenic organisms, which makes purple bacteria ideal model systems for dissecting the physiology, biochemistry and molecular biology of photosynthesis. Under oxic conditions, energy is derived from aerobic respiration and the synthesis of photosynthetic pigments and pigment-binding proteins is repressed. As conditions change through microoxic to anoxic, the ultrastructure of the cytoplasmic membrane forms invaginations towards the inside of the cell called intracytoplasmic membranes (ICM) (Hunter *et al.*, 2008); these can take the form of vesicles, tubes or lamellae. Fig. 1.2 shows a variety of different ICMs from different species.

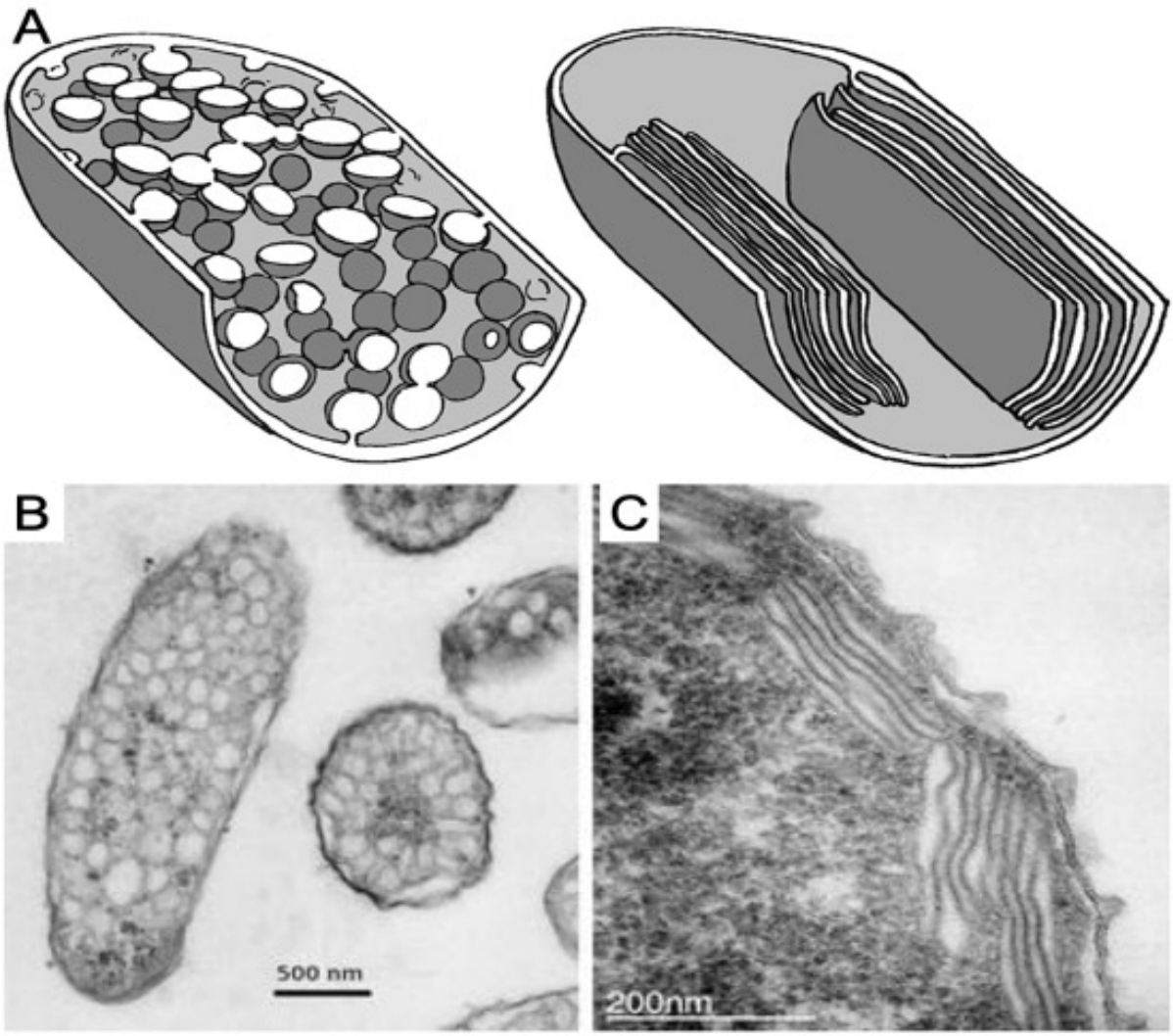


**Figure 1.2. Intracytoplasmic membranes of purple bacteria. A.** Schematic illustration of vesicular and lamellar ICM architectures (LaSarre *et al.,* 2018). **B.** Transmission electron micrograph of *Rhodospirillum (Rsp.) rubrum* cells, ICM vesicles are visible throughout the cytoplasm (Scheuring and Sturgis, 2009). **C.** TEM of photosynthetic membranes of *Phs. molischianum* cells containing stacked lamellar type ICM continuous with the cytoplasmic membrane (Scheuring and Sturgis, 2009).

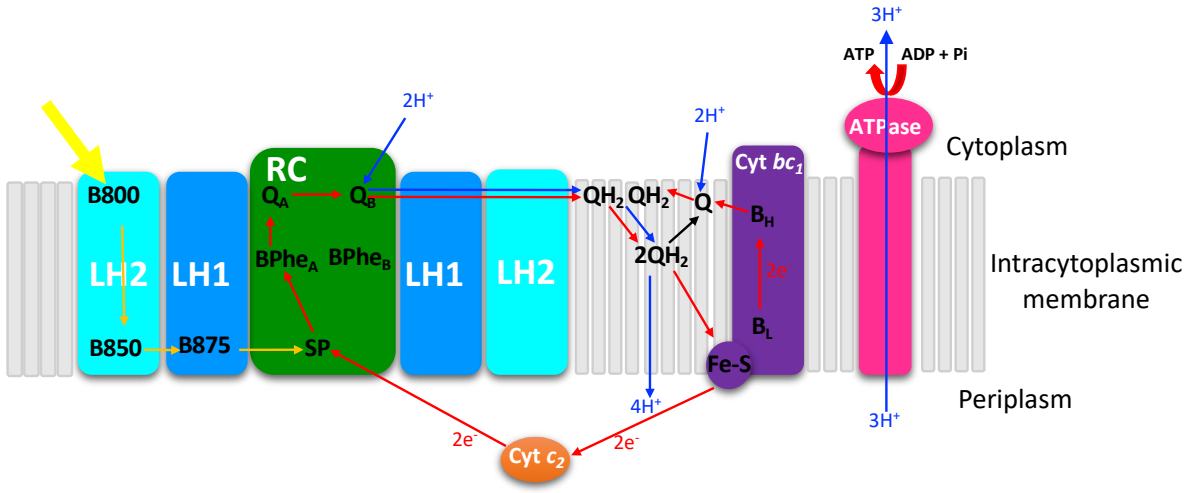


**Figure 1.3. Schematic of the Light-dependent reactions of purple bacterial photosynthesis.** Light energy is first absorbed by B800 in LH2; this is then transferred to lower energy BChls until it reaches and excites the special pair BChls in the RC. An electron is then passed along a series of electron donors to $Q_B$, and after a second charge separation $Q_B$ is fully reduced to quinol; the electrons are then passed to cyt $bc_1$ and cyt $c_2$ which re-reduces the special pair. This creates an electrochemical gradient across the membrane, which is used by ATPase to create ATP. Note, the exact locations of cyt $bc_1$ and ATPase are not known. Yellow arrows, excitation transfer; red arrows, electron transfer; blue arrows, proton transfer; *BChl* bacteriochlorophyll; *LH* light-harvesting; *RC* reaction centre; *SP* special pair; *BPhe* bacteriopheophytin; *Q* quinone; $QH_2$ quinol; *cyt* cytochrome; *ATPase* ATP synthase.

Photosynthesis occurs in two stages: the light-dependent reactions, followed by the light-independent reactions. The light-dependent reactions occur in the ICM, where the photosynthetic apparatus is housed. The pigments within light-harvesting (LH) antenna complexes absorb photons of light as resonance energy. The derived excitation energy is then transferred through a network of pigments in the LH complexes towards the reaction centre (RC), where a 'special pair' of BChl pigments

are housed. In the RC, charge separation occurs leading to the release of excited electrons, which are then passed down an electron transfer chain to RC-bound quinone electron carriers. This quinone is fully reduced to quinol after two electron transfers, at which point it is released from the RC and diffuses to cytochrome $bc_1$ (cyt $bc_1$). The quinol is then oxidised, releasing two protons into the periplasm of the cell; the electrons are passed to the soluble cytochrome $c_2$ (cyt $c_2$) and eventually back to the special pair in 'cyclic electron flow'. This results in an electrochemical gradient between the cytoplasm and the periplasm, generating a proton motive force (pmf) utilised by ATP synthase (ATPase) in the production of ATP (Hu *et al.*, 1998) (Fig. 1.3). In the light-independent stage the energy produced in the light-dependent reactions is used to fix $CO_2$ in the Calvin-Benison-Bassham Cycle (See details below) (Tabita, 2004; Blankenship, 2014).

Aerobic anoxygenic phototrophs (AAP) are a unique purple bacterial functional group that contain fully functional photosynthetic apparatus; however, this is assembled and operative under oxic conditions. Their photosynthetic machinery has various extensive modifications, including different peripheral antennas, and some organisms using zinc-chelated BChls in place of the more common magnesium-containing pigments (Wakao *et al.*, 1996). AAPs have a much lower number of photosynthetic complexes per cell and a huge abundance of carotenoids (Rathgeber *et al.*, 2004). Interestingly, although they are incapable of photoautrophy and rely on heterotrophy for 80% of their cellular metabolism, phototrophy can double organic carbon assimilatory efficiency (Kolber *et al.*, 2001). BChl synthesis in these organisms is inhibited by sunlight (Aagaard and Sistrom, 1972). Examples of these organisms can be seen in Table 1.1.

The majority of the genetic information needed to build the photosynthetic apparatus in purple bacteria is clustered into large (40-50 kbp) groups of genes called the photosynthesis gene cluster (PGC). The precise organisation of these genes within the cluster is highly variable. This cluster enables the precise control of expression levels and spatial proximity of the components (Alberti *et al.*, 2004). The discovery of a phototrophic member of the Gemmatimonadetes bacteria, carrying a PGC of purple bacterial origin, demonstrates that the organisation of these genes into this superoperon permitted horizontal gene transfer between distant bacterial phyla (Zeng and Koblizek, 2017).

## 1.2 Structural Components

### 1.2.1 *Peripheral antenna complexes*

The RC itself is a poor antenna, harvesting insufficient photons to support rapid growth via phototrophy. Purple bacteria have thus evolved specialised antenna complexes to increase the cross-sectional area available for light-harvesting and maximise photon capture. The energy absorbed by the antenna complexes is then passed to the RC. Purple bacteria typically contain two types of antenna complexes: the 'core' light-harvesting complex 1 (LH1) intimately associates with the RC, encircling it to form the 'core complex' or RC-LH1 complex, found in all purple bacterial species. There are also peripheral antenna, known as LH2, that are separated from the RC by the LH1 ring. These antenna complexes are embedded in the ICM of purple bacteria, bound non-covalently to the light-absorbing BChl and carotenoid pigments.

### *1.2.1.1 Light-Harvesting Complex 2*

The peripheral LH2 complexes funnel excitation energy to the RC via the core LH1 complexes (discussed in detail later). The LH2 complexes have been well studied across different species; all consist of symmetric ring structures with octa- or nonameric quaternary structures. The crystal structures of LH2 from *Rhodoblastus* (*Rbl.*) *acidophilus* (Fig. 1.4A) (McDermott *et al.*, 1995; Prince *et al.*, 1997; Papiz *et al.*, 2003) and *Phaeospirillum* (*Phs.*) *molischianum* (Fig. 1.4B) (Koepke *et al.*, 1996) have been solved to 2.0 Å and 2.4 Å resolution, respectively. Both structures adopt the same modular principle: oligomers consisting of numerous pairs of α- and β-polypeptides, known as the αβ-heterodimer, forming double ring structures with their associated pigments. The α- and β-polypeptides of the two species share 26% and 31% sequence identity, respectively.

The LH2 complex of *Rbl. acidophilus* is formed of a nonameric ring structure of 9 inner α- and 9 outer β-polypeptide chains (Fig. 1.4A), with ring diameters of 36 Å and 68 Å, respectively; each polypeptide crosses the membrane once, via an α-helical transmembrane domain (McDermott *et al.*, 1995). The LH2 structure acts as a scaffold for the associated pigments, including carotenoids and two populations of BChls. One BChl population in the *Rbl. acidophilus* LH2 contains 9 pairs of overlapping pigments held perpendicular to the plane of the membrane via histidine residues in the α- and β-polypeptides (Prince *et al.*, 1997); the short distances between these paired BChls (~9 Å) provide strong excitonic coupling between the pigments, shifting the absorption maximum to ~850 nm, thus this population is known as B850 (after their corresponding absorption maxima). The complex also contains 9 B800 BChl molecules inserted between the β-polypeptides, parallel to the membrane plane. The central Mg atom of

BChl is coordinated by methionine residues in the α-polypeptide (Papiz *et al.*, 2003); these pigments are not tightly coupled and so can be considered 'monomeric', thus contribute a band at ~800 nm, close to the absorption maximum of the pigment in solution. Finally, a carotenoid (rhodopin glucoside in the *Rbl. acidophilus* LH2) threads the space between the α- and β-pairs. Together, these pigments contribute to the structural and functional integrity of LH2 (Lang and Hunter, 1994).

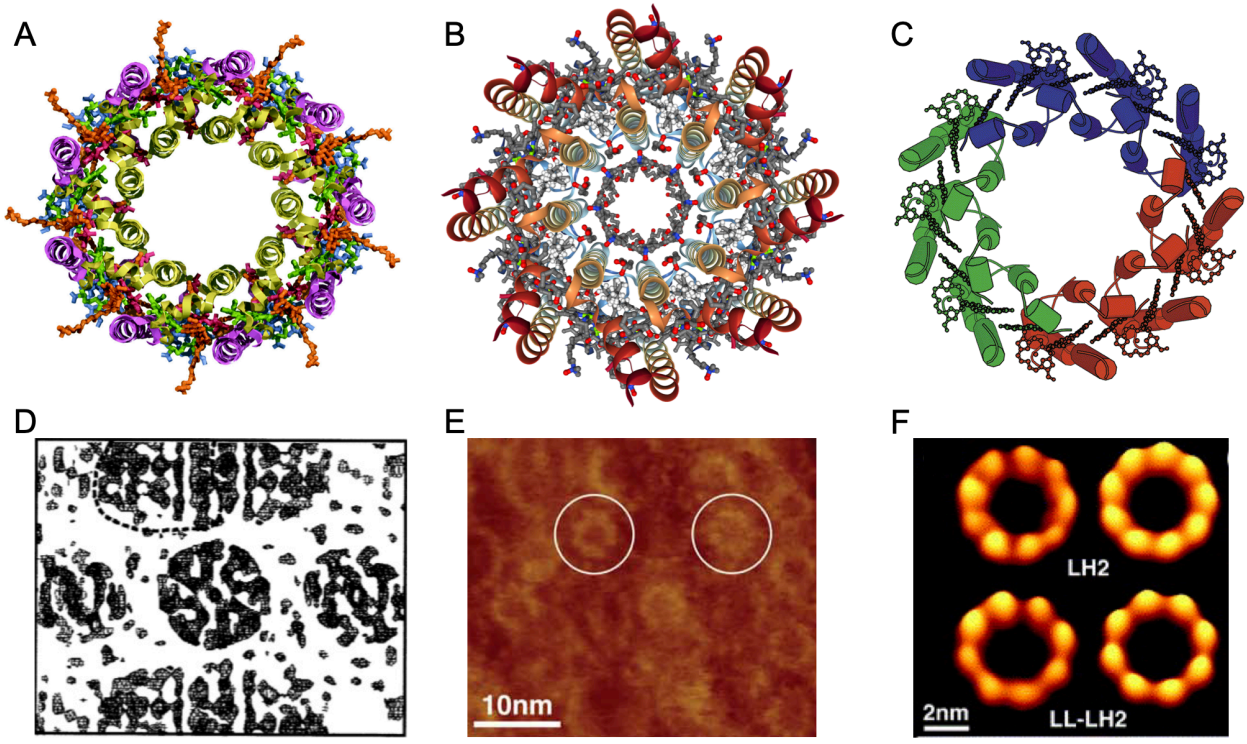


**Figure 1.4. Structures of different forms of light-harvesting antenna complexes in purple bacteria. A.** Structure of the LH2 complex from *Rbl. acidophila* 10050. Cartoon representation of the nonameric B800-B850 LH2 complex viewed from above. The α- and β-polypeptides are represented in light-green and purple, respectively. The BChls α-B850, β-B850, B800 are represented in red, green and blue, respectively, and the carotenoid is represented in orange (Papiz *et al.,* 2003). **B.** Crystal structure of the LH2 complex from *Phs. molischianum*. The octameric B800-B850 LH2 complex viewed from above with the N-termini pointing upwards. The α-

and β-polypeptides are represented in orange and red, respectively. The BChl a molecules are in grey (Koepke *et al.,* 1996). **C.** Structure of the LH3 complex from *Rbl. acidophilus* 7050. Schematic representation of the nonameric LH3 complex from *Rbl. acidophilus* 7050 (McLuskey *et al.,* 2001). **D.** Electron densities obtained from *Rps. palustris* LH4 X-ray data, revealing an octameric structure (Hartigan *et al.,* 2002). **E.** AFM analysis of peripheral antenna complexes from Rps. palustris grown under low-light; the white circles represent LH4 complexes (Scheuring *et al.,* 2006). **F.** Non-symmetrized (left) and symmetrized averages (right) of nonameric LH2 and octameric LH4 (LL-LH2) from *Rps. palustris* grown in low light (Scheuring *et al.,* 2006).

The overall structure of the B800-850 LH2 complex from *Phs. molischianum* is similar to that of *Rbl. acidophilus* (McDermott *et al.*, 1995; Koepke *et al.*, 1996), but with some key differences. The ring structure of this complex is made up of 8 αβ-pairs (Fig. 1.4B), thus possessing 3 BChls and 1 carotenoid fewer than that from *Phs. moliscianum*, as well as reduced diameters of the inner (31 Å) and outer rings (62 Å) (Koepke *et al.*, 1996). The 8 B800 molecules are coordinated by aspartate rather than methionine residues of α-polypeptides almost parallel to the membrane plane, with a distance of 2.45 Å. The acetyl carbonyl groups of BChl were also shown to interact with tryptophan residues in the α- and β-polypeptides; these residues were shown to be important in stabilising the BChl–LH1 interaction (Davis *et al.*, 1997; Kehoe *et al.*, 1998). The 8 carotenoids found in the complex are lycopene pigments stretched between the B800 and B850 molecules (Koepke *et al.*, 1996). The crystal structure of *Phs. molischianum* LH2, along with mutational studies (Olsen *et al.*, 1997), indicated that His residues also form a hydrogen bond with the carbonyl group of the coordinated BChl. The difference in oligomerisation seen between the two LH2 proteins was suggested to be

due to the differences in the interaction angle between subunits: 40° for nonameric rings and 45° for octomeric rings (Janosi *et al.*, 2006); these angles are believed to be determined by the surface interactions in the transmembrane regions (Janosi *et al.*, 2006). The intermolecular forces underlying the ring shape of the LH2 complex was shown to influence the structural and functional integrity of the LH2 complex in *Rhodospirillum* (*Psp.*) *photometricum* (Liu *et al.*, 2011).

### *1.2.1.2 Light-Harvesting Complexes 3 and 4*

Under stress conditions, such as low light or low temperature, absorption bands of several purple bacteria vary due to the expression of atypical peripheral light-harvesting complexes, known as LH3 and LH4 (Evans *et al.*, 1990; Mcluskey *et al.*, 2001; Hartigan *et al.*, 2002; Niedzwiedzki *et al.*, 2011). These are spectral variants of LH2, functioning to increase the size of the photosynthetic unit and broaden the spectral range of solar energy captured by the unit.

Both the *Rbl. acidophilus* 7050 and 7750 strains contain LH3 complexes (Fig. 1.4C) (Cogdell *et al.*, 1983; Angerhofer *et al.*, 1986). In the 7050 strain, LH3 complexes always coexist with LH2 complexes; however, low-light conditions can also induce the expression of LH3 (Cogdell *et al.*, 1983; Angerhofer *et al.*, 1986). LH2 was almost completely replaced with LH3 complexes in the 7750 strain under low light conditions (Gardiner *et al.*, 1993). The LH3 complexes absorb light at 800-820 nm, a blue shift from the 800-850 nm absorption seen in LH2. The overall structure of the LH3 complex from *Rbl. acidophilus* 7050 (Mcluskey *et al.*, 2001) is analogous to LH2 from *Rbl. acidophilus* 10050 (McDermott *et al.*, 1995), with the exception of reorientation of acetyl groups at the C3 position of B820 BChl in LH3 relative to the membrane plane;

this causes a change in the hydrogen bonding patterns between the protein and the coupled BChl *a* molecules, resulting in the change in spectral properties of the apoprotein (Mcluskey *et al.*, 2001).

*Rhodopseudomonas (Rps.) palustris* predominantly contains LH4 complexes in low-light conditions (Tharia *et al.*, 1999). This complex, also referred to as the low-light LH2 B800 complex, is composed of 8 αβ-peptide pairs, each pair contains 4 BChl molecules, distinct from the 3 BChls in LH2 complexes (Hartigan *et al.*, 2002); electron microscopy (EM) and atomic force microscopy (AFM) studies have confirmed its octameric structure (Scheuring *et al.*, 2006a) (Fig. 1.4D-4F).

The majority of purple phototrophic bacteria that use BChl *a* employ a peripheral antenna, but there are some exceptions; *Rhodospirillium (Rsp.) rubrum* and AAPs within the Eryth-Citro clde lack the genes that encode LH2 (and LH3 and LH4) (Munk *et al.*, 2011; Zheng *et al.*, 2011). To date, peripheral antenna have not been found in any BChl *b*-containing phototrophs, one possible explanation being that these antenna evolved in an ancestor using BChl *a*, after divergence of the two pigment pathways.

### *1.2.2 The core complex of purple bacterial photosynthesis*

Once light is harvested by LH2, the excitation energy is then passed to the BChl molecules housed in the LH1 antenna proteins, and subsequently to the special pair BChls in the RC, enabling charge separation. Across all species, the LH1 complex surrounds the RC forming a ring; this RC-LH1 supercomplex, central to purple bacterial photosynthesis, is known as the core complex. As mentioned above, some

purple bacteria, e.g. BChl *a*-containing *Rsp. rubrum* and BChl *b*-containing *Blastochloris (Blc.) viridis*, exclusively use the RC-LH1 core complex for both light harvesting and photochemical functions. The aggregation states of the RC-LH1 core complexes amongst different species are diverse (Fig. 1.5), with both monomeric and dimeric cores being found in the membranes.

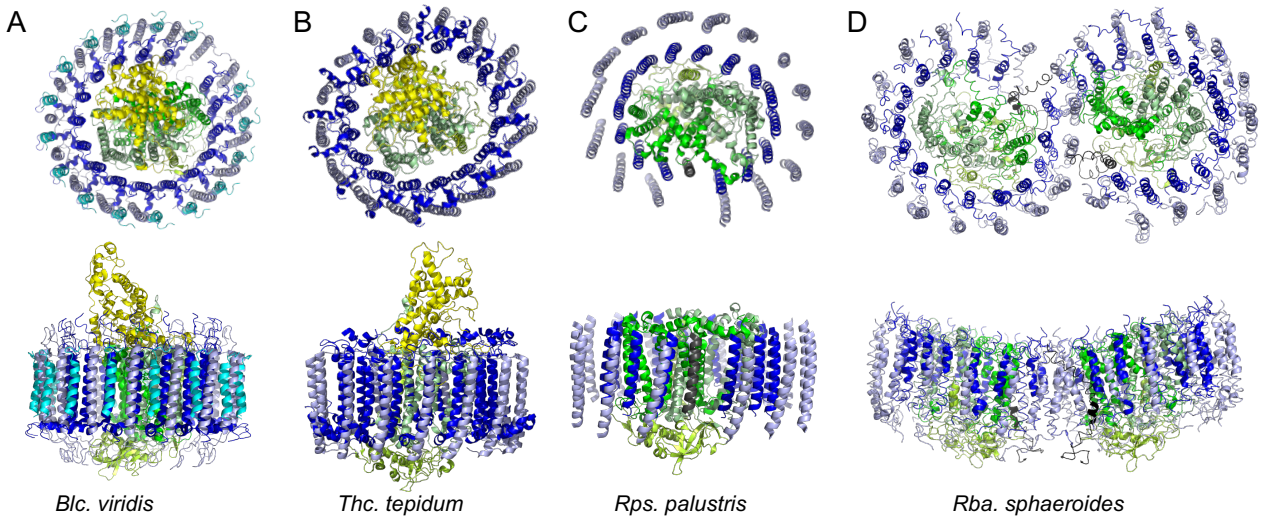


**Figure 1.5. Diverse structures of RC-LH1 complexes from different purple bacterial species.** Cartoon representations viewed from perpendicular to the membrane plane (top) and from the membrane plane (bottom) of **A.** RC-LH1 from *Blc. viridis* (PDB: 6ET5) (Qian *et al.,* 2018), **B.** RC-LH1 of *Thc. tepidum* (5Y5S) (L. J. Yu *et al.*, 2018), **C.** RC-LH1-PufW complex of *Rps. palustris* (PDB: 1PYH) (Roszak *et al.,* 2003), **D.** RC-LH1-PufX dimer of *Rba. sphaeroides* (PDB: 4V9G) (Qian *et al.,* 2013). The 4Hcyt, L, M and H subunits of the RC are represented in yellow, bright green, pale green and lime green respectively; α -, β – and γ - chains of LH1 are shown in blue, light blue and cyan, respectively. PufX and Protein W are represented in black and dark grey, respectively.

### *1.2.2.1 Light-Harvesting Complex 1*

The LH1 complex is composed of a ring of α- and β-polypeptides forming a heterodimer together with their associated pigment molecules: BChl *a* or *b* and carotenoids. These generally short, 40-70 amino acid residue, α-helical antenna polypeptides contain three domains: polar C- and N-terminal domains lying either side of a hydrophobic transmembrane domain (Brunisholz and Zuber, 1992; Zuber and Cogdell, 2004). A conserved Histidine residue acts as the ligand to the central Magnesium atom of the BChl (Qian, 2017); in *Blc. viridis,* the C3 acetyl groups of BChl *b* hydrogen bond to tryptophan residues in LH1 (Qian *et al.*, 2018), adopting an in-plane conformation similar to coordination in the LH2 of *Rbl.* acidophilus.

### *1.2.2.2 The photochemical Reaction Centre*

The RC, home of the light-induced charge separation across the intracytoplasmic membrane, of *Blc. viridis* was the first membrane protein structure to be solved by Deisenhofer et al. (Deisenhofer *et al.*, 1985; Deisenhofer and Michel, 1988). The RC consists of a common, basic structure of three transmembrane polypeptides, the L, H and M subunits (Fig. 1.6B), and their associated pigments, similar in all species of purple photosynthetic bacteria. L and M subunits each contain 5 transmembrane helices, and the LM heterodimer displays pseudo two-fold axis symmetry, perpendicular to the membrane plane. These subunits possess 25-30% sequence identity. L and M act as a scaffold for the arrangement of cofactors: 4 BChls, 2 bacteriopheophytin (BPhe) pigments, 1 non-haem iron, 2 quinones and 1 carotenoid. The cofactors are also arranged with a pseudo two-fold symmetry and form two separate branches, A and B, within the M and L subunits, respectively (Fig. 1.6C). Electron transfer has been shown to occur through branch A (Kirmaier *et al.*, 1985;

Bylina and Youvan, 1988; Kellogg *et al.*, 1989). The H subunit contains only 1 transmembrane helix, anchoring the subunit to the membrane, a cytoplasmic globular domain docks to L and M. The RC structure of *Blc. viridis* revealed an extra periplasmic tetrahaem cytochrome subunit (4Hcyt) attached to the membrane via a covalently attached fatty acid molecule (Deisenhofer *et al.*, 1985). The 4Hcyt houses four haem groups covalently attached to cyst(e)ine residues, arranged in a high-low-high-low redox potential pattern (Fig. 1.6C), functioning to re-reduce the special pair BChl (Ortega *et al.*, 1999). The conserved structure of RC is demonstrated by the crystal structures of *Rhodobacter (Rba.) sphaeroides* (Fig. 1.6D) (Allen and Holmes, 1986; Chang *et al.*, 1986) and *Thermochromatium (Thc.) tepidum* (Fig. 1.6E) (Nogi *et al.*, 2005) RC's, both of which are very similar to that of *Blc. viridis* (Qian *et al.*, 2018), however, *Rba. sphaeroides* (Allen and Holmes, 1986; Chang *et al.*, 1986) lacks the 4Hcyt subunit and both contain BChl *a* rather than BChl *b.*

*1.2.2.2.1 Quinones*

As well as being the home of charge separation, the RC also functions to produce fully reduced quinol ($QH_2$) to drive electron transfers through cyt $bc_1$, ultimately resulting in the formation of an electrochemical gradient driving ATPase. The RCs of purple bacteria consist of two acceptor quinones that act in series. The primary quinone, $Q_A$, is bound tightly to the RC, and cycles between oxidised quinone and singly reduced semiquinone. The secondary quinone, $Q_B$, is reduced twice by $Q_A$ to form a doubly reduced, fully protonated $QH_2$. The electron donor for these reactions is cyt $c_2$, so the RC can be thought of as a 'cytochrome $c_2$/ubiquinone' photo-oxidoreductase enzyme. After two turnovers of the RC, $QH_2$ is released from the $Q_B$ site and replaced by oxidised quinone to complete the quinone cycle. In the majority of purple bacteria both

$Q_A$ and $Q_B$ are ubiquinone (UQ) molecules, but in *Blc. viridis, Allochromatium vinosum*, and *Thc. tepidum* $Q_A$ is a menaquinone (MQ). The X-ray crystal structure of the RC from *Rba. sphaeroides* revealed hydrogen bonding to $Q_A$ (UQ-10) through carbonyl oxygens, a histidine residue and an amide backbone; a similar hydrogen bonding pattern was seen in $Q_A$ from *Blc. viridis* (MQ-9) (Gast *et al.*, 1985; Shopes and Wraight, 1985). The acceptor quinones are symmetrically positioned about a non-haem iron atom coordinated by four histidines and a glutamate residue, $Q_A$ is bound in the L subunit and $Q_B$ within the M subunit (Deisenhofer and Michel, 1988).

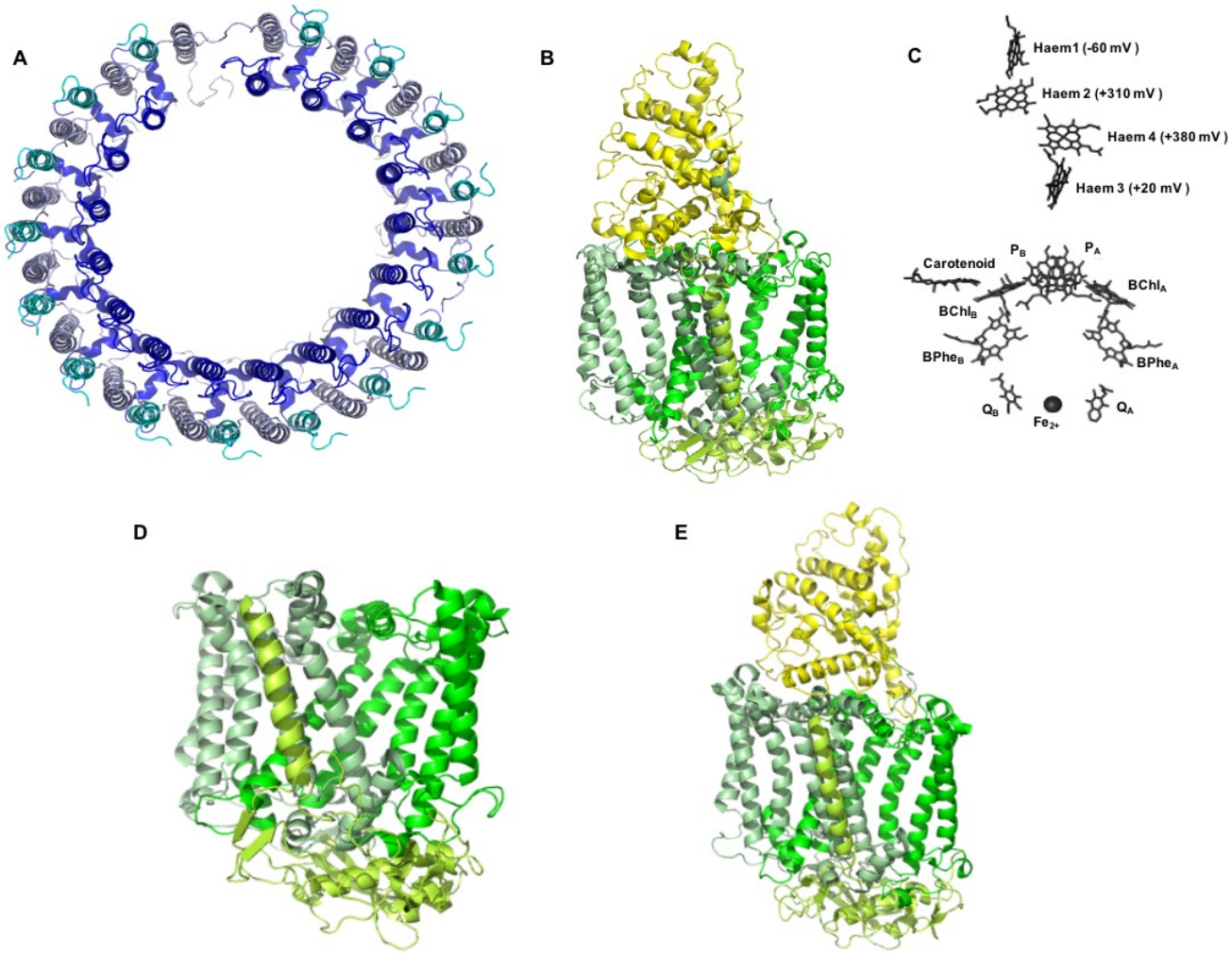


**Figure 1.6. Structures of LH1 and RC complexes.** Cartoon representation of **A** LH1 from *Blc. viridis* (PDB: 6ET5) (Qian *et al.,* 2018) from the periplasmic side of the

membrane and **B** RC from *Blc. viridis* (PDB: 6ET5) (Qian *et al.,* 2018) from the membrane plane. The RC resides in the center of the LH1 complex, this has been removed from the structure. **C.** Arrangement of cofactors in the RC from *Blc. viridis*; cofactors are represented as sticks. The redox potential of the haems are labelled. **D.** Crystal structure of the RC from *Rba. sphaeroides* (PDB: 2RCR) *(Camara-Artigas et al.*, 2002). **E.** Crystal structure of the RC from *Thc. tepidum* (PDB: 5Y5S) (L. J. Yu *et al.*, 2018). The α-, β- and γ-chains of LH1 are shown in blue, light blue and cyan, respectively. The 4Hcyt, L, M and H subunits are represented in yellow, bright green, pale green and limon respectively.

*1.2.2.3 Additional core complex components*

*1.2.2.3.1 PufX*

The core complex of many species within the *Rhodobacter* genus contains an extra transmembrane polypeptide, PufX (Youvan *et al.*, 1984; Sheng *et al.*, 1986; DeHoff *et al.*, 1988; Holden-Dye *et al.*, 2008). PufX creates a break in the LH1 ring, keeping it in an 'open' conformation to facilitate rapid quinone/quinol exchange between the RC and cyt $bc_1$ (Klug *et al.*, 1988; Farchaus *et al.*, 1990; Lilburn *et al.*, 1992). PufX represents an α-helical structure consisting of 34 residues (Tunnicliffe *et al.*, 2006); its N-terminus is largely unstructured, followed by a structured helical domain positioned to ensure basic residues are at the membrane interface to fulfil a membrane-anchoring role (Parkes-Loach *et al.*, 2000). Studies on *Rba. capsulatus* and *Rba. sphaeroides* indicated that deletion of the *pufX* gene led to the inability of these strains to grow phototrophically (Klug *et al.*, 1988; Farchaus *et al.*, 1990; Lilburn *et al.*, 1992). For a history of PufX, see the review by Holden-Dye et al. (Holden-Dye *et al.*, 2008).

*1.2.2.3.2 Protein W*

The X-ray crystal structure of the core complex from *Rps. palustris* revealed that the RC was surrounded by an incomplete elliptical ring of 15 αβ-polypeptide pairs. Electron density maps suggested that a single transmembrane helix, named protein W, prevented closure of the LH1 ring (Fig. 1.5C) (Roszak *et al.*, 2003). The break in the LH1 ring created by protein W is positioned adjacent to the secondary electron acceptor quinone ($Q_B$) binding site, as is the case for PufX, which suggested a similar potential role in quinone/quinol exchange with cyt $bc_1$. The identity of protein W remained unknown for many years, until proteomic analysis of purified core complexes from the sequenced *Rps. palustris* strain CGA009 identified a polypeptide (RPA4402) that was present in the preparation (Jackson *et al.*, 2018). Biochemical and electron microscopic analysis indicated that RPA4402/protein W is only present in ~10% of the purified core complexes, and deletion of the encoding gene had no measurable effect on phototrophic growth, thus the precise role of protein W remains enigmatic (Jackson *et al.*, 2018).

*1.2.2.3.3 The Gamma subunit*

An additional LH1 subunit was also identified in core complex preparations of *Blc. viridis* (Jay *et al.*, 1983); unlike protein W and PufX, this γ-polypeptide was found to be in apparent equimolar ratio with the LH1 α- and β-polypeptides (Brunisholz *et al.*, 1985). Subsequently, the structure of the core complex from this organism revealed the location of γ, packing between β-polypeptides on the outside of the LH1 ring (Qian *et al.*, 2018). The α:β:γ ratio was found to be 17:17:16, the 'missing' γ-subunit creating the channel for quinone diffusion, converse to the proposed roles for PufX and protein W, whose presence at a single location around the LH1 ring is believed to create this

channel. An additional role of the γ-polypeptide in increasing the packing of LH1 BChls was also proposed; the resulting shorter intra-subunit Mg–Mg distances increase excitonic coupling, making the *Blc. viridis* RC-LH1 complex the most red-shifted photosynthetic complexes described to date (Qian *et al.*, 2018).

**Table 1.2. Composition of RC-LH1 complexes in purple bacteria.** Species with '2x' subunits form dimeric complexes.

| Species | RC Components | | | | LH1 Components | | Additional Peptides | |
|---|---|---|---|---|---|---|---|---|
| | 4HCyt | L | M | H | αβ | αβγ | PufX | Protein W |
| *Blc. viridis* (PDB: 6ET5) (Qian *et al.*, 2018) | ✓ | ✓ | ✓ | ✓ | 1 | 16 | - | - |
| *Rba. sphaeroides*(PDB: 4V9G) (Qian *et al.*, 2013) | - | 2x | 2x | 2x | 28 | - | 2 | - |
| *Rps.palustris* (PDB:1PYH) (Roszak *et al.*, 2003) | - | ✓ | ✓ | ✓ | 15 | - | - | 1 |
| *Rsp. rubrum* (Jamieson *et al.*, 2002) | - | ✓ | ✓ | ✓ | 16 | - | - | - |
| *Thc. tepidum* (PDB: 5Y5S) (L. J. Yu *et al.*, 2018) | ✓ | ✓ | ✓ | ✓ | 16 | - | - | - |
| *Rba. blasticus* (Scheuring *et al.*, 2005a) | - | 2x | 2x | 2x | 26 | - | 2 | - |
| *Rba. veldkampii* (Busselez *et al.*, 2007b) | - | ✓ | ✓ | ✓ | 15 | - | 1 | - |

### *1.2.2.4 Architectures of core complexes*

The RC-LH1 complexes possess different forms across different purple photosynthetic bacteria (Fig. 1.5). Table 1.2 provides the RC-LH1 composition for several species of purple bacteria.

Early, low-resolution electron microscopy studies on membranes from *Blc. viridis* and *Halorhodospira* (*Hlr.*) *halochloris*, followed by single particle analysis on purified core complexes from *Phs. molischianum* indicated that the common structure of RC–LH1 complexes consisted of a circular LH1 antenna surrounding the RC (Stark *et al.*, 1984; Engelhardt *et al.*, 1986; Boonstra *et al.*, 1994). Later studies employing AFM to interrogate the topography of membranes from purple bacteria (Liu and Scheuring, 2013; Liu, 2016) achieved sufficient resolution to assign the number of αβ-polypeptide pairs in the LH1 antenna from *Blc. viridis*, *Rsp. rubrum*, *Psp. photometricum*, and *Phs. molischianum*; all considered the RC to be enclosed by 16 αβ dimers, with those from *Blc. viridis* and *Rsp. rubrum* interpreted to be elliptical in shape (Fig. 1.7A,B) (Fotiadis *et al.*, 2003; Scheuring *et al.*, 2003a; Scheuring *et al.*, 2004a; Gonçalves *et al.*, 2005). This elliptical shape was reinforced with the 4.8 Å crystal structure of the *Rps*. *palustris* core complex, although the LH1 ring was found to contain the W polypeptide in place of one of the 16 αβ pairs (Roszak *et al.*, 2012). The 'gap' in the elliptical ring created by protein W was also identified by AFM (Fig. 1.7C)(Scheuring *et al.*, 2006b). The contemporary, high-resolution structures of the RC–LH1 complexes from *Tch. tepidum* and *Blc. viridis*, which consist of 16 and 17 αβ heterodimers, respectively, the latter also containing 16 γ subunits, illustrate that monomeric core complexes do not have a uniform architecture.

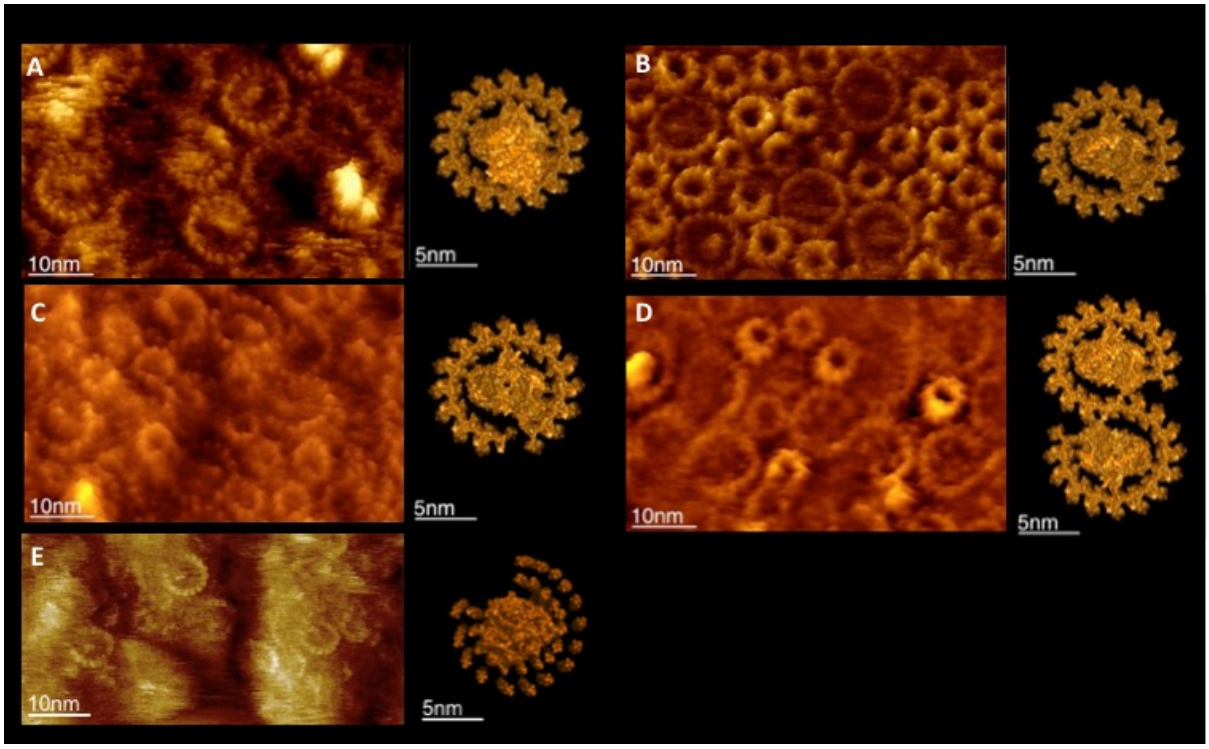


**Figure 1.7. Diversity of core-complex architectures among purple photosynthetic bacteria species.** Core complexes in their native membranes (left) and the models of individual core complexes (right) for **A** *Blc. viridis* ($LH1_{16}$-$RC_{L,M,H}$-4Hcyt) (Scheuring *et al.,* 2003a), **B** *Psp. photometricum* ($LH1_{16}$-$RC_{L,M,H}$) (Scheuring *et al.,* 2004a), **C** *Rps. palustris* (W-$LH1_{15}$-$RC_{L,M,H}$) (Scheuring *et al.,* 2006b), **D** *Rba. blasticus* ($PufX_2$-$LH1_{13}$-$RC_{L,M,H}$)$_2$ (Scheuring *et al.,* 2005a) and **E** *Rba. veldkampii (Liu et al.,* 2011).

This lack of uniformity is compounded by the presence of dimeric core complexes in species of Rhodobacter. Cryo-EM of negatively-stained membranes from an LH2 mutant of Rba. sphaeroides (the mutation causing the switch from its native vesicular to tubular membranes) revealed highly-ordered core complexes in S-shaped conformations, believed to be comprised of two RCs, each surrounded by a C-shaped LH1 (Jungas et al., 1999). Sucrose-density gradients of solubilised membranes from Rba. sphaeroides also revealed that monomeric and dimeric core complexes could be isolated in which PufX was detected in a 1:1 ratio with the RC,

but that when pufX was deleted, only monomeric RC-LH1 could be isolated, indicating that PufX promotes dimerization of the core complex (Francia et al., 1999). AFM analysis of membranes from *Rba. sphaeroides* and *Rba. blasticus* revealed that the majority of core complexes exist in dimeric form in the native membranes of these strains (Fig. 1.7D)(Bahatyrova et al., 2004; Scheuring et al., 2005a). A subsequent structure of the dimeric core from Rba. sphaeroides revealed that each RC was surrounded by 14 αβ heterodimers, with each PufX adjacent to the $Q_B$ site and interacting with the RC-H subunit via its N-terminal extension, and both N- and C-termini of PufX promoting dimerisation by interacting with a β polypeptide in the other half of the dimer (Qian et al., 2013). Interestingly, the core complex of *Rba. veldkampii* was found to contain a PufX polypeptide, but sedimentation and single particle analysis, and subsequent AFM analysis of its native membrane, demonstrated the complex exists solely as monomeric cores in this organism (Fig. 1.7E)(Gubellini et al., 2006; Liu et al., 2011). More recently, a systematic analysis of additional Rhodobacter species demonstrated that dimeric core complexes were also found in Rba. azotoformans and Rba. changlensis, but those of Rba. capsulatus and Rba. vinaykumarii were monomeric, yet all contained PufX (Crouch and Jones, 2012). This study also indicated that there was no clear motif with the amino acid sequences of PufX from the tested strains that could be identified as key for dimerisation, thus further work is required to clarify the biochemical basis of this morphological difference.

### *1.2.3 Cofactors and pigments*

### *1.2.3.1 Carotenoids*

Carotenoids have several essential functions within photosynthetic systems: (1) they are accessory pigments functioning in the collection and absorption of light energy and transferring this to BChl molecules. (2) They function in the photoprotection process, rapidly quenching triplet excited states of BChl and preventing them from reacting with oxygen and forming the highly reactive and damaging excited singlet state of oxygen. If singlet oxygen is formed, carotenoids can also quench this (Blankenship, 2014). (3) Carotenoids also play an important role in the assembly of LH complexes; in order to reversibly dissociate LH complexes, removal of carotenoids from the complex is required (Loach and Parkes-Loach, 1995). In LH2 complexes carotenoids extend between the subunits (McDermott *et al.*, 1995; Koepke *et al.*, 1996; Prince *et al.*, 1997), stabilising the complex and interacting with the BChls.

Structures of several carotenoids present in purple bacteria can be found in Fig. 1.8. All of these carotenoids are extended molecules with delocalised π electron systems. A number of common characteristics exist including, but not limited to, the presence of tertiary hydroxy and methoxy groups at C-1, keto groups at C-2, and frequent double bonds in the C-3,4 position (Takaichi, 2000).

### *1.2.3.2 Bacteriochlorophylls*

The main structural cofactors and LH pigments of photosynthetic antennae of purple bacteria are BChls, which also play a key role in photochemistry in the RC; energy is harvested and transferred from BChls within the LH complexes to the RC for charge separation at the special pair. Many different types of BChl exist within phototrophic prokaryotes, but only two types exist in purple photosynthetic bacteria, BChl *a* and

BChl *b* (Fig. 1.1). BChl *a* is the most common pigment found in purple bacteria, permitting absorption of wavelengths between 800 and 970 nm when assembled into LH complexes, shifting the Qy absorption band of the pigment in solution into the near-infrared (Imanishi *et al.*, 2019) (Table 1.1). BChl *b* is only found in a few species; it differs from BChl *a* in the presence of an exocyclic double bond at C-8 in ring B, known as an ethylidene substituent (Fig. 1.1). BChl *b* permits absorption between 960-1050 nm, the longest wavelength absorbance band of any chlorophyll-type pigment. The use of BChls *a* or *b* allow purple bacteria to absorb wavelengths of light outside the range of the chlorophylls used by plants and cyanobacteria.

#### *1.2.3.3 Bacteriopheophytins*

BPhe are easier to reduce than BChls, and hence function as electron acceptors within the sequence of electron carriers in places where BChls are not active (Fajer *et al.*, 1975). They are metal free BChls, lacking the central $Mg^{2+}$ present in BChls. They are predominantly recognised as breakdown products, due to their formation during the degradation of BChl. However, small amounts of BPhe are essential components of RCs, which are produced in specific, but yet unknown, pathways. In charge separation, BPhe (termed $H_A$) function as the first electron acceptor subsequent to the excitation of the special pair of BChls (Zinth and Wachtveitl, 2005; Jones, 2009).

### *1.2.4 Cofactor-cofactor and protein-protein interactions*

A large, overlapping array of BChl molecules is formed by dense packing of LH1 and LH2 proteins in the photosynthetic membranes. This ensures that absorbed energy and the excited state are both quickly delocalised among the array and thus can be

easily transferred to other LH complexes and eventually to the RC. Oligomerisation of B820 is required for the formation of LH1 and LH2 complexes (Miller *et al.*, 1987; Chang *et al.*, 1990). B820 subunits readily associate with the corresponding LH apoproteins to form LH1 and LH2 complexes with dependence on the details of cofactor-protein and protein-protein interactions. The heterodimeric B820 complex is stabilised by the interaction of the N-terminal regions of α- and β-polypeptides (Parkes-Loach *et al.*, 2004). Several studies have demonstrated that fine tuning of the absorption maximum of the associated LH complex may be due to evolution of the α-polypeptide (Todd *et al.*, 1998). Dissociation and reassociation experiments revealed that under *in vitro* conditions, B820 re-associates to form LH1 via several intermediate species, reflecting the different numbers of subunits which associate during growth of the complex and eventual formation of the ring. Once this structure is formed, some rearrangements of the protein segments occur on a slower timescale (Miller *et al.*, 1987; Pandit *et al.*, 2003).

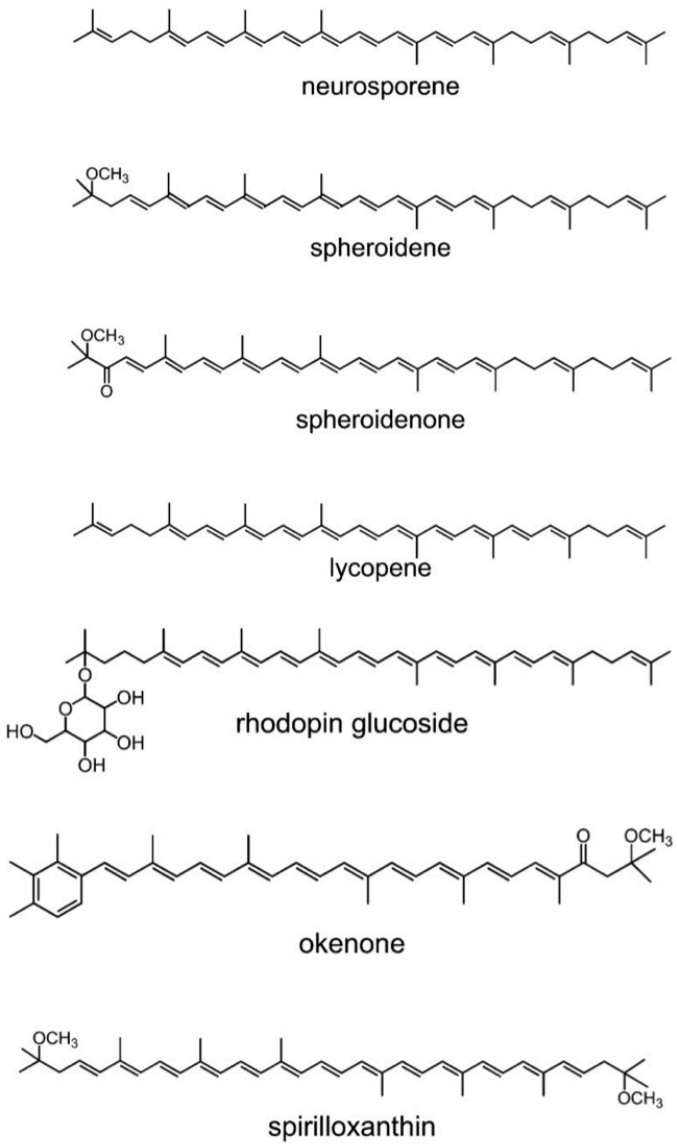


**Figure 1.8. Structures of common carotenoids in LH complexes of purple photosynthetic bacteria.**

### *1.2.5 Assembly of complexes*

Assembly factors LhaA and PucC are important, but not essential, in the specific assembly of LH1 and LH2 complexes *in vivo*, respectively. These factors form oligomers at sites of initiation of membrane invagination. LhaA makes associations with RCs, BChl synthase, the protein translocase subunit YajC and the membrane protein insertase YidC, aiding coordination of pigment delivery, co-translational

insertion of the LH polypeptides and the folding and assembly of these form functioning complexes (Mothersole *et al.*, 2016). Reconstitution experiments demonstrated that LH1 subunits possess the ability to re-associate with RCs to form functional, native-like core complexes, in the absence of LhaA (Bustamante and Loach, 1994). The RC-LH1 may follow a similar pattern of assembly *in vivo*. As is seen in *Rba. sphaeroides* (Pugh *et al.*, 1998), the RC is likely to form first, allowing the LH1 subunits to subsequently encircle it. This theory suggests that the LH1 subunits are static within the complete circle, however, these subunits may in reality be flexible (Jamieson *et al.*, 2002; Bahatyrova, Frese, Siebert, *et al.*, 2004). The forces underlying the stability of the B820 subunit may be minimal, allowing the subunit to readily dissociate; this would provide a possible pathway for Quinones on release from the $Q_B$ binding site (Hunter *et al.*, 2008).

### *1.2.6 Spectroscopic properties of light-harvesting complexes*

Understanding the spectroscopic properties of LH complexes is fundamental as they are the key factor in directing the flow of excitation energy towards the RC. Although many antenna proteins contain the same BChl molecules, their absorption spectra can differ. BChl *a* and BChl *b* (Fig. 1.1) molecules of LH1 complexes absorb at 870-890 nm and near 1000 nm, respectively; whereas, the BChl *a* molecules of LH2 complexes absorb at 800 and 850 nm. Additionally, a number of strains have been shown to synthesise modified antenna proteins absorbing at unusual wavelengths, for instance *Chromatium purpuratum* (830 nm) (Cogdell *et al.*, 1990) and *Roseococcus thiosulfatophilus* (856nm) (Gall *et al.*, 1999). The arrangement of BChl molecules within LH complexes could modify the spectroscopic properties of LH complexes. 24-

32 and 16-18 BChl molecules associate with LH1 and LH2 respectively, through van der Waals contacts, leading to the red-shifting of the absorption properties of the complexes (van Grondelle *et al.*, 1994), compared to the BChls in solution.

The absorption spectra of LH3 and LH4 complexes is shifted to be lower than 820 nm. The primary sequence of LH proteins between complexes and species differs; changes in the amino acid sequence in the protein environment of BChls can affect the hydrogen-bonding-state and the dielectric properties of the protein environment (Fowler *et al.*, 1994, 1997; Gall *et al.*, 1997); this explains part of the blue-shift observed. Recent experiments showed that a change in the hydrogen bonding network affected the $Q_y$ transition of BChls but also indirectly affected the role of charge-transfer states (Nottoli *et al.*, 2018), leading to a new explanation of the blue-shift seen in LH3 and LH4 complexes.

Homogenous LH proteins do not necessarily share the same electronic properties (van Mourik *et al.*, 1992); slight differences in the conformation of the immediate environment of the BChls or dynamic fluctuations in the system, known as the static and dynamic disorder respectively, lead to changes in the local physico-chemical properties of the BChl and heterogeneity in the electronic properties. This disorder in the structure changes the properties of otherwise chemically identical BChls, which results in the localisation of excited states onto a subset of BChls within the interacting group (Hunter *et al.*, 2008).

### *1.2.7 Cytochrome $bc_1$*

Cyt $bc_1$ is a multi-subunit membrane bound enzyme and an essential component of the energy transduction machinery in purple photosynthetic bacteria (Fig. 1.9) (Berry *et al.*, 2000, 2004; Crofts, 2004). The enzyme functions to electronically connect the quinone pool to the downstream electron transport chain (ETC) and translocate protons across the membrane helping to produce the pmf (Crofts, 2004). The cyt $bc_1$ oxidises $QH_2$ and donates the electron to the membrane soluble electron carrier cyt $c_2$ (Jenney and Daldal, 1993). Therefore, this enzyme can be thought of as a 'ubiquinol/cytochrome $c_2$ oxidoreductase', operating in the opposite direction to the RC, and completes the cyclic electron flow utilised by purple bacterial photosynthesis.

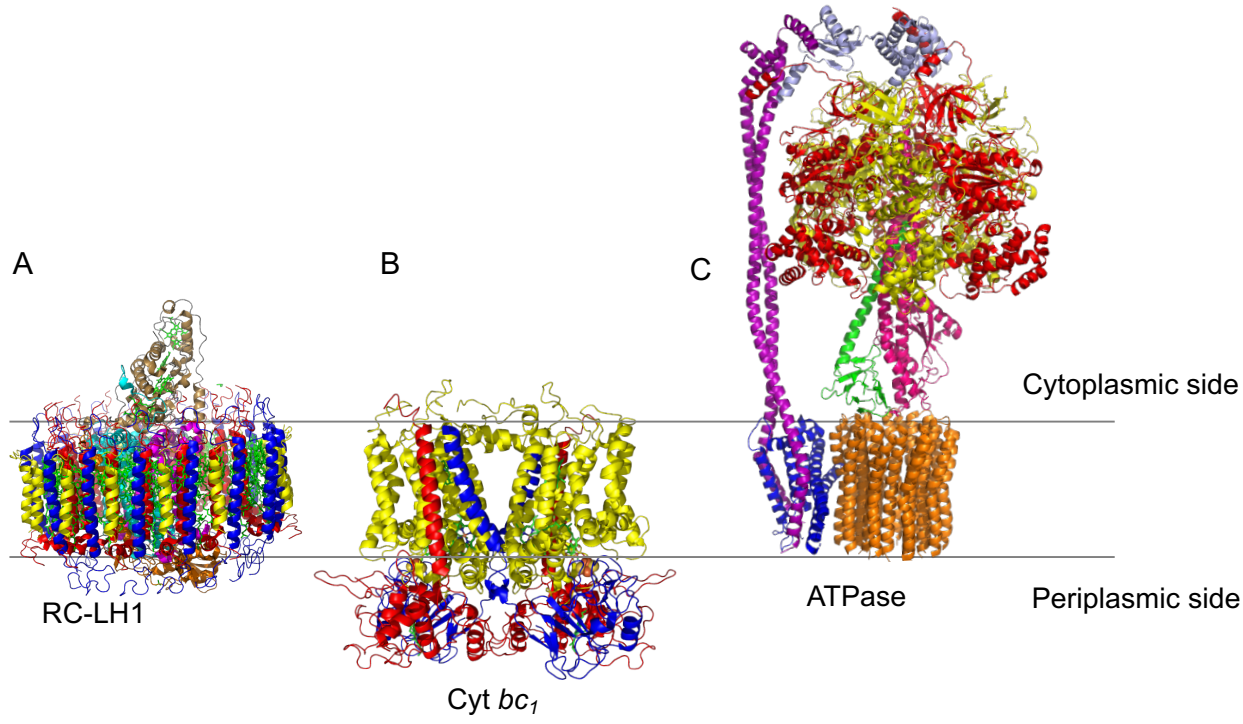


**Figure 1.9. Structures of cytochrome $bc_1$ and ATP synthase. A.** Structure of RC-LH1 from *Blc. viridis* (Qian *et al.,* 2018) shown for comparison, colour scheme identical to Fig. 1.5. **B.** Structure of cyt $bc_1$ from *Rba. capsulatus* (PDB: 1ZRT) (Berry *et al.,* 2000). The cyt b, cyt $c_1$ and Rieske subunits are represented in yellow, red and blue, respectively. **C.** Structure of the ATPase from *Bacillus* PS3 (PDB: 6N30) (Guo *et al.,*

2019). The c-ring, A, B, α, β, δ, γ and ε subunits are represented in orange, blue, purple, red, yellow, light blue, pink and green, respectively. The grey lines represent the intracytoplasmic membrane.

The overall structure of cyt $bc_1$ (Fig. 1.9B) consists of an intertwined homodimer with two monomers organised about a two-fold molecular axis; each monomer is comprised of three subunits: a high-potential [2Fe–2S] cluster-containing subunit, known as the Rieske protein (Rieske *et al.*, 1964), an integral membrane cyt *b* subunit, and a *c*-type cytochrome subunit, known as cyt $c_1$, in which the haem cofactor is covalently attached to the polypeptide (Berry *et al.*, 2000; Darrouzet *et al.*, 2004). Cyt *b* consists of two *b* type haems located on the positive (*p*) and negative (*n*) sides of the membrane. The central core of the monomer is formed by ten transmembrane helices, one from the Rieske protein, one from cyt $c_1$ and eight from cyt *b*. The large protrusion on the *p* side of the membrane consists mainly of the hydrophilic parts of the Rieske protein and the cyt $c_1$ subunits, whereas the *n* side is seemingly devoid of proteins (Fig. 1.9) (Berry *et al.*, 2004). Each monomer contains two $Q/QH_2$ binding sites referred to as $Q_o$ ($QH_2$ oxidation, $H^+$ output) and $Q_i$ (Q reduction, $H^+$ input) sites; the $Q_o$ site is at the interface of the Rieske protein and cyt *b* on the *p* side of the membrane and the $Q_i$ site is in the cyt *b* subunit, closer to the *n* side of the membrane (Sarıbaş *et al.*, 1998; Berry *et al.*, 2000).

### *1.2.8 ATP synthase*

The electrochemical gradient produced by the actions of the photosynthetic machinery is used by $F_0F_1$-ATPase, a membrane protein that synthesises ATP from ADP and inorganic phosphate (Pi). The enzyme contains two distinct portions of multi-subunit

complexes; a hydrophobic proton-translocating $F_0$ proton channel is embedded within the membrane, consisting of three subunits: A, B and C, and a hydrophilic, enzymatic $F_1$ portion, consisting of α, β, ε and γ subunits, protrudes from the plane of the membrane by ~100 Å (Fig. 1.9) (Guo *et al.*, 2019). Three αβ heterodimers in $F_1$ form a hexamer, with a long central cavity filled with the elongated portion of the γ-subunit comprising an N-terminal coiled-coil structure and an α-helical domain close to the C-terminus; this protrudes ~30 Å into the stalked region. A short α-helix of the γ-subunit is at a 45$^o$ incline to the coiled-coil domain at the bottom of the $F_1$. The γ-subunit makes up a coupling domain, coupling ATP hydrolysis with ion pumping (Capaldi *et al.*, 1996; Junge *et al.*, 1997).

The αβ heterodimer contains six nucleotide-binding sites within the six clefts between adjacent subunits; only three of these participate in catalysis (Weber *et al.*, 1994, 1995); the role of the other three clefts are not known, but are believed to play a regulatory role (Milgrom *et al.*, 1991; Jault and Allison, 1993; Jault *et al.*, 1995; Matsui *et al.*, 1997). The catalytic sites are mainly formed by the β subunit. Although they are all identical, at any given time they have different conformations and affinities to nucleotides (Kayalar *et al.*, 1977). Nucleotide binding to a particular site triggers the release of a nucleotide from another site, this is intimately linked to the rotation of the γ subunit within the αβ heterodimer (Senior *et al.*, 2002; Weber and Senior, 2003).

### *1.2.9 Cytochrome $c_2$*

The water-soluble c-type haem protein cyt $c_2$ (Fig. 1.10) serves as an electron donor to the RC, rapidly reducing the oxidised special pair created during the charge

separation step due to its optimisation for rapid association and dissociation (Tiede and Dutton, 1993). The haem group of cyt $c_2$ is covalently linked to the protein through thio-ether linkages, one edge of this haem group is exposed to solvent, which is important for reduction of the RC (Axelrod *et al.*, 1994). Many positively charged Lys and Arg residues surround the solvent-exposed haem edge; these interact electrostatically with a cluster of negatively charged residues on the surface of the RC, positioning the cyt $c_2$ in the centre of the periplasmic surface of the RC, so that the solvent exposed haem edge is directly over the BChl dimer, the primary donor, for rapid electron transfer (Rosen *et al.*, 1983; Caffrey *et al.*, 1992; Drepper *et al.*, 1997). This binding region exhibits close van der Waals contacts important for both binding and electron transfer. A crystal structure of the cyt $c_2$:RC complex from *Rba. sphaeroides* has been determined, confirming this binding position (Axelrod *et al.*, 2002). The position of the haem is similar to that found in the 4Hcyt subunit of the RC of *Blc. viridis* (Fig. 1.6B) (Deisenhofer and Michel, 1988). Binding of the cyt $c_2$ to RC leads to a slight conformational change creating a kink in the polypeptide chain of the RC, indicating a rigidly-fixed specific binding site of the cyt $c_2$ on the RC (Axelrod *et al.*, 2002).

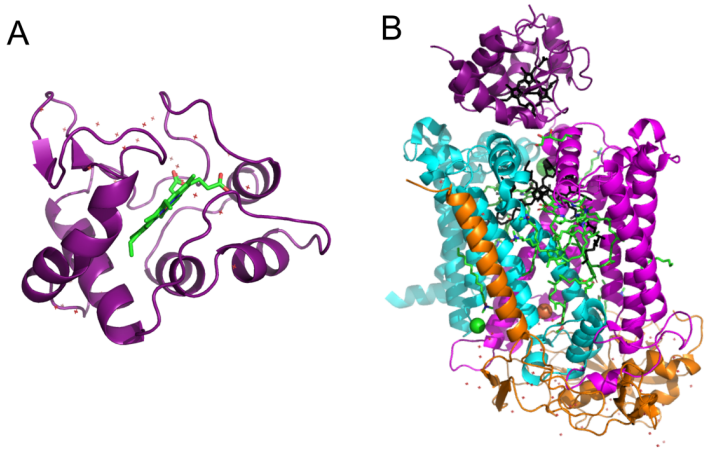


**Figure 1.10. Structure of cytochrome $c_2$. A.** Crystal structure of cyt $c_2$ from *Rba. sphaeroides* (PDB: 1CXC) (Axelrod *et al.,* 1994); the haem group is represented in green. **B.** Crystal structure of *Rba. sphaeroides* cyt $c_2$:RC (PDB: 1L9B) *(Axelrod et al.,* 2002). Cyt $c_2$ is represented in purple, the L, M and H subunits of the RC are represented in magenta, cyan and orange, respectively. The haem group in cyt $c_2$ and the special pair BChl in RC are represented in black to highlight their positioning in the complex.

## 1.3 Organisation and Assembly of Photosynthetic Membranes

Knowledge of the static structures of individual membrane proteins is insufficient to fully understand their function and physiological coordination. An appreciation of *in situ* assembly and distribution of the proteins within their native membrane, and analysis under near-native conditions, is fundamental. In addition, it is increasingly accepted that structural heterogeneity exists within these proteins, between proteins from different species, as well as between distinct gene products within a species and between individual complexes. In addition to studying the structures of individual membrane proteins, AFM has matured to be a powerful technique to visualise the organisation of different membrane-proteins in the native environment, enabling visualisation of the macromolecular structures in biological membranes and the

dynamics of adaptation to different conditions (Scheuring *et al.*, 2005b; Scheuring *et al.*, 2007). AFM imaging of photosynthetic membranes from various purple bacteria have shown a variety of different organisational patterns of the photosynthetic apparatus, ranging from highly ordered to less ordered arrangements of proteins (Liu and Scheuring, 2013; Liu, 2016).

The simplest purple bacterial photosynthetic membrane is that of *Blc. viridis* (Scheuring *et al.*, 2003a; Qian *et al.*, 2018), which contains simplified photosynthetic units lacking LH2 complexes. Small chromatophores were isolated from *Blc. viridis* and analysed using AFM (Scheuring *et al.,* 2003a), revealing a highly organised architecture composed of hexagonally dispersed single RCs, each surrounded by a closed ellipsoid of LH1 subunits (Fig. 1.11A), similar to the cryo-EM structure (Qian *et al.*, 2018). After removing the 4Hcyt subunit from the RC, AFM images revealed that the underlying RC-L and -M subunits adopt an asymmetric topography, whereby orientation of the long-axis of LH1 coincides with this, representing an important constraint for energy transfer (Scheuring *et al.*, 2005b). When the entire RC is removed, the LH1 units adopt a closed circular structure of ~100 Å diameter. This change reflects the flexibility of the LH1 heterotrimer assembly and the strong and specific interactions between the RC and LH1 components. This flexible motion could promote a 'breathing' motion to facilitate quine/quinol exchange, similar to that proposed for the LH1 of *Thc. tepidum* (Niwa *et al.*, 2014b).

The presence of LH2 complexes leads to a slightly more complex photosynthetic unit (PSU) arrangement; nevertheless, AFM images of the photosynthetic membrane of wild-type *Rba. sphaeroides* revealed a relatively ordered, interconnected network of

LH2 and dimeric RC-LH1-PufX core complexes, coexisting with ordered LH2-only domains (Fig. 1.11B). The RC-LH1-PufX dimers form linear arrays, composed of pairs of elliptical structures with a protruding protein in the centre (Fig. 1.11B), interconnected with rows of peripheral antenna LH2 complexes (Bahatyrova, Frese, Siebert, *et al.*, 2004). This physical continuity between the complexes ensures a highly efficient transfer of excitation energy from the peripheral LH2 to the LH1 complexes, and onto an active RC (Bahatyrova *et al.*, 2004; Scheuring *et al.*, 2005a). The LH1 complexes are positioned to serve as a hub for the collection of excitons from LH2; the excitons can migrate along a series of dimers until they reach an open RC (Bahatyrova, Frese, Siebert, *et al.*, 2004). LH2 was found to preferentially hexagonally pack within convex vesicular regions of the membrane (Scheuring *et al.*, 2014). Cyt $bc_1$ was postulated to localise in disordered areas adjacent to RC-LH1 complexes; cyt $bc_1$ is outnumbered by RC-LH1 by a 3:1 ratio, placing them out of direct contact with the core complexes (Michaël L. Cartron *et al.*, 2014; Scheuring *et al.*, 2014). Mutants of *Rba. sphaeroides* lacking PufX had a completely reorganised ICM with ordered arrays of monomeric RC-LH1 complexes from which LH2 is largely excluded and segregated to the curved membrane domains (Frese *et al.*, 2004). The interconnection of RC-LH1-PufX arrays interspersed with rows of LH2 complexes was also prevented in the mutant, suggesting that PufX plays a long-range organisational role within the membrane (Frese *et al.*, 2004).

Despite the similarity in the structures of the RC-LH1-PufX complex in *Rba. blasticus* (Scheuring *et al.*, 2005a) and *Rba. sphaeroides* (Jungas *et al.*, 1999; Qian *et al.*, 2008), AFM images revealed that the *Rba. blasticuus* RC-LH1-PufX complexes did not form rows that were seen in *Rba. sphaeroides* (Bahatyrova, Frese, Siebert, *et al.*,

2004). Instead individual S-shaped dimeric core complexes are interspersed with nonameric LH2 rings (Fig. 1.7D) (Scheuring *et al.*, 2005a).

Other LH2 containing species displayed much less regular arrangements of their PSUs. *Rsp. photometricum* ICMs, consisting of stacked, flattened thylakoid-like discs, contain a mixed, unordered arrangement of monomeric RC-LH1 complexes and circular nonameric LH2 rings (Fig. 1.11C) (Scheuring *et al.*, 2004a; Scheuring *et al.*, 2004b), and inter-complex clustering was visualised (Scheuring *et al.*, 2004b; Scheuring and Sturgis, 2005; Liu *et al.*, 2009). The membranes are heterogeneously organised with RC-LH1-rich domains separate from hexagonally packed, almost crystalline LH2 domains. Some of the core complexes were completely surrounded by 7 LH2 complexes, whereas others made multiple contacts with other core complexes, increasing the probability that excitons will find an open RC, enhancing rapid energy trapping as is seen in the more organised *Rba. sphaeroides* membranes (Bahatyrova, Frese, Siebert, *et al.*, 2004). This organisation provides efficient movement of excitons towards the RC whilst opening the ring of LH2 complexes to ensure all LH2 are in contact with one another. A heterogenous variability in ring sizes of LH2 was also observed including octamers, nonamers and decamers, representing a natural variability in ring sizes, suggesting a possible strategy for broadening absorption to maximise the collection of near-IR radiation, and optimisation of the packaging of photosynthetic components within the membrane (Scheuring *et al.*, 2004b). Although cyt $bc_1$ was demonstrated to be in the membrane preparations, it was not identified in AFM images (Scheuring *et al.*, 2004a).

Similarly, the ICMs of *Phs. molischianum* also consist of thylakoid-like structures giving rise to flat membrane sheets. The LH2 and core complexes are also arranged similarly to that in *Rsp. photometricum*; LH complexes are segregated into two structurally different types of domains: one consists of a mixture of core complexes and a small amount of octameric LH2 complexes, and the other consists of paracrystalline, hexagonally packed octameric LH2 rings (Fig. 1.7B) (Gonçalves *et al.*, 2005). The crystal structure of the LH2 complex from *Phs. molischianum* (Koepke *et al.*, 1996) enabled the exact pigment distances between LH2 complexes to be deduced (Hu *et al.*, 2002), intercomplex distances between central $Mg^{2+}$ atoms are ~16.3-28.3 Å, enabling efficient energy transfer.

The membranes of *Rps. palustris* consist of a complex ICM structure made of infoldings of the cytoplasmic membrane forming regular bundles of stacked and flattened thylakoid-like membrane sacs. AFM images of *Rps. palustris* membranes were obtained under differing light conditions, reflecting the versatility of photosynthetic apparatus in chromatic adaptation (Fig. 1.7C) (Scheuring *et al.*, 2006a). Under low light, mixed domains were commonly observed, along with paracrystalline domains of peripheral LH2 complexes, as is seen for other purple bacteria containing lamellar ICM structures. The mixed domains are likely to arise from the proximal layers within the lamellar ICM folds, whereas the LH2-only regions arise from distal layers formed subsequently; this is supported by the assembly sequence of complexes in developing ICMs (Koblízek *et al.*, 2005). Under high light, regions of crystalline RC-LH1 core complexes were observed, with a few LH2 complexes. This arrangement of randomly ordered RCs would be expected to facilitate efficient energy trapping under high photon fluxes. Chromatic adaptation also resulted in the

modification of LH2 ring sizes and absorption spectra (Scheuring *et al.*, 2006a). AFM images also confirmed the structures of the RC-LH1 complex, consisting of LH1 rings composed of 15 heterodimers interrupted by a gap, presumed to the location of protein W (Scheuring *et al.*, 2006a).

### *1.3.1 Common features of the photosynthetic membranes*

Although the organisations of photosynthetic membranes in differing species vary, there are a number of recurring features. All the species contain membranes densely clustered with photosynthetic complexes, ensuring efficient excitation energy capture and transfer between antenna, and ultimately to the RC for charge separation. In addition, the organisation of photosynthetic apparatus is never entirely random; clustering of RC-LH1 and formation of LH2 domains is often seen. Although the locations of cyt $bc_1$ and ATPase in most species remain enigmatic, the location of *Rba. sphaeroides* cyt $bc_1$ has been proposed (Michaël L. Cartron *et al.*, 2014; Scheuring *et al.*, 2014), and AFM on intact chromatophores from the same organism revealed a high protrusion from the membrane surface, speculated to be ATPase (Kumar *et al.*, 2016).

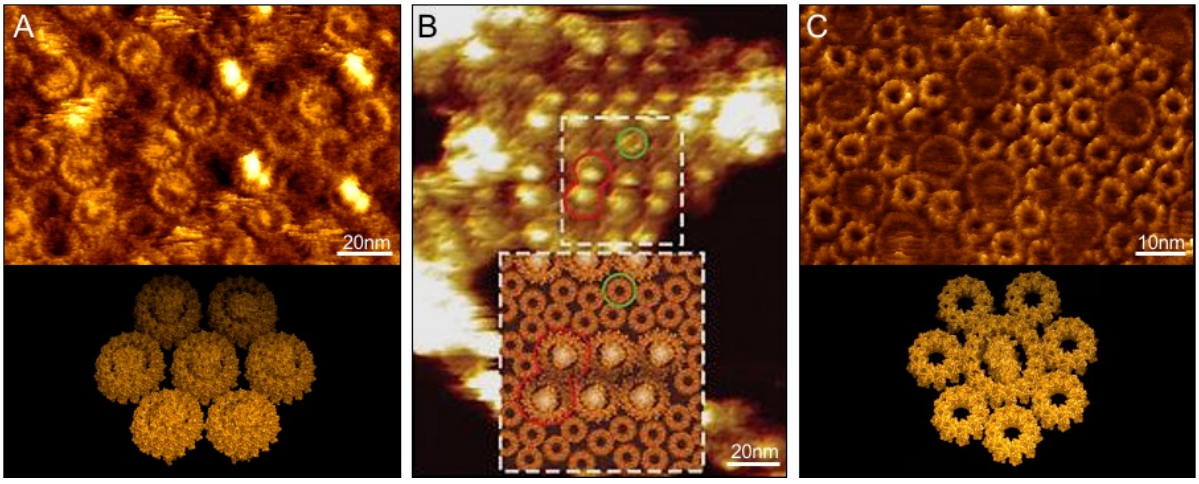


**Figure 1.11. Molecular-resolution AFM topographs of purple photosynthetic apparatus. A.** Protein organisation in the flat ICM of *Blc. viridis* (Scheuring *et al.*, 2003b). **B.** Protein organisation in the vesicular ICMs of *Rba. sphaeroides* (Scheuring *et al.*, 2003a). **C.** Protein organisation in the stacked ICMs of *Rsp. photometricum* (Scheuring *et al.*, 2004a).

### *1.3.2 Functional importance of photosynthetic membrane organisation*

The architectural variability of the photosynthetic membranes permits the systems to work efficiently in their native environments under various conditions. It is difficult to simultaneously satisfy the paradox of the organisation of the photosynthetic apparatus; these include firstly, the expectation that the LH system should completely surround the RC for maximum efficiency and to minimise the distances for energy to travel between complexes. Next, the core complexes should be connected in order to avoid energy loss from closed RCs by allowing energy transfer between core complexes (Bahatyrova *et al.*, 2004; Scheuring *et al.*, 2005a). And thirdly, the cyt $bc_1$ complex is expected to be in close proximity to the RC to close the electron circuit by quinol diffusion.

The first problem lies with the location of cyt $bc_1$ and the release of quinone/quinol. For *Rba. sphaeroides* and *Rps. palustris* whereby the RC-LH1 complexes contain PufX and Protein W, respectively, the diffusion of quinone is fairly simple due to the gap produced by these proteins creating a possible pathway (Roszak *et al.*, 2003; Bahatyrova *et al.*, 2004; Qian *et al.*, 2005). In other species, however, the ring of LH1 was observed to be closed, therefore quinone transfer across the LH1 wall would depend on the dynamics of the process by which the integrity of the ring is breached. Circular and elliptical closed forms of LH1 were observed in AFM images of *Rsp. rubrum* 2D crystals, suggesting the structural flexibility of LH1 that facilitates the transfer of quinone through molecular motions (Jamieson *et al.*, 2002; Siebert *et al.*, 2004). The missing 17$^{th}$ gamma-subunit of *Blc. viridis* RC-LH1 (Qian *et al.*, 2018) also provides a path for this diffusion, in this case through the absence of an additional subunit, rather than the presence of one.

Once the quinone is released from the RC, another problem arises in its rapid diffusion through a crowded membrane to cyt $bc_1$ complexes. A lipid environment was found to be created around the core complexes of *Rsp. photometricum*, due to a size mismatch of the LH2 and core complexes, providing a potential long-range pathway for quinones to travel (Liu *et al.*, 2009). However, it was revealed that static paracrystalline LH2 complexes in the photosynthetic membrane, with significantly restricted diffusion, provided no space for quinones to diffuse between them (Scheuring *et al.*, 2006a).

## 1.4 Energy Transfer

### *1.4.1 Transfer of excitation energy*

The knowledge of the structures and spatial arrangement of photosynthetic complexes and association with cofactors provides a basis for understanding energy transfer performed by the photosynthetic system. Energy is collected by antenna systems via the funnel concept; the pigments of the most peripheral antenna complexes, e.g. LH2, absorb shorter wavelengths than the pigments within RC. Photons of shorter wavelengths are higher in energy than longer wavelength photons and thus, ensure 'downhill' energy flow: LH2 → LH1 → RC. A certain amount of energy is lost as heat during each transfer, providing some irreversibility and resulting in the funnelling of excitation energy into the RC. This funnel model is enabled by the spatial and energetic organisation of the antenna pigments. This concept also applies within LH complexes in the energy transfer from carotenoids to BChls, however some energy transfers occur 'uphill' e.g. between LH1 and the RC in *Rba. sphaeroides* and *Blc. viridis* (Sumi, 2002).

Higher energy photons are first absorbed by carotenoids in LH2, or LH1 in species lacking LH2; carotenoids absorb short wavelengths, 400-550 nm, of light and subsequently transfer the energy to both $Q_x$ and $Q_y$ states of B800 in LH2. Upon absorption of light, carotenoids are promoted from the ground state, $S_0$, to the $S_2$ state (transition to $S_1$ state is symmetry forbidden), the molecule then quickly relaxes to the $S_1$ state in less than 300 fs. The lifetime of the $S_1$ state varies from 300 ps to ~1 ps, depending on the conjugation length of the carotenoid (Sundström, 2004). Once the excitation energy is passed from $S_1$, or sometimes $S_2$ (Polívka and Frank, 2010), to B800, it is quickly transferred to B850 in ~1 ps by Förster resonance energy transfer (FRET). The excitation energy is subsequently delocalised over the ring of tightly coupled B850 pigments, i.e. it hops rapidly around the ring, within 100 fs (van Oijen *et*

*al.*, 1999). The excited state is thus equally probable to transfer from any site within the ring, implying that no fixed arrangement of LH2 and LH1 complexes is required for efficient transfer (Cogdell *et al.*, 1999). If the energy does not reach another LH complex within 1 ns it will decay. Energy from B850 is subsequently transferred to the B875 pigments in ~3 ps and, again, it is delocalised over the tightly coupled B875 pigments. The relatively large distance between B875 and the RC makes the transfer between these pigments the slowest step, occurring in ~35-50 ps, which is essentially irreversible (Pullerits and Sundström, 1996; Sundstrom and Grondelle, 1999).

### *1.4.2 Charge separation in the RC*

The transfer of excitation energy to the RC induces the separation and stabilisation of charge across the photosynthetic membrane. A BChl dimer, known as the special pair (SP), acts as the primary electron donor and is excited to SP*; this excited state then transfers an electron to a BPhe molecule via a transient radical pair state, BPhe then subsequently transfers an electron to $Q_A$. A *c*-type cytochrome, or the 4HCyt subunit in certain species, reduces oxidised $SP^+$, whilst $Q_A^-$ transfers an electron to $Q_B$. At this point, an electron has been transferred across the membrane and the primary reactants are ready for the next electron transfer.

### *1.4.3 Electron transfer in cytochrome $c_2$*

In species that do not contain the 4Hcyt subunit, cyt $c_2$ re-reduces $SP^+$. *C*-type cytochromes contain covalently attached haem groups; the haem group is located in the crevice of cyt $c_2$, with one edge exposed to the outside of the protein (Axelrod *et al.*, 2002). This exposed edge is surrounded by a group of positively charged lysine

residues which interact with the negative charges of the reaction partner forming a tightly bound complex. Cyt $c_2$ thus binds the RC at a specific site with the haem optimally positioned for electron transfer (Fig. 1.9) (Axelrod *et al.,*, 2009). The oxidation kinetics of cyt $c_2$ are multiphasic; when bound to the RC the oxidation occurs within ~1 μs, however when the reduced cyt $c_2$ is unbound prior to electron transfer the phase is slower (Mathis *et al.*, 1994). The cytochrome needs to diffuse to the RC and dock in place ready for oxidation, this results in the slow phase.

In species that contain the 4Hcyt subunit, the cytochrome is permanently positioned for optimal electron transfer. After flash excitation, the haem located closest to P is oxidised within a few hundred ns; electron transfer then occurs down the chain of haems within 4Hcyt re-reducing the first haem in μs. The 4Hcyt is then reduced by cyt $c_2$ (Menin *et al.*, 1998; Myllykallio *et al.*, 1998). At this stage, protons have been taken up from the cytoplasmic side of the membrane and cyt $c_2$ has been oxidised in the periplasmic side.

### *1.4.3.1 Modified Q Cycle*

Cyt $bc_1$, located in the ICM (Xia *et al.*, 1997; Zhang *et al.*, 1998; Berry *et al.*, 2000; Crofts, 2004), mediates the completion of cyclic electron transfer in the modified Q cycle (Fig. 1.3) (Crofts, 2004). UQ binds the $Q_o$ site (see **section 1.2.3** for details on the structure of cyt $bc_1$) of cyt *b*. UQ then transfers the electron to the Rieske subunit, leaving ubisemiquinone in the $Q_o$ site and a proton is released to the periplasmic side of the membrane. Next, ubisemiquinone transfers a second electron to the lower redox potential haem and subsequently to the higher redox haem; a second proton is also released into the periplasmic side of the membrane. The Rieske subunit then

undergoes a large amplitude motion, moving from the cyt *b* to the cyt $c_1$ subunit, displacing the Fe-S centre. UQ next binds to the $Q_i$ site and is reduced to the semiquinone by the higher redox haem of cyt *b*. Oxidised UQ is then dissociated from the $Q_o$ site and the Rieske Fe-S centre reduces cyt $c_1$, which in turn reduces cyt $c_2$. The Rieske subunit then moves back to its original position. At this stage, one quinol has been oxidised, an electron has traversed the full electron transport chain, and another has reduced the oxidised UQ to the semiquinone state for the following turnover. A new UQ binds to the $Q_o$ site and transfers its electron to the Rieske subunit, which then subsequently passes it to cyt $c_1$ and then cyt $c_2$ along one branch and then the two haem groups from cyt *b* on the other branch. The electron on the higher redox potential haem then reduces semiquinone to quinol, taking two protons from the cytoplasmic side. Finally, the reduced quinol dissociates from the complex (Crofts, 2005).

Two turnovers of cyt $bc_1$ result in the transfer of two electrons to cyt $c_2$, two UQ oxidised to quinone form and one UQ reduced to hydroquinone quinol form and four protons transferred from the cytoplasmic to the periplasmic side of the membrane. Overall, this electron flow across the RC gives rise to pmf across the membrane which is subsequently utilised by ATPase.

### *1.4.4 Proton translocation and ATP synthase*

ATPase exploits the proton motive force created by the photosynthetic electron transfer chain to produce ATP from ADP and $SP_i$. Specifically, the $F_0$ portion of the enzyme uses the proton motive force to generate a torque, which is then used by the

$F_1$ portion in the synthesis of ATP (Noji *et al.*, 1997; Wada *et al.*, 1999; Pänke *et al.*, 2000; Kinosita, Adachi and Itoh, 2004; Junge, Sielaff and Engelbrecht, 2009) (Fig. 1.8). ATPase operates via the binding change mechanism (Boyer, 1993). The major energy-requiring step is the simultaneous binding of substrates to, and release of products from, the ATP catalytic sites (Boyer *et al.*, 1973; Kayalar *et al.*, 1977). The rotation of subunits extending through the ATPase complex couples these affinity changes to proton transport. Three ATP catalytic sites located in the β-subunit of the complex sequentially alternate between open, loose and tight binding sites. As the γ subunit rotates, it acts as a camshaft alternatively distorting the β-subunit, leading to the cycling between the three binding sites (Hunter *et al.*, 2008). Rotation of the γ-subunit in the centre of the $F_1$ portion deforms the surrounding catalytic subunits, giving rise to the three binding sites (Cross, 2000). Rotation of the c subunit relative to the α subunit, however, is required for completion of the proton pathway (Vik and Antonio, 1994; Duncan *et al.*, 1995; Hatch *et al.*, 1995; Junge *et al.*, 1996). The energy from this conformational change is transduced into the ATP phosphoanhydride bond. Entrance and exit channels for protons are contained within the $F_0$ subunit, but there is no connection between the two channels (Junge *et al.*, 1997). An essential glutamic acid residue in a transmembrane helices within the entrance channel is protonated by residing protons; this conformational change ratchets the c subunit with respect to the α subunit (Rastogi and Girvin, 1999; Junge *et al.*, 2009; Pogoryelov *et al.*, 2009). The c ring rotates, in turn each σ subunit picks up a proton and releases it through the exit channel. Therefore, during one complete cycle, a proton is transported through each c subunit, and each of the three β-subunits goes through open, loose and tight conformations, each producing and releasing a molecule of ATP.

## 1.5 Calvin-Benson-Bassham Cycle

The final stage in purple bacterial photosynthesis is the use of the energy generated in the steps discussed to drive the conversion of inorganic carbon into organic compounds. Purple photosynthetic bacteria contain the most diverse metabolism of carbon compounds. Both purple non-sulfur and sulfur bacteria assimilate $CO_2$ into 3-phosphoglycerate (3-PG) and reduce $CO_2$ mainly via the Calvin-Benson-Bassham (CBB) cycle (Fig. 1.12) (Benson, 2002; Tabita, 2004). The CBB cycle is a complex series of reactions, which can be broken down into three phases: carboxylation, reduction and regeneration (Heldt and Piechulla, 2011).

Carboxylation is the first stage of the cycle and utilises ribulose-biphosphate carboxylase/oxygenase (RuBisCO) to incorporate carbon from $CO_2$ into an organic molecule. Ribulose-1,5-bisphosphate (RuBP) is attached to a molecule of $CO_2$ to form a six-carbon compound, this spontaneously breaks down into two molecules of 3-phosphoglyceric acid (3-PGA). The next stage of the cycle is reduction (Heldt and Piechulla, 2011), 3-PGA molecules are converted to 3-PG by phosphorylation. First ATP donates a phosphate group to each of the two 3-PGA molecules producing 1,3-bisphosphoglycerate. This is then reduced by NADPH releasing a phosphate group and producing 3-PG. The final stage is regeneration, in which some of the 3-PG molecules are used to make glucose, while others are recycled to regenerate the RuBP acceptor.

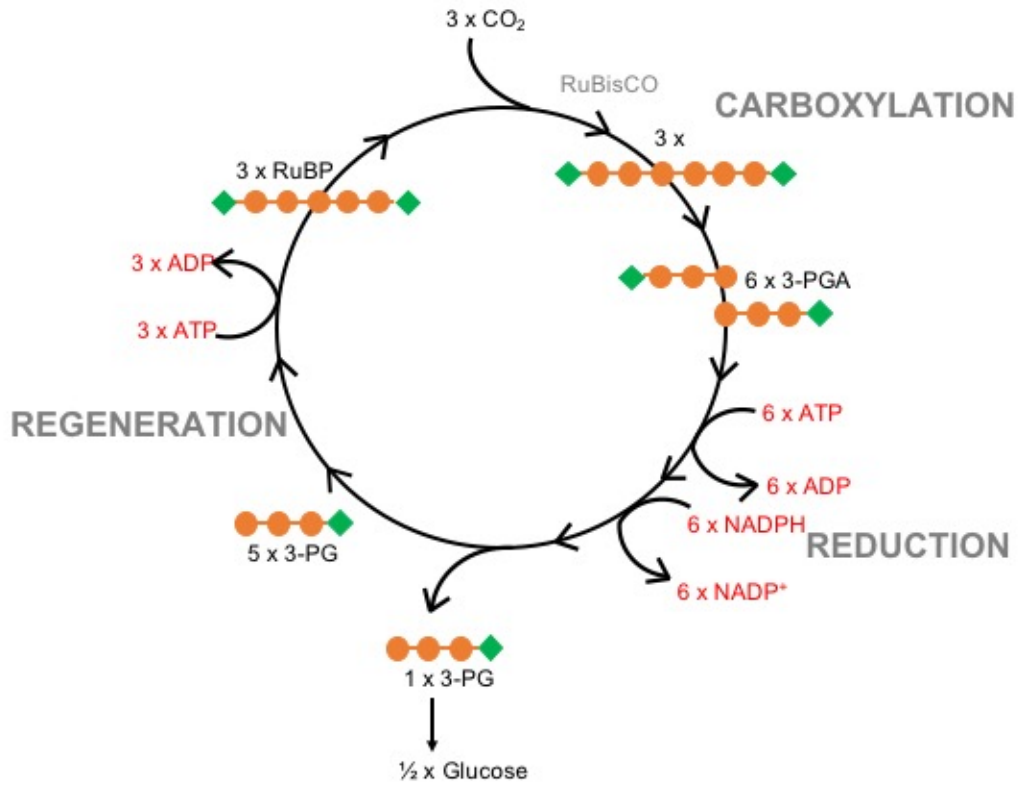


**Figure 1.12. Schematic of the Calvin-Benson-Bassham (CBB) Cycle.** The CBB cycle occurs in three main stages, RuBisCO is first used in carboxylation to produce 6 molecules of 3-PGA from the incorporation of inorganic carbon (CO2) and RuBP. ATP and NADPH are then utilized to phosphorylate and reduce 3-PGA to produce 3-PG in the reduction stage. Finally, in the regeneration stage, 5 3-PG molecules are recycled to regenerate RuBP and 1 molecule of 3-PG is used to make glucose; two cycles of the cycle are required to make a molecule of glucose. Orange circle, carbon; green diamond, phosphate.

AAPs are obligate photoheterotrophs, no autotrophic carbon assimilation pathways have been reported (Yurkov and Beatty, 1998; Fuchs *et al.*, 2007; Swingley *et al.*, 2007). AAPs and some anaerobic anoxygenic phototrophs have been reported to

grow heterotrophically on acetate using the ethylmalonyl-CoA pathway and the oxidative glyoxylate cycle (Tang *et al.,* 2011; De Meur *et al.*, 2018).

## 1.6 Thesis Aims

This thesis aims to further our understanding of the organisation, interactions and dynamics of photosynthetic apparatus of purple photosynthetic bacteria using AFM and AFM-based SMFS. Specifically, the main aims of this thesis are as follows:

- To elucidate the native organisation of the photosynthetic apparatus of *Blc. viridis*;
- Characterise at single-molecule level the mechanical unfolding process of the core complex of *Blc. viridis*;
- Use AFM and TEM to study the cross-species effects of PufX from *Rba. veldkampii* on the organisation and architecture of the RC-LH1 complex and ICM of *Rba. sphaeroides;*
- Engineer the photosynthetic membrane *Blc. viridis* by overexpressing LH1 and expressing LH2 to analyse the effects on the organisation and function of the membrane.

# CHAPTER II
# Materials and Methods

# 2 Materials and Methods

## 2.1 Bacterial Strains and Maintenance

### *2.1.1* Blastochloris viridis *growth conditions*

*Blastochloris viridis* (*Blc. viridis*) was provided by Dr Luning Liu at the University of Liverpool. *B. viridis* cells were initially grown on solid Medium 27 (M27) (DMSZ) 1.5% (w/v) agar plates at 30°C under normal light in anaerobic conditions. Single colonies formed after around 1 week, these were then used to inoculate liquid Medium 27 at 30°C under normal light, under anaerobic conditions in screw cap bottles. All sub-culturing was carried out in an anaerobic chamber to maintain anaerobic conditions. For long-term storage, a 50ml culture of *Blc. viridis* in exponential growth phase was pelleted by centrifugation at 10,000g and re-suspended in 0.8ml M27; this was then thoroughly mixed with 0.8ml filter-sterilised 50% (w/v) glycerol in water, flash-frozen in liquid nitrogen and stored at -80°C. The strains were revived using a pipette tip to put a small amount of frozen culture into an Eppendorf tube and then used to inoculate 5ml M27.

### *2.1.2* Rhodobacter sphaeroides *growth conditions*

*Rhodobacter sphaeroides* 158 (*Rba. sphaeroides*) dry culture was purchased from DMSZ. Cells were rehydrated with 0.5ml Medium $22^+$ (see **Appendix A**) for 30 minutes in room temperature and normal light conditions, 5ml of $M22^+$ was then added to the rehydrated cells and grown at 30°C under normal light, under anaerobic conditions in screw cap bottles. Rehydrated cells were also grown on $M22^+$ solid 1.5% (w/v) agar plates in anaerobic conditions; single colonies grew after around 1 week. All sub-culturing was carried out in an anaerobic chamber to maintain anaerobic

conditions. For long-term storage, a 50ml culture of *Rba. sphaeroides* in exponential growth phase was pelleted by centrifugation at 10,000g and re-suspended in 0.8ml $M22^+$; this was then thoroughly mixed with 0.8ml filter-sterilised 50% (w/v) glycerol in water, flash-frozen in liquid nitrogen and stored at -80°C. The strains were revived using a pipette tip to put a small amount of frozen culture into an Eppendorf tube and then used to inoculate 5ml $M22^+$.

*Rba. sphaeroides* ΔpufX and ΔLH2ΔpufX (provided by Dr Canniffe, University of Liverpool) were grown in identical medium to the above strains, however they were grown under aerobic conditions in the dark.

### *2.1.3* Escherichia coli *growth*

*E. coli* strains TOP 10, DH5α and BL21 DE3 were obtained from lab stocks. These were grown at 37 °C in liquid Lysogeny Broth (LB) medium with shaking at 220rpm, unless stated otherwise. Cells were also grown on solid LB 1.5% (w/v) agar plates for longer term storage. Antibiotics were used for selective growth in both liquid and solid LB medium where necessary. For long-term storage, 1 ml of an overnight liquid LB cell culture was thoroughly mixed with 0.5 ml filter-sterilised 50% (v/v) glycerol in water, flash-frozen in liquid nitrogen, and stored at -80°C. Strains were revived by streaking solid LB plates with appropriate antibiotics. Mu-free *E. coli* strain MFD*pir* cells require 0.3mM DAP to grow.

### *2.1.4 Optical density of liquid cultures*

The OD of *E. coli* liquid cultures were measured at 600nm against an LB blank, *Blc. viridis* liquid cultures were measured at 680nm against a $M22^+$ blank and *Rba.*

*sphaeroides* liquid cultures were measured at 680nm, also against a $M22^+$ blank. In all three cases, 1ml of culture was pipetted into a Sarstedt polystyrene cuvette with a 0.394 " path length, 45 mm height and 3 ml capacity. The OD was then measured in a UV-1600PC Spectrophotometer.

## 2.2 Molecular Biology Techniques

### *2.2.1 Plasmids*

Plasmids generated or acquired for this study were stored in Mili-Q water at -20°C.

### *2.2.2 DNA transformation of cells*

#### *2.2.2.1 Transformation of chemically competent cells*

Chemically competent DH5α, S17 and MFD*pir E. coli* (Ferrieres *et al.*, 2010) cells were thawed on ice for 10 minutes and mixed with ~1µg plasmid DNA or 10µl ligation mix and incubated on ice for 1 hour. The cells were subjected to heat shock at 42°C for 30 seconds and incubated for 2 minutes on ice. Cells were recovered by the addition of 1 ml of LB medium and incubated at 37°C for 45 minutes. Cells were then centrifuged at 6000g and the pellet resuspended in ~100µl LB, ~50µl of the mix was spread onto LB 1.5% (w/v) agar plates supplemented with appropriate antibiotics and incubated overnight at 37°C. For MFD cells, 0.3mM DAP was required in the medium for growth.

#### *2.2.2.2 Transformation of electro-competent cells*

Electro-competent DH5α E. coli cells were thawed on ice for 10 minutes and mixed with ~1µg plasmid DNA or 10µl ligation mix and transferred to a chilled electroporation cuvette on ice. Cells were electroporated at 200ohms, 2.5µFD and 2.5Kv. 500µl of LB was then added to recover the cells. This was transferred to an Ependorf tube and

incubated for 1 hour at 37°C with shaking at 220rpm. Cells were then centrifuged at 6000g and the pellet resuspended in ~100µl LB, ~50µl of the mix was spread onto LB 1.5% (w/v) agar plates supplemented with appropriate antibiotics and incubated overnight at 37°C.

### *2.2.3 DNA conjugation of cells*

Plasmids were transformed into S17 *E. coli* and MFD*pir*. 25ml of *Blc. viridis* cells were pelleted by 4000rpm for 5 minutes at room temperature, and resuspended in LB broth, slowly. 25µl of transformed *E. coli* cells were added to this and lightly shaken. 3 50µl spots of this mixture was spotted onto $LB^-$ plates and left to dry for 20 minutes. This was incubated at 37°C overnight. Each spot was then spread on antibiotic resistance plates of M27 medium and placed in an anaerobic box. Once anaerobic, the box was placed under light and 30°C for growth. Once grown, the colonies were transferred to liquid cultures of M27 with antibiotic.

### *2.2.4 Extraction and purification of genomic DNA*

A 1ml culture was pelleted and resuspended in 200µl of Mili-Q water, 200µl of phenol-chloroform was added to the mixture. This was then spun down at full-speed for 5 minutes and 150µl of the aqueous phase was carefully removed. $1/10^{th}$ volume of 3M sodium acetate, pH 5.2 and 2 times volume of ethanol was added and the mixture was incubated at -20°C for 1 hour. This was then immediately spun-down at full-speed for 5 minutes, the supernatant was removed and the pellet was left to dry for 5 minutes.

*2.2.4.1 Plasmid purification from E. coli cells*

*E. coli* cells were harvested from a 10ml overnight liquid culture by centrifugation at 6000g. Plasmids were purified using a GeneJET Plasmid Miniprep Kit (ThermoFisher Scientific), according to the manufacturer's instructions.

*2.2.4.2 DNA fragment purification*

DNA fragments from PCR or restriction digestions were purified using magnetic beads. Magnetic beads were added to the DNA fragments in a 0.2ml PCR tube in a 1:1 ratio, mixed and incubated at room temperature for ~15 minutes. The PCR tube was then placed in the magnetic holder, beads were then washed twice with 80% ethanol and left to dry for ~3 minutes. The beads were then resuspended in ~10µl of MQ-water and incubated at room temperature for ~3minutes. The PCR tube was then placed in the magnetic holder and DNA removed.

*2.2.4.3 Estimation of DNA concentration*

The concentration of DNA was determined using a Nanodrop at wavelengths 260nm and 280nm.

*2.2.5 DNA manipulation*

*2.2.5.1 Agarose gel electrophoresis*

DNA fragments were separated by their size by agarose gel electrophoresis using 1% (w/v) agarose dissolved in 10X Tris-acetate-EDTA (TAE) buffer with 1 µg $ml^{-1}$ ethidium bromide for visualisation of DNA under UV illumination using a gel imaging system. DNA samples were mixed with 6x Purple DNA Loading Buffer (Bioline) to monitor the migration of DNA. Samples were ran alongside 3µl of HyperLadder 1kb (Bioline) which was used as a molecular weight marker. Gels were run in TAE buffer at 120V.

*2.2.5.1.1 Agarose gel Extraction*

ThermoScientific gel extraction kit was used according to the manufacturer's instructions.

*2.2.5.2 Polymerase chain reaction*

*2.2.5.2.1 DNA polymerases*

Q5 DNA polymerase was used for PCR to isolate gene fragments using primers listed in the text. A typical 50µl reaction mixture contained: 10µl 5 x Q5 reaction buffer, 1µl 10mM dNTPs, 0.8µl 50% dimethyl sulfoxide (DMSO), 0.8µl 10µM forward primer, 0.8µl 10µM reverse primer, 0.2µl plasmid DNA template and 0.5µl Q5 DNA polymerase made up to 50µl with Mili-Q water. DMSO and Q5 DNA polymerase were used due to the high GC content of the DNA.

*2.2.5.2.2 Conditions for standard PCR*

The standard PCR program consisted of the initial denaturation step at 98°C for 3 minutes, and 35 subsequent cycles of the denaturation stage at 98°C for 20 seconds, the primer annealing stage at 60-72°C for 20 seconds and a primer extension stage at 72°C for 30 seconds, with a final extension at 72°C for 2 minutes. The PCR program was varied when the standard procedure did not yield optimal results.

*2.2.5.2.3 Colony PCR*

A typical 50µl reaction mixture contained: 5µl BioMix Red, 3.2µl Mili-Q-water, 0.5µl 10µM forward primer, 0.5µl 10µM reverse primer, 0.8µl 50% DMSO and colony cells.

#### *2.2.5.3 Restriction endonuclease digestion*

High-Fidelity (HF) Restriction Endonucleases (New England BioLabs) were used to perform restriction digestions under conditions suggested by the manufacturer's instructions. Typically, the reaction mixtures were incubated for 1 hour at 37°C, and contained: 10 units of each HF restriction enzyme, 5µl appropriate NEBuffer, and 1µg DNA, made up to 50µl with Mili-Q-water.

#### *2.2.5.4 DNA ligation*

T4 DNA ligase (New England BioLabs) was used to ligate DNA fragments, according to manufacturer's instructions. The reaction mixture was incubated overnight at 16$^{o}$C.

#### *2.2.5.5 DNA sequencing*

DNA sequencing was performed by Eurofins.

### *2.2.6 Proteomic Analysis*

#### *2.2.6.1 SDS-PAGE*

Samples of purified photosynthetic membranes were treated with SDS sample buffer (0.06 M Tris-HCl pH 6.8, 10% glycerol, 2% SDS, 0.1% bromophenol blue, 1.5% dithiothreitol) at 100$^{o}$C for 15–20 min. Proteins were loaded onto a 15% denaturing SDS-PAGE gel and run at 120 V for 45 mins. The gels were stained with Coomassie Blue stain for 20 mins and destained for 1 hr.

## 2.3 Antibiotic Usage

The antibiotics used for the growth of each mutant strain can be seen in Table 2.1.

**Table 2.1 Antibiotics used in bacterial strains**

| Bacterial Strain | Antibiotic |
|---|---|
| *Rba. sphaeroides ΔpufX* | Kanamycin |
| *Rba. sphaeroides* $\Delta pufXR_s::pufXR_v$ | Kanamycin |
| *Blc. viridis* LH1-overexpressed | Kanamycin |
| *Blc. viridis* LH2 expression | Kanamycin |

## 2.4 Intracytoplasmic Membrane Isolation

### *2.4.1* Blc. viridis *ICM isolation*

*Blc. viridis* wild-type and mutant cultures were harvested by centrifugation at 10,000g, 4$^{o}$C for 10 minutes. The pellet was rinsed twice with 2mM Tris, 2mM EDTA pH 7.5 and resuspended in 20mM HEPES pH 8.0 to ~ 35% cells, a final concentration of 0.1% DNase and 1% protease inhibitor cocktail (PIC) was added to the resuspended cells. The cells were broken via one pass through a French Press at 15,000psi, -10$^{o}$C. Cell debris was pelleted via centrifugation at 10,000g, 4$^{o}$C for 10 minutes. The supernatant, containing the ICM, was pelleted by centrifugation at 36,900g for 16 minutes and resuspended in 20mM HEPES, pH 8. This was then loaded onto a five-step sucrose gradient (4 ml – 60% sucrose, 2 ml-35% sucrose, 2 ml-25% sucrose, 2 ml-15% sucrose, 1 ml-5% sucrose made with 20 mM HEPES pH 8.0 + 1% PIC and ~2 ml sample). This was ultracentrifuged at 120,000g (16.9,000rpm on rotor: Hitachi RPS40T-832), 4$^{o}$C for 3 hours. The ICM was collected from the appropriate green coloured fractions.

### *2.4.2* Rba. sphaeroides *ICM isolation*

*Rba. sphaeroides* wild-type and mutant cultures were harvested by centrifugation at 10,000g, 4°C for 10 minutes. The pellet was rinsed twice with 2 mM Tris, 2 mM EDTA pH 7.5 and resuspended in 20 mM HEPES pH 8.0 to ~ 35% cells, a final concentration of 0.1% DNase and 1% PIC was added to the resuspended cells. The cells were broken via one pass through a French Press at 15,000 psi, -10°C. Cell debris was pelleted via centrifugation at 10,000g, 4°C for 10 minutes. The supernatant, containing the ICM, was pelleted by centrifugation at 36,900g for 16 minutes and resuspended in 20 mM HEPES, pH 8. This was then loaded onto a five-step sucrose gradient (4 ml – 60% sucrose, 2 ml-35% sucrose, 2 ml-25% sucrose, 2 ml-15% sucrose, 1 ml-5% sucrose made with 20 mM HEPES pH 8.0 + 1% PIC and ~2 ml sample). This was ultracentrifuged at 120,000g (16.9,000 rpm on rotor: Hitachi RPS40T-832), 4°C for 3 hours. The ICM was collected from the appropriate coloured fractions.

## 2.5 ICM Fractionation

*Rba. sphaeroides* wild-type and mutant cultures were harvested by centrifugation at 10,000g, 4°C for 10 minutes. The pellet was rinsed twice with 2mM Tris, 2mM EDTA pH 7.5 and resuspended in 20mM HEPES pH 8.0 to ~ 35% cells, a final concentration of 0.1% DNase and 1% PIC was added to the resuspended cells. The cells were broken via three passes through a French Press at 15,000psi, -10°C. Cell debris was pelleted via centrifugation at 10,000g, 4°C for 10 minutes. The supernatant, containing the ICM, was ultracentrifuged at 125,000g for 90 minutes (AH-629 rotor), before being resuspended in 1 ml 20 mM HEPES, pH 8.0. The membrane was then solubilized in 3% n-Dodecyl β-D-maltoside (β-DDM) for 15 minutes at 4 °C in the dark. The solubilized membrane was then centrifuged at 21,000g for 30 minutes. The solubilized

membrane was then loaded onto a continuous sucrose gradient (10-25% w/v) with 0.1% β-DDM and ultracentrifuged at 36,000 rpm for 19 hours.

## 2.6 Atomic Force Microscopy

### *2.6.1 Substrates*

Mica was used as the substrate for the *Blc.viridis* and *Rba. sphaeroides* wild-type and mutant ICM AFM samples.

### *2.6.2 Sample Preparation*

A 1 in 200µl dilution of ICM was prepared in absorption buffer (10mM Tris-Hcl pH 7.2, 150mM KCl, 25mM MgCl2), 40µl of this was loaded onto the freshly cleaved highly ordered pyrolytic graphite (HOPG) or mica (or PLL-GD mica), covered and left to absorb for at least 1 hour at room temperature. The sample was then rinsed with 4 washes of 40µl imaging buffer (10mM Tris-Hcl pH 7.2, 150mM KCl), pipetting up and down each time thoroughly, ensuring no buffer touched the metal in which the mica is held on, before being imaged in 40µl imaging buffer.

### *2.6.3 Probe Stiffness Calibration*

A contact-based method was used to calibrate the probes in imaging buffer on a flat, empty area of substrate, prior to the AFM experiment. Deflection sensitivity was estimated from an average curve, the probe was then withdrawn >100nm from the surface for thermal tuning. The Lorentzian model was used to fit the data and estimate the spring constant of the probe.

### *2.6.4 AFM Imaging*

A Bruker Multimode 8.0 equipped with a 97 μm J-scanner and SNL or ScanAsystAir HR probes (spring constants 0.06 $N \cdot m^{-1}$ and 0.4 $N \cdot m^{-1}$, respectively), operated in PeakForce Quantitative Nanoscale Mechanical (PeakForce QNM) mode, ScanAsyst mode or contact mode, or JPK Nanowizard with USC-F0.3-K0.3 (Nanoworld, Windsor scientific UK; spring constant 0.3 $N \cdot m^{-1}$) probes in tapping mode were used to image the samples. Forces of 70-120pN were used in imaging to avoid sample damage and scanning-induced artefacts. Slow speeds of 3-5Hz were used for overview scans of areas of interest. Patches of interest were then scanned by incrementally decreasing the scan size and increasing the scan speed whilst optimizing other parameters to maintain high resolution images of the area of interest. For high-speed images speeds of ~20-30Hz were used.

#### *2.6.4.1 Image Processing and Analysis*

Image analysis was carried out using Gwyiddion 2.4.7. AFM images were flattened by plane fitting and any noise was removed using median filters and the look-up table colours were adjusted manually to obtain optimal contrast. Subsequent processing and analysis was then carried out depending on individual image and requirements. Diameters and heights were measured from the respective height profile graphs.

## 2.7 Single Molecule Force Spectroscopy

### *2.7.1 Force Measurements*

A Bruker Multimode 8.0 equipped with a 97 μm J-scanner and SNL tip, or ScanAsystFluid+ tip (spring constants (spring constants 0.06 $N \cdot m^{-1}$ and 0.7 $N \cdot m^{-1}$, respectively), operated in PeakForce Quantitative Nanoscale Mechanical (PeakForce

QNM) mode, ScanAsyst mode or contact mode was used for force measurements. Force measurements were performed by repeating tip approach and retraction cycles with a z-ramp size of 200 nm, and at a tip velocity of 200 nm·s$^{-1}$. The tip adhered to the protein by a controlled loading force of ≤1 nN for ≤1 s. Many of the force curves had to be rejected because the force rupture events were incompatible with a polymer-unfolding model. Finally, 100 curves entered the final analysis.

### *2.7.2 Data Analysis*

Data analysis of force measurements was carried out by SPIP™ software program (Image Metrology).

### *2.7.3 Worm-Like Chain Fitting*

The unfolding events in the force-distance curves were fitted using the worm-like chain (WLC) model, following

$$\mathrm{F}(\chi) = \left({}^{\kappa_\mathrm{B}\mathrm{T}}/_{b}\right) \cdot \left(0.25 \cdot \sqrt{(1 - {}^{\chi}/_{L}} - 0.25 + {}^{\chi}/_{L}\right)$$

where $\mathrm{F}(\chi)$ is the force at distance $\chi$, $\kappa_\mathrm{B}$ is the Boltzmann constant, $b$ = 4Å is the persistence length (the approximate length of amino acid residues), $L$ the contour length of the unfolded polypeptide chain, and $\mathrm{T}$ is the temperature = 298 K.

## 2.8 Structure Representation

The RC-LH1 structure (PDB ID code: 6ET5) representation was generated using PyMOL.

## 2.9 Thin-Section Transmission Electron Microscopy

Purple bacterial cell cultures were pelleted by centrifugation (6000g, 10 minute) and processed for thin section using a Pelco BioWave Pro laboratory microwave system. The cells were fixed with 2.5% glutaraldehyde in 0.1 M sodium cacodylate buffer at pH 7.2 using two steps of 100W for 1 minute each (P1). After embedding in 4% agarose, samples were then stained with 2% osmium tetroxide and 3% Potassium Ferrocyanide using three steps of 100W for 20 seconds each (P2). The reduced osmium stain is then set using a solution of 1% Thiocarbohydrazide for 10 minutes. The second osmium stain is applied using P2 with 2% osmium tetroxide. The sample is made electron dense with 2% Uranyl Acetate incubated at 4$^{o}$C overnight. Dehydration is achieved with a series of increasing alcohol concentrations (30 to 100%),and embedded in medium resin. Thin sections of 70 nm were cut with a diamond knife and poststained with 3% lead citrate. Images were recorded using an FEI Tecnai G2 Spirit BioTWIN transmission electron microscope. This was carried out by Greg Dykes at the University of Liverpool.

## 2.10 Absorbance Spectra

The absorbance spectra of samples was measured by pipetting 1 ml of sample into a Sarstedt polystyrene cuvette with a 0.394 " path length, 45 mm height and 3 ml capacity. The spectra was then measured in a UV-1600PC Spectrophotometer at specific wavelengths.

### *2.10.1 $A_{LH1}/A_{RC}$ Ratio Calculation*

The $A_{LH1}/A_{RC}$ ratio was calculated by the following equation:

$$A_{LH1}/A_{RC}$$

where $A_{LH1}$ is absorbance of LH1 and $A_{RC}$ is the absorbance of RC, both taken from the absorption spectra.

## 2.11 Two Sample *t*-test assuming Unequal Variances

The two-sample T-test assuming unequal variances (Welch's t-test) was calculated by the following equation:

$$t = \frac{\overline{X_1} - \overline{X_2}}{\sqrt{\frac{s_1^2}{N_1} + \frac{s_2^2}{N_2}}}$$

Where $\overline{X_1}$ and $\overline{X_2}$ are the sample means, $s^2$ is the sample standard deviation, $N_1$ and $N_2$ are the sample sizes.

The degrees of freedom, $v$, associated with this variance estimate is approximated using the Welch–Satterthwaite equation:

$$v \approx \frac{\left(\frac{s_1^2}{N_1} + \frac{s_2^2}{N_2}\right)^2}{\frac{s_1^4}{N_1^2 v_1} + \frac{s_2^4}{N_2^2 v_2}}$$

where $v_1 = N_1 - 1$ is the degrees of freedom associated with the first variance estimate) and $v_2 = N_2 - 1$ is the degrees of freedom associated with the 2nd variance estimate.

# CHAPTER III
# Mini-review: The Application of Single-Molecule Force Spectroscopy in Studying Proteins

# 3 Mini-review: The Application of Single-Molecule Force Spectroscopy in Studying Proteins

## 3.1 General Introduction

To fully understand the structure and function of biological molecules, and hence biological processes, it is vital to understand the folding and assembly of these molecules, as well as the forces underlying the specific inter- and intra-molecular interactions (Kedrov *et al.*, 2007; Müller and Engel, 2007; Alessandrini *et al.*, 2011). Although the structural techniques, such as X-ray crystallography and electron microscopy, have given us a wealth of information on the static structures of proteins, this alone cannot decipher the folding and interactions of such proteins. The invention of AFM (Binnig *et al.*, 1986) has revolutionised the studies of biological processes due to the ability to probe biological samples in their native environments at the nanometer resolution. Additionally, AFM-based single-molecule force spectroscopy (SMFS) has opened new horizons for force measurements, transforming this field. This chapter will focus on the use of AFM-based SMFS to study inter- and intra-molecular interactions in biological macromolecules.

## 3.2 The Principles of AFM and SMFS

AFM (Liu and Scheuring, 2013) is a form of scanning probe microscopy, consisting of a sharp tip mounted at the end of a flexible cantilever (Fig. 3.1), used to probe the topological and mechanical properties of a sample surface. A laser beam is reflected off the back of the cantilever onto a position-sensitive photodiode detector, this measures the precise deflection of the cantilever as it moves over the sample surface by converting the incident beam into a voltage difference. A piezo-electric feedback

loop is used to control the height of the tip in relation to the sample, maintaining a constant position of the laser beam and generating a precise topography of the sample surface features (Binnig *et al.*, 1985).

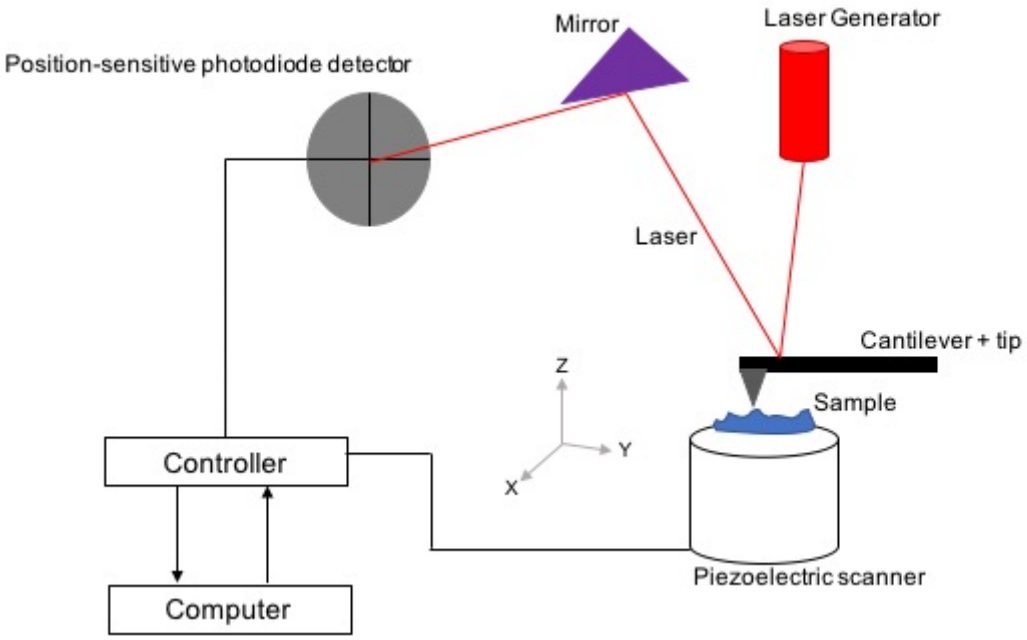


**Figure 3.1. Principle of Atomic Force Microscopy.** A schematic diagram of an atomic force microscope is shown.

### *3.2.1 Principles of SMFS*

Although AFM was originally developed for the topographic imaging described above, the technique has since become a 'multifunctional molecular toolkit' (Müller and Dufrêne, 2011) providing imperative data on the mechanical and physical properties of a sample. The use of AFM for SMFS allows the measurement of forces with 10-1000s picoNewton (pN) sensitivity and changes in length of nm resolution on a milisecond timescale (Liu et al., 2011); SMFS has hence been utilised for probing the inter- and intramolecular interactions of biological macromolecules.

In SMFS (Scholl and Marszalek, 2018), AFM is used to extend a protein, by bringing the tip into contact with the surface of a sample at a constant velocity (Fig. 3.2A) (e.g. 200 $nm \cdot s^{-1}$) and a controlled loading force is applied (e.g. ≤ 1 nN) for ≤ 1 s (Liu *et al.*, 2011); this increases the probability of the protein adsorbing to the tip. As the tip is retracted, again at constant velocity, the attached protein is stretched, eventually causing the protein to unravel, releasing amino acids and resulting in the end to end length of the protein increasing (Fig. 3.2A). After the amino acids are released, the tension between the tip and sample is lost, resulting in a decrease in the force (Fig. 3.2B). These steps are repeated as further segments of the protein are unfolded, until the unfolded protein peptide is eventually detached from the tip and a detachment peak is observed (Fig. 3.2B). The resulting curve is known as the force-distance (F-D) curve, an example of which is shown in Fig. 3.2B. As the tip is retracted, the force initially increases as the distance between the tip and sample increases and the protein resists the change in entropy. The bonds within the protein then break at a certain force, elongating the chain and the force drops back down; the process begins again in the next folded domain of the protein, producing a saw-like tooth pattern (Fig. 3.2C). Each individual peak represents the unfolding of a particular protein domain.

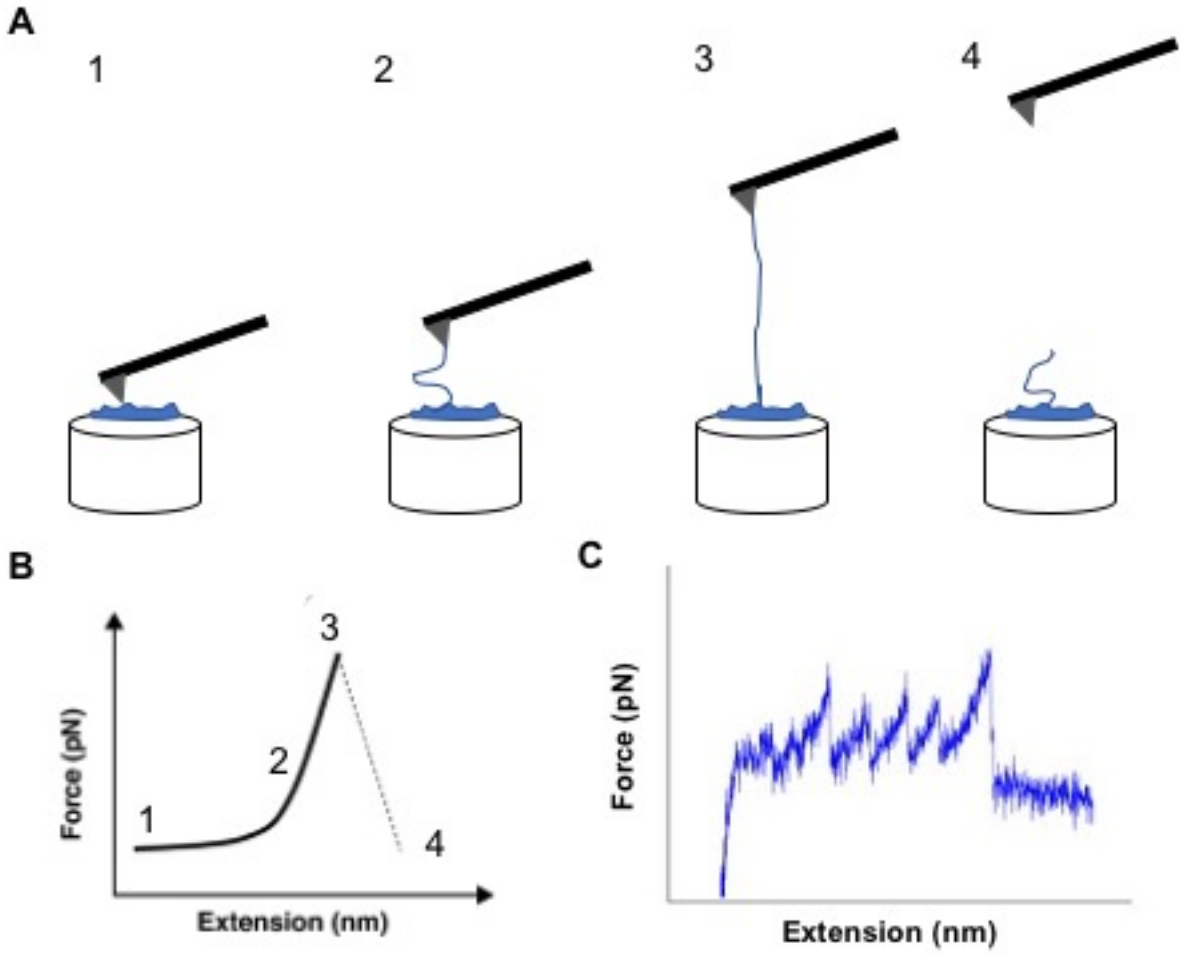


**Figure 3.2. Principle of Single-molecule force spectroscopy. A.** Schematic diagram of a typical single-molecule force spectroscopy experiment. (1) The tip is first brought into contact with the sample at a constant velocity for ~1 s. (2) The tip is then retracted, causing the attached protein to elongate (3) until it is eventually released (4). **B.** The corresponding force-distance curve, only the retraction curve is shown. **C.** Example of a saw-like tooth F-D curve.

### *3.2.2 Worm-like Chain Model*

The F-D curves require fitting to a model in order to extract useful information from them. There are two potential polymer models which could be used (Fig. 3.3); the first is the freely-jointed chain model (Mark, 2004) whereby a polymer is flexible only

between discrete freely hinged segments, the second is the WLC model which describes polymers as a continuously flexible isotropic rod (Doi and Edwards, 1988). The WLC model is most suited to the semi-flexible behaviors of proteins. The model is as follows:

$$F(\chi) = \left(\kappa_B T / b\right) \cdot \left(0.25 \cdot \sqrt{(1 - \chi / L}\right) - 0.25 + \chi / L)$$

where $F(\chi)$ is the force at distance $\chi$, $\kappa_B$ is the Boltzmann constant, $b$ = 4Å is the persistence length (the approximate length of amino acid residues), $L$ the contour length of the unfolded polypeptide chain, and $T$ is the temperature = 298 K. This is used to calculate the contour lengths of the unfolded segments, which can then be converted into the number of amino acids. This can then be related to the amino acid sequence of the protein to determine the individual domains which have unfolded at certain forces.

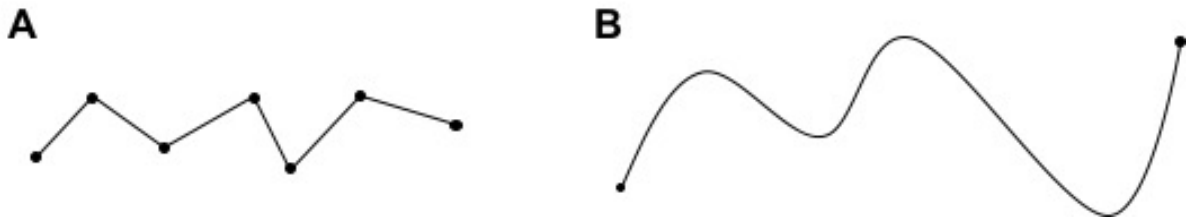


**Figure 3.3. Polymer models. A.** Schematic of the freely jointed chain model. **B.** Schematic of the worm-like chain model.

### *3.2.3 Principles of Topography and Recognition imaging*

Topography and recognition (TREC) imaging is another imaging mode of AFM using tip functionalization (Stroh *et al.*, 2004). This technique allows for the specific recognition of biomolecules from a complex biological sample using a probe modified with specific molecules, e.g. an antibody, via a flexible PEG linker (Fig. 3.4A) (Haselgrübler *et al.*, 1995). The sample is scanned with a modified probe, as the

antibody tethered to the AFM tip binds to its antigen on the sample surface (Fig. 3.4B), the oscillation of the tip is altered (Fig. 3.4C). The height map of the sample is recorded (Fig. 3.4D) and the change in amplitude is converted to a recognition image (Fig. 3.4E), whereby the molecule can be localized (Stroh *et al.*, 2004).

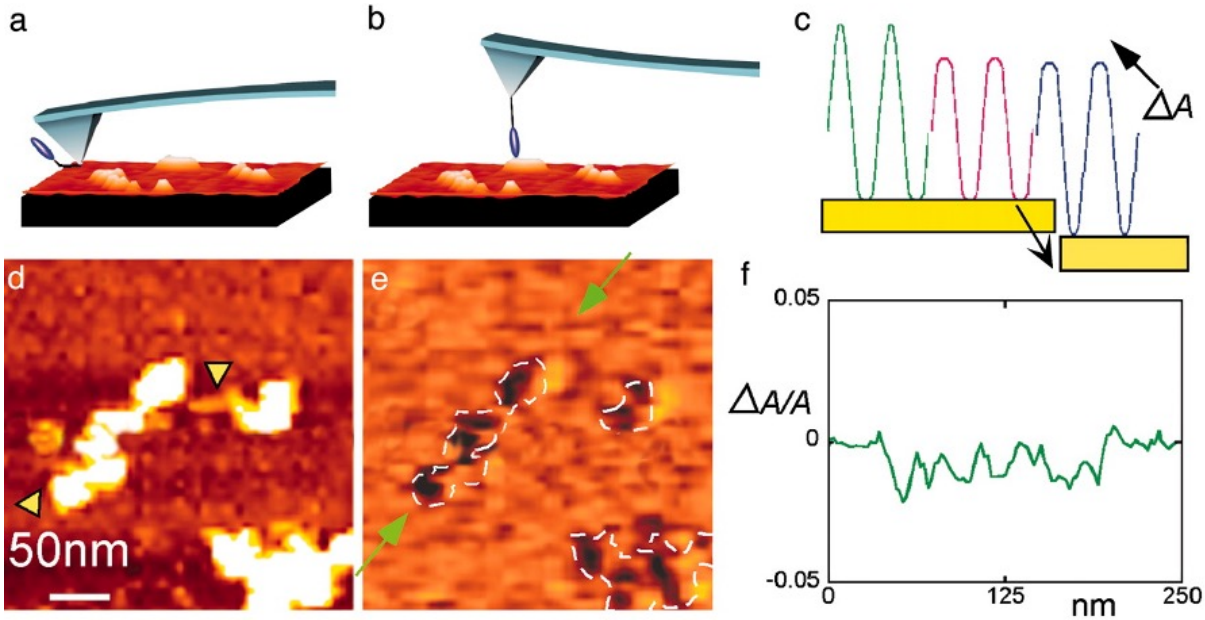


**Figure 3.4. TREC Schematic. A.** The sample is scanned with a modified probe, **B** the antibody then binds to the antigen when they come into contact. **C.** Binding of the antibody to the antigen reduces the amplitude value and is converted to a molecular recognition image by a feedback loop. **D**. The height topograph of the sample, **E**. the corresponding recognition map, the black dots represent the recognition signal. **F.** The cross-sectional analysis of **E**. Taken from Stroh et al. 2004.

### *3.2.4 Tip Selection*

Choosing the correct tip for imaging and mechanical measurement of samples is a vital aspect of AFM experiments; the diameter, morphology, material, spring constant and length of the cantilever of tips are critical factors. For low-resolution, large scans a larger tip is suitable. To gain high-resolution images, a sharper tip is required for the

measurement of proteins and other nanoscale materials. Delicate biological samples, such as cell membranes, can be damaged through repeated contact with high spring constant probes, therefore probes with smaller spring constants (0.01-0.5 $N \cdot m^{-1}$) are most suitable (Du and Li, 2007).

### *3.2.5 Sample Preparation*

Another important factor in AFM experiments is the preparation of samples; this can have a huge impact on the quality of the imaging. Common substrates for AFM samples include mica, treated mica, HOPG and silicon. Mica and HOPG are both layered materials and can therefore be cleaved with cellotape to reveal an atomic level, clean surface suitable for high-resolution AFM imaging (Rodriguez-Ramos, *et al.,*, 2018).

The sample must be immobilized onto the substrate for good quality imaging, therefore the substrate chosen depends on the sample being imaged; negatively charged samples can be immobilized using mica treated with 3-aminopropyltriethoxysilane (APTES) which makes the surface positively charged. This can be further modified with glutaraldehyde to facilitate the interaction with amino groups in the side chains of proteins, enhancing protein adsorption to the substrate. For other samples, such as the ICM of bacteria, the electrostatic interactions between the freshly cleaved mica, when a buffer containing divalent cations is used, and the sample is sufficient for high-resolution imaging. The absorption time between samples varies. It must be noted that for certain experiments, such as SMFS, the interaction between the sample and substrate may alter the forces measured and therefore needs to be carefully considered.

## 3.3 Biological Applications of SMFS

### *3.3.1 Receptor-Ligand Interactions*

Receptor-ligand interactions play key roles in controlling and mediating cell communication and signaling. Understanding these interactions is imperative to the full understanding of many biological processes. Receptors interact with multiple ligands with differing levels of affinity and binding-related conformational changes. SMFS has been used to characterise the binding landscape of various receptor-ligand interactions (Fuhrmann and Ros, 2010; Wildling *et al.*, 2011).

In these experiments, the ligands were attached to the AFM tip and used to probe the corresponding receptor on the surface of the sample (Fig 3.5). The specific interaction between these two molecules was detected by the AFM. This technique was first utilised by Hinterdorfer and colleagues (Hinterdorfer *et al.*, 1996) to measure the unbinding force between human serum albumin (HAS) and anti-HAS. Many other researchers have since used this method to detect the specific recognition of receptors immobilised on artificial surfaces (Zhang *et al.*, 2004) and on cell surfaces (Pfister *et al.*, 2005; Puntheeranurak *et al.*, 2006; Shi *et al.*, 2009).

This technique was also applied to detect the interactions of HER2 and epidermal growth factor receptors (EGFRs). SMFS demonstrated that cancer therapy antibodies Trastuzumab and Pertuzumab target HER2, interrupting its interaction with EGFR and decreasing the downstream signalling of EGFRs (Zhang *et al.*, 2013).

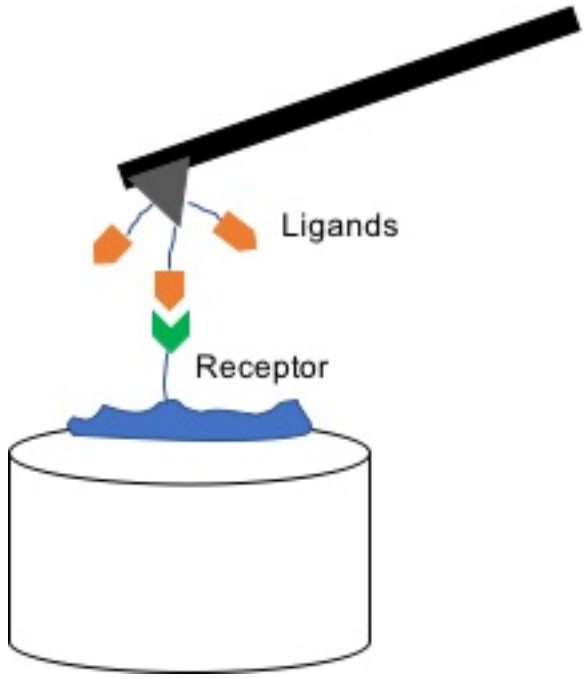


**Figure 3.5. Receptor-ligand SMFS experiment.** The ligands are attached to the AFM tip by linker molecules and used to probe the sample surface. The interaction between the ligand and receptor can then be measured.

### *3.3.2 Folding and Unfolding Pathways of Proteins*

The function of a protein is acquired through the specific folding of their polypeptide chains; the unfolding of a plethora of proteins using SMFS has revealed that the mechanical stability of a protein can be related to its secondary structure (Carrion-Vazquez *et al.*, 2000). Unfolding of the I27 domain of the muscle protein Titin, composed of β-sheets, at pulling speed 0.6 $nm \cdot ms^{-2}$ revealed an unfolding force of ~200 pN (Carrion-Vazquez *et al.*, 2000). Comparatively, calmodulin, a calcium-dependent regulator, consisting of 7 α-helices does not show mechanical barriers to its unfolding, when the protein is subject to SMFS at the same pulling speed (Carrion-Vazquez *et al.*, 2000). SMFS on a third protein, spectrin which forms bundles of α-helices reveals unfolding forces of 25-35 pN (Fisher *et al.*, 1999; Rief *et al.*, 1999);

these forces are intermediate between the single α-helix and the β-sheets. β-sheet proteins were shown to withstand the most mechanical force, and hence the parallel beta-sheet is the most stable structural element.

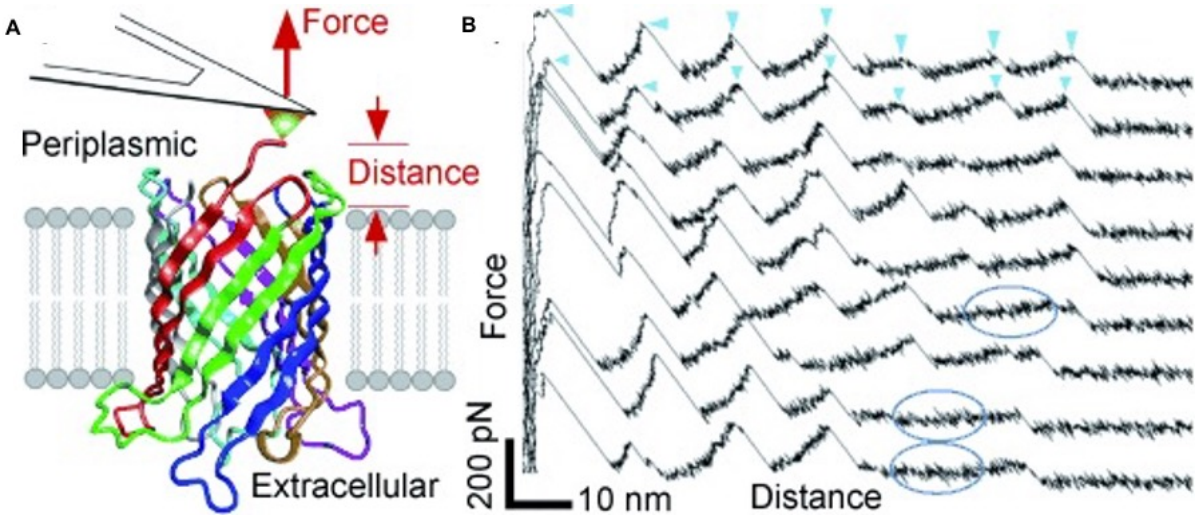


**Figure 3.6. Unfolding of OmpG. A.** Schematic of the SMFS experiment on the structural model of OmpG. OmpGs were non-specifically attached to the tip by their N-terminal end (26). **B**. F-D curves recorded during the unfolding of OmpG. Taken from Sapra *et al.,* 2009.

The first transmembrane protein to be unfolded was the β-barrel protein, OmpG, found in the outer membrane of *E. coli*, which comprises of 14 β-strands and occurs as monomer (Fajardo *et al.*, 1998; Conlan *et al.*, 2000). The protein produced a fingerprint of seven distinct force peaks when unfolded from its N-terminus. Fitting these peaks with the WLC model revealed the length of each (Sapra *et al.*, 2009), assignment of these segments to the tertiary structure of the protein showed that the unfolding occurred via the sequential removal of the seven β-hairpins (Fig. 3.6), with forces ranging from 250 pN at the N-terminal β-hairpins to 150 pN for the C-terminal β-hairpins (Sapra *et al.*, 2009). OmpG consists of two functional states, open and closed, SMFS was repeated on both states. The unfolding pathway was identical for the first

four and the last β-hairpins, however the pathways diverge in at the middle β-hairpins, whereby there is a conformational change in part of the extracellular loop L6 (Fig. 3.7)(Damaghi *et al.*, 2010). This demonstrates that the unfolding pathway of a membrane protein and the forces measured are dependent on its functional state; the forces required to mechanically unfold a protein reflect the strength of the intra- and intermolecular interactions.

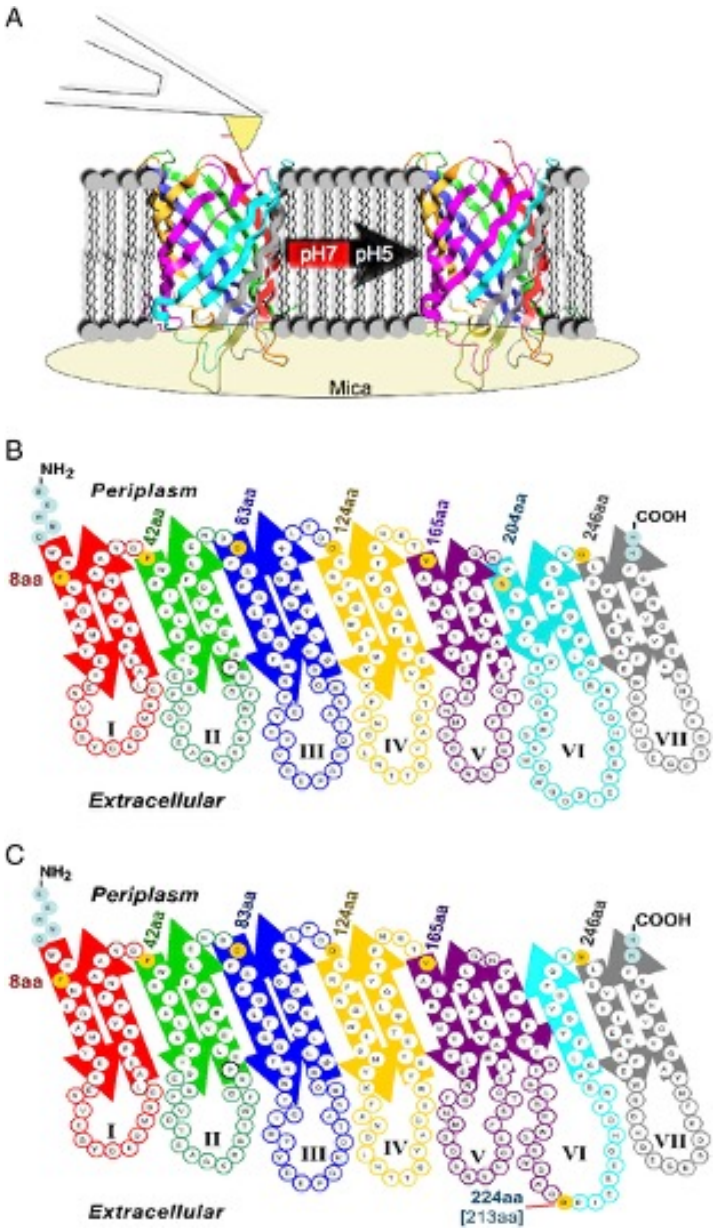


**Figure 3.7. Unfolding intermediates of OmpG at different functional states detected using SMFS. A**. Schematic of the SMFS experiment. OmpGs were non-

specifically attached to the tip by their N-terminal end (26). **B**. In the Open/closed (pH7) state, single β-hairpins formed the unfolding steps. **C.** In the open/closed state, β-hairpins 9-11 formed one unfolding step and β-hairpin 12 also formed one. Taken from Damaghi *et al.,* 2010.

### *3.3.3 Membrane Proteins*

As well as the specific folding of the protein, the interactions with the lipid bilayer and adjacent proteins are also imperative to the stability and function of membrane proteins. SMFS provides the ability to measure the forces anchoring proteins into the membrane. Bacteriorhodopsin (BR) from purple bacteria was the first protein to be unfolded by SMFS (Oesterhelt *et al.*, 2000). The membrane patch was first imaged at high resolution, the AFM was then used to unfold the protein before imaging the membrane again; the protein had disappeared implying that the protein had been unfolded (Fig. 3.8). The resulting F-D curve revealed several peaks at up to 75 nm distance (248 amino acids), corresponding to the length of an entire unfolded BR (Fig. 3.9).

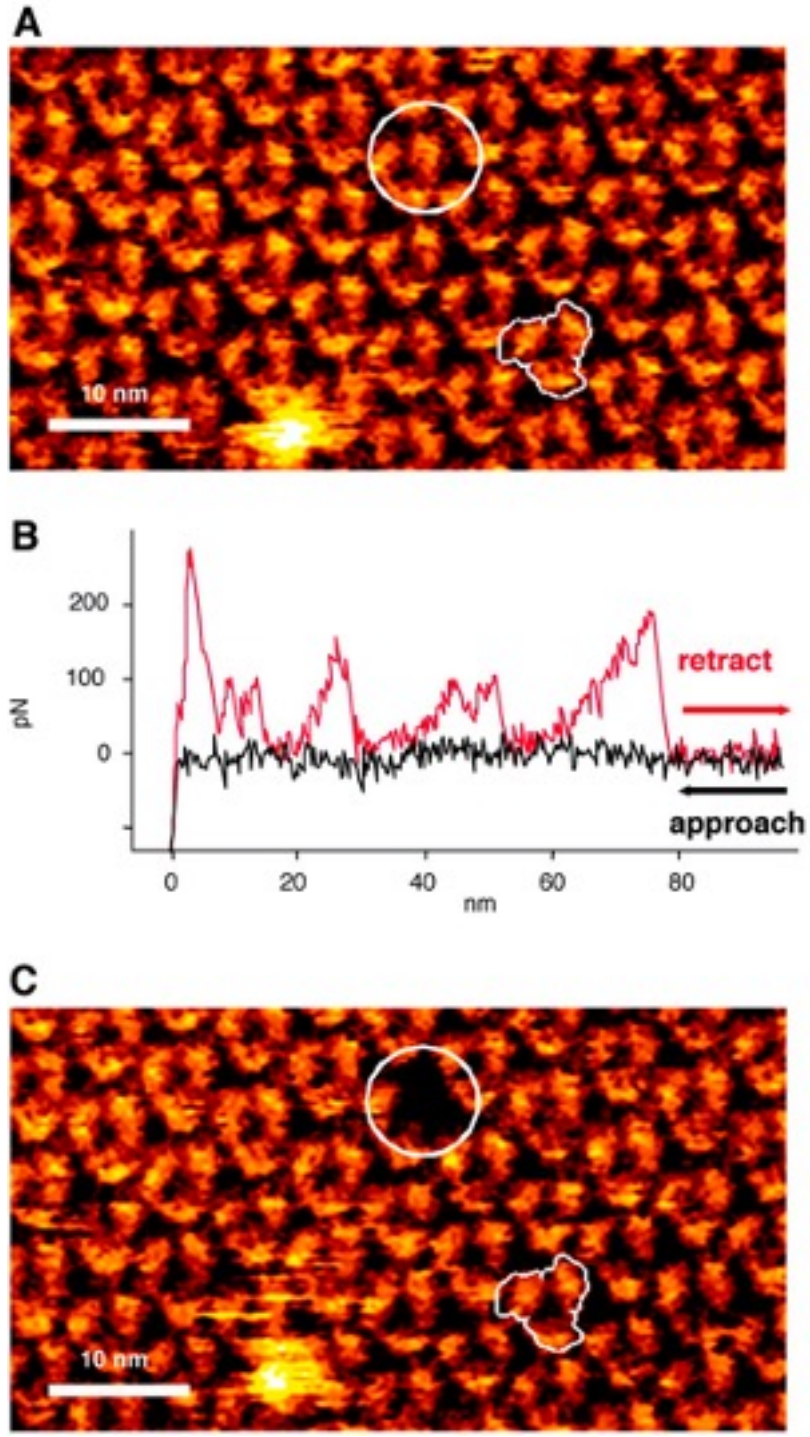


**Figure 3.8. Single-molecule force spectroscopy of bacteriorhodopsin. A.** High-resolution AFM image of BR trimers in the purple bacterial membrane before SMFS. **B.** Typical force curve from the extraction of a BR molecule from the membrane. **C.** High-resolution AFM image of the purple bacterial membrane after the SMFS

experiment, revealing the removal of a BR molecule from the membrane. Taken from Oesterhelt et al., 2000.

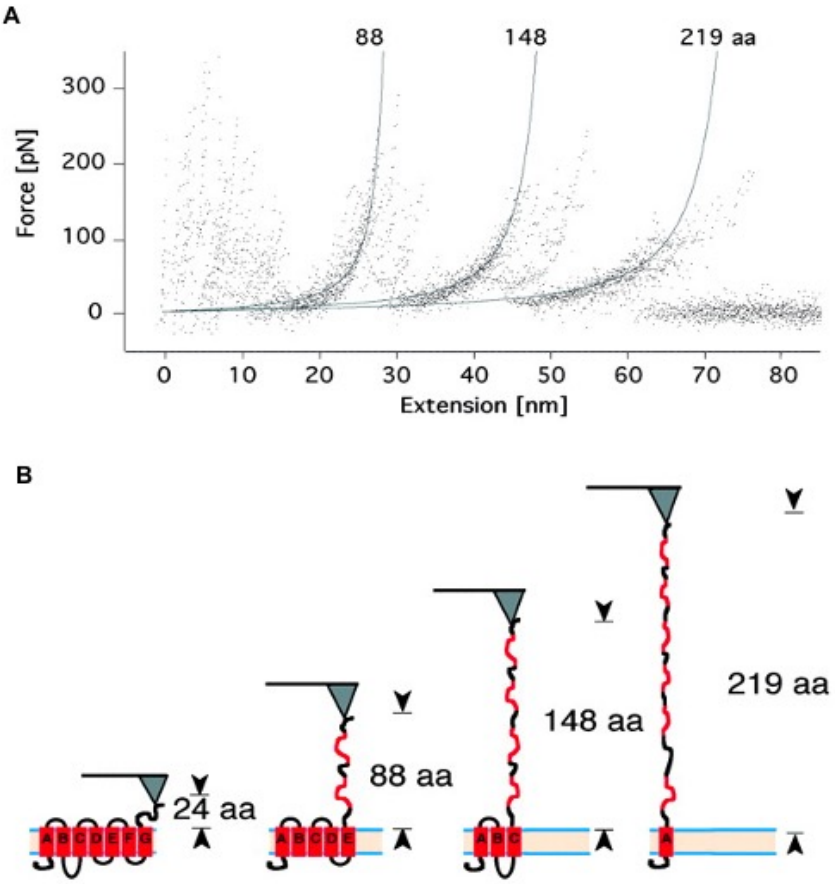


**Figure 3.9. Force-distance curves resulting from SMFS of Bacteriorhodopsin. A.** 13 F-D curves are superimposed revealing various common peaks. The worm-like chain model has been fitted to these in grey. **B.** Model explaining the peaks in the F-D curve as the sequential unfolding of a BR molecule. Taken from Oesterhelt et al., 2000.

The technique was also used to probe the light-harvesting complex 2 (LH2) from purple bacteria (Liu *et al.*, 2011); during this study the tip was brought into contact with the sample at a constant velocity of 200 nm·s$^{-1}$ with a loading force of ≤ 1 nN for ≤1 s. High-resolution AFM imaging before and after the unfolding event confirmed the unfolding of individual complexes. The unfolding of the complex resulted in periodic

unfolding of the LH2 ring subunits (Fig. 3.10). One- and two-step unfolding events were detected (Fig. 3.10A); the major unfolding events consisted of an unfolding force of approximately 150 pN (Fig. 3.10C). A high variability of the lengths of the unfolding curves was revealed (Fig. 3.10D), this was due to the presence of a sequence of tightly associated polypeptides, rather than a single protein chain. The one- and two-step unfolding curves where overlaid separately and fitted with the WLC model (Fig. 3.10E,F); the one-step subunit unfolding had a periodicity of 53 amino acids, whereas the two-step subunit unfolding contained an intermediate step at 23 amino acids. Both had an unfolding force of 150 pN. The study revealed that weakly bound subunits of the complex self-assembled into ring structures, as this shape guarantees the stability of the entire complex. The specific molecular environment within the membrane enables the stability. This study highlighted the importance of intermolecular forces in maintaining the structural and functional integrity of membrane proteins (Liu *et al.*, 2011).

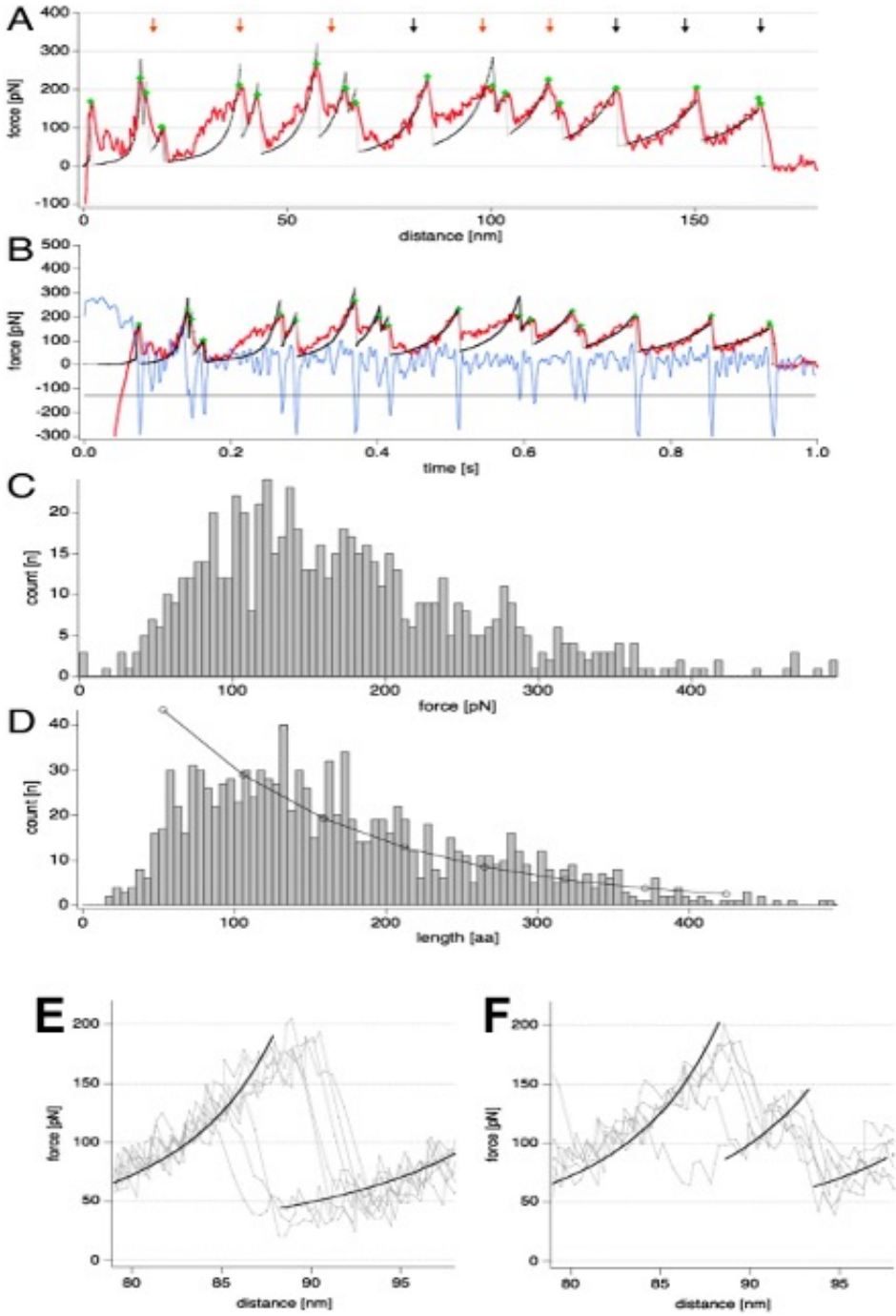


**Figure 3.10. The unfolding of LH2. A.** Force-distance curve and **B** force-time curve of an individual LH2 complex unfolding. The WLC fits of unfolding events are shown in black on the red raw-data force curve. Black and red arrows indicate one-step and two-step unfolding events, respectively, during the subunit unfolding. The blue trace in **B** is the derivative of the measured force-time curve and the horizontal black line

depicts five times the standard deviation (5σ) of the noise of the force curve. Automated unfolding events detection was defined by cross-over of the force derivative plot with the 5σ-trace, indicated by green crosses. **C.** Rupture force, and **D** force curve length histograms of unfolding curves analysis and an exponential fit to the decay. Overlay of force curves of **E** the one-step subunit unfolding with a periodicity of 53 amino acids and **F** two-step subunit unfolding with an intermediate unfolding barrier at 23 amino acids. Taken from (Liu et al., 2011).

In a recent study which forms part of this thesis (see **Chapter IV**), SMFS has been used to elucidate the multi-step unfolding process of the non-membranous 4Hcyt subunit of the RC-LH1 membrane-bound complex from *Blc. viridis* and its interaction with the RC-L subunit (Miller *et al.*, 2020). The tip was brought into contact with the C-terminus of the protein and subsequently retracted; AFM images taken before and after SMFS experiments demonstrate the removal of the subunit from the membrane protein. The resulting F-D curves were superimposed revealing seven pronounced peaks. Fitting to the WLC model and relating this to the secondary and tertiary structure of the protein subunit revealed the unfolding pathway. Unfolding of the 4Hcyt also lead to the unfolding of the L subunit, indicating strong interactions between the 4Hcyt and RC transmembrane subunit (Miller *et al.*, 2020).

### *3.3.4 High-speed single molecule force spectroscopy*

Although SMFS experiments at conventional AFM speeds provide a wealth of information on proteins, higher pulling rates and times are required to get a more complete picture of mechanisms by direct comparison with experiments with molecular dynamic simulations. High-speed force spectroscopy was developed to unfold titin at velocities identical to those reached by simulations (~4 $mm \cdot s^{-1}$) (Rico *et*

*al.*, 2013). The experiments reveal detailed mechanisms of the unfolding steps of Titin I91; the protein fluctuates between native and intermediate states at zero and moderate forces, however under increasing force only the intermediate state is populated. This shows slow diffusion along the unfolding pathway resulting in a high mechanical stability (Rico *et al.*, 2013).

## 3.4 Conclusions

The examples discussed above are just a handful of examples of the use of AFM for SMFS to enhance our understanding of protein structure and function in biological processes. The combination of AFM imaging with single-molecule mechanical manipulation by force spectroscopy has proven a powerful approach in studying the inter- and intramolecular interactions of proteins and membrane-proteins, greatly enhancing our understanding of biological processes. High-resolution imaging of the sample before and after SMFS experiments helps to confirm the nature of the interactions measured.

# CHAPTER IV
# Interactions Underlying the Folding and Assembly of Photosynthetic Reaction Centers in Native Membrane Environment

# 4 Interactions Underlying the Folding and Assembly of Photosynthetic Reaction Centers in Native Membrane Environment

## 4.1 Introduction

Photosynthesis is one of the most important biological processes, providing the energy for almost all life on Earth. The photosynthetic light reactions occur in the specialized biological membranes, termed the photosynthetic membranes, which accommodate a set of pigment–protein photosynthetic complexes. Light is absorbed by the pigments in the antenna complexes, and the energy is transferred efficiently to the reaction center (RC), where primary charge separation takes place and electron transfer is initiated. Defined protein organization and interaction in photosynthetic membranes are paramount to high-efficiency light-harvesting and energy conversion.

In purple photosynthetic bacteria, the light-harvesting system is predominantly made up of two pigment–protein antennas: the peripheral light-harvesting (LH) complexes LH2 and the core light- harvesting complexes LH1. LH2 funnels the excitation energy to an LH1 complex that encircles an RC to form the RC–LH1 core complexes. *Blastochloris (Blc.) viridis* is an unusual, bacteriochlorophyll (BChl) *b*-producing purple bacterium, possessing a simplified photosynthetic apparatus that lacks LH2 (Liu *et al.*, 2016). The RC of *Blc. viridis* was the first membrane protein to be structurally characterized (Deisenhofer *et al.*, 1984). It is formed by four subunits (Fig. 4.1): three core subunits L (PufL), M (PufM), H (PuhA) that are bound to the cytoplasmic face of the L and M subunits, as well as a non- membranous tetraheme cytochrome subunit (4Hcyt, PufC) with its N-terminal cysteine covalently linked to a diglyceride at the periplasmic surface of the photosynthetic membrane; the 4Hcyt subunit is non-

covalently linked to the L and M subunits (Weyer *et al.*, 1987; Wöhri *et al.*, 2010; Roszak *et al.*, 2012). In addition, the RC consists of four BChl *b* molecules, two bacteriopheophytin *b* molecules, one nonheme iron, two quinones, and one carotenoid (Deisenhofer and Michel, 1988). The *Blc. viridis* LH1 complex is composed of α-, β- and γ-polypeptides. A recent cryo-electron microscopy structure of the *Blc. viridis* RC-LH1 complex revealed that the LH1 ring consists of 16 heterotrimers of α–β–γ-polypeptides and one α–β-heterodimer; the 'missing' 17th γ- polypeptide creates a gap in the LH1 ring, potentially allowing for quinone diffusion (Qian *et al.*, 2018).

The 4Hcyt subunit contains four covalently bound heme groups and is attached to the periplasmic face of the L and M subunits, transferring electrons from the soluble electron carrier cytochrome (Cyt) $c_2$ molecule to the RC "special pair" of BChls (Fig. 4.1). The conformation of the 4Hcyt subunit is designed for rapid electron flow between the vertically stacked heme groups and the binding of Cyt $c_2$ to the RC is speculated to be the limiting step of electron transfer (Olson *et al.*, 2014). Recent structural analysis has provided information about the Cyt−RC association in several species (Niwa *et al.*, 2014a; L.-J. Yu *et al.*, 2018; Qian *et al.*, 2018; Xin *et al.*, 2018). However, the 4Hcyt subunit is not a crucial RC component in all purple photosynthetic bacteria. Some species, such as *Rhodobacter (Rba.) sphaeroides* (Axelrod and Okamura, 2005), *Rhodospirillum rubrum* (Jamieson *et al.*, 2002), and *Rhodopseudomonas palustris* (Roszak *et al.*, 2003), do not contain a 4Hcyt subunit and rely on Cyt $c_2$ or other electron carriers (such as Cyt $c_y$) for electron donation. Despite many structural studies at close to atomic resolution of bacterial RCs, how the 4Hcyt subunit folds to position its heme cofactors and interact with the RC subunits in the native complex remains enigmatic.

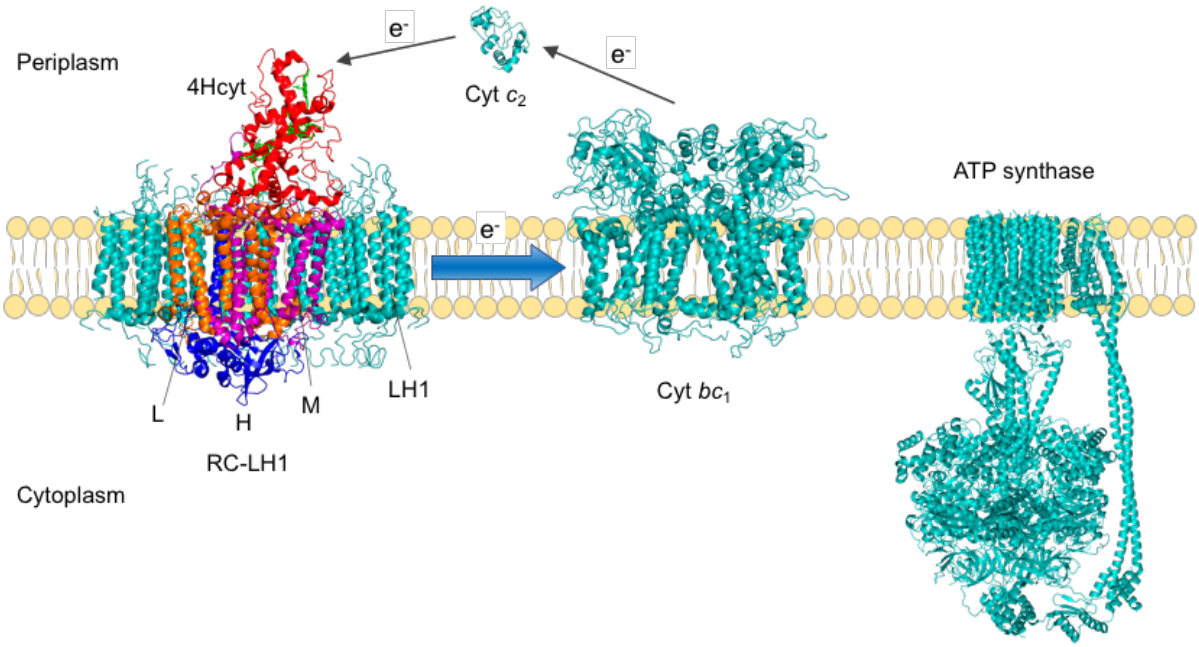


**Figure 4.1. Schematic model of the photosynthetic apparatus of *Blc. viridis*.** The electron transport chain of *Blc. viridis* comprises the RC-LH1 complex (PDB ID: 6ET5, *Blc. viridis*), Cyt $bc_1$ (PDB ID: 1ZRT, *Rhodobacter capsulatus*), and ATP synthase (PDB ID: 6N30, *Bacillus sp.* strain PS3). The 4Hcyt subunit (red) at the periplasmic side of the photosynthetic RC contains four heme groups (green). It interacts with the transmembrane subunits L (orange) and M (purple). The H subunit is at the cytoplasmic side of the RC (blue). LH1 complexes (teal) associate with the RC, forming the RC-LH1 core complex. The Cyt $c_2$ functions as the soluble electron carriers and transfers electrons from the Cyt $bc_1$ complex to the RC.

In this work, we apply AFM imaging and AFM-based SMFS to elucidate the native organization of the photosynthetic apparatus from *Blc. viridis* and characterize, at the single-molecule level, the mechanical unfolding process of the 4Hcyt subunit. Our study provides new insights into the strength of protein folding segments and intermolecular interactions of photosynthetic multiprotein complexes.

## 4.2 Results and Discussion

### *4.2.1 Preparation of native photosynthetic membranes*

Photosynthetic membranes from *Blc. viridis* were isolated using sucrose gradient centrifugation (Fig. 4.2A), without freeze-thawing as reported previously (Scheuring, Jérôme Seguin, *et al.*, 2003). The absorption spectrum of isolated photosynthetic membranes exhibits a characteristic absorption maximum at 1015 nm and a peak at 831 nm (Fig. 4.3), arising from BChl *b* in the RC–LH1 (Qian *et al.*, 2018). SDS-PAGE revealed the presence of the most predominate photosynthetic proteins based on their molecular weights (Fig. 4.2B), consistent with the previous study (Scheuring *et al.*, 2003), demonstrating the structural integrity of the isolated photosynthetic membranes.

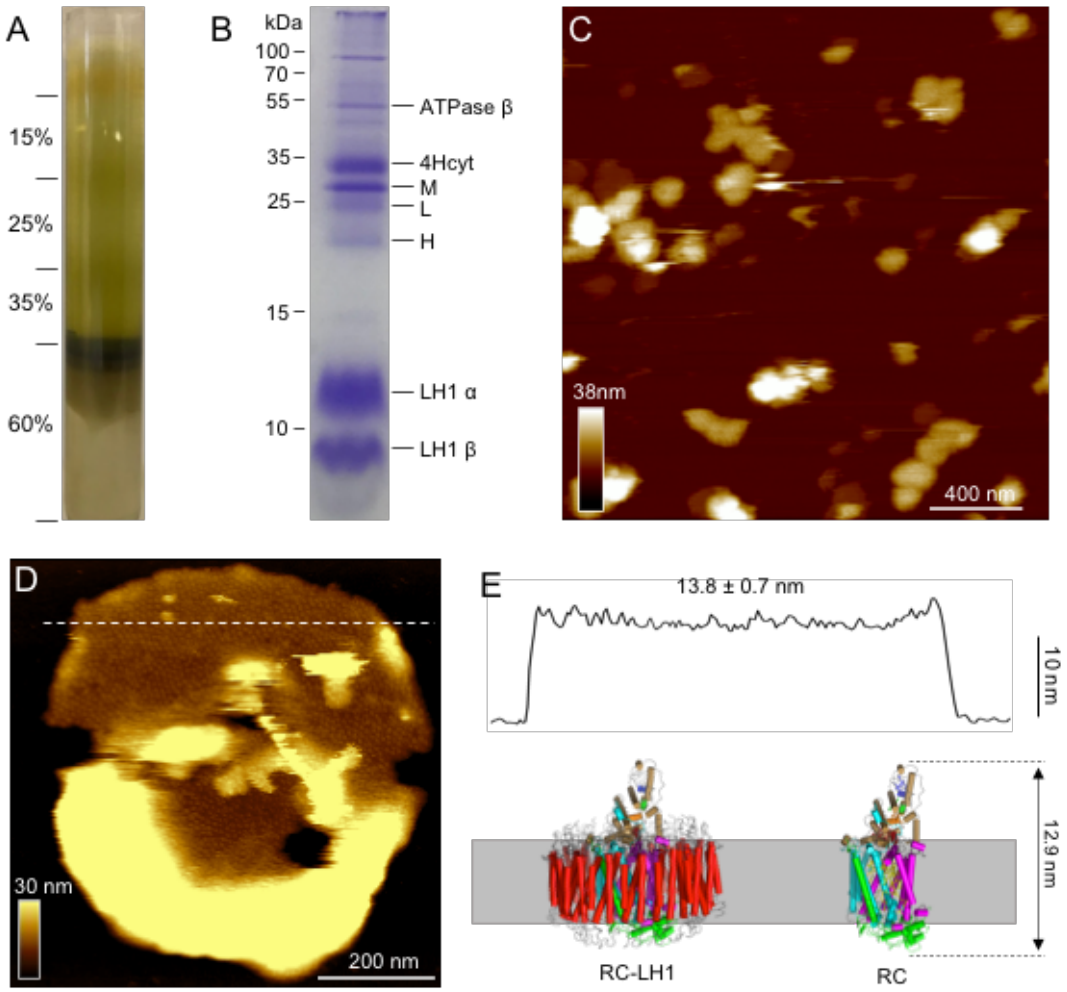


**Figure 4.2. Isolation and AFM imaging of photosynthetic membranes from *Blc. viridis*.** **A.** Step sucrose gradient centrifugation of the photosynthetic membranes, containing 0.03% n-Dodecyl β-D-maltoside (β-DDM). Photosynthetic membranes at the 35%-60% interface were extracted for further analysis. **B.** SDS-PAGE of the isolated photosynthetic membranes stained with Coomassie blue. The assigned components are labelled on the right. L: L subunit (PufL), M: M subunit (PufM), H: H subunit (PuhA). **C.** AFM overview image of isolated *Blc. viridis* photosynthetic membrane patches. **D.** AFM topograph of an isolated photosynthetic membranes patch in liquid. **E.** Cross-section analysis along the dashed line in **D** reveals an average height of 13.8 ± 0.7 nm (*n* = 6) of the photosynthetic membranes containing the RC-LH1 complexes (bottom). The RC-LH1 and RC complexes were presented using the cryo-EM structure of RC-LH1 (PDB ID: 6ET5).

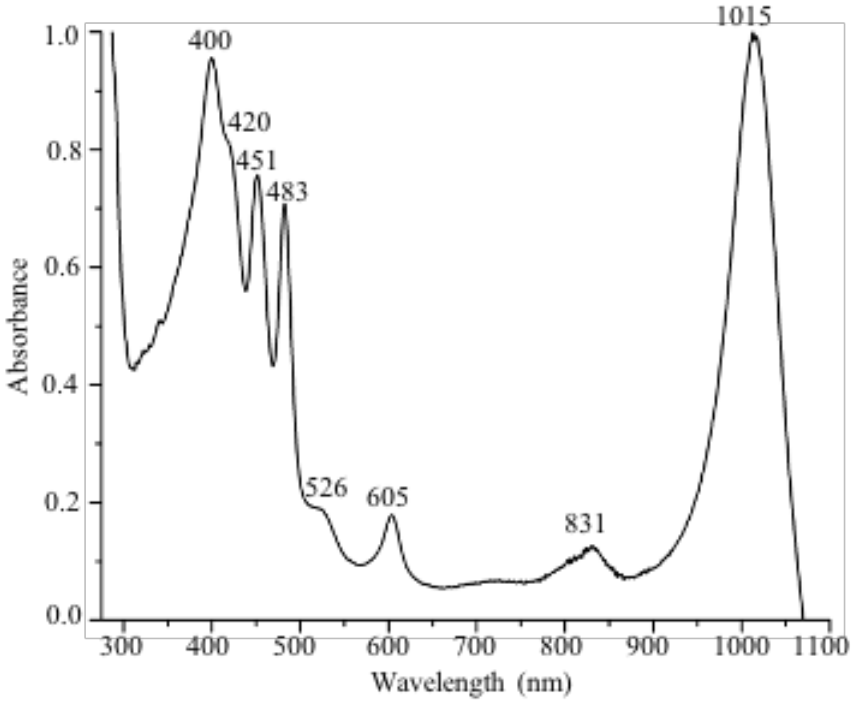


**Figure 4.3. Room-temperature absorption spectrum of isolated photosynthetic membranes from *Blc. viridis.***

### *4.2.2 RC-LH1 complexes are densely packed in the photosynthetic membranes*

The resulting photosynthetic membranes were then immobilized on freshly cleaved mica substrate for AFM imaging. AFM has demonstrated its extraordinary power in high-resolution imaging of native photosynthetic membranes (Yamashita *et al.*, 2009; Casuso *et al.*, 2012; Liu and Scheuring, 2013; Sutter *et al.*, 2016) and force measurements to delineate the mechanical unfolding of photosynthetic antenna membrane complexes (Bustamante and Loach, 1994). AFM screening showed that the isolated photosynthetic membranes appear as two-dimensional patches with the sizes larger than 150 nm (Fig. 4.2C), allowing for AFM visualization of the long-range protein arrangement in the photosynthetic membranes. Fig. 4.2D shows a representative membrane patch that exhibits arrays of RC-LH1 complexes. Cross-section analysis (Fig. 4.2E) reveals that the membrane patches have an average

thickness of 13.8 ± 0.7 nm (mean ± standard error of the mean (SEM), n = 6), comparable to the overall height of the RC-LH1 complex from the cytoplasmic face of the H subunit (Ser189) to the periplasmic extremity of the 4Hcyt subunit (Pro49) (12.9 nm, PDB ID: 6ET5)(Qian *et al.*, 2018).

Closer AFM inspection provided an overview of the distribution of RC-LH1 complexes in the photosynthetic membranes (Fig. 4.4A). On the periplasmic surface, the RC-LH1 complexes, represented as individual protruding particles due to the presence of 4Hcyt, are densely packed and form regular arrays in a ~60$^{o}$ staggered pattern, resulting from the inherent circular structures packing in the densest manner. The protruding height of 4Hcyt above the membrane surface is 5.1 ± 0.7 nm (n = 32) (Fig. 4.4B), similar to the protrusion of 4Hcyt above the membrane plane as indicated by the reported cryo-EM structure (Qian *et al.*, 2018). The distance between adjacent RC-LH1 complexes is 14.8 ± 2.6 nm (*n* = 30) (Fig. 4.4B), consistent with the pair correlation function results that indicate the closest distance between two RC-LH1 complexes of ~14 nm (Fig. 4.4C). Higher- magnification AFM topograph illustrates the structures of individual circular RC-LH1 complexes and their lateral arrangement in the membrane, with the angle between RC-LH1 arrays of 55-60$^{o}$ (Fig. 4.4D, 4.4E). During high-resolution AFM imaging, the 4Hcyt heads could be removed by scanning forces exerted by the AFM tip, resulting in better characterization of the associated LH1 organization (Fig. 4.4D). The density of RC-LH1 complexes and the space between neighbouring RC-LH1 complexes differ in different membrane regions, implying the inherent variability of the protein organization of these photosynthetic membranes (Fig. 4.5).

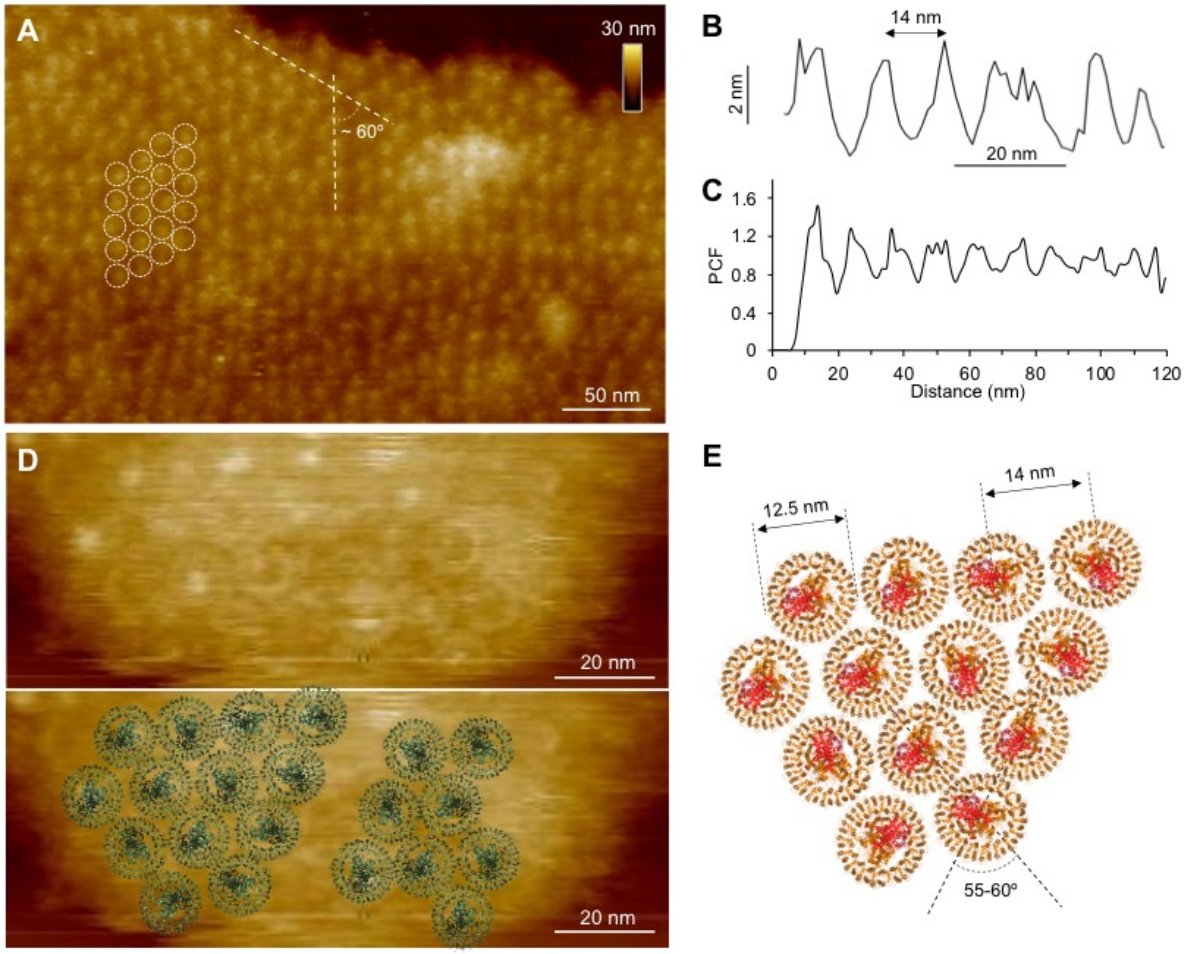


**Figure 4.4. Arrangement of RC-LH1 complexes in photosynthetic membranes from *Blc. viridis.*** **A**. Medium-resolution AFM image of the photosynthetic membrane in liquid. White circles indicate individual RC-LH1 complexes, revealing a regular array of core complexes, with an angle of ~60º. **B**. Height analysis indicates that the 4Hcyt heads are 14.8 ± 2.6nm apart in the periplasmic surface of photosynthetic membranes. **C**. Pair correlation function (PCF) analysis of the RC-LH1 distribution in the periplasmic surface reveals a ~14 nm distance between adjacent RC-LH1 complexes. **D**. High-resolution image of the photosynthetic membranes in liquid demonstrates a compact arrangement of RC-LH1 complexes (upper). The cryo-EM structure of RC-LH1 (PDB ID: 6ET5) is superimposed in the AFM image (lower). **E**. Schematic arrangement of RC-LH1 complexes as revealed by AFM imaging. Each RC-LH1

complex is 12.5 nm in size and the space between neighbouring RC-LH1 complexes is ~14 nm.

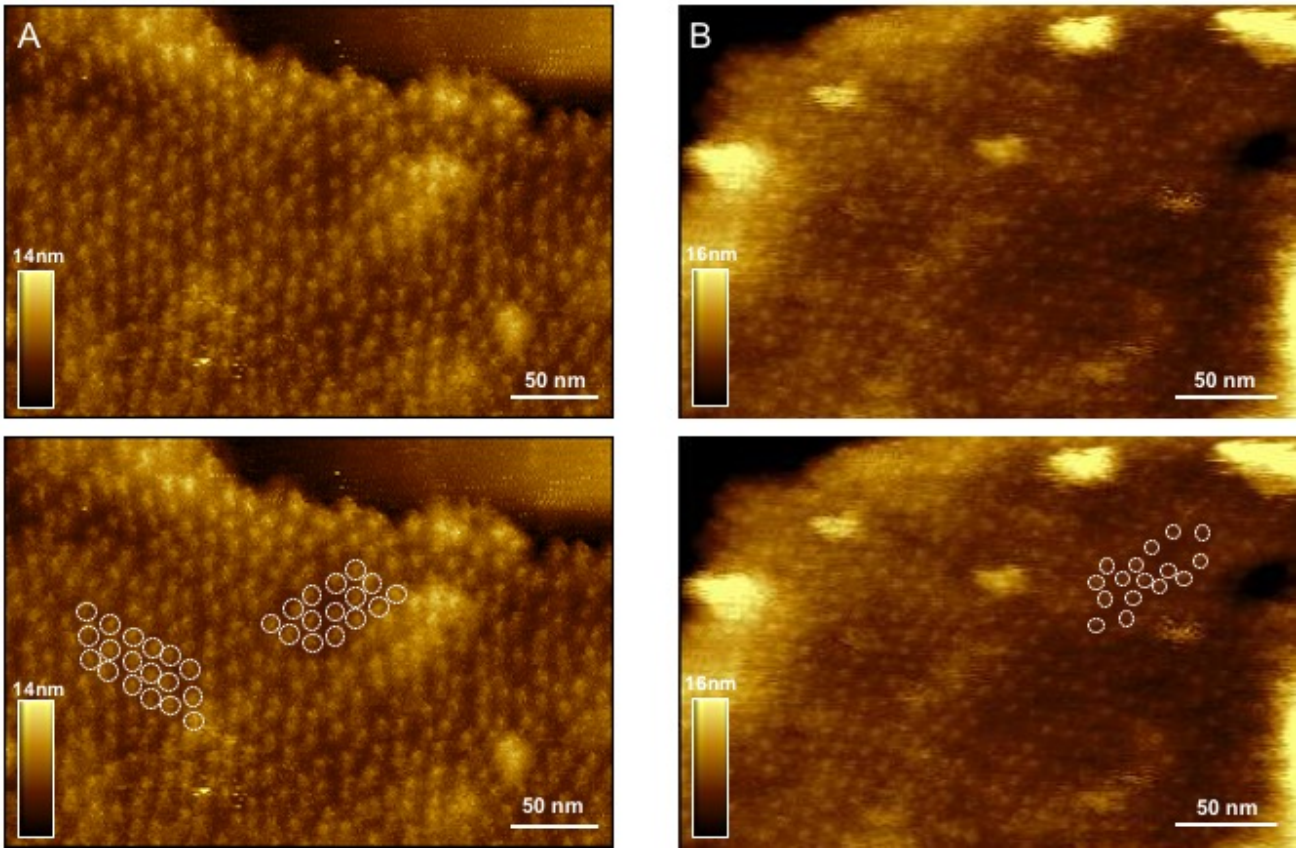


**Figure 4.5. Variability of the distribution of RC-LH1 complexes in native photosynthetic membranes. A.** A densely-packed photosynthetic membrane patch containing 112 RC-LH1 complexes per 15640 $nm^2$, covering ~81% of the total membrane. The RC-LH1 complexes are 14.8 ± 2.6 nm apart. Circles indicate individual 4Hcyt heads. **B.** A less densely- packed photosynthetic membrane patch containing 73 RC-LH1 complexes per 15640 $nm^2$, covering 53% of the total membrane. The RC-LH1 complexes are 17.9 ± 5.6 nm (*n* = 70) apart. Circles indicate individual 4Hcyt heads.

RC-LH1 complexes account for over 90% of the total proteins in the *Blc. viridis* photosynthetic membranes (Gonçalves and Scheuring, 2006). In such a highly

crowded membrane environment, RC-LH1 complexes are presumed to possess restricted diffusion due to the lack of space in the membrane. High-speed AFM imaging confirmed the highly stable organization of RC-LH1 complexes. No detectable lateral movement of the strongly protruded 4Hcyt heads was observed during continuous AFM scanning over 85 seconds (Fig. 4.6), indicating a higher restriction of protein diffusion than those of packed membrane proteins and self-assembling proteins (Deisenhofer *et al.*, 1995; Oberhauser *et al.*, 1998; Oesterhelt *et al.*, 2000), although the influences caused by sample-substrate absorption cannot be discounted.

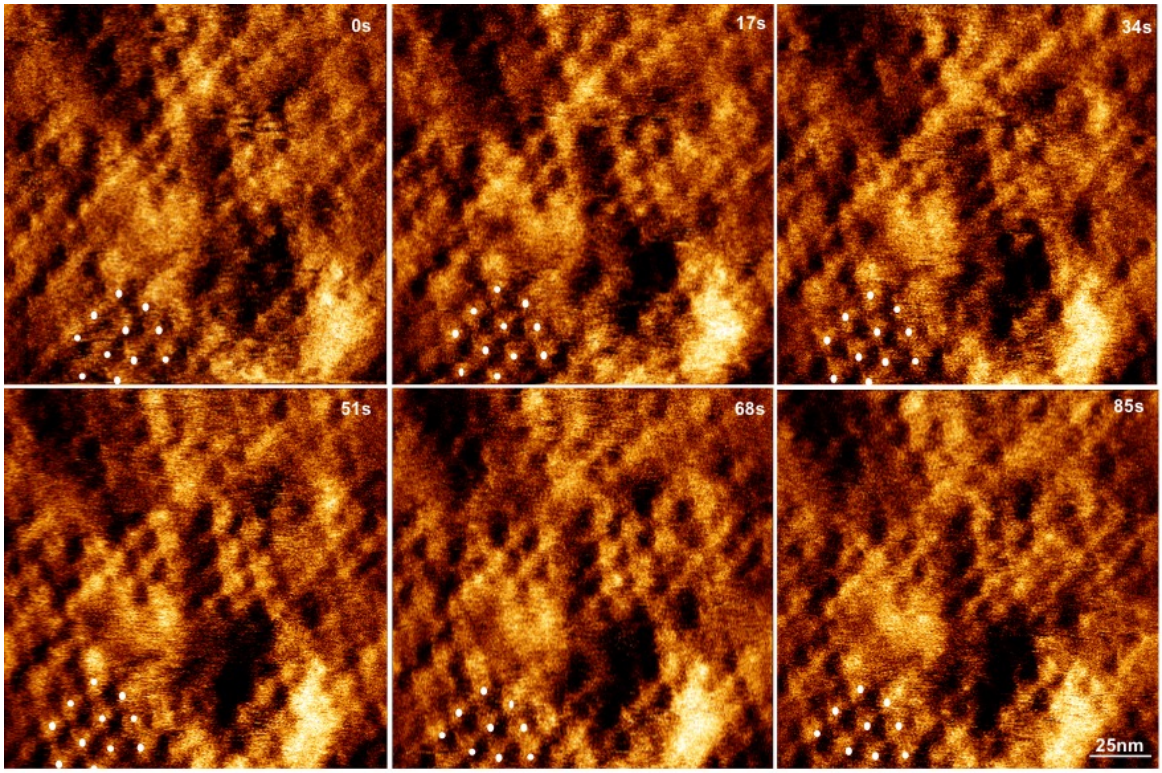


**Figure 4.6. High-speed AFM imaging reveals the stable organization of RC-LH1 complexes in isolated photosynthetic membranes.** Time-lapse AFM amplitude error signal images were captured at 17 sec per frame, revealing no detectable changes in the 4Hcyt subunit (white dots) organization within 85 sec.

### *4.2.3 Mechanical unfolding of the 4Hcyt subunit*

By applying the scanning force of ~200 pN during AFM imaging, previous studies have reported that the globular 4Hcyt structure could be mechanically removed (Liu *et al.*, 2011), indicating its flexible binding with the RC subunits. To examine the mechanical properties of 4Hcyt, AFM-based single-molecule force measurement was exploited to unfold the 4Hcyt heads of the RC-LH1 complex in the native membrane environment. The C-terminal end of 4Hcyt is exposed away from periplasmic side of the photosynthetic membranes (Fig. 4.7). We placed the AFM probe onto a *Blc. viridis* photosynthetic membrane patch to non-specifically attach the C-terminus of 4Hcyt with a controlled loading force ≤1 nN for ~1 s. Then the probe was retracted from the membrane surface at a constant velocity of 200 nm·s−1 (Fig. 4.8A) and the force was recorded as a function of the distance between the AFM probe and membrane surface (shown as force−distance curves).

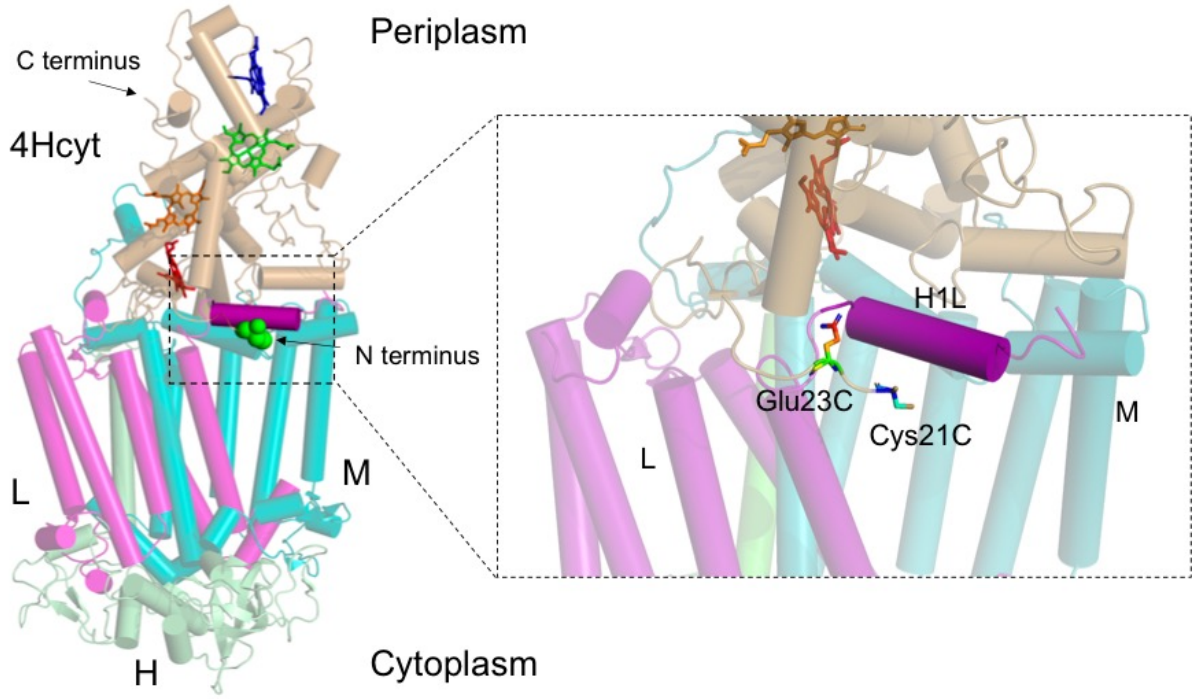


**Figure 4.7. Interactions of 4Hcyt with the L subunit in the RC complex.** The structure was presented using the atomic structure of RC (PDB ID: 1PRC). The four coloured heme groups are shown in sticks. The residues Cys21C and Glu23C at the

N-terminal end of 4Hcyt have close contacts with the first α-helix from the C-terminus of the L subunit.

AFM topographic analysis of the membranes before and after force measurements allowed us to determine the specific unfolding events. Individual RC-LH1 complexes were visualized in their associations with neighbouring RC-LH1 structures prior to force measurements (Fig. 4.8B). Imaging the same membrane region after force measurements and cross-section analysis demonstrated the physical removal of 4Hcyt subunits from the RC-LH1 complex in the native photosynthetic membrane (Fig. 4.8C-E).

The force−distance curves that were compatible with a polymer-unfolding model (Liu *et al.*, 2008) were finally selected for further analysis (Fig. 4.9). Superposition of 200 force curves reveals a pattern of seven pronounced peaks, corresponding to 7 unfolding events (Fig. 4.8F), revealing a consistent unfolding pattern. By fitting each of the 7 force peaks with the WLC model using a persistence length of 0.4 nm (the approximate length of amino acid residues), we determined the contour lengths of the polypeptide segments unfolded in each unfolding event: 114, 173, 229, 306, 390, 475, and 508 amino acids (Fig. 4.8F, Table 4.1).

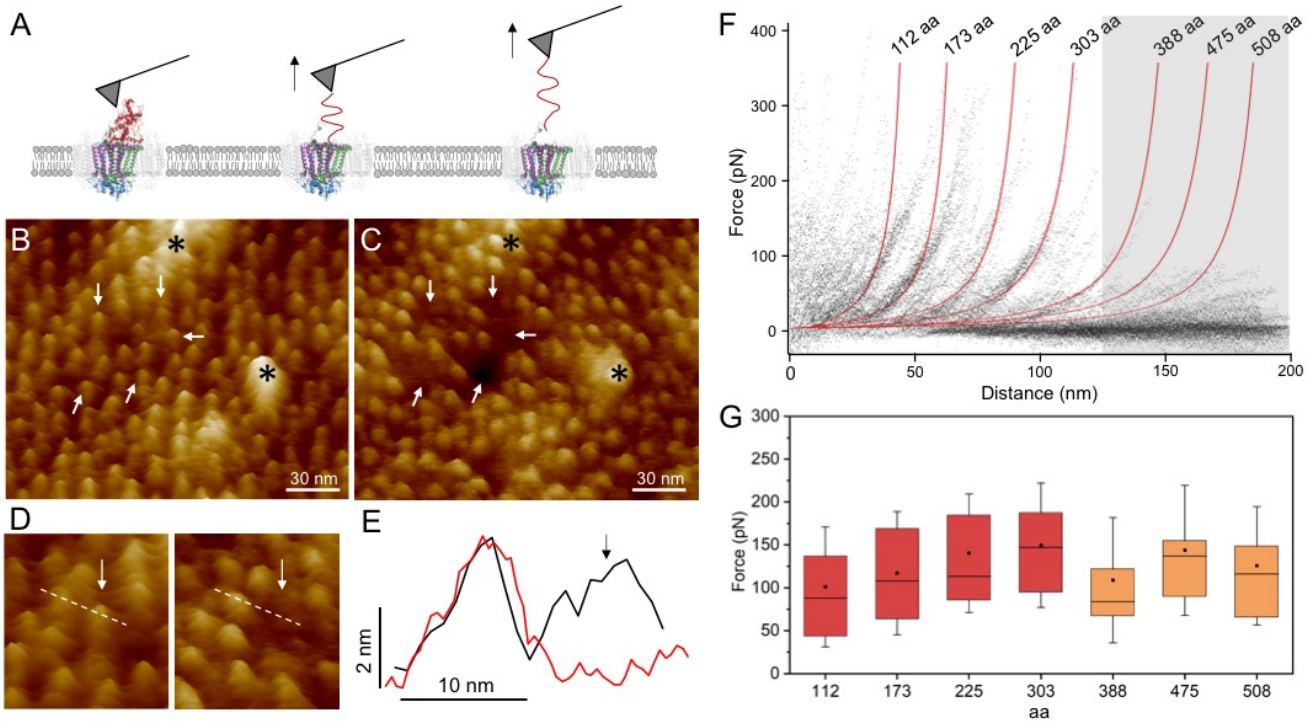


**Figure 4.8. Force measurements of 4Hcyt unfolding. A**. Schematic representation of single-molecule force spectroscopy (SMFS) on the *Blc. viridis* RC-LH1 complex. **B** and **C**. AFM images of the photosynthetic membrane fragment before and after force measurement. Medium-resolution AFM images allow precise alignment of images (stars indicate unchanged protein complexes). Force measurements have removed and unfolded the 4Hcyt subunits from the RC-LH1 complexes (white arrows). **D**. An example of the mechanical removal of a protruding 4Hcyt head. **E**. Height analysis along the dashed lines in D confirms the removal of the 4Hcyt subunit. **F**. Superimposed force-distance curves, each recorded upon mechanically unfolding a single 4Hcyt subunit from the RC-LH1 complex in the native membrane, reveal the unfolding pattern of 4Hcyt. Red and orange force-extension curves are Worm-Like Chain (WLC) curves, indicating the mean contour lengths of seven detected force peaks in the force-distance curves, 114, 173, 229, 306, 390, 475, and 508 amino acids (aa). **G**. Forces required in individual unfolding steps are 101.2 ± 9.7 pN for 114 aa ($n$ = 62), 117.1 ± 12.1 pN for 173 aa ($n$ = 42), 140.3 ± 12.4 pN for 229 aa ($n$ =

37), 149.5 ± 18.1 pN for 306 aa (*n* = 19), 108.9 ± 18.9 pN for 390 aa (*n* = 18), 143.7 ± 21.0 pN for 475 aa (*n* = 15), and 125.7 ± 28.1 pN for 508 aa (*n* = 7)(see Table 4.1).

**Table 4.1. Analysis of the unfolding events**

| Contour length | Force (pN) | Unfolding subunit | Residues | Helices |
|---|---|---|---|---|
| 114 aa | 101.2 ± 9.7 | 4Hcyt | Gly349C − Arg236C | H1-H8 |
| 173 aa | 117.1 ± 12.1 | 4Hcyt | Ser235C − Arg177C | H9-H10 |
| 229 aa | 140.3 ± 12.4 | 4Hcyt | Asn176C − Lys121C | H11-H12 |
| 306 aa | 149.5 ± 18.1 | 4Hcyt | Ala120C − His44C | H13-H16 |
| 390 aa | 108.9 ± 18.9 | 4Hcyt, L | Leu43C − Cys21C Asp269L − Thr209L | H1-H3 |
| 475 aa | 143.7 ± 21.0 | L | Lys208L − Cys123L | H4-H5 |
| 508 aa | 125.7 ± 28.1 | L | Phe122L − Ile90L | H6 |

The forces required in individual unfolding steps within the 4Hcyt subunit are 101.2 ± 9.7 pN for 114 aa (*n* = 62), 117.1 ± 12.1 pN for 173 aa (*n* = 42), 140.3 ± 12.4 pN for 229 aa (*n* = 37), and 149.5 ± 18.1 pN for 306 aa (*n* = 19)(Fig. 4.8G, Table 4.1). An average rupture force is approximately 121.2 ± 5.6 pN (*n* = 200), with comparable magnitudes as those determined for unfolding of the muscle protein titin (Nogi *et al.*, 2005), the extracellular matrix glycoprotein tenascin (Vasilev *et al.*, 2014), the transmembrane protein in an LH2 complex (Bustamante *et al.*, 1994) and bacteriorhodopsin (Wöhri *et al.*, 2009) at similar pulling velocities. The determined rupture force is slightly lower than the AFM scanning force of 200 pN, explaining to some extent why AFM nanodissection could cause removal of 4Hcyt (Liu *et al.*, 2011).

In addition, the rupture force increases as more of the peptide fragments are unfolded (Fig. 4.8G), indicative of an increase in the strength of each consecutive structural segment. The locations of these structural components are specified below.

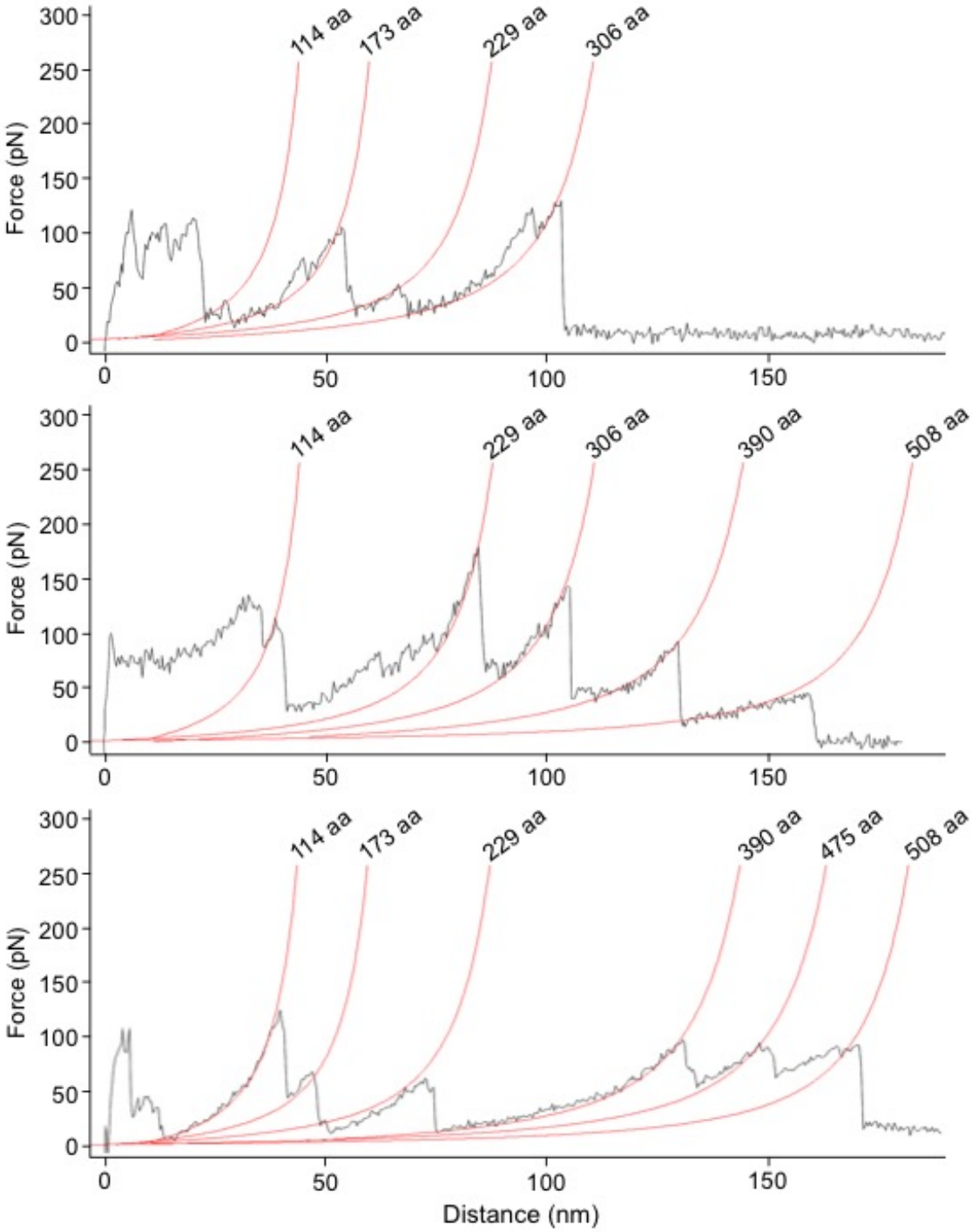


**Figure 4.9. Selected single force-distance curves (black) with individual peaks fitted by the WLC model (red) denote different structural intermediates in the**

**unfolding pathways.** The mean contour lengths of detected force peaks are indicated.

To investigate the detailed gradual unfolding pattern, we analyzed the secondary and three- dimensional structures of the *Blc. viridis* 4Hcyt subunit (Fig. 4.10, Fig. 4.11). The 4Hcyt subunit is 356 amino acids long (Uniprot ID: P07173). The predominant elements of the 4Hcyt secondary structure are α-helices, and β-sheets are rare. Residues Lys356C to Pro350C (C represents the PufC subunit) at the C-terminus of the Cyt subunit are completely disordered and were not structurally solved (Liu *et al.*, 2009). The tip−sample separation led to unfolding of the 4Hcyt subunit from the C-terminus. The first peak of the force curve displays an unfolding length of 114 aa (Fig. 4.8F), revealing the unfolding of α-helices 1-8 of the 4Hcyt subunit from residues Gly349C to Arg236C (Fig. 4.10A, B, Fig. 4.11, Table 4.1). This unfolding event requires approximately 101.2 pN. Subsequently, the α-helices 9-10 (Ser235C−Arg177C), 11-12 (Asn176C−Lys121C) and 13-16 (Ala120C−His44C) were unfolded, corresponding to the second, third, and forth peaks of the force curve with the unfolding length of 173, 229, and 306 aa, respectively (Fig. 4.10A, B, Fig. 4.11, Table 4.1). The covalent binding of heme to the 4Hcyt protein subunit might perturb these contour lengths slightly.

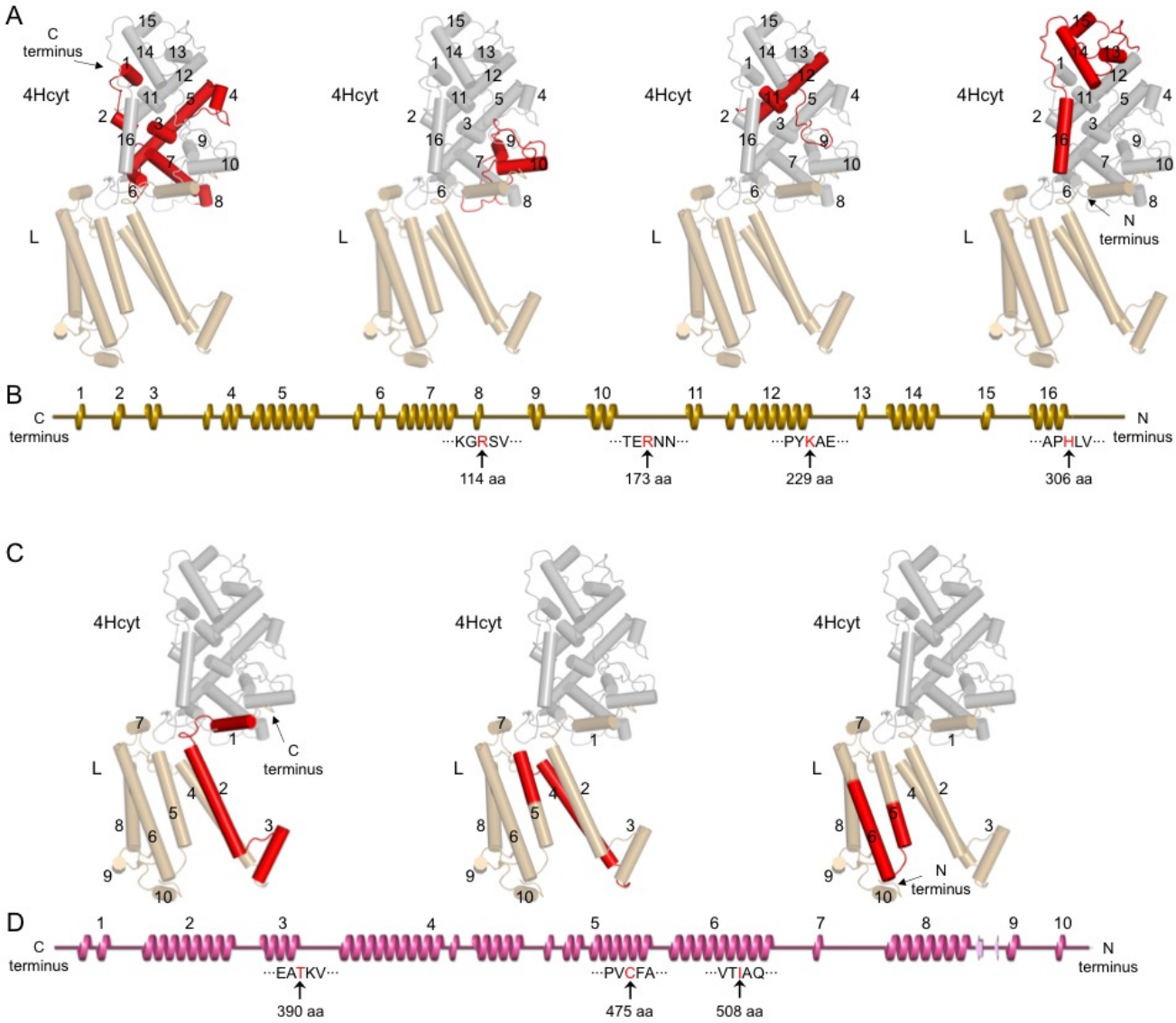


**Figure 4.10. Proposed unfolding pathways of the *Blc. viridis* RC-LH1 4Hcyt and L subunits. A.** Sequential unfolding of the 4Hcyt subunit (grey) of the RC complex (PDB ID: 1PRC), starting from the C-terminal end to the N-terminus. The 15 α-helices of 4Hcyt are numbered and the structural segments unfolding in each unfolding step are highlighted in red. The interacting L subunit is shown in brown. **B.** Secondary structure model of the 4Hcyt subunit with the residues (red, indicated by arrows) unfolded in each unfolding step. The 15 α-helices of 4Hcyt are numbered. **C.** Sequential unfolding of the L subunit (brown) of the RC complex induced by 4Hcyt unfolding, starting from the C-terminal end to the N-terminus. The N-terminal end of

the 4Hcyt subunit interacts with the first α-helix at the C-terminus of the L subunit. The structural segments unfolding in each unfolding step are highlighted in red. **D.** Secondary structure model of the L subunit with the residues (red, indicated by arrows) unfolded in each unfolding step. The 10 α-helices of the L subunit are labelled.

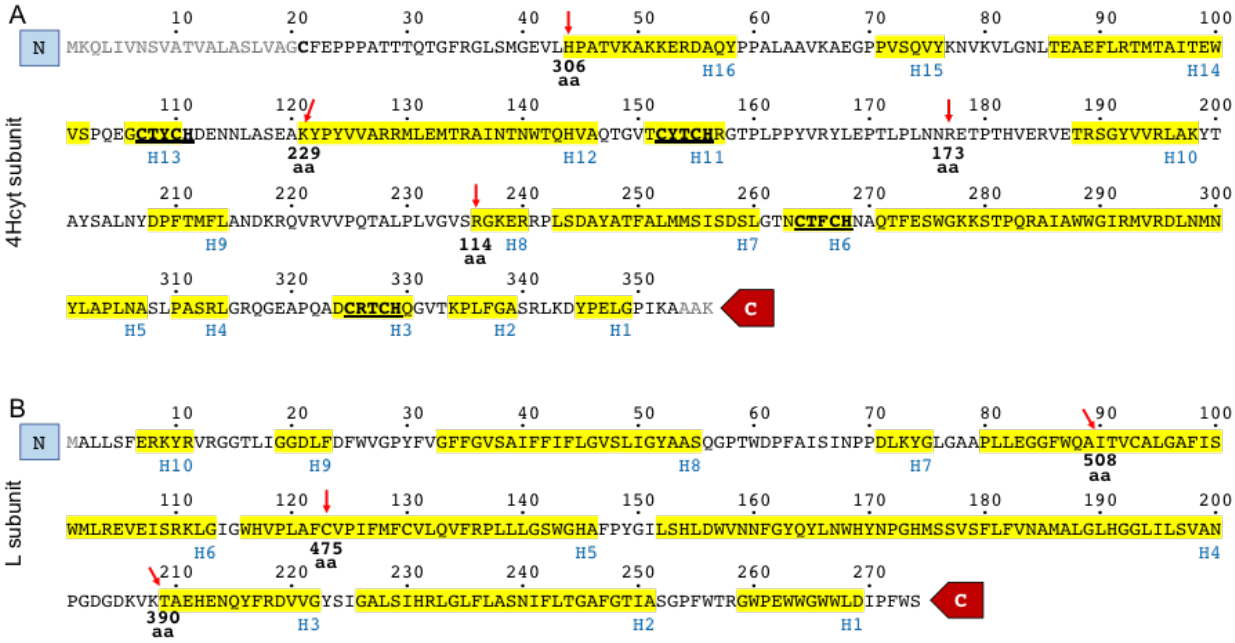


**Figure 4.11. Peptide sequence analysis of the *Blc. viridis* 4Hcyt and L subunit.** Protein sequences were acquired in Uniprot: 4Hcyt (Uniprot ID: P07173) and L subunits (Uniprot ID: P06009). The α-helices are highlighted in yellow and numbered. Red arrows indicate the key residues in the unfolding events. The heme-binding residues were indicated by underlines.

### *4.2.4 Unfolding of 4Hcyt could result in unfolding of the RC L subunit*

Interestingly, there are only 328 amino acids from the first α-helix at the C-terminus (Gly349C) to the Cys21C at the N-terminal region of the 4Hcyt subunit. The occurrence of the remaining three unfolding events with contour lengths of 388, 475 and 508 aa (fitted with orange curves) indicated that the unfolding of 4Hcyt resulted in

the unfolding of the transmembrane RC L and M subunits that interact with 4Hcyt. Structural analysis revealed that the Cyt residues in the connecting sequences between heme-binding segments form interactions with the M subunit, whereas the Cyt N-terminal segment (residues 1-40) contacts only with the L subunit (Liu *et al.*, 2009). In particular, the residues Cys21C and Glu23C have close contacts with the first α-helix from the C-terminus of the L subunit (Fig. 4.7).

The fifth force peak with the unfolding length of 390 aa indicates that pulling the 4Hcyt peptide by the AFM probe resulted in unfolding of α-helices 1-3 from residues Asp269L to Thr209L (L represents the PufL subunit) (Fig. 4.10C, D). This unfolding event requires a force of 108.9 ± 18.9 pN ($n$ = 18). The last two unfolding events occur with the unfolding lengths of 475 and 508 aa, corresponding to the unfolding of α-helices 4-5 (Lys208L−Cys123L) and the α-helix 6 (Phe122L−Ile90L) with the required forces of 143.7 ± 21.0 pN ($n$ = 15) and 125.7 ± 28.1 pN ($n$ = 7), respectively. These results demonstrate that the interacting force between the 4Hcyt N-terminus and the C-terminus of the L subunit is larger than the maximum unfolding force detected in unfolding of the L subunit (143.7 pN). The strong binding between 4Hcyt and the transmembrane RC subunits may provide the foundation for efficient electron flow. It is also worth noting that the chance to record longer unfolding events over 306 aa is lower than shorter unfolding events, suggesting that the L subunit could break at any amino acid residue during the unfolding events due to the unspecific binding between the AFM probe and 4Hcyt and relatively weak interactions between 4Hcyt and the L subunit. This may explain the fact that only partial unfolding of α-helices 5 and 6 was detected in the 475 and 508 aa unfolding events (Fig. 4.10C, D).

In some purple photosynthetic bacteria that lack the 4Hcyt subunit in the RC complex, the soluble electron carrier Cyt $c_2$ docks directly to the RC complex through electrostatic interactions (Weyer *et al.*, 1987). The specific binding has allowed the recognition of the *Rba. sphaeroides* RC complexes using the AFM probes pre-modified with Cyt $c_2$ (Canniffe and Hunter, 2014). Interestingly, the measured unbinding force was above 160 pN, higher than the average force required for the unfolding of the 4Hcyt subunit. It remains unclear whether the AFM-induced unbinding of Cyt $c_2$ from the RC could result in unfolding of RC subunits.

The CysC-1 at the N-terminus of the *Blc. viridis* 4Hcyt subunit (Fig. 4.10A) has been characterized to bind with a covalently bound lipid through a thioether bond and function as a membrane anchor for 4Hcyt to associate with the periplasmic surface of the photosynthetic membrane prior to interacting with other RC subunits (Bahatyrova, Frese, Siebert, *et al.*, 2004; Roszak *et al.*, 2012). However, the binding between 4Hcyt and the lipid membrane may be relatively small to measure in SMFS.

### 4.3 Concluding Remarks

Using AFM imaging and SMFS, this study provides quantitative insight into the organisation of photosynthetic complexes and the assembly mechanisms of the RC complex from the BChl *b*-producing purple bacterium *Blc. viridis*. The RC-LH1 complexes are densely organized in native photosynthetic membranes. Mechanical unfolding of the globular 4Hcyt subunit at the periplasmic side of the RC represents a stepwise process. Removal of the 4Hcyt subunit also resulted in the unfolding of the L subunit of the RC complex, indicating strong binding of the non-membranous 4Hcyt structure to the RC transmembrane subunit. We anticipate that our approach will

provide a means of studying the folding and interactions of membrane-associated proteins and the assembly of membrane protein complexes at the single-molecule level, allowing the exploration and reprogramming of native and synthetic biological membranes.

# CHAPTER V
# The Roles of PufX in Determining the RC-LH1 Core Complex Structure

# 5 The Roles of PufX in Determining the RC-LH1 Core Complex Structure

## 5.1 Introduction

In purple bacteria, a set of highly organised pigment-protein complexes are responsible for the absorption of light energy and its subsequent conversion into biochemical energy. As discussed in Chapter I of this thesis, light is initially collected by a peripheral LH complex, LH2, and transduced to a second antenna complex, LH1. The excitation energy from LH1 is funnelled to the special pair of BChl in the RC for light-driven charge separation to take place. Reducing equivalents are then passed from the RC to the cytochrome (cyt) $bc_1$ complex via quinol exchange at the $Q_B$ site of RC (Okamura *et al.*, 2000; Francia *et al.*, 2004).

*Rba. sphaeroides* is an important model species to uncover the molecular mechanisms underlying photosynthetic energy transduction, due to the well-established genetic modification procedure, as well as extensive biochemical and spectroscopic characterisations. The structures of the photosynthetic complexes in *Rba. sphaeroides* are well documented (see **Chapter I** of this thesis); the LH1 antenna are made up of α- and β-polypeptides (*pufA* and *pufB*) which non-covalently bind to the bacteriochlorophyll (BChl) and carotenoid pigments (Brunisholz and Zuber, 1992; Zuber and Cogdell, 2004; Qian, 2017). The *Rba. sphaeroides* RC complex is composed of L, M and H subunits (*pufL, pufM, puhA*); LH1 forms a stoichiometric complex with the RC, completely surrounding the complex (Qian *et al.*,, 2005). In the native photosynthetic membranes of *Rba. sphaeroides,* the RC-LH1 complexes associate in two forms, a dimeric form whereby two RCs are surrounded by an S-

shaped LH1 aggregate (Jungas *et al.*, 1999; Bahatyrova *et al.*, 2004; Scheuring *et al.,*, 2005) and a monomeric form whereby one RC is surrounded by a C-shaped LH1 aggregate, some also consist of a complete LH1 ring or with a small gap (see details in **Chapter I** of this thesis) (Jungas *et al.*, 1999; Scheuring *et al.*, 2006; Liu *et al.*, 2011). The RC-LH1 complexes of *Rba. sphaeroides* have been documented by EM as dimers (Jungas *et al.*, 1999; Siebert *et al.*, 2004; Qian *et al.*, 2005); the dimeric structures have also been visualised in their native membranes by AFM in both *Rba. sphaeroides* and *Rba. blasticus* (Bahatyrova *et al.*, 2004; Scheuring *et al.*, 2004; Scheuring *et al.*, 2005). However, another *Rhodobacter* species, *Rba. veldkampii*, contains monomeric RC-LH1 complexes, as visualised by AFM of intact membranes and cryo-EM of isolated complexes (Busselez *et al.*, 2007; Liu *et al.*, 2011).

Some LH1 antennas also contain additional subunits; the *Rhodopseudomonas* (*Rps.*) *palustris* LH1 ring contains a single transmembrane helix known as protein W (Jackson *et al.*, 2018), and the *Rhodobacter* species contain a PufX polypeptide (Klug *et al.*, 1988; Farchaus *et al.*, 1990; Lilburn *et al.*, 1992). PufX and Protein W create a channel in their respective LH1 rings allowing quinone/quinol exchange between the RC and the cytochrome (cyt) $bc_1$ complex (Barz *et al.*, 1995; Francia *et al.*, 1999; Qian *et al.*, 2013). An additional LH1 γ subunit was also identified in BChl *b*-containing Blc*. viridis*; all studied BChl *a*-containing organisms lack a γ subunit in LH1.

The PufX protein consists of a single membrane-spanning α-helix preventing the complete encirclement of the LH1 around the RC (Walz *et al.*, 1998; Siebert *et al.*, 2004). Removal of the *pufX* gene from *Rba. sphaeroides* results in the loss of photosynthetic growth (Klug *et al.*, 1988; Farchaus *et al.*, 1990; Lilburn *et al.*, 1992)

and the formation of exclusively monomeric RC-LH1 complexes (Walz *et al.*, 1998; Siebert *et al.*, 2004). PufX is considered a major factor in the dimerization of RC-LH1 complexes in *Rba. sphaeroides*; truncation 18 of the N-terminus residues of PufX resulted in the loss of dimeric RC-LH1 complexes (Francia *et al.*, 2002; Ratcliffe *et al.*, 2011). However, despite possessing a PufX protein, *Rba. veldkampii* RC-LH1 complexes are exclusively monomeric (Busselez *et al.*, 2007; Liu *et al.*, 2011), therefore other factors must also play a role in the dimerization.

*Rba. sphaeroides* chromatophores do contain a minor population of monomeric RC-LH1 complexes alongside the dimeric RC-LH1 complexes (Bahatyrova, Frese, Siebert, *et al.*, 2004; Adams *et al.*, 2011); the atomic-level model of a 50 nm ICM vesicle revealed that it consists of 67 LH2, 11 LH1–RC dimers, 2 RC–LH1 monomers, 4 cyt $bc_1$ dimers, and 2 ATP synthases (ATPase) (Cartron *et al.*, 2014). Similarly, *Rba. blasticus* chromatophores contains 25% monomeric RC-LH1 complexes (Scheuring *et al.*, 2005a). The advantage of the dimeric architecture and the reasons why some species do not contain dimeric complexes remain unknown. The PufX polypeptide contains a relatively low degree of sequence identity across the *Rhodobacter* species (Tsukatani *et al.*, 2004); *Rba. sphaeroides* contains 23% sequence identity with *Rba. veldkampii* (Table 5.1) and *Rba. capsulatus,* and 26% with *Rba. blasticus*. This is much lower than for the RC and LH1 polypeptides making up the remainder of the RC-LH1 complexes. A possible dimerization motif is present in *Rba. sphaeroides* PufX in the sequence $G^{31}xxxG^{35}xxxG^{39}$, whereas the equivalent sequence in *Rba.* v*eldkampii*, as can be seen in the multiple sequence alignment between the two PufX's (Fig. 5.1A), is GxxxVxxxG (Busselez *et al.*, 2007); Leu substitutions at the Gly residues in *Rba. sphaeroides* had no effect on the monomer and dimer amounts (Crouch *et al.*, 2010).

In a mutant species of *Rba. sphaeroides* in which PufX was replaced by the *Rba. capsulatus* PufX that has a low sequence identity with *Rba. sphaeroides* PufX, the dimeric architecture of the complex was lost (Crouch and Jones, 2012), although the photosynthetic growth of the mutant was retained. The role of PufX in the organisation and architecture of the RC-LH1complex is still unclear.

In this work, we apply spectroscopy, TEM and AFM to study the cross-species effects of PufX on the organisation and architecture of the RC-LH1 complex and the ICM in a strain of *Rba. sphaeroides* containing PufX of *Rba. veldkampii*.

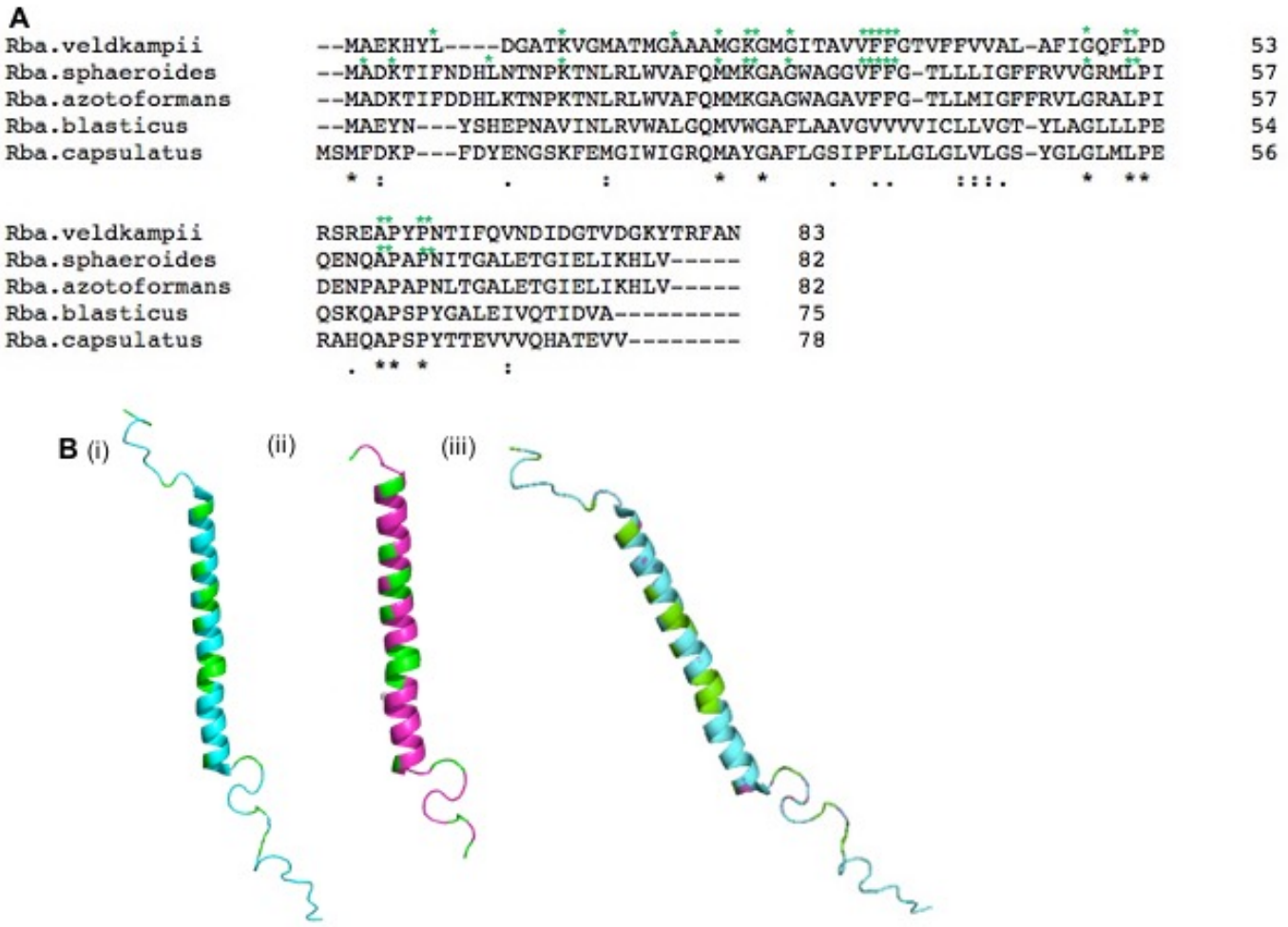


**Figure 5.1. PufX protein from *Rhodobacter* species. A.** Multiple sequence alignment of PufX sequences from different species. The green stars highlight the conserved residues in *Rba. sphaeroides* and *Rba. veldkampii* shown in **B**. **B.**

Comparison of PufX 3D Structure. (i) NMR solution structure of *Rba. sphaeroides* WT PufX (Wang *et al*., 2007; PDB: 2DW3), (ii) Phyre2 structural prediction of *Rba. veldkampii* PufX (Kelley *et al*., 2015) and (iii) overlay of both structures. PufXs and PufXv are represented in cyan and magenta, respectively. Conserved residues are represented in green.

**Table 5.1. RC-LH1-PufX component sequence identities.**

| ***Rba. sphaeroides*** **protein** | **Encoding gene** | **Percentage identity** ***Rba. veldkampii*** |
|---|---|---|
| LH1 β (PufB) | *pufB* | - |
| LH1 α (PufA) | *pufA* | - |
| RC L (PufL) | *pufL* | 70 |
| RC M (PufM) | *pufM* | 74 |
| RC H (PuhA) | *puhA* | - |
| PufX | *pufX* | 23 |

## 5.2 Results

### *5.2.1 Cell growth*

Cultures of *Rba. sphaeroides* wild-type (WT) (DSMZ 158, Germany), *Rba. sphaeroides* $\Delta pufX_{Rs}::pufX_{Rv}$ (Fig. 5.2) (provided by Dr Dan Canniffe, University of Liverpool) and *Rba. veldkampii* (WT) were grown in M22$^{+}$ medium (**Appendix A**) under anaerobic conditions at 30 $^{o}$C under normal white light. *Rba. sphaeroides ΔpufX* culture was also grown in M22$^{+}$ medium (**Appendix A**) at 30 $^{o}$C, but under aerobic

conditions in the dark; a second *Rba. sphaeroides* WT culture was also grown in these conditions. The room-temperature absorption spectra of these cultures (Fig. 5.3) reveal the characteristic peaks at 800 and 850 nm corresponding to the LH2 complex, with a shoulder at 875 nm corresponding to the LH1 complex and the group of peaks around 500 nm corresponding to the carotenoids; this shows that the cultures contain all the necessary pigments for photosynthetic growth. There is no difference in the absorption spectra of the different strains. This shows that photosynthetic growth of *Rba. sphaeroides* is not impaired if the *Rba. sphaeroides* PufX ($PufX_{Rs}$) is replaced by the PufX from *Rba. veldkampii*, and implies that some roles of the native $PufX_{Rs}$ are fulfilled by $PufX_{Rv}$.

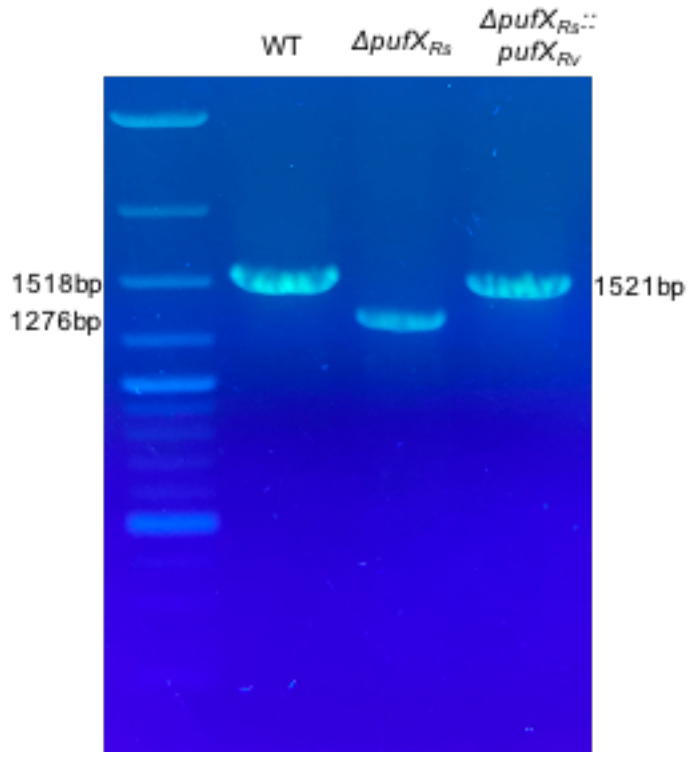


**Figure 5.2. PCR verification of the strains.**

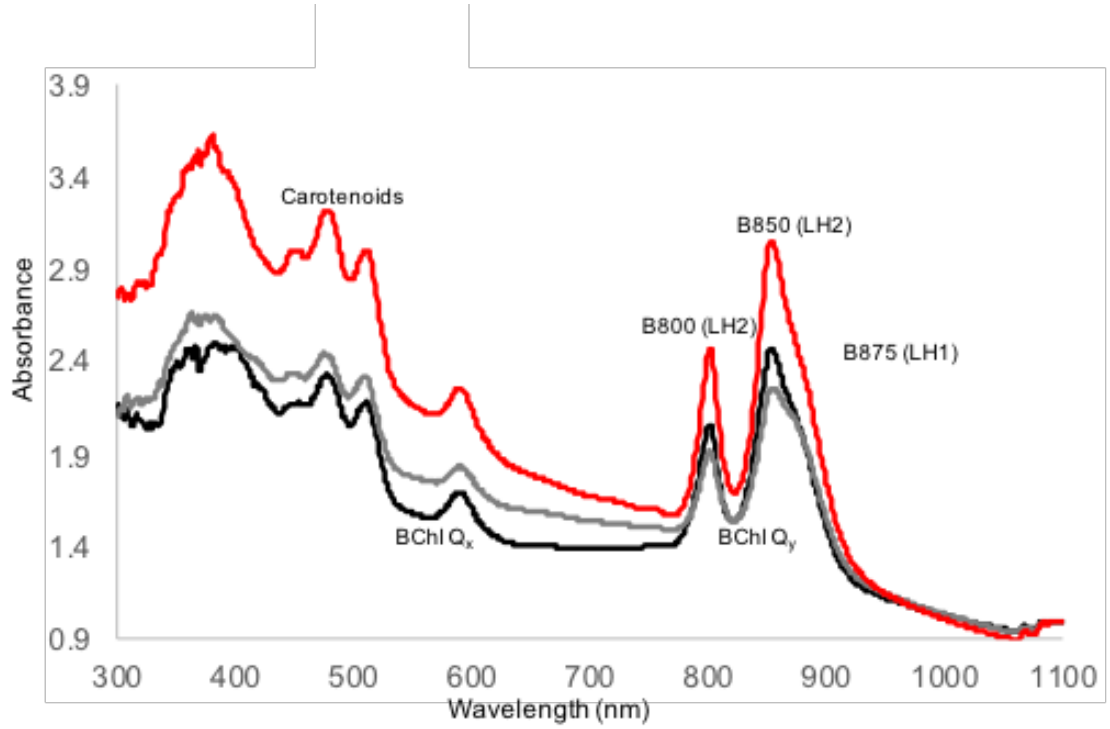


**Figure 5.3. Absorption spectra of purple bacterial cultures.** The absorption spectra of *Rba. sphaeroides* WT, *Rba. sphaeroides* Δ*pufX*$_{Rs}$::*pufX*$_{Rv}$ and *Rba. veldkampii* WT cultures are shown in black, grey and red, respectively.

### *5.2.2 Assessing the composition of RC-LH1-PufX complexes*

The pigment-protein complexes in *Rba. sphaeroides* WT (grown in light) and *Rba. sphaeroides* Δ*pufX*$_{Rs}$::*pufX*$_{Rv}$ were analysed by the extraction of the RC-LH1-PufX and LH2 complexes using mild concentration of detergent β-DDM (0.03%) and fractionation by sucrose gradient ultracentrifugation (Fig. 5.4A, carried out by Laura Bracun at the University of Liverpool). The sucrose gradients from these species resulted in varied numbers of pigmented bands; the faint orange band at the top of the first two sucrose gradients is attributable to free carotenoid spheroidene, which is the main carotenoid in *Rba. sphaeroides* when grown under photosynthetic conditions. The intense green bands further down are attributable to the peripheral LH2 antenna. The middle green bands are attributable to the monomeric RC-LH1-PufX complexes,

present in both species. The band below representing RC-LH1-PufX dimers was only present in photosynthetically grown *Rba. sphaeroides* WT. This reveals that *Rba. sphaeroides* $\Delta pufX_{Rs}::pufX_{Rv}$ forms a monomeric RC-LH1-PufX complex similar to the complex from *Rba. veldkampii* (Gubellini *et al.*, 2006; Liu *et al.*, 2011). The absorption spectra (Fig. 5.4B) reveals similar line shapes for the different species and contain all the expected peaks. The $A_{LH1}/A_{RC}$ of the *Rba. sphaeroides* $\Delta pufX_{Rs}::pufX_{Rv}$ RC-LH1-PufX complex is 3.7, reduced from both WT *Rba. sphaeroides* (4.2) and *Rba. veldkampii* (4.8) (Table 5.2, $n$ = 1). This reduced ratio suggests that there are fewer LH1 proteins per RC, further indicating a monomer assembly. This phenomenon has been seen previously in mutant studies by Crouch and Jones, 2012 and McGlynn and colleagues (McGlynn, Hunter and Jones, 1994; Crouch and Jones, 2012).

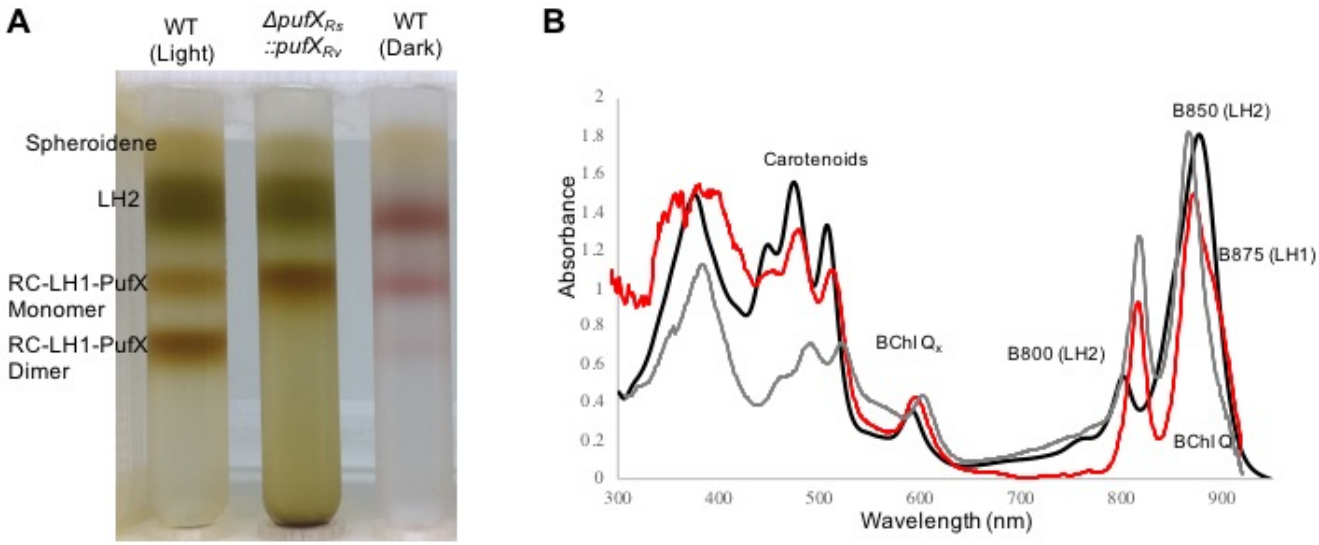


**Figure 5.4. Comparative sucrose gradient shows that PufX is a monomer in *Rba. sphaeroides* $\Delta pufX_{Rs}::pufX_{Rv}$. A.** Comparative sucrose gradients of *Rba. sphaeroides* WT (left) and *Rba. sphaeroides* $\Delta pufX_{Rs}::pufX_{Rv}$ (right) both reveal a faint orange band at the top of the first two sucrose gradients attributable to free carotenoid spheroidene. The intense green bands further down are attributable to the peripheral LH2 antenna. The middle green bands are attributable to the monomeric RC-LH1-

PufX complex. The absorption spectra of *Rba. sphaeroides* WT RC-LH1-PufX dimer, *Rba. sphaeroides* ΔpufX$_{Rs}$::pufX$_{Rv}$ RC-LH1-PufX complex and *Rba. veldkampii* WT RC-LH1-PufX complexes (sucrose gradient not shown) are shown in **B** represented by grey, black and red lines, respectively.

**Table 5.2. LH1:RC ratios.**

| **Strain** | **$A_{LH1}/A_{RC}$** | **Monomeric/dimeric RC-LH1-PufX** | **References** |
|---|---|---|---|
| *Rba. sphaeroides* WT (light) | 4.2 | Dimer, some monomers | Current study |
| *Rba. sphaeroides* WT (dark) | 4.4 | Monomer, some dimer | Current study |
| *Rba. veldkampii* WT | 4.8 | Monomer | Current study |
| *Rba. sphaeroides* *ΔpufX$_{Rs}$::pufX$_{Rv}$* | 3.6 | Monomer | Current study |
| *Rba. sphaeroides* RC-LH1 *Rba. capsulatus* PufX (light) | 3.9 | Dimer | Crouch and James, 2012 |
| *Rba. capsulatus* RC-LH1-PufX (light) | 3.7 | Monomer | Crouch and James, 2012 |
| *Rba. capsulatus* RC-LH1 *Rba. sphaeroides* PufX, no LH2 (dark) | 3.9 | Monomer | Crouch and James, 2012 |

### *5.2.3 Difference in the ICM and cell morphology of PufX mutants*

In order to study the morphologies of the ICMs *in vivo*, thin-section electron microscopy of whole cells was performed (supported by Greg Dykes at the University of Liverpool). As can be seen in Fig. 5.5, in the *Rba. sphaeroides* WT cells that contain mainly dimeric RC-LH1-PufX complexes according to comparative sucrose gradients (Fig 5.4A), the outer-membrane (OM) and cytoplasmic membrane (CM) were both visible; the ICMs were visualised as vesicles with an average diameter of 48 ± 8 nm ($n$ = 50, Fig 5.5A). Similar ICM morphologies were seen in *Rba. sphaeroides* grown in the dark (Fig. 5.5B), which contained mainly monomeric RC-LH1-PufX complexes (Fig. 5.4A), however the number of the ICMs were increased by ~16 (Fig. 5.5Bii). The diameter of the vesicles seen in *Rba. sphaeroides* grown in the dark were significantly larger than those seen in the cells grown in light (Fig. 5.5B, 52 ± 6 nm, $p < 0.05$, $n$ = 50). *Rba. sphaeroides ΔpufX* cells also contain vesicular ICMs, however the ICMs were far less well defined (Fig. 5.5C); the vesicles which were present were significantly smaller (40 ± 4 nm, $p < 0.05$, $n$ = 10) than WT *Rba. sphaeroides*.

Ovoid *Rba. veldkampii* cells, containing monomeric RC-LH1-PufX complexes, also contain vesicular ICMs. The diameters of the vesicular ICMs were significantly smaller than WT *Rba. sphaeroides* (Fig 5.5D, 44 ± 6 nm, $p < 0.05$, $n$ = 50). In the *Rba. sphaeroides ΔpufX::pufX*$_{Rv}$ cells that contain only monomeric RC-LH1-PufX complexes (Fig. 5.4A), the ICMs have both vesicular and lamellar morphologies (Fig. 5.5E). The vesicular ICMs were significantly larger (51 ± 7 nm, $p < 0.05$, $n$ = 50) than those in *Rba. sphaeroides* WT grown in the light and *Rba. veldkampii* WT. However, they were not significantly different from the diameter of the vesicles seen in *Rba. sphaeroides* WT grown in the dark ($p > 0.05$, $n$ = 50). *Rps. palustris* also contain monomeric RC-LH1 complexes, however with the extra component protein W rather

than PufX (Jackson *et al.*, 2018); the ICM of these cells consist of lamellar structures, differing from the vesicular structures seen in *Rba. veldkampii* but similar to those seen in *Rba. sphaeroides ΔpufX$_{Rs}$::pufX$_{Rv}$* (Fig. 5.5F). This may suggest that the specific sequence and structure of PufX also has an influence on the morphology of the cell and the *in vivo* vesicular ICMs, rather than the monomeric or dimeric state of the PufX complex alone. Both RC-LH1$_{Rs}$-PufX$_{Rv}$ and RC-LH1$_{Rv}$-PufX$_{Rv}$ complexes form monomer assemblies. However, the interactions between LH1$_{Rs}$-PufX$_{Rv}$ appear to result in the formation of both vesicular and lamellar ICMs, whereas the LH1$_{Rv}$-PufX$_{Rv}$ interactions result in the formation of only vesicular ICMs. This indicates that the interaction between PufX and LH1 may play roles in determining the morphology of the ICM.

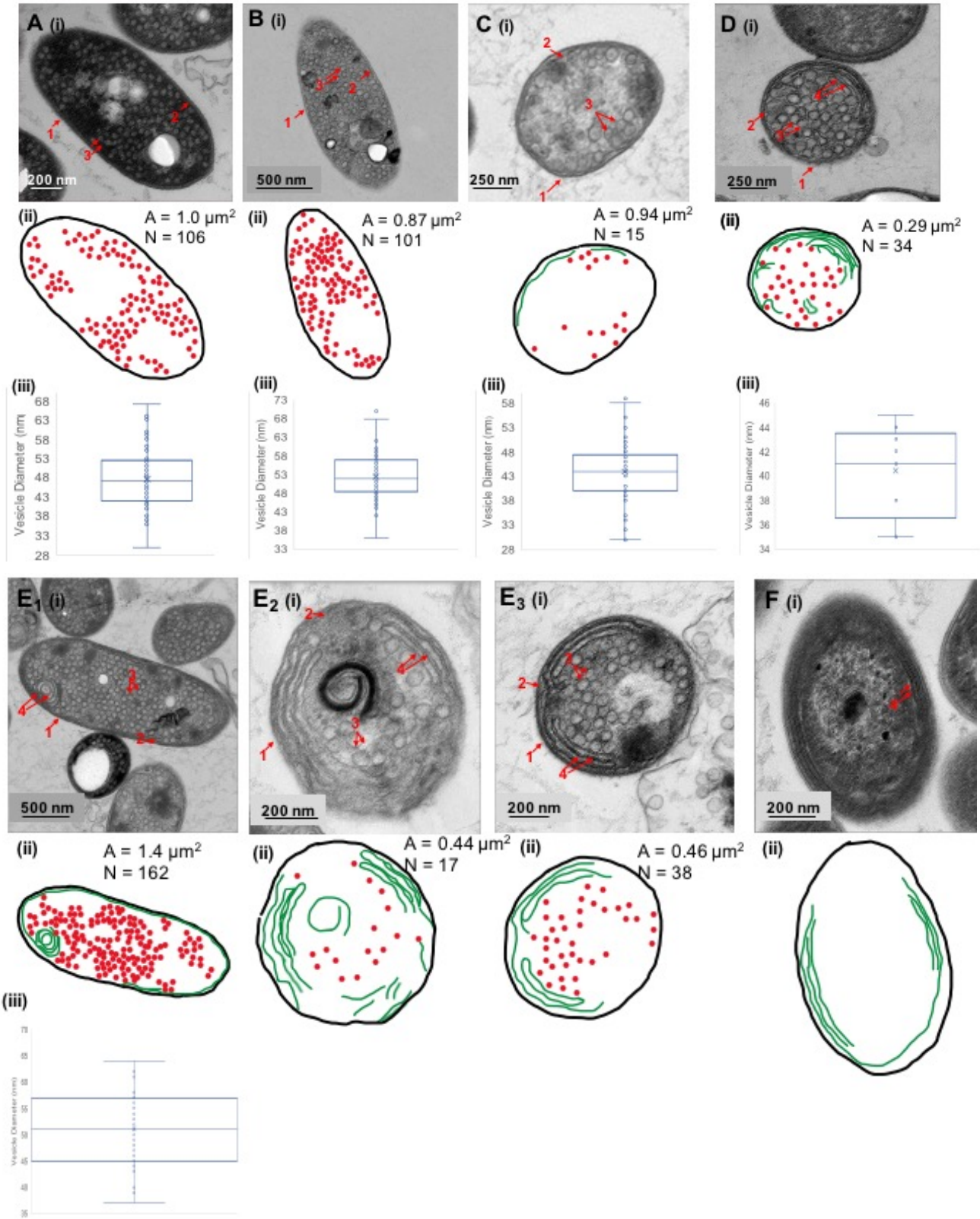


**Figure 5.5. Thin-section Transmission Electron Microscope images of purple bacterial cells. A.** *Rba. sphaeroides* WT cells grown in light containing vesicular ICMs with a diameter of 48 ± 8 nm (*n* = 50). **B.** *Rba. sphaeroides* WT cells grown in the dark

containing vesicular ICMs with a diameter of 52 ± 6 nm (*n* = 50). **C.** *Rba. veldkampii* WT cells containing vesicular ICMs with a diameter of 44 ± 6 nm (n = 50) and lamellar ICMs. **D.** *Rba. sphaeroides ΔpufX* cells containing vesicular ICMs with a diameter of 40 ± 4 nm (*n* = 10). **E.** *Rba. sphaeroides* $\Delta pufX_{Rs}::pufX_{Rv}$ cells containing vesicular ICMs with a diameter of 51 ± 7 nm (*n* = 50) and lamellar ICMs. **F.** *Rps. palustris* WT cells containing lamellar ICMs. (i) Thin-section transmission electron microscope (TEM) images of the purple bacterial cells. (ii) Schematic map of the manual identification of vesicular (red dots) and lamellar (green lines) ICMs in the respective TEM image. The area analysed is outlined by aa black line. (iii) Graph showing an analysis of the diameter of vesicles in the respective TEM images. 1 = outer membrane, 2 = cytoplasmic membrane, 3 = vesicular ICM and 4 = lamellar ICM. Vesicular and lamellar ICMs are represented in red and green respectively.

### 5.2.4 *Isolation of* Rba. sphaeroides WT *and* Rba. sphaeroides $\Delta pufX_{Rs}::pufX_{Rv}$ *photosynthetic membranes*

To assess the effects of $PufX_{Rv}$ on the composition of *Rba. sphaeroides* RC-LH1-PufX complex, the photosynthetic membranes from *Rba. sphaeroides* $\Delta pufX::pufX_{Rv}$ were isolated using sucrose gradient centrifugation (Fig. 5.6A). The absorption spectrum of the ICM (Fig. 5.6B) reveals characteristic peaks at 800 and 850 nm corresponding to the LH2 complex, with a shoulder at 875 nm corresponding to the LH1 complex and the group of peaks around 500 nm corresponding to the carotenoid. The $A_{LH1}/A_{RC}$ ratio of this complex was decreased (3.7, *n* = 1) compared to the WT structure (4.2, *n* = 1), however it was similar to a strain of *Rba. sphaeroides* containing PufX from *Rba. capsulatus* (Crouch and Jones, 2012), suggesting a monomer composition (Table 5.2). The lower LH1:RC ratio, and hence fewer LH1 per RC, suggests that $PufX_{Rv}$ has

increased the effectiveness with which the excitation energy from LH1 is used by the RC, suggesting a direct interaction between $PufX_{Rv}$ and *Rba. sphaeroides* RC-LH1 ($RC\text{-}LH1_{Rs}$).

SDS-PAGE revealed the presence of the most predominate photosynthetic proteins based on their molecular weights (Fig. 5.6C), comparable to previous studies of both *Rba. sphaeroides* and *Rba. veldkampii* photosynthetic membranes (Jungas *et al.*, 1999; Liu *et al.*, 2011). The LH1 α-polypeptide is not visible on the gel, however, the absorption spectra of the whole cell were identical to the isolated ICM spectra, indicating that the isolation process had no major effect on the photosynthetic machinery structure. This suggests either the LH1 α-polypeptide is present at very low amounts or that the polypeptide has no significant effect on the machinery. These spectroscopic and biochemical results demonstrated the structural integrity of the isolated photosynthetic membranes.

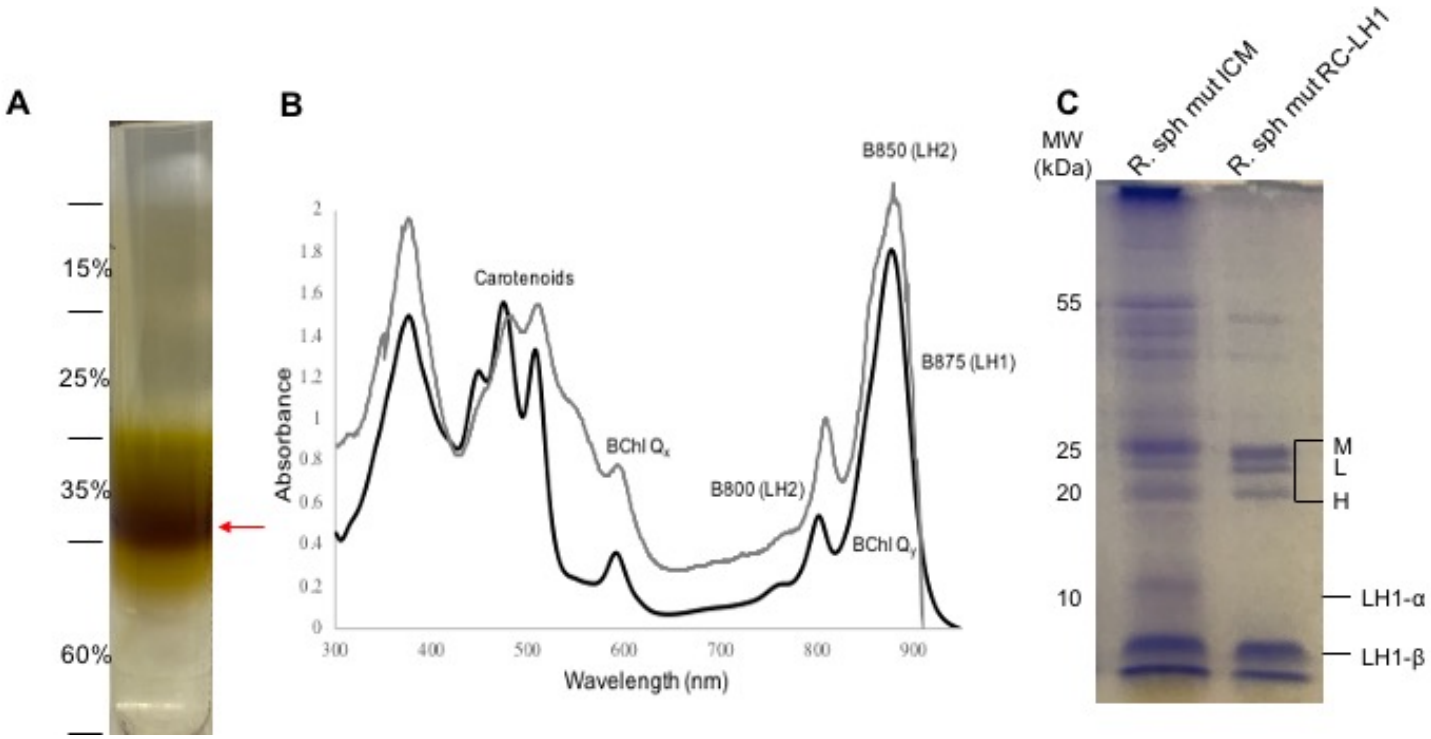


**Figure 5.6. Isolation and absorption spectra of the ICM from *Rba. sphaeroides* *ΔpufX$_{Rs}$::pufX$_{Rv}$*. A.** Step sucrose gradient centrifugation of the photosynthetic

membranes, containing 0.03% n-Dodecyl β-D-maltoside (β-DDM). Photosynthetic membranes at the 35%-60% interface were extracted for further analysis. **B.** Absorption spectra of the isolated photosynthetic membrane of *Rba. sphaeroides* *ΔpufX$_{Rs}$::pufX$_{Rv}$* and *Rba. sphaeroides* WT in black and grey, respectively. **C**. SDS-PAGE of the isolated photosynthetic membranes stained with Coomassie blue. The assigned components are labelled on the right. L: L subunit (PufL), M: M subunit (PufM), H: H subunit (PuhA).

### *5.2.5 PufX$_{Rv}$ reduces the ICM curvature compared to PufX$_{Rs}$*

To further determine the effects of PufX composition on the curvature of the ICM, we used AFM imaging to measure the curvature of the WT *Rba. sphaeroides* and *Rba. sphaeroides ΔpufX$_{Rs}$::pufX$_{Rv}$* ICMs. The isolated ICMs of *Rba. sphaeroides* WT and *Rba. sphaeroides ΔpufX$_{Rs}$::pufX$_{Rv}$* were immobilised on freshly cleaved mica substrate for AFM imaging. This revealed the curved ICM patches are larger than 200 nm for both strains, with the height of over 30 nm (Fig. 5.7). The WT vesicular structures are significantly more curved (height = 50 ± 22 nm, $n$ = 210) than the mutant vesicles (42 ± 16 nm, $p < 0.05$, $n$ = 206). This is in line with the TEM images of the whole cells which have larger and less curved vesicular ICMs (Fig. 5.5). PufX$_{Rv}$ appears to reduce the membrane curvature of the *Rba. sphaeroides* ICMs than both the native PufX$_{Rs}$ and PufX$_{Rv}$ in their native ICMs (Fig. 5.5). As discussed previously, *Rba. sphaeroides ΔpufX$_{Rs}$::pufX$_{Rv}$* has fewer LH1s per RC ($A_{LH1}/A_{RC}$ = 3.6, Table. 5.2); this reduction in LH1 complexes appears to also reduce the curvature of the vesicles and may even induce the formation of lamellar structures.

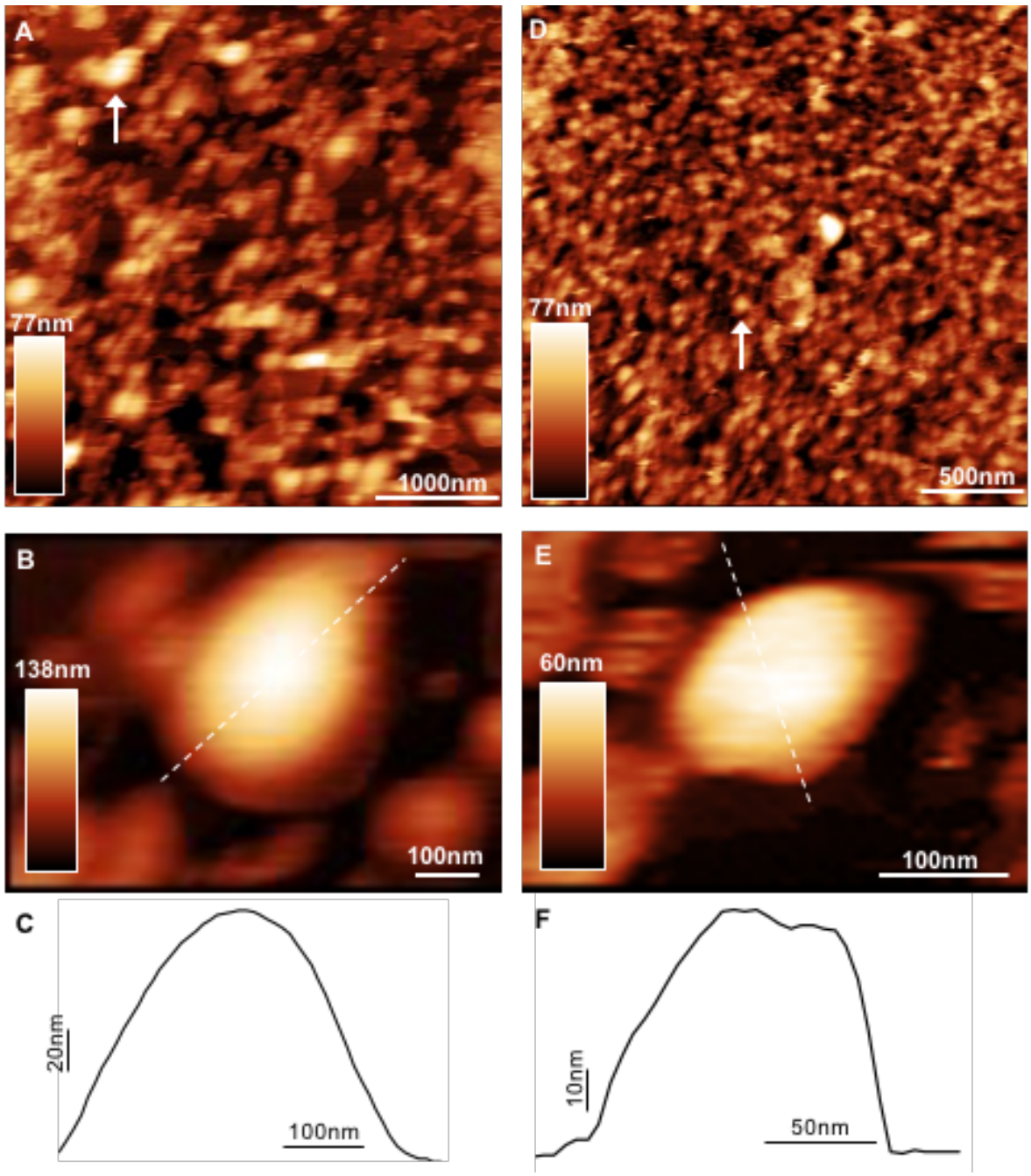


**Figure 5.7. Curvature analysis of the ICMs from *Rba. sphaeroides* WT and *Rba. sphaeroides* $\Delta pufX_{Rs}::pufX_{Rv}$. A.** AFM overview image of isolated ICM vesicles from *Rba. sphaeroides* WT. **B.** AFM topograph of an isolated ICM vesicle from *Rba. sphaeroides* WT. **C.** Cross-section analysis along the dashed line in **B** reveals an average height of 50 ± 22 nm (*n* = 211) of the vesicles. **D.** AFM overview image of isolated ICM vesicles from *Rba. sphaeroides* $\Delta pufX_{Rs}::pufX_{Rv}$. **E.** AFM topograph of an isolated ICM vesicle from *Rba. sphaeroides* $\Delta pufX_{Rs}::pufX_{Rv}$. **F.** Cross-section

analysis along the dashed line in B reveals an average height of 42 ± 16 nm (*n* = 207) of the vesicles. The white arrows represent example ICMs.

### *5.2.6 The ICM of* Rba. sphaeroides ΔpufX$_{Rs}$::pufX$_{Rv}$ *contains regular arrays of RC-LH1-PufX monomers*

The ICMs were isolated from *Rba. sphaeroides ΔpufX$_{Rs}$::pufX$_{Rv}$* again, however a 0.03% β-DDM sucrose gradient was used to slightly flatten the membranes for higher resolution images (Fig. 5.8) to study the organisation of the membranes. The resulting isolated ICMs appear as two-dimensional flat membrane patches of ~ 300 nm with a height of 7 ± 1 nm (*n* = 50), as opposed to the curved ICMs isolated with 0.00% β-DDM with heights of ~50 nm (Fig. 5.8). This allows the visualization of the RC-LH1$_{Rs}$-PufX$_{Rv}$ complexes and the long-range protein arrangement in the photosynthetic membranes. AFM images (Fig. 5.8) reveal regular arrays of monomeric RC-LH1$_{Rs}$-PufX$_{Rv}$ complexes with a diameter of 11.3 ± 3.3 nm (*n* = 50), similar to the 12.5 nm diameter of monomer RC-LH1 complex from *Blc. viridis* (Miller *et al.*, 2020), confirming the presence of monomer complexes.

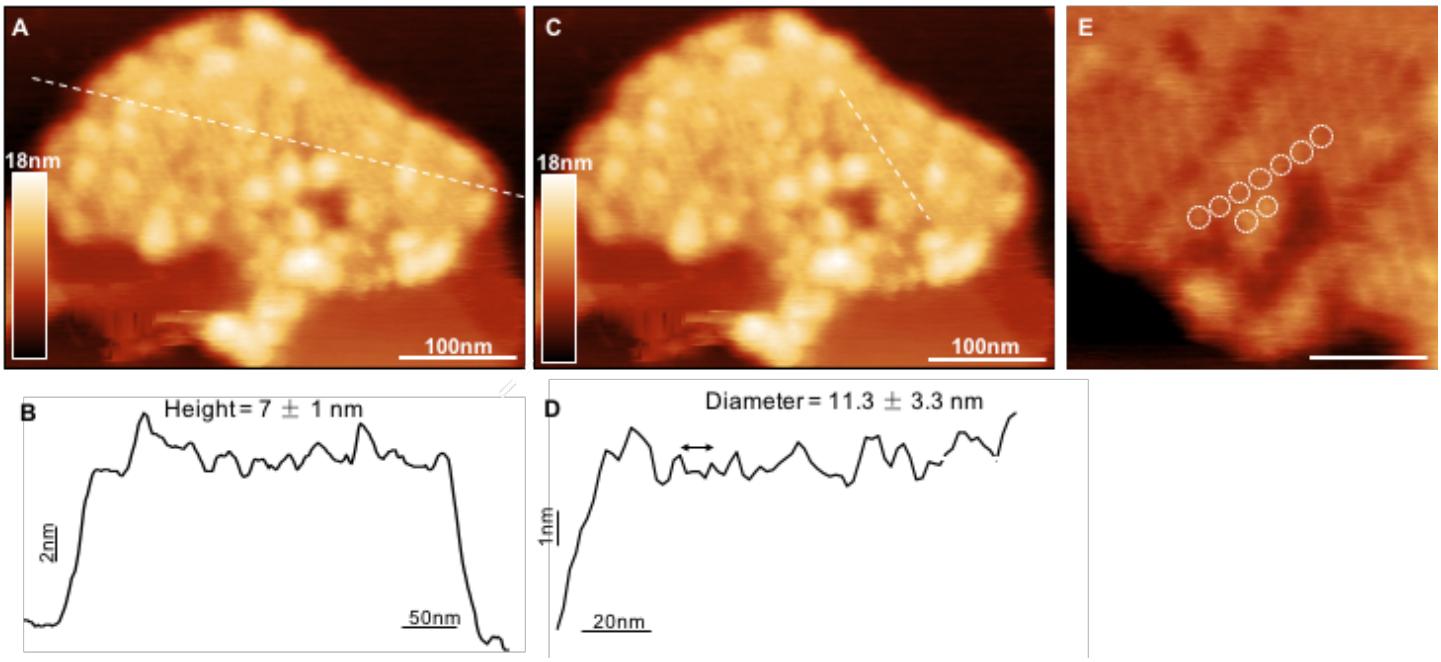


**Figure 5.8. AFM analysis of ICMs from *Rba. sphaeroides* Δ*pufX*$_{Rs}$::*pufX*$_{Rv}$. A.** AFM topograph of an isolated photosynthetic membranes patch in liquid. **B**. Cross-section analysis along the dashed line in A reveals an average height of the RC-LH1-PufX complexes of 7 ± 1 nm (*n* = 50). **C.** Medium-resolution AFM image of the photosynthetic membrane in liquid. **D.** Cross-section analysis along the dashed line in C reveals the RC-LH1-PufX complexes have a diameter of 11.3 ± 3.3 nm. **E.** The white circles highlight RC-LH1-PufX complexes.

## 5.3 Discussion

This study demonstrated that PufX$_{Rv}$ altered the composition of the *Rba. sphaeroides* core complex, as well as the architecture and organisation of the photosynthetic membrane.

The similarity in the absorption spectra of WT and mutant strains demonstrated that photosynthetic growth of the strain is not completely impaired by replacing PufX$_{Rs}$ with PufX$_{Rv}$ and that some of the roles of the former are fulfilled by PufX$_{Rv}$, despite the PufX$_{Rv}$ and PufX$_{Rs}$ proteins consisting of a low sequence identity (Table 5.1). The

assembly of the core complex is, however, impaired by the replacement of $PufX_{Rs}$ with $PufX_{Rv}$; the level of LH1 per RC is reduced, as can be seen in the reduction of the $A_{LH1}/A_{RC}$ ratio in the *Rba. sphaeroides* $\Delta pufX_{Rs}::pufX_{Rv}$ strain compared to WT (Table 5.2), indicating a monomer composition. This may also suggest that $PufX_{Rv}$ improved the effectiveness with which LH1 excitation is utilised by the RC, further studies are needed to confirm this.

The structure of the PufX protein could be a requirement of its function and organisation. However, the NMR solution structure of $PufX_{Rs}$ (Wang *et al.*, 2007) (PDB: 2DW3) and the Phyre2 predicted structure of $PufX_{Rv}$ (Kelley *et al.*, 2015) show almost identical structures (Fig. 5.1B). Although there are some conserved residues between the two structures (Fig. 5.1A,B), there are also many residue variations, some of these residues may be key to determining the function of PufX in their interactions with LH1, rather than the entire structure.

Previous studies have suggested that the dimerization of *Rba. sphaeroides* PufX is facilitated by a GxxxG dimerisation motif (Lemmon *et al.*, 1992, 1994), of which it contains two adjacent in the sequence $G^{31}xxxG^{35}xxxG^{39}$, in monomeric *Rba. veldkampii* the equivalent sequence is GxxxVxxxxG (Busselez *et al.*, 2007). However, previous studies have shown that replacing Leu for $Gly^{31}$, $Gly^{35}$ and $Gly^{39}$ has no effect on the dimerization of the complex (Crouch *et al.*, 2010). Replacing the PufX of *Rba. sphaeroides* (GxxxGxxxG) with the PufX of *Rba. veldkampii* (GxxxVxxxxG) interestingly leads to the assembly of exclusively monomeric complexes.

The effects of PufX on the organisation of the photosynthetic membrane are likely dictated not only by the PufX itself, but the interactions of PufX with LH1. The interaction of $PufX_{Rv}$ with $LH1_{Rs}$ appears to have an effect on the ICM architecture of

the cell, resulting in not only significantly larger vesicular ICM structures (Fig. 5.5), but also particularly, the formation of lamellar ICM structures simultaneously (Fig. 5.5).

# CHAPTER VI
# Re-engineering of *Blc. viridis* photosynthetic membrane

# 6 Re-engineering of *Blc. viridis* photosynthetic membrane

## 6.1 Introduction

Purple photosynthetic bacteria are remarkable in their ability to carry out photosynthesis via a simple system of highly organised components. The general mechanism of photosynthesis, the absorption of light by antenna components and the subsequent transfer of excitation energy to the RC, is similar among species, however, (as is discussed in **chapter I** of this thesis) different species consist of different component structures and organisations and, hence, utilise light of different wavelengths.

LH1 complexes are composed of a ring of α- and β-polypeptides forming a heterodimer together with their associated pigment molecules: BChl *a* or *b* and carotenoids. These subunits associate in a closed ellipsoid structure surrounding the RC, known as the RC-LH1 complex; in different species of purple bacteria, the RC-LH1 complexes possess different forms (see **chapter I** of this thesis). In *Blc. viridis,* the closed ellipsoid structure adapts to form a completely circular structure when the entire RC is removed (Scheuring *et al.*, 2005b); this reveals an inherent flexibility of the complex. In order to fully understand the flexibility and assembly of the LH1 complex, it must be examined in the absence of the RC.

Studies in *Rba. sphaeroides* (Hunter *et al.*, 1990; Jones *et al.*, 1992; Bahatyrova *et al.*, 2004; Olsen *et al.*, 2014) revealed that the LH1 can adopt a smaller, circular structure when the entire RC is removed and indicates a simple assembly of the system, lacking rigid quality control. The RC-LH1 complex of *Rba. sphaeroides* has been proposed to assemble by association of a single $\alpha_1\beta_1(Bchl)_2$ subunit with the RC, followed by

cooperative forces of self-association between the $\alpha_1\beta_1(Bchl)_2$ subunits which drive the encirclement of the subunits for form a complete core complex (Olsen *et al.*, 2014). Previous studies have also demonstrated the ability of the LH1 complex to form a ring-shaped structure in the absence of the RC (Bustamante and Loach, 1994).

The LH1 complex of *Blc. viridis* contains an additional *γ*-polypeptide in apparent equimolar ratio with the LH1 α- and β-polypeptides, encoded by *pufγ* (Brunisholz *et al.*, 1985); this additional subunit is located between the β-polypeptides (Qian *et al.*, 2018). The assembly of this RC-LH1 from *Blc. viridis* has not been investigated in such detail; it is not clear if *Blc. viridis* LH1 complexes assemble in the same way as proposed for *Rba. sphaeroides*, nor whether they are capable of assembling in the absence of the RC.

*Blc. viridis* houses one of the simplest photosynthetic systems, consisting of a single LH component surrounding the RC, two quinones (Q), cyt $c_2$ and $bc_1$ and ATPase; *Blc.* viridis is also unique in its production of Bchl *b*. Other purple bacteria species produce BChl *a* and consist of an additional peripheral antenna, LH2 (see **chapter I** of this thesis). The peripheral LH2 complex capture photons and funnel the excitation energy to the core LH1 complexes and ultimately the RC. These antenna, similar to LH1, form symmetric ring structures made up of numerous pairs of α- and β-polypeptides (McDermott *et al.*, 1995; Koepke *et al.*, 1996; Prince *et al.*, 1997; Papiz *et al.*, 2003).

LH1 complexes generally absorb wavelengths between 870-890 nm; the BChl *b*-containing LH1 complex of *Blc. viridis* shifts the absorb capabilities of the species ~150 nm into the infrared up to 1023 nm. Comparatively, the LH2 complex absorbs shorter

wavelengths of 800-850 nm. Engineering *Blc. viridis* to contain these LH2 complexes could increase the range of wavelengths utilised by the species.

In this chapter, we aim to engineer the *Blc. viridis* in two different ways; the first in the overexpression of the LH1 complex in order to investigate the flexibility and assembly of the complex. Second, by expressing the LH2 complex in *Blc. viridis* to study the effects on the absorption spectra and function of the species, as well as the effects on the organisation of the photosynthetic machinery in the membrane.

## 6.2 Results and Discussion

### *6.2.1* Blc. viridis *LH1-overexperession*

#### *6.2.1.1 Construction of a BioBrick™ LH1-overexpression plasmid*

To create a vector system for the overexpression of LH1 proteins in *Blc. viridis*, we chose to utilise the BioBrick™ system (Shetty *et al.*, 2008; Vick *et al.*, 2011; Tikh *et al.*, 2014). The BioBrick™ pBBRBB-P*puf* vector shown in Fig. 6.1 has shown expression levels in purple photosynthetic bacteria comparable to that of reporter proteins expressed in *E. coli* using the $P_{lac}$ promoter (Tikh *et al.*, 2014). The mobility (mob) genes present in the plasmid allow rapid plasmid transfer into multiple host strains via conjugation (Saltikov and Newman, 2003). The plasmid also contains a broad-host-range origin of replication and is capable of maintenance in a diverse range of bacteria using kanamycin selection (Kovach *et al.*, 1995). As well as this, the system also contains the *puf* promoter (Gong *et al.*, 1996) that drives the expression of the *pufBALMX* operon coding for LH1, RC and PufX in *Rba. sphaeroides*; we chose to use the full length of this strong promoter region in the design of our plasmid.

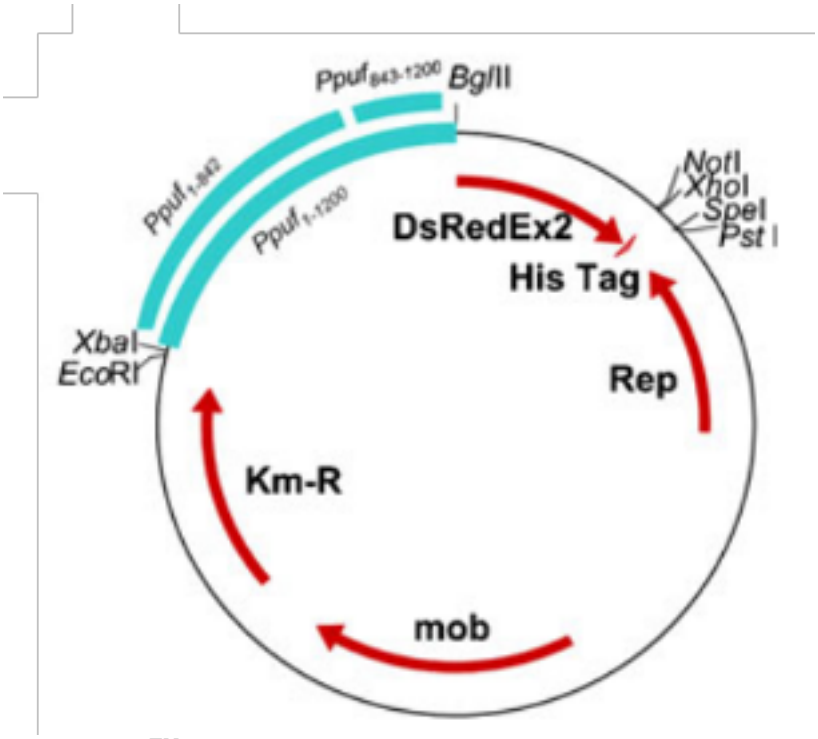


**Figure 6.1. BioBricks™ plasmid map.** The pBBRBB-P*puf* (Tikh *et al.,*2014) vector used as the backbone for the construction of the pBBRBB-P*puf-pufBA*-P*puf*-puf*γ* plasmid.

The overall design of the pBBRBB-P*puf-pufBA*-P*puf-pufγ* plasmid and step-process used is displayed in Figure 6.2. The *pufBA* and *pufγ* gene fragments, encoding LH1 α, β and γ polypeptides respectively, were first PCR amplified from respective plasmids (provided by Dr Daniel Canniffe, University of Liverpool) using the primers indicated in Table 6.1 and purified using magnetic beads (Fig. 6.2A). The first step in the process is the construction of two plasmids: pBBRBB-P*puf-pufBA* and pBBRBB-P*puf-pufγ* (Fig. 6.2). The confirmed *pufBA* and *pufγ* fragments and the pBBRBB-P*puf* plasmid were each restriction digested with *Bgl*II and *Spe*I (Fig. 6.2B). The resulting fragments were gel extracted and purified. The cut *pufBA* and *pufγ* fragments were then individually ligated together with the cut pBBRBB-P*puf* plasmid to produce the two individual plasmids and transformed into *E. coli* TOP10 cells (Fig. 6.2C,D). The

successful transformants were identified by colony PCR and their growth scaled-up into liquid cultures. The cultures were mini-prepped to isolate the plasmid and the sequences of the plasmid were confirmed by sequencing by Eurofins.

**Table 6.1. Primers used in this chapter.**

| Primer | Sequence (5'-3') |
|---|---|
| *pufBA* Forward Primer | gcgcagatctatggctgacttgaaaccg |
| *pufBA* Reverse Primer | ccggactagttcagccgacagccggcgg |
| *pufγ* Forward Primer | gcgcagatctatgaaactttcagctatt |
| *pufγ* Reverse Primer | ccggactagttcaacgataggtcagcgcg |

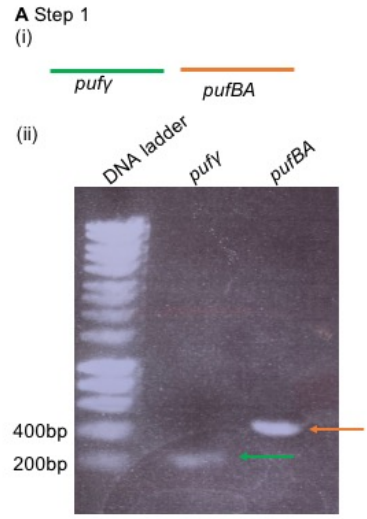
A Step 1
(i)
pufγ
pufBA
(ii)
DNA ladder
pufγ
pufBA
400bp
200bp

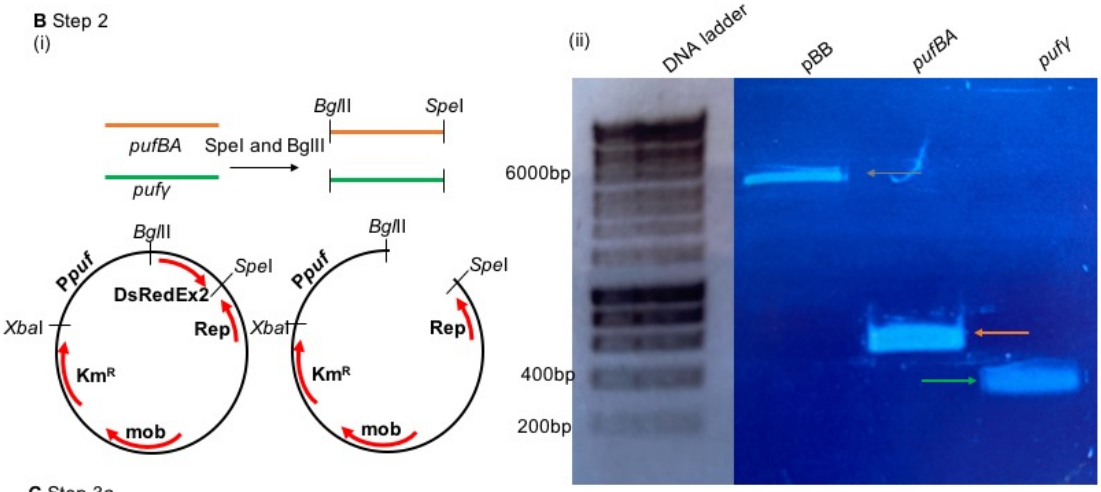
B Step 2
(i)
pufBA
pufγ
SpeI and BglII
BglII
SpeI
Ppuf
DsRedEx2
Rep
KmR
mob
XbaI
(ii)
DNA ladder
pBB
pufBA
pufγ
6000bp
400bp
200bp

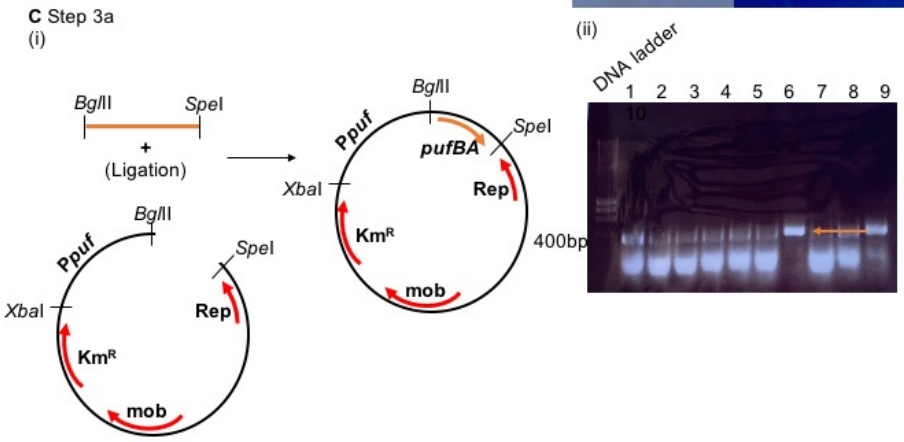
C Step 3a
(i)
BglII
SpeI
(Ligation)
Ppuf
pufBA
Rep
KmR
mob
XbaI
(ii)
DNA ladder
1 2 3 4 5 6 7 8 9 10
400bp

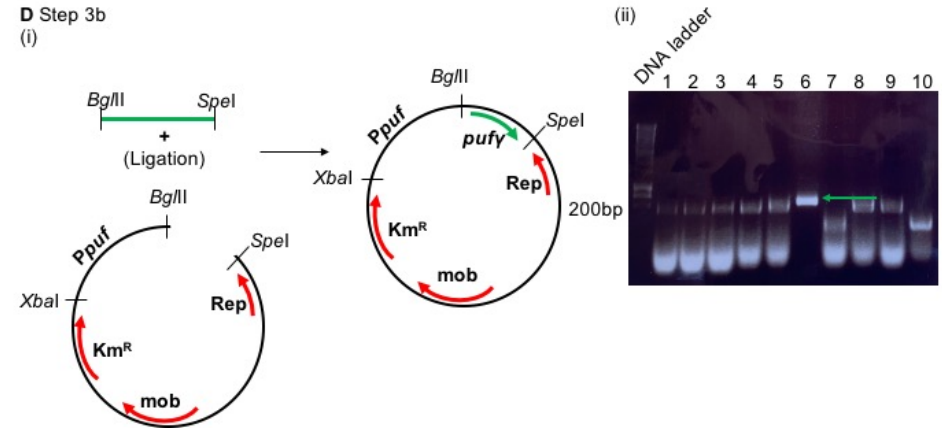
D Step 3b
(i)
BglII
SpeI
(Ligation)
Ppuf
pufγ
Rep
KmR
mob
XbaI
(ii)
DNA ladder
1 2 3 4 5 6 7 8 9 10
200bp

**Figure 6.2. Construction of pBBRBB-*pufBA* and pBBRBB- *pufγ* plasmids. A.** Step 1, (i) schematic of the PCR amplified *pufγ* and *pufBA* fragments, represented by red and orange lines, respectively. (ii) Agarose gel showing the *pufγ* and *pufBA* PCR fragments after PCR. Red and orange arrows indicate the *pufγ* (0.17kb) and *pufBA* (0.44kb) fragments, respectively. **B.** Step 2, (i) schematic of the amplified *pufγ* and *pufBA* fragments and the pBBRBB-P*puf* plasmid (Tikh *et al.,* 2014) restriction digestions with *Spe*I and *Bgl*II. (ii) Agarose gel showing pBBRBB-P*puf* plasmid, *pufBA* and *pufγ* fragments after restriction digestion. The grey, orange and red arrows indicate the pBB, *pufBA* and *pufγ* fragments extracted for ligation, respectively. **C.** Step 3a , (i) schematic of the ligation of the digested *pufBA* fragment together with the digested *pBBRBB-Ppuf plasmid* to create the pBBRBB-P*puf*-p*ufBA* plasmid. (ii) Agarose gel showing colony PCR of the transformants after transformation of the respective plasmid into *E. coli* TOP10 cells. The orange arrow indicates the successful colony selected for sequencing. **D.** Step 3b, this is identical to **C**, however, with the *pufγ* fragment.

The pBBRBB-P*puf-pufγ* plasmid was then digested with *Xba*I and *Spe*I (Fig 6.3A) to produce the P*puf-pufγ* fragment; the pBBRBB-P*puf-pufBA* plasmid was digested with *Spe*I (Fig 6.3A) and ligated together with the P*puf-pufγ* fragment to produce pBBRBB-P*puf-pufBA*-P*puf-pufγ* (Fig 6.3). The ligation product was transformed into *E. coli* TOP10 cells and the successful transformants were selected by colony PCR (Fig. 6.3B), scaled up into liquid culture and the sequence confirmed by sequencing by Eurofins. The resultant plasmid was transformed into S17 and MFD*pir* (Ferrières *et al.*, 2010) *E. coli* donor strains; the plasmid was then successfully conjugated into *Blc. viridis* WT strain (Fig. 6.4).

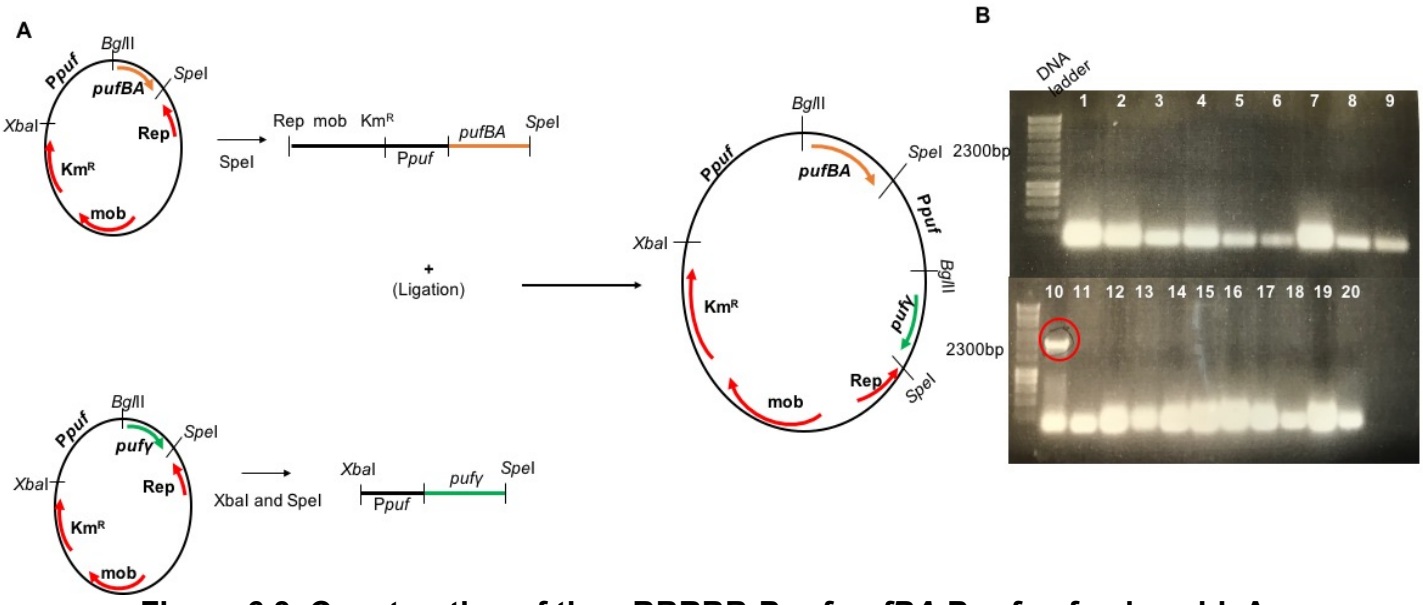


**Figure 6.3. Construction of the pBBRBB-P*puf-pufBA*-P*puf*-pufγ plasmid. A**. Schametic of the restriction digestion of pBBRBB-P*puf-pufBA* plasmid with *Spe*I (top) and pBBRBB-P*puf-pufγ with* Xba*I and* SpeI (bottom). The resulting fragments were ligated together to produce the pBBRBB-P*puf-pufBA*-P*puf*-pufγ plasmid. **B.** Agarose gel showing the colony PCR of *E. coli* DH5alpha pBBRBB-P*puf-pufBA*-P*puf*-pufγ plasmid (2.3 kb) successful transformants. The red circle indicates the successful transformant, which was sent for sequencing.

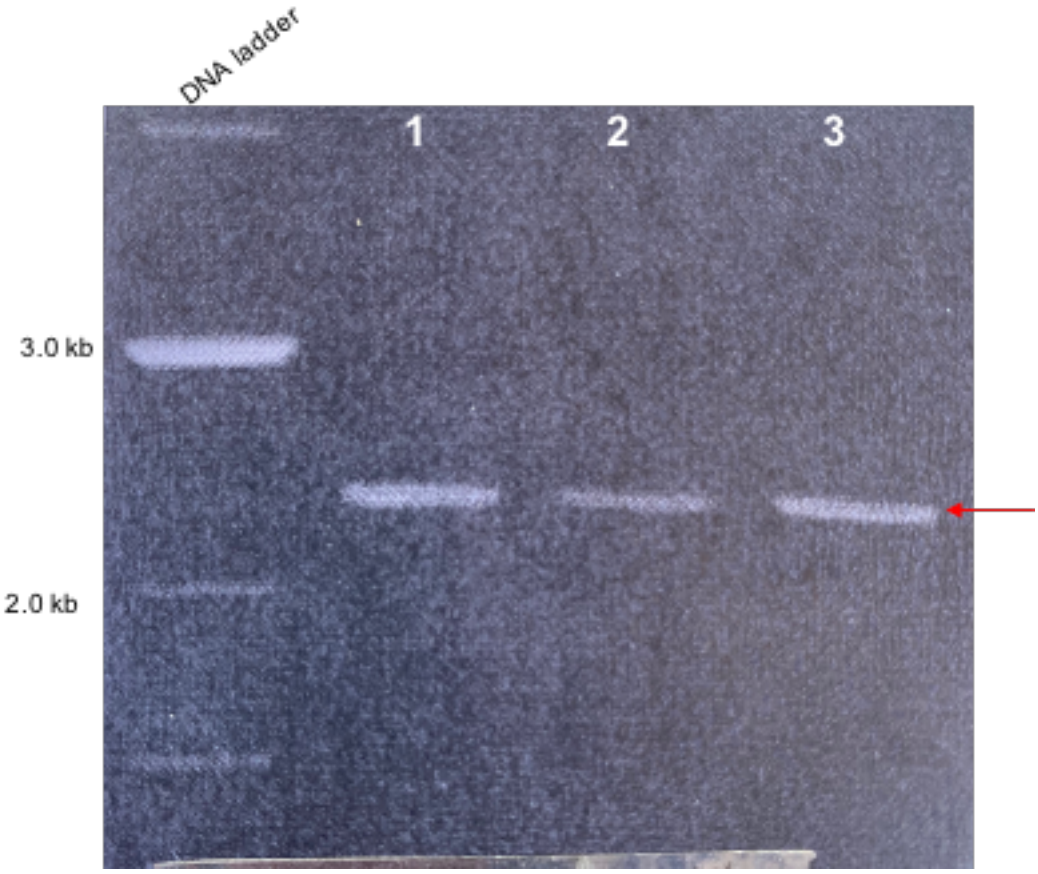


**Figure 6.4. LH1-overexpressed *Blc. viridis* strain.** Agarose gel showing the PCR of three cultures of *Blc. viridis* pBBRBB-*pufBA*-puf*y* plasmid – containing strain. The colonies each contain the pBB-*pufBA*-puf*y* plasmid (2.3 kb) plasmid, indicated by red arrow.

### *6.2.1.2 Characterisation of* Blc. viridis *LH1-overexpression strain*

The successfully conjugated *Blc. viridis* LH1-overexpression strain was grown anaerobically in normal light at 30°C in $M22^+$ medium (**Appendix A**); the absorption spectra (Fig. 6.5) of the culture shows that the strain is capable of carrying out photosynthetic growth as the line spectra reveals a similar pattern to WT and contains all the relevant carotenoids and Bchl for photosynthetic growth.

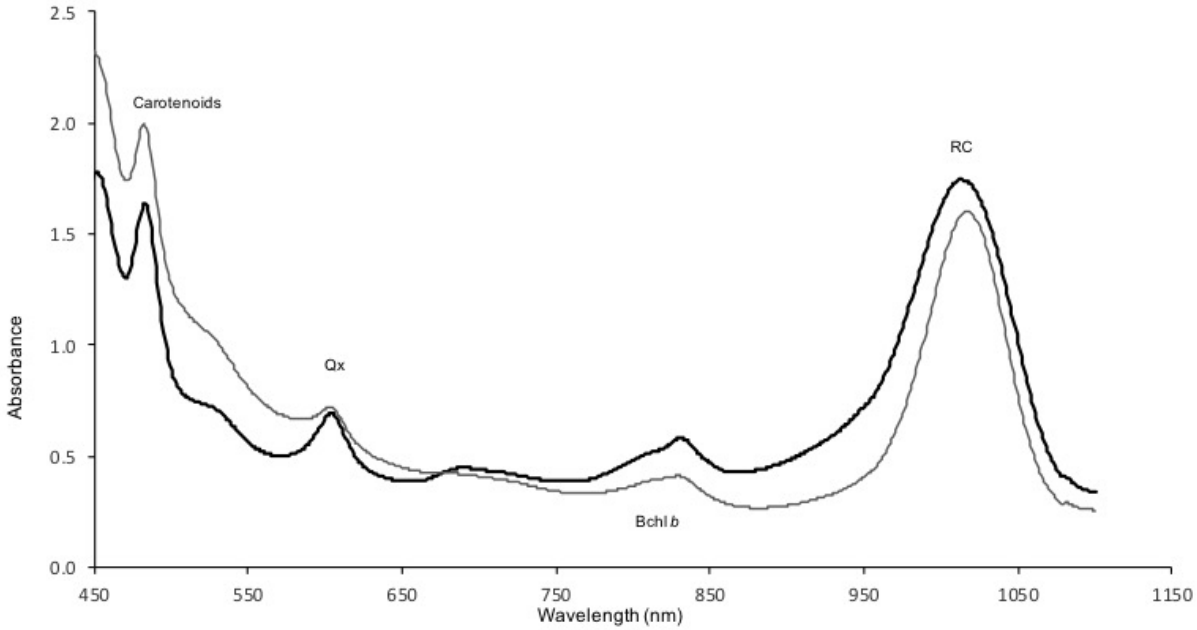


**Figure 6.5. Absorption spectra of *Blc. viridis* LH1-overexpression mutant.** The absorption spectra of *Blc. viridis* WT and LH1-overexpression mutant are represented in black and grey, respectively.

### *6.2.1.3 Isolation and Characterisation of the ICM*

The ICM of the LH1-overexpression strain was isolated using sucrose gradient centrifugation (Fig. 6.6A); the absorption spectra of the isolated ICM (Fig. 6.6B) reveals a similar pattern to that of the WT. This indicates no difference in the expression of the LH1 complex in the mutant compared to WT. SDS-PAGE analysis (Fig. 6.6C) of the ICM also reveals little difference in the expression levels of the LH1-polypeptide chains between the mutant and WT ICMs, there appears to be a slight reduction in the expression levels of the LH1 polypeptides in the mutant compared to WT. The expression of the H subunit of the mutant RC is notably increased compared to WT. Furthermore, AFM analysis of the isolated ICMS (Fig. 6.7A,B) reveals membrane patches of 12.3 ± 0.9 nm ($n$ = 32) heights, this is comparable to the composition of WT ICMs (Miller *et al.*, 2020) (see **chapter IV** of this thesis). The RC-

LH1 complexes are 14.0 ± 2.6 nm (*n* = 32) apart from each other (Fig. 6.7C,D) in a regular array (Fig. 6.7E), also comparable to the arrangement of WT *Blc. viridis* ICMs (Miller *et al.*, 2020) (see **chapter IV** of this thesis) indicating no presence of LH1-only complexes. Although the plasmid has been successfully conjugated into the *Blc. viridis* strain (Fig. 6.4), it appears that the strain has not successfully overexpressed the LH1 complex.

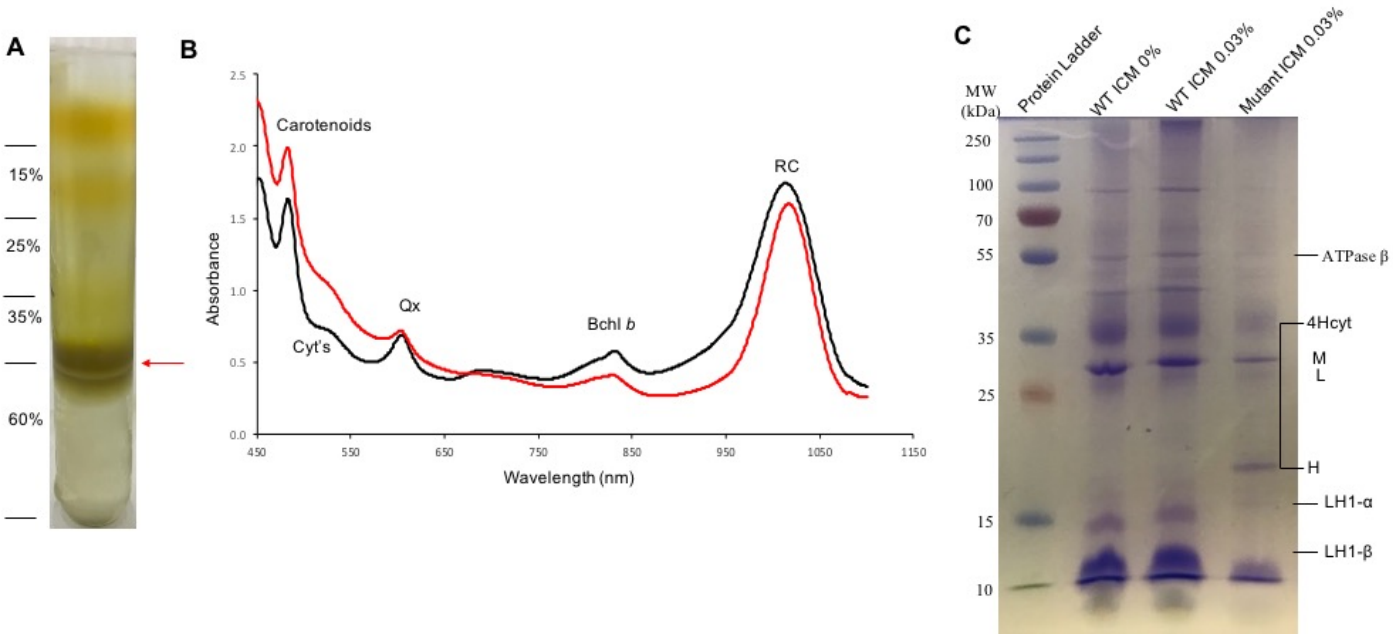


**Figure 6.6. Characterisation of the ICM from *Blc viridis* LH1-overexpressed mutant. A.** Sucrose gradients used to collect and purify the mutant ICM, the red arrow indicates the band extracted for further characterisation **B.** Absorption spectra of isolated WT (black) and mutant (red) ICM. **C.** SDS-PAGE gel of the 60% sucrose gradient band from WT and mutant.

### *6.2.2 LH2 Expression in* Blc. viridis

#### *6.2.2.1 Construction of a BioBrick™ LH2-expression plasmid*

The BioBrick™ system (Shetty *et al.*, 2008; Vick *et al.*, 2011; Tikh *et al.*, 2014) was also utilised to create a vector system for the expression of *Rba. sphaeroides* LH2 in *Blc. viridis*. Two pBBRBB-*pucBAC* plasmids, containing the LH2 gene (*pucBAC*) and

pBBRBB-LONG, containing a long P*puf* promoter were both digested with *Bgl*II and *Bcu*I and gel extracted (Fig. 6.8A). These two fragments were ligated together and transformed into *E. coli* DH5α cells; colony PCR of the resulting colonies revealed many successful transformants (Fig. 6.8B). The plasmid from these transformants were transformed into S17 and MFD*pir E. coli* cells and subsequently conjugated into *Blc. viridis* WT (carried out by Dowrung Namoon, University of Liverpool), however this was not successful (Fig. 6.9).

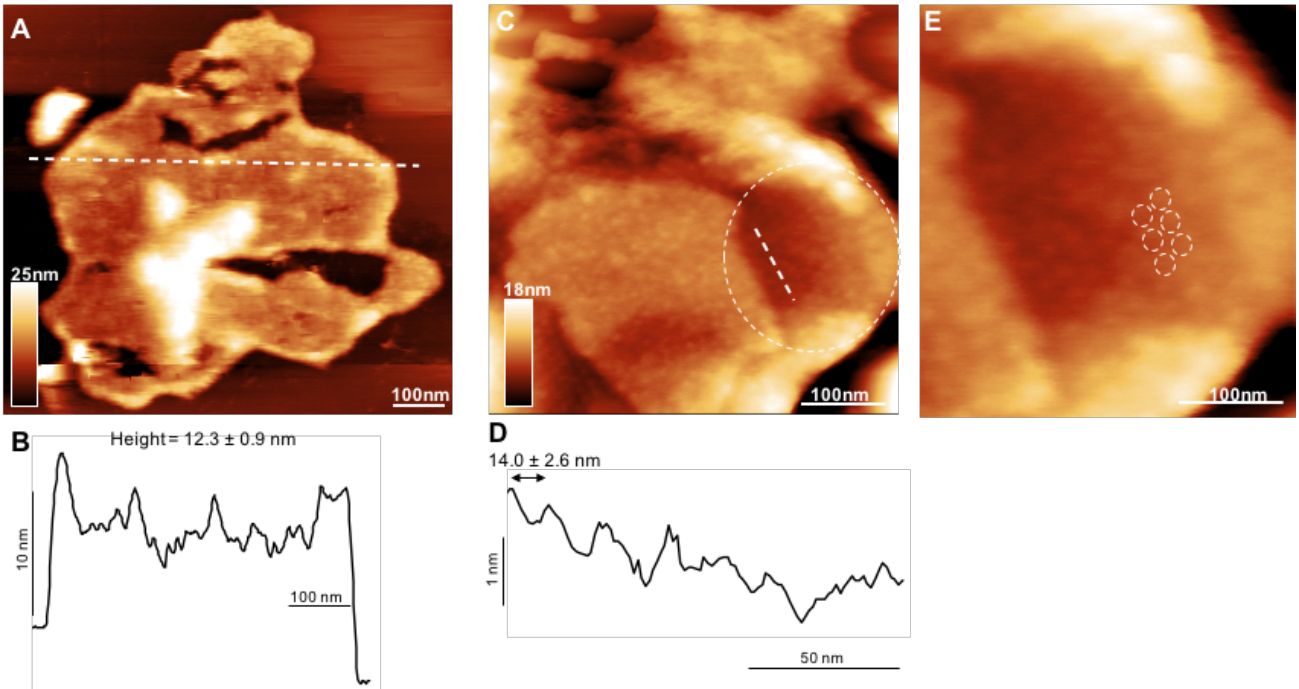


**Figure 6.7. AFM analysis of the ICMs from *Blc viridis* LH1-overexpressed mutant.** **A.** Medium resolution AFM image of an ICM patch, height profile along the white dotted line is shown in **B**, the ICM patches are 12.3 ± 0.9 nm (*n* = 32) high. **C.** High resolution AFM image of an ICM patch, revealing a regular pattern of RC complexes with x nm height at 14.0 ± 2.6 nm (*n* = 32) distances from each other. **D.** Height profile along the white dotted line. **E.** Zoomed in on the highlighted circle on **C**, the white circles represent the RC heads.

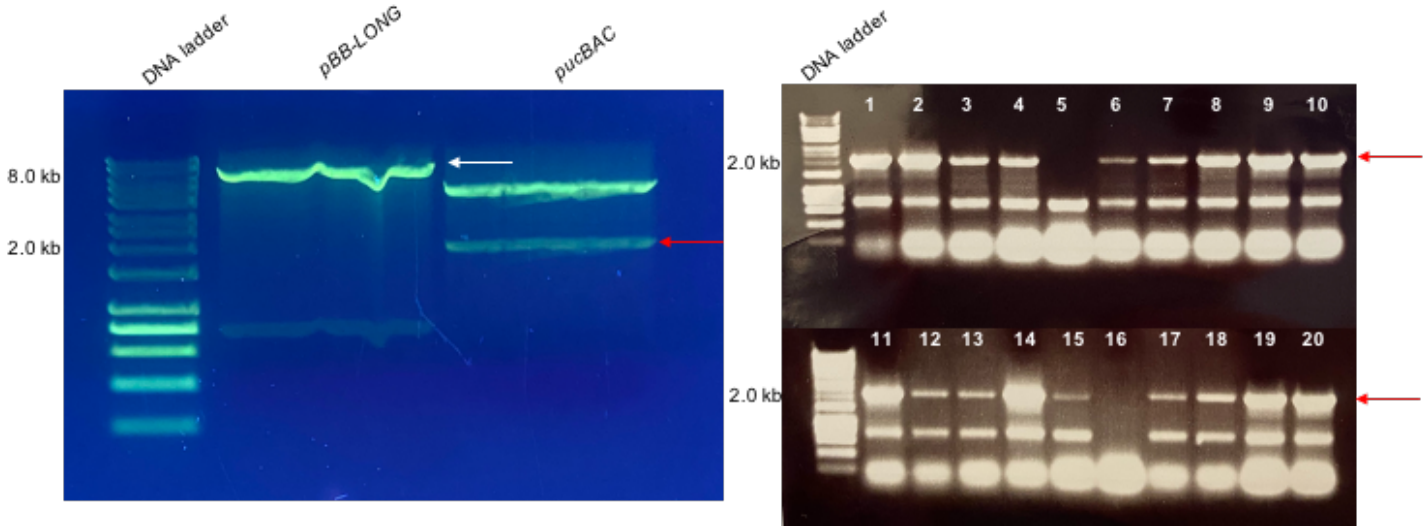


**Figure 6.8. Production of pBBRBB-LONG-pucBAC plasmid**. **A.** Agarose gel showing pBBRBB-LONG (8kb) and *pucBAC* (2kb) fragments, represented by white and red arrows, respectively. **B.** Agarose gel showing the colony PCR of *E. coli* DH5alpha pBB-LONG-*pucBAC* plasmid (2 kb) successful transformants. The red arrow indicates the size of successful transformants.

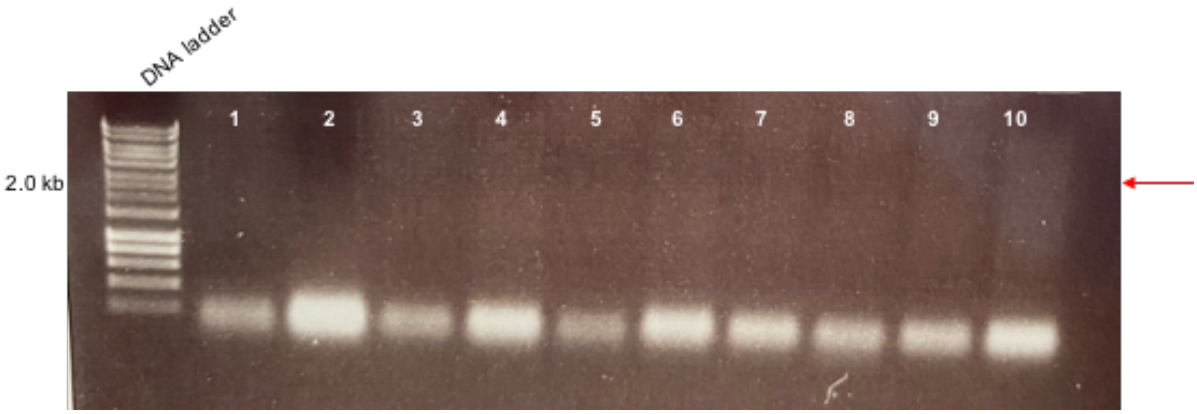


**Figure 6.9. *Blc. viridis* LH2 expression strain**. Agarose gel showing the PCR of ten cultures of *Blc. viridis* pBB-LONG-*pucBAC* plasmid – containing strains, this reveals no strains were successfully conjugated. The expected size of the successful band (2 kb) is highlighted by the red arrow.

## 6.3 Concluding Remarks

The overexpression of LH1 in *Blc. viridis* was not successful, it must be noted however, that this was tested only in light growth conditions; testing the growth of this strain under dark conditions may result in altered membrane constitution. The overexpression of LH1 would have resulted in empty rings of LH1 complexes containing no RC complexes; LH1 antenna would, therefore, be capturing light energy with nowhere to transduce this energy to. Primary charge separation would not occur and hence, the captured light energy cannot be utilized; as this is not energetically favorable to the strain, this is likely the reason the LH1 complexes have not been overexpressed. There are no documented species of purple bacteria which contain empty LH1 complexes as peripheral antennas; in species such as *Rba. sphaeroides* LH2 complexes act as peripheral antennas transducing light energy to the LH1 and subsequently the RC complexes (Sumi, 2002). The lack of overexpression of LH1 suggests that this antenna complex is not an efficient peripheral antenna, hence they are not utilised for this. Interestingly, an LH1-only mutant strain of *Rba. sphaeroides* has been studied (Hunter *et al.*, 1990; Jones *et al.*, 1992; Bahatyrova *et al.*, 2004; Olsen *et al.*, 2014); this would suggest it is possible to overexpress LH1 complexes in *Blc. viridis* also. A different approach to this study in the future could be to delete the genes coding for the RC using transposon mutagenesis, rather than overexpressing the LH1 genes.

A vector for the expression of LH2 in *Blc. viridis* was successful, however the conjugation was not. There are several reasons that the conjugation may have failed, including a low ratio of recipient to donor strain, too short of an incubation period or

incorrect antibiotic concentrations. Future experiments could be set up changing slightly these aspects of the protocol. A vector system containing the same gene, however with a shorter promoter region was successfully created and conjugated within the lab (Namoon, unpublished). In the future, these strains can be characterised and the changes in their growth and absorption spectra analysed to investigate whether this increases the wavelength of light utilised by the strain. The ICM can also be isolated and analysed by AFM to visualise the effects of introducing the LH2 complex into the membrane on the long-range organisation of the photosynthetic machinery.

# CHAPTER VII
# Discussion

# 7 Discussion

## 7.1 General Introduction

The research in this thesis has deepened the understanding of the forces influencing the organisation of purple bacterial photosynthetic membranes, as well as the protein folding and the interactions of membrane-associated proteins at the single-molecule level using AFM and SMFS. The application of SMFS methods used in this thesis represent a new way to study the mechanical properties of membrane-associated proteins which can be applied in future studies enabling us to explore and reprogram native and synthetic biological membranes. The most important findings in this study include elucidating the forces underlying the organisation of the *Blc. viridis* photosynthetic membrane (**Section 7.2**) and the understanding of the effects of the PufX protein on membrane and ICM architecture (**Section 7.3**). Some progress was also made in the engineering of the *Blc. viridis* photosynthetic membrane (**Section 7.4**). During this chapter, I will briefly discuss the findings made and the outlook for future studies.

## 7.2 Forces influencing the organisation of *Blc. viridis* photosynthetic membranes

The precise folding and organisation of multicomponent photosynthetic assemblies to form functional entities are fundamental to efficient photosynthetic electron transfer; although there is a wealth of knowledge on the static structures of the photosynthetic machinery of purple photosynthetic bacteria, the forces underlying these structures and their long-range remains somewhat enigmatic. This chapter aimed to deepen our understanding of these two issues.

We used AFM imaging (Fig. 4.2, 4.4) to reveal the precise arrangement of the RC-LH1 complexes in the photosynthetic membranes of *Blc. viridis*. These complexes are densely packed, forming regular arrays of ~60$^{o}$ staggered pattern at ~14 nm distances, supported by PCF (Fig. 4.4). We also demonstrate the inherent variability of the protein organisation (Fig. 4.5); membrane regions more densely packed with RC-LH1 complexes contain a more regular arrangement of complexes compared with less densely packed regions. High-speed (HS)-AFM images (Fig. 4.6) confirm the high stability of the RC-LH1 organizations suggesting a higher restriction of protein diffusion compared to packed membrane proteins and self-assembled proteins (Deisenhofer *et al.*, 1995; A. F. Oberhauser *et al.*, 1998; Oesterhelt *et al.*, 2000). HS-AFM on the LH1 ring itself following removal of the 4Hcyt complex would be an interesting future study, to determine the dynamics of the LH1 ring in the exchange of quinol molecules.

It should also be noted that across numerous patches of membranes, there was no apparent space for cyt $bc_1$ or ATPase complexes; quantitative mass spectrometry has shown an average of two ATPase complexes per chromatophore vesicle is sufficient to efficiently convert light energy to ATP in *Rba. sphaeroides* (Kumar *et al.*, 2016). The lack of ATPase structures in the AFM images suggests that the few ATPase complexes present per ICM could be located on the periphery of the ICMs, not within the densely packed antennas. ATPase relies on the proton gradient created across the membrane to drive ATP production, therefore a location independent of the densely packed antennas is not unexpected. It may be an interesting future study to apply TREC imaging (see **Chapter III** of this thesis) using an antibody for each of the structures to localize these two components on the photosynthetic membrane.

SMFS was used to unfold the 4Hcyt subunit of the *Blc. viridis* RC (Fig. 4.8), this revealed strong forces comparable to the unfolding of the muscle protein titin (Nogi *et al.,* 2005), the extracellular matrix glycoprotein tenascin (Vasilev *et al.*, 2014), the transmembrane protein in an LH2 complex (Bustamante *et al.*, 1994) and bacteriorhodopsin (Wöhri *et al.*, 2009) (Table 4.1). The resultant forces demonstrated the increased strength of consecutive structural segment of the protein. We modeled the unfolding pattern of the subunit (Fig. 4.10), revealing strong binding between the 4Hcyt and L subunits of the RC which may provide a strong foundation for efficient electron flow.

## 7.3 The effects of PufX in the membrane and on the architecture of the ICM

The *Rhodobacter* species of purple photosynthetic bacteria contain an extra protein in their RC-LH1 complexes, PufX. The structure of PufX, in isolation and in complex with RC-LH1 has been studied (Walz *et al.*, 1998; Siebert *et al.*, 2004), as well as the function of the protein (Klug and Cohen, 1988; Farchaus *et al.,* 1990; Lilburn *et al.*, 1992; Francia *et al.*, 2002; Ratcliffe *et al.*, 2011). The protein is considered to play a role in the dimerization of the RC-LH1 complex, however *Rba. veldkampii* contain exclusively monomeric RC-LH1-PufX complex (Busselez *et al.*, 2007a; L.-N. Liu, Sturgis and Scheuring, 2011), hence other factors must also play important roles. The role of PufX in the organisation and architecture of the RC-LH1 complex is still unclear, this chapter aimed to further our understanding on the role of PufX by cross-species investigations.

We used AFM and TEM imaging to demonstrate that $PufX_{Rv}$ alters the composition of not only the *Rba. sphaeroides* RC-LH1 complex, but also the organisation of the ICM

and the architecture of the ICM vesicles. Despite the low sequence identity of $PufX_{Rv}$ and $PufX_{Rs}$ (Table 5.1), the absorption spectra of *Rba. sphaeroides* WT and *Δ$pufX_{Rs}$::$pufX_{Rv}$* were comparable (Fig. 5.3), demonstrating that composition of the photosynthetic pigments in the mutant strain are not completely impaired by the replacement with $PufX_{Rs}$ and hence, some of the roles of the native $PufX_{Rv}$ must be fulfilled by $PufX_{Rs}$. This is not true, however, of the assembly of the two core complexes; a monomer composition of RC-LH1-$PufX_{Rs}$ replaces the native dimeric structure (Table 5.2, Fig. 5.4, Fig. 5.8). The reduction in the level of LH1 per RC may suggest that $PufX_{Rv}$ improves the effectiveness with which LH1 excitation is utilised by the RC; spectral and fluorescence studies in the future could be used to study this further.

Previous mutagenic studies have shown that replacing key Gly amino acids residues in the dimerization motif (GxxxGxxxG) of *Rba. sphaeroides* with Leu reisdues has no effect on the dimerization of the complex (Crouch *et al.*, 2010); interestingly, however, we demonstrate that replacing $PufX_{Rs}$ with $PufX_{Rv}$, and hence essentially replacing the dimerization motif with that of *Rba. veldkampii* (GxxxVxxxG) results in the assembly of exclusively monomer RC-LH1-PufX complexes. The dimerization motif may have some effect on the dimerization of the complex, despite not strictly acting as a dimerization motif. The interaction of the PufX with specific LH1 proteins likely also plays a role in dimerization, it would be interesting to replace $PufX_{Rv}$ in the native *Rba. veldkampii* membrane with $PufX_{Rs}$ and analyse the assembly of the core complex. The three-dimensional structures of $PufX_{Rv}$ and $PufX_{Rs}$ appeared to be almost identical (Fig. 5.1). There are many residues variations between the two structures however, these may play key roles in the interactions of PufX with LH1; another interesting future

study would be to perform site-directed mutagenesis on specific residues and analyse the effects on the strain.

Replacement of $PufX_{Rs}$ with $PufX_{Rv}$ also effected the architecture of the ICM vesicles (Fig. 5.5, Fig. 5.8) in the formation of not only larger vesicles but also lamellar ICM structures similar to WT *Rba. veldkampii* (Fig. 5.5). Again, this may be due to the interaction between $LH1_{Rs}$ and $PufX_{Rv}$.

## 7.4 Engineering of the *Blc. viridis* photosynthetic membrane

Under the conditions tested, the overexpression of LH1 in *Blc. viridis* was not successful. As the overexpression of the LH1 rings would result in empty rings of LH1 complexes containing no RC complexes, the LH1 antenna would be capturing light but the strain would be unable to transfer energy to the RC for primary charge separation. The light captured would therefore not be utilized; this is not energetically favorable to the strain and may be the reason for the lack of overexpression. In nature, LH1 antenna are not used as peripheral antennas, instead LH2 complexes act as the peripheral antenna by capturing sunlight energy and transducing this to the RC via LH1 (Sumi, 2002). Our results perhaps suggest that the LH1 antenna is not efficient to act as a peripheral antenna to *Blc. viridis* RC-LH1 complexes. A second theory may be that the LH1 complex of *Blc. viridis* is not capable of assembling in the absence of the RC; an LH1-only mutant strain of *Rba. sphaeroides* has been studied (Hunter *et al.*, 1990; Jones *et al.*, 1992; Bahatyrova *et al.*, 2004; Olsen *et al.*, 2014), in which aberrant LH1 complexes form, consisting of varying ring sizes with the occurrence of arcs and spirals. Perhaps in *Blc. viridis,* the RC template is required for the assembly to be initiated.

We have successfully created a vector for the expression of LH2 in *Blc. viridis* (Fig. 6.8); however, the conjugation into *E. coli* strains was unsuccessful. There are several potential reasons for this, which need to be altered in future experiments; these include: increasing the ratio of recipient to donor strain, increasing the incubation period of the conjugation and changing the concentration of the antibiotics. Once the vector is successfully conjugate into *Blc. viridis,* the effects of the LH2 complex on the *Blc. viridis* photosynthetic membrane can be analysed using AFM and spectroscopic effects. Introducing the LH2 complex to the *Blc. viridis* membrane may increase the wavelengths of light which can be utilised by the strain, leading to more efficient photosynthesis.

## 7.5 Concluding Remarks

There are still many unanswered questions regarding the organisation and dynamics underlying the efficient photosynthesis carried out by purple photosynthetic bacteria. In this thesis, we have utilized AFM and SMFS to elucidate the forces influencing the organisation and function of the 4Hcyt subunit of the RC complex from *Blc. viridis* and further our knowledge on the organisation and inherent flexibility of the RC-LH1 complexes, which enables efficient electron transfer. The use of SMFS in this work has proven a powerful way to study the mechanical properties of membrane-associated proteins which can be applied in future studies of membrane-associated proteins. AFM was also used in conjunction with TEM to further our understanding of the role of the PufX protein on the organisation and assembly of the RC-LH1-PufX complex of *Rba. sphaeroides.* Lastly, we have made some progress on the

engineering of the *Blc. viridis* photosynthetic membrane, providing a strong base for future studies.

## Bibliography

Aagaard, J. and Sistrom, W. R. (1972) 'CONTROL OF SYNTHESIS OF REACTION CENTER BACTERIOCHLOROPHYLL IN PHOTOSYNTHETIC BACTERIA', *Photochemistry and Photobiology*, 15(2), pp. 209–225. doi: 10.1111/j.1751-1097.1972.tb06240.x.

Adams, P. G. *et al.* (2011) 'Monomeric RC–LH1 core complexes retard LH2 assembly and intracytoplasmic membrane formation in PufX-minus mutants of Rhodobacter sphaeroides', *Biochimica et Biophysica Acta (BBA) - Bioenergetics*. Elsevier, 1807(9), pp. 1044–1055. doi: 10.1016/J.BBABIO.2011.05.019.

Alberti, M., Burke, D. H. and Hearst, J. (2004) *Advances in Photosynthesis. Anoxygenic Photosynthetic Bacteria*. Available at: https://link.springer.com/content/pdf/10.1007%2F0-306-47954-0.pdf (Accessed: 29 August 2019).

Alessandrini, A. *et al.* (2011) 'High-resolution atomic force microscopy and spectroscopy of native membrane proteins The physics of pulling polyproteins: a review of single molecule force spectroscopy using the AFM to study protein unfolding Megan L Hughes and Lorna Dougan - Recent citations High-resolution atomic force microscopy and spectroscopy of native membrane proteins', *Reports on Progress in Physics Rep. Prog. Phys*, 74, pp. 86601–43. doi: 10.1088/0034-4885/74/8/086601.

Allen, J. F. and Holmes, N. G. (1986) 'A general model for regulation of photosynthetic unit function by protein phosphorylation', *FEBS Letters*. doi: 10.1016/0014-5793(86)80682-2.

and, T. P. and Sundström, V. (2004) 'Ultrafast Dynamics of Carotenoid Excited States−From Solution to Natural and Artificial Systems'. American Chemical Society . doi: 10.1021/CR020674N.

Angerhofer, A., Cogdell, R. J. and Hipkins, M. F. (1986) 'A spectral characterisation of the light-harvesting pigment-protein complexes from Rhodopseudomonas acidophila', *Biochimica et Biophysica Acta (BBA) - Bioenergetics*, 848(3), pp. 333–341. doi: 10.1016/0005-2728(86)90208-2.

Axelrod, H. L. *et al.* (1994) 'Crystallization and X-ray structure determination of cytochrome c2 from Rhodobacter sphaeroides in three crystal forms', *Acta Crystallographica Section D*

*Biological Crystallography*. International Union of Crystallography (IUCr), 50(4), pp. 596–602. doi: 10.1107/S0907444994001319.

Axelrod, H. L. *et al.* (2002) 'X-ray Structure Determination of the Cytochrome c2: Reaction Center Electron Transfer Complex from Rhodobacter sphaeroides', *Journal of Molecular Biology*. Academic Press, 319(2), pp. 501–515. doi: 10.1016/S0022-2836(02)00168-7.

Axelrod, H. L. and Okamura, M. Y. (2005) 'The structure and function of the cytochrome c2: Reaction center electron transfer complex from Rhodobacter sphaeroides', *Photosynthesis Research*. Springer, pp. 101–114. doi: 10.1007/s11120-005-1368-8.

Axelrod, H., Miyashita, O. and Okamura, M. (2009) 'Structure and Function of the Cytochrome c 2:Reaction Center Complex from Rhodobacter sphaeroides', in. Springer, Dordrecht, pp. 323–336. doi: 10.1007/978-1-4020-8815-5_17.

Bahatyrova, S., Frese, R. N., Werf, K. O. van der, *et al.* (2004) 'Flexibility and Size Heterogeneity of the LH1 Light Harvesting Complex Revealed by Atomic Force Microscopy', *Journal of Biological Chemistry*. American Society for Biochemistry and Molecular Biology, 279(20), pp. 21327–21333. doi: 10.1074/JBC.M313039200.

Bahatyrova, S., Frese, R. N., Siebert, C. A., *et al.* (2004) 'The native architecture of a photosynthetic membrane', *Nature*. Nature Publishing Group, 430(7003), pp. 1058–1062. doi: 10.1038/nature02823.

Barz, W. P. *et al.* (1995) 'Role of the PufX protein in photosynthetic growth of Rhodobacter sphaeroides. 2. PufX is required for efficient ubiquinone/ubiquinol exchange between the reaction center QB site and the cytochrome bc1 complex.', *Biochemistry*, 34(46), pp. 15248–15258. doi: 10.1021/bi00046a033.

Benson, A. A. (2002) 'P AVING THE P ATH', *Annual Review of Plant Biology*. Annual Reviews 4139 El Camino Way, P.O. Box 10139, Palo Alto, CA 94303-0139, USA , 53(1), pp. 1–25. doi: 10.1146/annurev.arplant.53.091201.142547.

Berry, E. A. *et al.* (2000) *STRUCTURE AND FUNCTION OF CYTOCHROME bc COMPLEXES*. Available at: http://www.life.illinois.edu/crofts/pdf_files/ARB_review.pdf (Accessed: 30 August 2019).

Berry, E. A. *et al.* (2004) 'X-Ray Structure of Rhodobacter Capsulatus Cytochrome bc $_1$ : Comparison with its Mitochondrial and Chloroplast Counterparts', *Photosynthesis Research*, 81(3), pp. 251–275. doi: 10.1023/B:PRES.0000036888.18223.0e.

Binnig, G. *et al.* (1985) *Atomic Force Microscope*. Available at: https://journals.aps.org/prl/pdf/10.1103/PhysRevLett.56.930 (Accessed: 14 July 2020).

Blankenship, R. E. (2014) *Molecular Mechanisms of Photosynthesis Robert E. Blankenship Second Edition*. Second. St Louis: Wiley Blackwell.

Boonstra, A. F., Germeroth, L. and Boekema, E. J. (1994) 'Structure of the light harvesting antenna from Rhodospirillum molischianum studied by electron microscopy', *Biochimica et Biophysica Acta (BBA) - Bioenergetics*. Elsevier, 1184(2–3), pp. 227–234. doi: 10.1016/0005-2728(94)90227-5.

Boyer, P. D. (1993) 'The binding change mechanism for ATP synthase — Some probabilities and possibilities', *Biochimica et Biophysica Acta (BBA) - Bioenergetics*. Elsevier, 1140(3), pp. 215–250. doi: 10.1016/0005-2728(93)90063-L.

Boyer, P. D., Cross, R. L. and Momsen, W. (1973) 'A new concept for energy coupling in oxidative phosphorylation based on a molecular explanation of the oxygen exchange reactions.', *Proceedings of the National Academy of Sciences of the United States of America*. National Academy of Sciences, 70(10), pp. 2837–9. doi: 10.1073/pnas.70.10.2837.

Brune, D. (2004) *Advances in Photosynthesis. Anoxygenic Photosynthetic Bacteria*. Available at: https://link.springer.com/content/pdf/10.1007%2F0-306-47954-0.pdf (Accessed: 29 August 2019).

Brunisholz, R. A. *et al.* (1985) 'The light-harvesting polypeptides of Rhodopseudomonas viridis. The complete amino-acid sequences of B1015-alpha, B1015-beta and B1015-gamma.', *Biological chemistry Hoppe-Seyler*, 366(1), pp. 87–98. doi: 10.1515/BCHM3.1985.366.1.87.

Brunisholz, R. A. and Zuber, H. (1992) 'Structure, function and organization of antenna polypeptides and antenna complexes from the three families of Rhodospirillaneae', *Journal of Photochemistry and Photobiology, B: Biology*. doi: 10.1016/1011-1344(92)87010-7.

Busselez, J. *et al.* (2007a) 'Structural basis for the PufX-mediated dimerization of bacterial photosynthetic core complexes.', *Structure (London, England : 1993)*. Elsevier, 15(12), pp. 1674–83. doi: 10.1016/j.str.2007.09.026.

Busselez, J. *et al.* (2007b) 'Structural Basis for the PufX-Mediated Dimerization of Bacterial Photosynthetic Core Complexes', *Structure*, 15(12), pp. 1674–1683. doi: 10.1016/j.str.2007.09.026.

Busselez, J. *et al.* (2007c) 'Structural Basis for the PufX-Mediated Dimerization of Bacterial Photosynthetic Core Complexes', *Structure*, 15(12), pp. 1674–1683. doi: 10.1016/j.str.2007.09.026.

Bustamante, C. *et al.* (1994) 'Entropic Elasticity of X-Phage DNA', *Science*, 265(5178), pp. 1599–1600.

Bustamante, P. L. and Loach, P. A. (1994) 'Reconstitution of a Functional Photosynthetic Receptor Complex with Isolated Subunits of Core Light-Harvesting Complex and Reaction Centers', *Biochemistry*, 33(45), pp. 13329–13339. doi: 10.1021/bi00249a020.

Bylina, E. J. and Youvan, D. C. (1988) 'Directed mutations affecting spectroscopic and electron transfer properties of the primary donor in the photosynthetic reaction center.', *Proceedings of the National Academy of Sciences of the United States of America*. National Academy of Sciences, 85(19), pp. 7226–30. doi: 10.1073/pnas.85.19.7226.

Caffrey, M. *et al.* (1992) 'Cytochrome c2 mutants of Rhodobacter capsulatus.', *Archives of biochemistry and biophysics*, 292(2), pp. 419–26. doi: 10.1016/0003-9861(92)90011-k.

Camara-Artigas, A., Brune, D. and Allen, J. P. (2002) 'Interactions between lipids and bacterial reaction centers determined by protein crystallography.', *Proceedings of the National Academy of Sciences of the United States of America*, 99(17), pp. 11055–60. doi: 10.1073/pnas.162368399.

Canniffe, D. P. and Hunter, C. N. (2014) 'Engineered biosynthesis of bacteriochlorophyll b in Rhodobacter sphaeroides', *Biochimica et Biophysica Acta - Bioenergetics*. Elsevier, 1837(10), pp. 1611–1616. doi: 10.1016/j.bbabio.2014.07.011.

Capaldi, R. A. *et al.* (1996) 'Structural changes in the γ and ε subunits of theEscherichia coli

F1F0-type ATPase during energy coupling', *Journal of Bioenergetics and Biomembranes*. Kluwer Academic Publishers-Plenum Publishers, 28(5), pp. 397–401. doi: 10.1007/BF02113980.

Carrion-Vazquez, M. *et al.* (2000) 'Mechanical design of proteins studied by single-molecule force spectroscopy and protein engineering.', *Progress in biophysics and molecular biology*. Prog Biophys Mol Biol, 74(1–2), pp. 63–91. doi: 10.1016/s0079-6107(00)00017-1.

Cartron, Michaël L. *et al.* (2014) 'Integration of energy and electron transfer processes in the photosynthetic membrane of Rhodobacter sphaeroides', *Biochimica et Biophysica Acta (BBA) - Bioenergetics*, 1837(10), pp. 1769–1780. doi: 10.1016/j.bbabio.2014.02.003.

Cartron, Micha??l L. *et al.* (2014) 'Integration of energy and electron transfer processes in the photosynthetic membrane of Rhodobacter sphaeroides', *Biochimica et Biophysica Acta - Bioenergetics*. doi: 10.1016/j.bbabio.2014.02.003.

Casuso, I. *et al.* (2012) 'Characterization of the motion of membrane proteins using high-speed atomic force microscopy', *NATURE NANOTECHNOLOGY*, 7(8), p. 525. doi: 10.1038/NNANO.2012.109.

Chang, C.-H. *et al.* (1986) *Structure of Rhodopseudomonas sphaeroides R-26 reaction center*.

Chang, M. C. *et al.* (1990) 'Spectroscopic characterization of the light-harvesting complex of Rhodospirillum rubrum and its structural subunit', *Biochemistry*. American Chemical Society, 29(2), pp. 421–429. doi: 10.1021/bi00454a017.

Cogdell, R. J. *et al.* (1983) 'The isolation and partial characterisation of the light-harvesting pigment-protein complement of Rhodopseudomonas acidophila', *BBA - Bioenergetics*, 722(3), pp. 427–435. doi: 10.1016/0005-2728(83)90058-0.

Cogdell, R. J. *et al.* (1990) 'Isolation and characterisation of an unusual antenna complex from the marine purple sulphur photosynthetic bacterium Chromatium purpuratum BN5500', *Biochimica et Biophysica Acta (BBA) - Bioenergetics*. Elsevier, 1019(3), pp. 239–244. doi: 10.1016/0005-2728(90)90199-E.

Cogdell, R. J. *et al.* (1999) 'How photosynthetic bacteria harvest solar energy.', *Journal of*

*bacteriology*. American Society for Microbiology (ASM), 181(13), pp. 3869–79. Available at: http://www.ncbi.nlm.nih.gov/pubmed/10383951 (Accessed: 6 September 2019).

Conlan, S. *et al.* (2000) 'Biochemical and biophysical characterization of OmpG: A monomeric porin.', *Biochemistry*. Biochemistry, 39(39), pp. 11845–54. doi: 10.1021/bi001065h.

Crofts, A. R. (2004) 'THE CYTOCHROME BC 1 COMPLEX: Function in the Context of Structure', *Annu. Rev. Physiol*, 66, pp. 689–733. doi: 10.1146/annurev.physiol.66.032102.150251.

Crofts, A. R. (2005) 'The Q-cycle — a personal perspective', in *Discoveries in Photosynthesis*. Berlin/Heidelberg: Springer-Verlag, pp. 479–499. doi: 10.1007/1-4020-3324-9_46.

Cross, R. L. (2000) 'The rotary binding change mechanism of ATP synthases', *Biochimica et Biophysica Acta (BBA) - Bioenergetics*. Elsevier, 1458(2–3), pp. 270–275. doi: 10.1016/S0005-2728(00)00079-7.

Crouch, L. I., Holden-Dye, K. and Jones, M. R. (2010) 'Dimerisation of the Rhodobacter sphaeroides RC–LH1 photosynthetic complex is not facilitated by a GxxxG motif in the PufX polypeptide', *Biochimica et Biophysica Acta (BBA) - Bioenergetics*. Elsevier, 1797(11), pp. 1812–1819. doi: 10.1016/J.BBABIO.2010.07.007.

Crouch, L. I. and Jones, M. R. (2012) 'Cross-species investigation of the functions of the Rhodobacter PufX polypeptide and the composition of the RC–LH1 core complex', *Biochimica et Biophysica Acta (BBA) - Bioenergetics*, 1817(2), pp. 336–352. doi: 10.1016/j.bbabio.2011.10.009.

Damaghi, M. *et al.* (2010) 'Dual energy landscape: The functional state of the β-barrel outer membrane protein G molds its unfolding energy landscape', *PROTEOMICS*. John Wiley & Sons, Ltd, 10(23), pp. 4151–4162. doi: 10.1002/pmic.201000241.

Darrouzet, E., Cooley, J. W. and Daldal, F. (2004) 'The Cytochrome bc $_1$ Complex and its Homologue the b $_6$ f Complex: Similarities and Differences', *Photosynthesis Research*, 79(1), pp. 25–44. doi: 10.1023/B:PRES.0000011926.47778.4e.

Davis, C. M. *et al.* (1997) 'Evaluation of structure-function relationships in the core light-harvesting complex of photosynthetic bacteria by reconstitution with mutant polypeptides', *Biochemistry*. American Chemical Society , 36(12), pp. 3671–3679. doi: 10.1021/bi962386p.

DeHoff, B. S. *et al.* (1988) 'In vivo analysis of puf operon expression in Rhodobacter sphaeroides after deletion of a putative intercistronic transcription terminator.', *Journal of bacteriology*, 170(10), pp. 4681–4692. doi: 10.1128/jb.170.10.4681-4692.1988.

Deisenhofer, J. *et al.* (1984) 'X-ray structure analysis of a membrane protein complex', *Journal of Molecular Biology*, 180(2), pp. 385–398. doi: 10.1016/S0022-2836(84)80011-X.

Deisenhofer, J. *et al.* (1985) 'Structure of the protein subunits in the photosynthetic reaction center of', *Nature*. Available at: https://www.nature.com/articles/318618a0.pdf (Accessed: 3 July 2019).

Deisenhofer, J. *et al.* (1995) 'Crystallographic refinement at 2.3 Å Resolution and Refined Model of the Photosynthetic Reaction Centre fromRhodopseudomonas viridis', *Journal of Molecular Biology*. Academic Press, 246(3), pp. 429–457. doi: 10.1006/JMBI.1994.0097.

Deisenhofer, J. and Michel, H. (1988) *The Photosynthetic Reaction Center from the Purple Bacterium Rhodops eudomonas viridis*. Available at: http://science.sciencemag.org/ (Accessed: 4 July 2019).

Doi, M. and Edwards, S. F. (no date) *The Theory of Polymer Dynamics CLARENDON PRESS " OXFORD*. Available at: https://cds.cern.ch/record/346518/files/0198520336_TOC.pdf (Accessed: 10 June 2020).

Drepper, F. *, Dorlet, P. A. and Mathis, P. (1997) 'Cross-Linked Electron Transfer Complex between Cytochrome c2 and the Photosynthetic Reaction Center of Rhodobacter sphaeroides†'. American Chemical Society. doi: 10.1021/BI961350U.

Duncan, T. M. *et al.* (1995) 'Rotation of subunits during catalysis by Escherichia coli F1-ATPase.', *Proceedings of the National Academy of Sciences of the United States of America*. National Academy of Sciences, 92(24), pp. 10964–8. doi: 10.1073/pnas.92.24.10964.

Ehrenreich, A. and Widdel, F. (1994) *Anaerobic Oxidation of Ferrous Iron by Purple Bacteria, a New Type of Phototrophic Metabolism*, *APPLIED AND ENVIRONMENTAL MICROBIOLOGY*. Available at: https://www.ncbi.nlm.nih.gov/pmc/articles/PMC202013/pdf/aem00029-0311.pdf (Accessed: 29 August 2019).

Engelhardt, H., Engel, A. and Baumeister, W. (1986) 'Stoichiometric model of the photosynthetic unit of Ectothiorhodospira halochloris', *Proceedings of the National Academy of Sciences*, 83(23), pp. 8972–8976. doi: 10.1073/pnas.83.23.8972.

Evans, M. B., Hawthornthwaite, A. M. and Cogdell, R. J. (1990) 'Isolation and characterisation of the different B800–850 light-harvesting complexes from low- and high-light grown cells of Rhodopseudomonas palustris, strain 2.1.6', *Biochimica et Biophysica Acta (BBA) - Bioenergetics*, 1016(1), pp. 71–76. doi: 10.1016/0005-2728(90)90008-R.

Fajardo, D. A. *et al.* (1998) 'Biochemistry and regulation of a novel Escherichia coli K-12 porin protein, OmpG, which produces unusually large channels.', *Journal of bacteriology*. American Society for Microbiology (ASM), 180(17), pp. 4452–9. Available at: http://www.ncbi.nlm.nih.gov/pubmed/9721282 (Accessed: 8 July 2020).

Fajer, J. *et al.* (1975) 'Primary charge separation in bacterial photosynthesis: oxidized chlorophylls and reduced pheophytin', *Proceedings of the National Academy of Sciences*. National Academy of Sciences, 72(12), pp. 4956–4960. doi: 10.1073/PNAS.72.12.4956.

Farchaus, J. W., Gruenberg, H. and Oesterhelt, D. (1990) *Complementation of a Reaction Center-Deficient Rhodobacter sphaeroides pufLMX Deletion Strain in trans with pufBALM Does Not Restore the Photosynthesis-Positive Phenotype*, *JOURNAL OF BACTERIOLOGY*. Available at: https://www.ncbi.nlm.nih.gov/pmc/articles/PMC208526/pdf/jbacter01044-0475.pdf (Accessed: 29 August 2019).

Ferrieres, L. *et al.* (2010) 'Silent Mischief: Bacteriophage Mu Insertions Contaminate Products of Escherichia coli Random Mutagenesis Performed Using Suicidal Transposon Delivery Plasmids Mobilized by Broad-Host-Range RP4 Conjugative Machinery', pp. 6418–6427.

Ferrières, L. *et al.* (2010) 'Silent mischief: Bacteriophage Mu insertions contaminate products of Escherichia coli random mutagenesis performed using suicidal transposon delivery plasmids mobilized by broad-host-range RP4 conjugative machinery', *Journal of Bacteriology*, 192(24), pp. 6418–6427. doi: 10.1128/JB.00621-10.

Fisher, T. E. *et al.* (1999) 'The study of protein mechanics with the atomic force microscope.', *Trends in biochemical sciences*. Elsevier, 24(10), pp. 379–84. doi: 10.1016/s0968-0004(99)01453-x.

Fotiadis, D. *et al.* (2003) *Structural analysis of the RC-LH1 photosynthetic core complex of Rhodospirillum rubrum using atomic force microscopy Downloaded from*. JBC Papers in Press. Available at: http://www.jbc.org/ (Accessed: 20 February 2019).

Fowler, G. J. S. *et al.* (1994) 'Blue shifts in bacteriochlorophyll absorbance correlate with changed hydrogen bonding patterns in light-harvesting 2 mutants of Rhodobacter sphaeroides with alterations at α-Tyr-44 and α-Tyr-45: Figure 2', *Biochemical Journal*, 299(3), pp. 695–700. doi: 10.1042/bj2990695.

Fowler, G. J. S. *et al.* (1997) 'The Role of βArg $_{-10}$ in the B800 Bacteriochlorophyll and Carotenoid Pigment Environment within the Light-Harvesting LH2 Complex of *Rhodobacter sphaeroides* †', *Biochemistry*, 36(37), pp. 11282–11291. doi: 10.1021/bi9626315.

Francia, F. *et al.* (2002) 'Role of the N- and C-terminal regions of the PufX protein in the structural organization of the photosynthetic core complex of Rhodobacter sphaeroides', *European Journal of Biochemistry*. John Wiley & Sons, Ltd, 269(7), pp. 1877–1885. doi: 10.1046/j.1432-1033.2002.02834.x.

Francia, F. *et al.* (2004) 'Light-Harvesting Complex 1 Stabilizes P + Q B-Charge Separation in Reaction Centers of Rhodobacter sphaeroides †'. doi: 10.1021/bi048629s.

Francia, F. ‡ *et al.* (1999) 'The Reaction Center−LH1 Antenna Complex of Rhodobacter sphaeroides Contains One PufX Molecule Which Is Involved in Dimerization of This Complex'. American Chemical Society. doi: 10.1021/BI982891H.

Frese, R. N. *et al.* (2004) 'The long-range organization of a native photosynthetic membrane', *Proceedings of the National Academy of Sciences of the United States of*

*America*, 101(52), pp. 17994–17999. doi: 10.1073/pnas.0407295102.

Frigaard, N. U. and Dahl, C. (2008) 'Sulfur Metabolism in Phototrophic Sulfur Bacteria', *Advances in Microbial Physiology*. doi: 10.1016/S0065-2911(08)00002-7.

Fuchs, B. M. *et al.* (2007) 'Characterization of a marine gammaproteobacterium capable of aerobic anoxygenic photosynthesis', *Proceedings of the National Academy of Sciences*, 104(8), pp. 2891–2896. doi: 10.1073/pnas.0608046104.

Fuhrmann, A. and Ros, R. (2010) 'Single-molecule force spectroscopy: a method for quantitative analysis of ligand–receptor interactions', *Nanomedicine*. Future Medicine Ltd London, UK , 5(4), pp. 657–666. doi: 10.2217/nnm.10.26.

G, P. *et al.* (2005) 'Detection of HSP60 on the Membrane Surface of Stressed Human Endothelial Cells by Atomic Force and Confocal Microscopy', *Journal of cell science*. J Cell Sci, 118(Pt 8). doi: 10.1242/JCS.02292.

Gall, A. *et al.* (1997) 'Influence of the Protein Binding Site on the Absorption Properties of the Monomeric Bacteriochlorophyll in Rhodobacter sphaeroides LH2 Complex†'. American Chemical Society. doi: 10.1021/BI9717237.

Gall, A. *et al.* (1999) 'Certain species of theProteobacteria possess unusual bacteriochlorophylla environments in their light-harvesting proteins', *Biospectroscopy*, 5(6), pp. 338–345. doi: 10.1002/(SICI)1520-6343(1999)5:6<338::AID-BSPY3>3.0.CO;2-D.

Gardiner, A. T., Cogdell, R. J. and Takaichi, S. (1993) *The effect of growth conditions on the light-harvesting apparatus in Rhodopseudomonas acidophila*, *Photosynthesis Research*. Kluwer Academic Publishers. Available at: https://link.springer.com/content/pdf/10.1007%2FBF00146415.pdf (Accessed: 9 July 2019).

Gast, P. *et al.* (1985) *Determination of the amount and the type of quinones present in single crystals from reaction center protein from the photosynthetic bacterium Rhodopseudomonas viridis*, *FEBS Letters*. doi: 10.1016/0014-5793(85)80544-5.

Gonçalves, R. P. *et al.* (2005) 'Architecture of the native photosynthetic apparatus of Phaeospirillum molischianum', *Journal of Structural Biology*, 152(3), pp. 221–228. doi: 10.1016/j.jsb.2005.10.002.

Gonçalves, R. P. and Scheuring, S. (2006) 'Manipulating and imaging individual membrane proteins by AFM', *Surface and Interface Analysis*. John Wiley & Sons, Ltd, 38(11), pp. 1413–1418. doi: 10.1002/sia.2350.

Gong, D.-W. *et al.* (1996) 'Genomic Structure and Promoter Analysis of the Human *obese* Gene', *Journal of Biological Chemistry*, 271(8), pp. 3971–3974. doi: 10.1074/jbc.271.8.3971.

van Grondelle, R. *et al.* (1994) 'Energy transfer and trapping in photosynthesis', *Biochimica et Biophysica Acta (BBA) - Bioenergetics*. Elsevier, 1187(1), pp. 1–65. doi: 10.1016/0005-2728(94)90166-X.

Gubellini, F. *et al.* (2006) 'Functional and Structural Analysis of the Photosynthetic Apparatus of *Rhodobacter veldkampii* †', *Biochemistry*, 45(35), pp. 10512–10520. doi: 10.1021/bi0610000.

Guo, H., Suzuki, T. and Rubinstein, J. L. (2019) 'Structure of a bacterial ATP synthase', *eLife*, 8. doi: 10.7554/eLife.43128.

Gupta, R. S. and Khadka, B. (2016) 'Evidence for the presence of key chlorophyll-biosynthesis-related proteins in the genus Rubrobacter (Phylum Actinobacteria) and its implications for the evolution and origin of photosynthesis', *Photosynthesis Research*, 127(2), pp. 201–218. doi: 10.1007/s11120-015-0177-y.

Hansen, T. A. and Gemerden, H. (1972) 'Sulfide utilization by purple nonsulfur bacteria', *Archiv f□r Mikrobiologie*. Springer-Verlag, 86(1), pp. 49–56. doi: 10.1007/BF00412399.

Hartigan, N. *et al.* (2002) 'The 7.5-Å electron density and spectroscopic properties of a novel low-light B800 LH2 from Rhodopseudomonas palustris', *Biophysical Journal*. doi: 10.1016/S0006-3495(02)75456-8.

Haselgrübler, T. *et al.* (1995) 'Synthesis and applications of a new poly(ethylene glycol) derivative for the crosslinking of amines with thiols.', *Bioconjugate chemistry*. Bioconjug Chem, 6(3), pp. 242–8. doi: 10.1021/bc00033a002.

Hatch, L. P., Cox, G. B. and Howitt, S. M. (1995) 'The essential arginine residue at position 210 in the alpha subunit of the Escherichia coli ATP synthase can be transferred to position 252 with partial retention of activity.', *The Journal of biological chemistry*. American Society

for Biochemistry and Molecular Biology, 270(49), pp. 29407–12. doi: 10.1074/jbc.270.49.29407.

Heldt, H.-W. and Piechulla, B. (2011) *Plant biochemistry*. Academic.

Hinterdorfer, P. *et al.* (1996) 'Detection and localization of individual antibody-antigen recognition events by atomic force microscopy.', *Proceedings of the National Academy of Sciences of the United States of America*. National Academy of Sciences, 93(8), pp. 3477–81. doi: 10.1073/pnas.93.8.3477.

Holden-Dye, K., Crouch, L. I. and Jones, M. R. (2008) 'Structure, function and interactions of the PufX protein', *Biochimica et Biophysica Acta*, 1777, pp. 613–630. doi: 10.1016/j.bbabio.2008.04.015.

Hu, X. *et al.* (1998) 'Architecture and mechanism of the light-harvesting apparatus of purple bacteria', *Computational Biomolecular Science*, 95, pp. 5935–5941.

Hu, X. *et al.* (2002) 'Photosynthetic apparatus of purple bacteria', *Quarterly Reviews of Biophysics*. Cambridge University Press, 35, pp. 1–62. doi: 10.1017/S0033583501003754.

Hunter, C. *et al.* (2008) 'The Purple Phototrophic Bacteria'. Dordrecht: Springer.

Imanishi, M. *et al.* (2019) 'A Dual Role for $Ca^{2+}$ in Expanding the Spectral Diversity and Stability of Light-Harvesting 1 Reaction Center Photocomplexes of Purple Phototrophic Bacteria', *Biochemistry*. American Chemical Society, 58(25), pp. 2844–2852. doi: 10.1021/acs.biochem.9b00351.

Imhoff, J. F., Hiraishi, A. and Süling, J. (2005) *Anoxygenic Phototrophic Purple Bacteria*, *Bergey's Manual® of Systematic Bacteriology*. doi: 10.1007/0-387-28021-9_15.

Jackson, P. J. *et al.* (2018) 'Identification of protein W, the elusive sixth subunit of the Rhodopseudomonas palustris reaction center-light harvesting 1 core complex', *Biochimica et Biophysica Acta (BBA) - Bioenergetics*. Elsevier, 1859(2), pp. 119–128. doi: 10.1016/j.bbabio.2017.11.001.

Jamieson, S. J. *et al.* (2002) 'Projection structure of the photosynthetic reaction centre-antenna complex of Rhodospirillum rubrum at 8.5 ?? resolution', *EMBO Journal*. doi: 10.1093/emboj/cdf410.

Janosi, L. *et al.* (2006) 'Influence of subunit structure on the oligomerization state of light-harvesting complexes: A free energy calculation study', *Chemical Physics*. doi: 10.1016/j.chemphys.2005.08.038.

Jault, J.-M. *et al.* (1995) *Complex of the Fi-ATPase from Thermophilic Bacillus PS 3 Containing the CX.D261N Substitution Fails To Dissociate Inhibitory MgADP from a Catalytic Site When ATP Binds to Noncatalytic Sites1"*, *Biochemistry*. Available at: https://pubs.acs.org/sharingguidelines (Accessed: 30 August 2019).

Jault, J. and Allison, W. (1993) *Slow binding of ATP to noncatalytic nucleotide binding sites which accelerates catalysis is responsible for apparent negative cooperativity exhibit... - PubMed - NCBI*, *J Biol Chem*. Available at: https://www.ncbi.nlm.nih.gov/pubmed/8420930 (Accessed: 30 August 2019).

Jay, F., Lambillotte, M. and Mühlethaler, K. (1983) 'Localisation of Rhodopseudomonas viridis reaction centre and light harvesting proteins using ferritin-antibody labelling.', *European journal of cell biology*, 30(1), pp. 1–8. Available at: http://www.ncbi.nlm.nih.gov/pubmed/6189715 (Accessed: 18 September 2019).

Jenney, F. E. and Daldal, F. (1993) 'A novel membrane-associated c-type cytochrome, cyt cy, can mediate the photosynthetic growth of Rhodobacter capsulatus and Rhodobacter sphaeroides.', *The EMBO journal*. European Molecular Biology Organization, 12(4), pp. 1283–92. doi: 10.1002/J.1460-2075.1993.TB05773.X.

Jones, M. R. *et al.* (1992) 'Mutants of Rhodobacter sphaeroides lacking one or more pigment-protein complexes and complementation with reaction-centre, LH1, and LH2 genes', *Molecular Microbiology*, 6(9), pp. 1173–1184. doi: 10.1111/j.1365-2958.1992.tb01556.x.

Jones, M. R. (2009) 'The petite purple photosynthetic powerpack', *Biochemical Society Transactions*, 37(2), pp. 400–407. doi: 10.1042/BST0370400.

Jungas, C. *et al.* (1999) 'Supramolecular organization of the photosynthetic apparatus of Rhodobacter sphaeroides', *The EMBO Journal*, 18(3), pp. 534–542.

Junge, W., Lill, H. and Engelbrecht, S. (1997) 'ATP synthase: an electrochemical ransducer

with rotatory mechanics', *Trends in Biochemical Sciences*. Elsevier Current Trends, 22(11), pp. 420–423. doi: 10.1016/S0968-0004(97)01129-8.

Junge, W., Sabber, D. and Engelbrecht, S. (1996) 'ATP-synthesis. Rotatory catalysis by F-ATPase: Real-time recording of intersubunit rotation', *Berichte der Bunsengesellschaft für physikalische Chemie*. John Wiley & Sons, Ltd, 100(12), pp. 2014–2019. doi: 10.1002/bbpc.19961001215.

Junge, W., Sielaff, H. and Engelbrecht, S. (2009) 'Torque generation and elastic power transmission in the rotary FOF1-ATPase', *Nature*, 459(7245), pp. 364–370. doi: 10.1038/nature08145.

Kayalar, C. *et al.* (1977) *An Alternating Site Sequence for Oxidative Phosphorylation Suggested by Measurement of Substrate Binding Patterns and Exchange Reaction Inhibitions**, *THE JOURNAL OF BIOLGGICAL CHEMISTRY*. Available at: http://www.jbc.org/ (Accessed: 30 August 2019).

Kedrov, A. *et al.* (2007) 'Deciphering Molecular Interactions of Native Membrane Proteins by Single-Molecule Force Spectroscopy', *Annu. Rev. Biophys. Biomol. Struct*, 36, pp. 233–60. doi: 10.1146/annurev.biophys.36.040306.132640.

Kehoe, J. W. *et al.* (1998) 'Reconstitution of Core Light-Harvesting Complexes of Photosynthetic Bacteria Using Chemically Synthesized Polypeptides. 2. Determination of Structural Features That Stabilize Complex Formation and Their Implications for the Structure of the Subunit Complex †', *Biochemistry*, 37(10), pp. 3418–3428. doi: 10.1021/bi9722709.

Kelley, L. A. *et al.* (2015) 'The Phyre2 web portal for protein modeling, prediction and analysis', *Nature Protocols*. Nature Publishing Group, 10(6), pp. 845–858. doi: 10.1038/nprot.2015.053.

Kellogg, E. C. *et al.* (1989) 'Measurement of the extent of electron transfer to the bacteriopheophytin in the M-subunit in reaction centers of Rhodopseudomonas viridis', *Photosynthesis Research*. Kluwer Academic Publishers, 22(1), pp. 47–59. doi: 10.1007/BF00114766.

Kinosita, K., Adachi, K. and Itoh, H. (2004) 'Rotation of F $_1$ -ATPase: How an ATP-Driven Molecular Machine May Work', *Annual Review of Biophysics and Biomolecular Structure*, 33(1), pp. 245–268. doi: 10.1146/annurev.biophys.33.110502.132716.

Kirmaier, C., Holten, D. and Parson, W. W. (1985) 'Picosecond-photodichroism studies of the transient states in Rhodopseudomonas sphaeroides reaction centers at 5 K. Effects of electron transfer on the six bacteriochlorin pigments', *Biochimica et Biophysica Acta (BBA) - Bioenergetics*. Elsevier, 810(1), pp. 49–61. doi: 10.1016/0005-2728(85)90205-1.

Klug, G. *et al.* (1988) *Pleiotropic Effects of Localized Rhodobacter capsulatus puf Operon Deletions on Production of Light-Absorbing Pigment-Protein Complexes*, *JOURNAL OF BACTERIOLOGY*. Available at: https://www.ncbi.nlm.nih.gov/pmc/articles/PMC211687/pdf/jbacter00190-0422.pdf (Accessed: 29 August 2019).

Klug, G. and Cohen, S. N. (1988) 'Pleiotropic effects of localized Rhodobacter capsulatus puf operon deletions on production of light-absorbing pigment-protein complexes.', *Journal of Bacteriology*, 170(12), pp. 5814–5821. doi: 10.1128/jb.170.12.5814-5821.1988.

Koblízek, M. *et al.* (2005) 'Sequential assembly of photosynthetic units in Rhodobacter sphaeroides as revealed by fast repetition rate analysis of variable bacteriochlorophyll a fluorescence', *Biochimica et Biophysica Acta (BBA) - Bioenergetics*, 1706(3), pp. 220–231. doi: 10.1016/j.bbabio.2004.11.004.

Koepke, J. *et al.* (1996) 'The crystal structure of the light-harvesting complex II (B800-850) from Rhodospirillum molischianum', *Structure*, 4(5), pp. 581–597. doi: 10.1016/S0969-2126(96)00063-9.

Kolber, Z. S. *et al.* (2001) 'Contribution of aerobic photoheterotrophic bacteria to the carbon cycle in the ocean.', *Science (New York, N.Y.)*. American Association for the Advancement of Science, 292(5526), pp. 2492–5. doi: 10.1126/science.1059707.

Kovach, M. E. *et al.* (1995) 'Four new derivatives of the broad-host-range cloning vector pBBR1MCS, carrying different antibiotic-resistance cassettes', *Gene*. Elsevier, 166(1), pp. 175–176. doi: 10.1016/0378-1119(95)00584-1.

Kumar, S. *et al.* (2016) 'Direct Imaging of Protein Organization in an Intact Bacterial Organelle Using High-Resolution Atomic Force Microscopy'. doi: 10.1021/acsnano.6b05647.

Lang, H. P. and Hunter, C. N. (1994) 'The relationship between carotenoid biosynthesis and the assembly of the light-harvesting LH2 complex in Rhodobacter sphaeroides', *Biochemical Journal*, 298(1), pp. 197–205. doi: 10.1042/bj2980197.

LaSarre, B. *et al.* (2018) 'Restricted localization of photosynthetic intracytoplasmic membranes (ICMs) in multiple genera of purple nonsulfur bacteria', *mBio*, 9(4), pp. 780–798. doi: 10.1128/mBio.00780-18.

Lemmon, M. A. *et al.* (1992) 'Sequence specificity in the dimerization of transmembrane .alpha.-helixes', *Biochemistry*. American Chemical Society, 31(51), pp. 12719–12725. doi: 10.1021/bi00166a002.

Lemmon, M. A. *et al.* (1994) 'A dimerization motif for transmembrane alpha-helices.', *Nature structural biology*. Nat Struct Biol, 1(3), pp. 157–63. doi: 10.1038/nsb0394-157.

Lilburn, T G *et al.* (1992) 'Pleiotropic effects of pufX gene deletion on the structure and function of the photosynthetic apparatus of Rhodobacter capsulatus.', *Biochimica et biophysica acta*, 1100(2), pp. 160–70. doi: 10.1016/0005-2728(92)90077-f.

Lilburn, Timothy G. *et al.* (1992) 'Pleiotropic effects of pufX gene deletion on the structure and function of the photosynthetic apparatus of Rhodobacter capsulatus', *Biochimica et Biophysica Acta (BBA) - Bioenergetics*, 1100(2), pp. 160–170. doi: 10.1016/0005-2728(92)90077-F.

Liu, L.-N. *et al.* (2008) 'Watching the Native Supramolecular Architecture of Photosynthetic Membrane in Red Algae TOPOGRAPHY OF PHYCOBILISOMES AND THEIR CROWDING, DIVERSE DISTRIBUTION PATTERNS *'. doi: 10.1074/jbc.M805114200.

Liu, L.-N. *et al.* (2009) 'Quinone Pathways in Entire Photosynthetic Chromatophores of Rhodospirillum photometricum', *Journal of Molecular Biology*, 393, pp. 27–35. doi: 10.1016/j.jmb.2009.07.044.

Liu, L.-N. *et al.* (2011) 'Forces guiding assembly of light-harvesting complex 2 in native membranes', *Proceedings of the National Academy of Sciences*, 108(23), pp. 9455–9459.

doi: 10.1073/pnas.1004205108.

Liu, L.-N. (2016) 'Distribution and dynamics of electron transport complexes in cyanobacterial thylakoid membranes.', *Biochimica et biophysica acta*. Elsevier, 1857(3), pp. 256–65. doi: 10.1016/j.bbabio.2015.11.010.

Liu, L.-N. *et al.* (2016) 'Revised Genome Sequence of the Purple Photosynthetic Bacterium Blastochloris viridis'. doi: 10.1128/genomeA.01520-15.

Liu, L.-N. and Scheuring, S. (2013) 'Investigation of photosynthetic membrane structure using atomic force microscopy', *Trends in Plant Science*, 18, pp. 277–286. doi: 10.1016/j.tplants.2013.03.001.

Liu, L.-N., Sturgis, J. N. and Scheuring, S. (2011) 'Native architecture of the photosynthetic membrane from Rhodobacter veldkampii', *Journal of Structural Biology*, 173, pp. 138–145. doi: 10.1016/j.jsb.2010.08.010.

Liu, L. N., Sturgis, J. N. and Scheuring, S. (2011) 'Native architecture of the photosynthetic membrane from Rhodobacter veldkampii', *Journal of Structural Biology*. doi: 10.1016/j.jsb.2010.08.010.

Loach, P. A. and Parkes-Loach, P. S. (1995) 'Structure-Function Relationships in Core Light-Harvesting Complexes (LHI) As Determined by Characterization of the Structural Subunit and by Reconstitution Experiments', in *Anoxygenic Photosynthetic Bacteria*. Dordrecht: Kluwer Academic Publishers, pp. 437–471. doi: 10.1007/0-306-47954-0_21.

Madigan, M. T. (2003) *Anoxygenic phototrophic bacteria from extreme environments*, *Photosynthesis Research*. Available at: http://www.life.illinois.edu/govindjee/Part2/14_Madigan.pdf (Accessed: 29 August 2019).

Mark Editor, J. E. (no date) *Physical Properties of Polymers Handbook Second Edition*. Available at: https://link.springer.com/content/pdf/10.1007%2F978-0-387-69002-5.pdf (Accessed: 14 July 2020).

Mathis, P., Ortega, J. M. and Venturoli, G. (1994) 'Interaction between cytochrome c and the photosynthetic reaction center of purple bacteria: Behaviour at low temperature', *Biochimie*, 76(6), pp. 569–579. doi: 10.1016/0300-9084(94)90181-3.

Matsui, T. *et al.* (1997) *Catalytic Activity of the 3 3 Complex of F 1-ATPase without Noncatalytic Nucleotide Binding Site**. Available at: http://www-jbc.stanford.edu/jbc/ (Accessed: 30 August 2019).

McDermott, G. *et al.* (1995) *Crystal structure of an integral membrane light-harvesting complex from photosynthetic bacteria*, *Nature*. doi: 10.1038/374517a0.

McGlynn, P., Hunter, C. N. and Jones, M. R. (1994) 'The *Rhodobacter sphaeroides* PufX protein is not required for photosynthetic competence in the absence of a light harvesting system', *FEBS Letters*. John Wiley & Sons, Ltd, 349(3), pp. 349–353. doi: 10.1016/0014-5793(94)00701-2.

Mcluskey, K. *et al.* (2001) 'The Crystallographic Structure of the B800-820 LH3 Light-Harvesting Complex from the Purple Bacteria Rhodopseudomonas Acidophila Strain 7050 †'. doi: 10.1021/bi010309a.

Menin, L. *et al.* (1998) 'Role of HiPIP as electron donor to the RC-bound cytochrome in photosynthetic purple bacteria', *Photosynthesis Research*. Kluwer Academic Publishers, 55(2/3), pp. 343–348. doi: 10.1023/A:1005989900756.

De Meur, Q. *et al.* (2018) 'Genetic Plasticity and Ethylmalonyl Coenzyme A Pathway during Acetate Assimilation in Rhodospirillum rubrum S1H under Photoheterotrophic Conditions.', *Applied and environmental microbiology*. American Society for Microbiology, 84(3), pp. e02038-17. doi: 10.1128/AEM.02038-17.

Milgrom, Y. M., Ehler, L. L. and Boyer, P. D. (1991) 'The characteristics and effect on catalysis of nucleotide binding to noncatalytic sites of chloroplast F1-ATPase.', *The Journal of biological chemistry*, 266(18), pp. 11551–8. Available at: http://www.ncbi.nlm.nih.gov/pubmed/1828802 (Accessed: 30 August 2019).

Miller, J. F. *et al.* (1987) 'Isolation and characterization of a subunit form of the light-harvesting complex of Rhodospirillum rubrum', *Biochemistry*. American Chemical Society, 26(16), pp. 5055–5062. doi: 10.1021/bi00390a026.

Miller, L. *et al.* (2020) 'Unfolding pathway and intermolecular interactions of the cytochromesubunit in the bacterial photosynthetic reaction center', *BBA-Bioenergetics*.

Available at:
https://reader.elsevier.com/reader/sd/pii/S0005272820300542?token=BF6C9D33C23A12AAE405A4B041D506D5512C6A187ABC578837D3A6D1FF64674AF6CEFB9AF9C54F8D5463B03078F12DCE (Accessed: 25 June 2020).

Mothersole, D. J. *et al.* (2016) 'PucC and LhaA direct efficient assembly of the light-harvesting complexes in Rhodobacter sphaeroides', *Molecular Microbiology*. doi: 10.1111/mmi.13235.

van Mourik, F., Visschers, R. W. and van Grondelle, R. (1992) 'Energy transfer and aggregate size effects in the inhomogeneously broadened core light-harvesting complex of Rhodobacter sphaeroides', *Chemical Physics Letters*. North-Holland, 193(1–3), pp. 1–7. doi: 10.1016/0009-2614(92)85674-Y.

Müller, D. J. and Dufrêne, Y. F. (2011) 'Atomic force microscopy: a nanoscopic window on the cell surface.', *Trends in cell biology*. Elsevier, 21(8), pp. 461–9. doi: 10.1016/j.tcb.2011.04.008.

Müller, D. J. and Engel, A. (2007) 'Atomic force microscopy and spectroscopy of native membrane proteins', *Nature Protocols*. Nature Publishing Group, 2(9), pp. 2191–2197. doi: 10.1038/nprot.2007.309.

Munk, A. C. *et al.* (2011) 'Complete genome sequence of Rhodospirillum rubrum type strain (S1T)', *Standards in Genomic Sciences*, 4(3), pp. 293–302. doi: 10.4056/sigs.1804360.

Myllykallio, H. *et al.* (1998) 'Membrane-Anchored Cytochrome $c_y$ Mediated Microsecond Time Range Electron Transfer from the Cytochrome $bc_1$ Complex to the Reaction Center in *Rhodobacter c apsulatus* †', *Biochemistry*, 37(16), pp. 5501–5510. doi: 10.1021/bi973123d.

Neil Hunter, C. *et al.* (1990) *Energy-Transfer Dynamics in Three Light-Harvesting Mutants of Rhodobacter sphaeroides: A Picosecond Spectroscopy Study* 1"*, *Biochemistry*. Available at: https://pubs.acs.org/sharingguidelines (Accessed: 7 July 2020).

Niedzwiedzki, D. M. *et al.* (2011) 'Energy transfer in an LH4-like light harvesting complex from the aerobic purple photosynthetic bacterium Roseobacter denitrificans', *Biochimica et Biophysica Acta (BBA) - Bioenergetics*, 1807(5), pp. 518–528. doi:

10.1016/j.bbabio.2011.03.004.

Nieto, F. *et al.* (2010) 'Electron microscopy: SEM/TEM', *Handbook of Physics in Medicine and Biology*, pp. 40-1-40–16. doi: 10.1201/9781420075250.

Niwa, S. *et al.* (2014a) 'Structure of the LH1-RC complex from Thermochromatium tepidum at 3.0 A °', *Nature*, 508. doi: 10.1038/nature13197.

Niwa, S. *et al.* (2014b) 'Structure of the LH1–RC complex from Thermochromatium tepidum at 3.0 Å', *Nature*, 508(7495), pp. 228–232. doi: 10.1038/nature13197.

Nogi, T., Hirano, Y. and Miki, K. (2005) *Structural and functional studies on the tetraheme cytochrome subunit and its electron donor proteins: The possible docking mechanisms during the electron transfer reaction*, *Photosynthesis Research*. doi: 10.1007/s11120-004-2416-5.

Noji, H. *et al.* (1997) 'Direct observation of the rotation of F1-ATPase', *Nature*, 386(6622), pp. 299–302. doi: 10.1038/386299a0.

Nottoli, M. *et al.* (2018) 'The role of charge-transfer states in the spectral tuning of antenna complexes of purple bacteria', *Photosynthesis Research*. Springer Netherlands, 137(2), pp. 215–226. doi: 10.1007/s11120-018-0492-1.

Oberhauser, A. *et al.* (1998) 'The molecular elasticity of the extracellular matrix protein tenascin', *Nature*, 393.

Oberhauser, A. F. *et al.* (1998) 'The molecular elasticity of the extracellular matrix protein tenascin', *Nature*. Nature Publishing Group, 393(6681), pp. 181–185. doi: 10.1038/30270.

Oesterhelt, F. *et al.* (2000) 'Bacteriorhodopsin unfolding pathway', *Science*, 288, pp. 143–146.

van Oijen, A. M. van *et al.* (1999) 'Unraveling the electronic structure of individual photosynthetic pigment-protein complexes', *Science (New York, N.Y.)*. American Association for the Advancement of Science, 285(5426), pp. 400–2. doi: 10.1126/science.285.5426.400.

Okamura, M. . *et al.* (2000) 'Proton and electron transfer in bacterial reaction centers', *Biochimica et Biophysica Acta (BBA) - Bioenergetics*. Elsevier, 1458(1), pp. 148–163. doi:

10.1016/S0005-2728(00)00065-7.

Olsen, J. D. *et al.* (1997) 'Site-Directed Modification of the Ligands to the Bacteriochlorophylls of the Light-Harvesting LH1 and LH2 Complexes of Rhodobacter sphaeroides†', *Biochemistry*. American Chemical Society, 36, pp. 12625–12632. doi: 10.1021/BI9710481.

Olsen, John D. *et al.* (2014) 'Aberrant Assembly Complexes of the Reaction Center Light-harvesting 1 PufX (RC-LH1-PufX) Core Complex of Rhodobacter sphaeroides Imaged by Atomic Force Microscopy', *The Journal of Biological Chemistry*. American Society for Biochemistry and Molecular Biology, 289(43), p. 29927. doi: 10.1074/JBC.M114.596585.

Olsen, John D *et al.* (2014) 'Aberrant Assembly Complexes of the Reaction Center Light-harvesting 1 PufX (RC-LH1-PufX) Core Complex of Rhodobacter sphaeroides Imaged by Atomic Force Microscopy *', *Published JBC Papers in Press*. doi: 10.1074/jbc.M114.596585.

Olson, T. L., Williams, J. C. and Allen, J. P. (2014) 'The three-dimensional structures of bacterial reaction centers', *Photosynthesis Research*, 120(1–2), pp. 87–98. doi: 10.1007/s11120-013-9821-6.

Ortega, J. M., Drepper, F. and Mathis, P. (1999) 'Electron transfer between cytochrome c(2) and the tetraheme cytochrome c in Rhodopseudomonas viridis', *Photosynthesis Research*, 59(2–3), pp. 147–157. doi: 10.1023/A:1006149621029.

Pandit, A. *et al.* (2003) 'Investigations of intermediates appearing in the reassociation of the light-harvesting 1 complex of Rhodospirillum rubrum.', *Photosynth Res.*, 3(75), pp. 235–48. Available at: https://www.ncbi.nlm.nih.gov/pubmed/16228604 (Accessed: 6 September 2019).

Pänke, O. *et al.* (2000) 'F-ATPase: specific observation of the rotating c subunit oligomer of EF(o)EF(1).', *FEBS letters*, 472(1), pp. 34–8. doi: 10.1016/s0014-5793(00)01436-8.

Papiz, M. Z. *et al.* (2003) 'The structure and thermal motion of the B800-850 LH2 complex from Rps. acidophila at 2.0 Å resolution and 100 K: New structural features and functionally relevant motions', *Journal of Molecular Biology*. doi: 10.1016/S0022-2836(03)00024-X.

Parkes-Loach, P. S. *et al.* (2000) 'Articles Role of the Core Region of the PufX Protein in

Inhibition of Reconstitution of the Core Light-Harvesting Complexes of Rhodobacter sphaeroides and Rhodobacter capsulatus †'. doi: 10.1021/bi002580i.

Parkes-Loach, P. S. *et al.* (2004) 'Interactions Stabilizing the Structure of the Core Light-Harvesting Complex (LH1) of Photosynthetic Bacteria and Its Subunit (B820) †', *Biochemistry*, 43(22), pp. 7003–7016. doi: 10.1021/bi049798f.

Pogoryelov, D. *et al.* (2009) 'High-resolution structure of the rotor ring of a proton-dependent ATP synthase', *Nature Structural & Molecular Biology*, 16(10), pp. 1068–1073. doi: 10.1038/nsmb.1678.

Polívka, T. and Frank, H. A. (2010) 'Molecular Factors Controlling Photosynthetic Light Harvesting by Carotenoids', *Accounts of Chemical Research*. American Chemical Society, 43(8), pp. 1125–1134. doi: 10.1021/ar100030m.

Prince, S. M. *et al.* (1997) 'Apoprotein structure in the LH2 complex from Rhodopseudomonas acidophila strain 10050: Modular assembly and protein pigment interactions', *Journal of Molecular Biology*. doi: 10.1006/jmbi.1997.0966.

Pugh, R. J. *et al.* (1998) 'The LH1–RC core complex of Rhodobacter sphaeroides: interaction between components, time-dependent assembly, and topology of the PufX protein', *Biochimica et Biophysica Acta (BBA) - Bioenergetics*. Elsevier, 1366(3), pp. 301–316. doi: 10.1016/S0005-2728(98)00131-5.

Pullerits, T. and Sundström, V. (1996) 'Photosynthetic Light-Harvesting Pigment−Protein Complexes: Toward Understanding How and Why'. American Chemical Society. doi: 10.1021/AR950110O.

Puntheeranurak, T. *et al.* (2006) 'Ligands on the string: single-molecule AFM studies on the interaction of antibodies and substrates with the Na+-glucose co-transporter SGLT1 in living cells.', *Journal of cell science*. J Cell Sci, 119(Pt 14), pp. 2960–7. doi: 10.1242/jcs.03035.

Qian, P. *et al.* (2013) 'Three-dimensional structure of the Rhodobacter sphaeroides rc-lh1-pufx complex: Dimerization and quinone channels promoted by PufX', *Biochemistry*, 52(43), pp. 7575–7585. doi: 10.1021/bi4011946.

Qian, P. (2017) 'Structure and Function of the Reaction Centre – Light Harvesting 1 Core

Complexes from Purple Photosynthetic Bacteria', in *Photosynthesis: Structures, Mechanisms, and Applications*. Cham: Springer International Publishing, pp. 11–31. doi: 10.1007/978-3-319-48873-8_2.

Qian, P. *et al.* (2018) 'Cryo-EM structure of the Blastochloris viridis LH1-RC complex at 2.9 Å', *Nature*, 556(7700), pp. 203–208. doi: 10.1038/s41586-018-0014-5.

Qian, P., Bullough, P. A. and Hunter, C. N. (2008) 'Three-dimensional reconstruction of a membrane-bending complex: The RC-LH1-PufX core dimer of rhodobacter sphaeroides', *Journal of Biological Chemistry*. doi: 10.1074/jbc.M800625200.

Qian, P., Hunter, C. N. and Bullough, P. A. (2005) 'The 8.5 Å projection structure of the core RC-LH1-PufX dimer of Rhodobacter sphaeroides', *Journal of Molecular Biology*. doi: 10.1016/j.jmb.2005.04.032.

Rastogi, V. K. and Girvin, M. E. (1999) 'Structural changes linked to proton translocation by subunit c of the ATP synthase', *Nature*, 402(6759), pp. 263–268. doi: 10.1038/46224.

Ratcliffe, E. C. *et al.* (2011) 'Experimental evidence that the membrane-spanning helix of PufX adopts a bent conformation that facilitates dimerisation of the Rhodobacter sphaeroides RC–LH1 complex through N-terminal interactions', *Biochimica et Biophysica Acta (BBA) - Bioenergetics*. Elsevier, 1807(1), pp. 95–107. doi: 10.1016/J.BBABIO.2010.10.003.

Rathgeber, C., Beatty, J. T. and Yurkov, V. (2004) *Aerobic phototrophic bacteria: New evidence for the diversity, ecological importance and applied potential of this previously overlooked group*, *Photosynthesis Research*. doi: 10.1023/B:PRES.0000035036.49977.bc.

Rico, F. *et al.* (2013) 'High-speed force spectroscopy unfolds titin at the velocity of molecular dynamics simulations', *Science*, 342(6159), pp. 741–743. doi: 10.1126/science.1239764.

Rief, M. *et al.* (1999) 'Single molecule force spectroscopy of spectrin repeats: low unfolding forces in helix bundles 1 1Edited by W. Baumeister', *Journal of Molecular Biology*, 286(2), pp. 553–561. doi: 10.1006/jmbi.1998.2466.

Rieske, J. S., MacLennan, D. H. and Coleman, R. (1964) 'Isolation and properties of an iron-protein from the (reduced coenzyme Q)-cytochrome C reductase complex of the respiratory

chain', *Biochemical and Biophysical Research Communications*. doi: 10.1016/0006-291X(64)90171-8.

Rodriguez-Ramos, J., Faulkner, M. and Liu, L.-N. (2018) 'Nanoscale Visualization of Bacterial Microcompartments Using Atomic Force Microscopy', in. Humana Press, New York, NY, pp. 373–383. doi: 10.1007/978-1-4939-8591-3_22.

Rosen, D. *et al.* (1983) 'Interaction of cytochrome c with reaction centers of Rhodopseudomonas sphaeroides R-26: localization of the binding site by chemical crosslinking and immunochemical studies', *Biochemistry*, 22(2), pp. 335–341. doi: 10.1021/bi00271a016.

Roszak, A. W. *et al.* (2003) 'Crystal Structure of the RC-LH1 core complex from Rhodopseudomonas palustris', *SCIENCE*, 302. Available at: http://science.sciencemag.org/ (Accessed: 22 July 2019).

Roszak, A. W. *et al.* (2012) 'New insights into the structure of the reaction centre from Blastochloris viridis: evolution in the laboratory', *Biochem. J*, 442, pp. 27–37. doi: 10.1042/BJ20111540.

Saltikov, C. W. and Newman, D. K. (2003) 'Genetic Identification of a Respiratory Arsenate Reductase', *Proceedings of the National Academy of Sciences of the United States of America*. Proc Natl Acad Sci U S A, 100(19). doi: 10.1073/PNAS.1834303100.

Sapra, K. T. *et al.* (2009) 'One beta hairpin after the other: exploring mechanical unfolding pathways of the transmembrane beta-barrel protein OmpG.', *Angewandte Chemie (International ed. in English)*. Angew Chem Int Ed Engl, 48(44), pp. 8306–8. doi: 10.1002/anie.200904361.

Sarıbaş, S. *et al.* (1998) 'Interactions between the Cytochrome b, Cytochrome c1, and Fe−S Protein Subunits at the Ubihydroquinone Oxidation Site of the bc1 Complex of Rhodobacter capsulatus†'. American Chemical Society. doi: 10.1021/BI973146S.

Scheuring, S., Seguin, Jerome, *et al.* (2003) 'AFM characterization of tilt and intrinsic flexibility of Rhodobacter sphaeroides light harvesting complex 2 (LH2).', *Journal of molecular biology*, 325(3), pp. 569–80. doi: 10.1016/s0022-2836(02)01241-x.

Scheuring, S., Seguin, Jérôme, *et al.* (2003) 'Nanodissection and high-resolution imaging of the Rhodopseudomonas viridis photosynthetic core complex in native membranes by AFM. Atomic force microscopy.', *Proceedings of the National Academy of Sciences of the United States of America*. National Academy of Sciences, 100(4), pp. 1690–3. doi: 10.1073/pnas.0437992100.

Scheuring, S., Francia, F., *et al.* (2004) 'Structural Role of PufX in the Dimerization of the Photosynthetic Core Complex of Rhodobacter sphaeroides', *Journal of Biological Chemistry*. doi: 10.1074/jbc.M310050200.

Scheuring, S., Rigaud, J., *et al.* (2004) 'Watching the photosynthetic apparatus in native membranes', *Sciences-New York*, 101(31), pp. 11293–112967.

Scheuring, S. *et al.* (2006a) 'The photosynthetic apparatus of Rhodopseudomonas palustris: Structures and organization', *Journal of Molecular Biology*. doi: 10.1016/j.jmb.2006.01.085.

Scheuring, S. *et al.* (2006b) 'The photosynthetic apparatus of Rhodopseudomonas palustris: Structures and organization', *Journal of Molecular Biology*, 358(1), pp. 83–96. doi: 10.1016/j.jmb.2006.01.085.

Scheuring, S. *et al.* (2014) 'The architecture of Rhodobacter sphaeroides chromatophores', *BBA - Bioenergetics*, 1837, pp. 1263–1270. doi: 10.1016/j.bbabio.2014.03.011.

Scheuring, S., Boudier, T. and Sturgis, J. N. (2007) 'From high-resolution AFM topographs to atomic models of supramolecular assemblies', *Journal of Structural Biology*, 159(2 SPEC. ISS.), pp. 268–276. doi: 10.1016/j.jsb.2007.01.021.

Scheuring, S., Busselez, J. and Lé, D. (2004) 'Structure of the Dimeric PufX-containing Core Complex of Rhodobacter blasticus by in Situ Atomic Force Microscopy* Downloaded from', *THE JOURNAL OF BIOLOGICAL CHEMISTRY*. JBC Papers in Press, 280(2), pp. 1426–1431. doi: 10.1074/jbc.M411334200.

Scheuring, S., Busselez, J. and Lévy, D. (2005) 'Structure of the Dimeric PufX-containing Core Complex of *Rhodobacter blasticus* by *in Situ* Atomic Force Microscopy', *Journal of Biological Chemistry*, 280(2), pp. 1426–1431. doi: 10.1074/jbc.M411334200.

Scheuring, S., Lévy, D. and Rigaud, J.-L. (2005) 'Watching the components of

photosynthetic bacterial membranes and their in situ organisation by atomic force microscopy', *Biochimica et Biophysica Acta (BBA) - Biomembranes*. Elsevier, 1712(2), pp. 109–127. doi: 10.1016/J.BBAMEM.2005.04.005.

Scheuring, S., Rigaud, J. L. and Sturgis, J. N. (2004) 'Variable LH2 stoichiometry and core clustering in native membranes of Rhodospirillum photometricum', *EMBO Journal*, 23(21), pp. 4127–4133. doi: 10.1038/sj.emboj.7600429.

Scheuring, S. and Sturgis, J. N. (2005) 'Chromatic Adaptation of Photosynthetic Membranes', *Science*, 309(5733), pp. 484–487. doi: 10.1126/science.1110879.

Scheuring, S. and Sturgis, J. N. (2009) 'Atomic force microscopy of the bacterial photosynthetic apparatus: Plain pictures of an elaborate machinery', *Photosynthesis Research*, 102(2), pp. 197–211. doi: 10.1007/s11120-009-9413-7.

Scholl, Z. N. and Marszalek, P. E. (2018) 'AFM-Based Single-Molecule Force Spectroscopy of Proteins.', *Methods in molecular biology (Clifton, N.J.)*. Methods Mol Biol, 1814, pp. 35–47. doi: 10.1007/978-1-4939-8591-3_3.

Senior, A. E., Nadanaciva, S. and Weber, J. (2002) 'The molecular mechanism of ATP synthesis by F1F0-ATP synthase', *Biochimica et Biophysica Acta (BBA) - Bioenergetics*. Elsevier, 1553(3), pp. 188–211. doi: 10.1016/S0005-2728(02)00185-8.

Shaorong Du and Yangmin Li (2007) 'Micromanipulation based on AFM: Probe tip selection', in *2007 7th IEEE Conference on Nanotechnology (IEEE NANO)*. IEEE, pp. 506–510. doi: 10.1109/NANO.2007.4601242.

Sheng, Y. U., And, Z. and Hearst, J. E. (1986) *Regulation of expression of genes for light-harvesting antenna proteins LH-I and LH-II; reaction center polypeptides RC-L, RC-M, and RC-H; and enzymes of bacteriochlorophyll and carotenoid biosynthesis in Rhodobacter capsulatus* by light and oxygen (photosynthetic bacteria/Rhodopseudomonas capsulata/puf operon/polycistronic mRNA/photooxidadve damage)*, *Proc. Natl. Acad. Sci. USA*. Available at: https://www.pnas.org/content/pnas/83/20/7613.full.pdf (Accessed: 29 August 2019).

Shetty, R. P., Endy, D. and Knight, T. F. (2008) 'Engineering BioBrick vectors from BioBrick parts', *Journal of Biological Engineering*. BioMed Central, 2(1), p. 5. doi: 10.1186/1754-

1611-2-5.

Shi, X. *et al.* (2009) 'Study of inhibition effect of herceptin on interaction between heregulin and erbB receptors HER3/HER2 by single-molecule force spectroscopy.', *Experimental cell research*. Exp Cell Res, 315(16), pp. 2847–55. doi: 10.1016/j.yexcr.2009.05.023.

Shopes, R. J. and Wraight, C. A. (1985) 'The acceptor quinone complex of Rhodopseudomonas viridis reaction centers', *BBA - Bioenergetics*. doi: 10.1016/0005-2728(85)90242-7.

Siebert, C. A. *et al.* (2004) 'Molecular architecture of photosynthetic membranes in Rhodobacter sphaeroides: the role of PufX', *The EMBO Journal*, 23, pp. 690–700. doi: 10.1038/sj.emboj.7600092.

Stark, W. *et al.* (1984) 'The structure of the photoreceptor unit of *Rhodopseudomonas viridis*; The structure of the photoreceptor unit of *Rhodopseudomonas viridis*', *The EMBO Journal*, 3(4), pp. 777–783. doi: 10.1002/j.1460-2075.1984.tb01884.x.

Stroh, C. *et al.* (2004) 'Detection and localization of individual antibody-antigen recognition events by atomic force microscopy.', *PNAS*. National Academy of Sciences, 93(8), pp. 3477–3481. doi: 10.1073/pnas.93.8.3477.

Sumi, H. (2002) 'Uphill Energy Trapping by Reaction Center in Bacterial Photosynthesis: Charge Separation Unistep from Antenna Excitation, Virtually Mediated by Special-Pair Excitation', *J. Phys. Chem. B*. American Chemical Society, 106(51), pp. 13370–13383. doi: 10.1021/JP021716E.

Sundstrom, V. and Grondelle, R. Van (1999) 'Photosynthetic Light-Harvesting: Reconciling Dynamics and Structure of Purple Bacterial LH2 Reveals Function of Photosynthetic Unit', *J. Phys. Chem. B*, pp. 2327–2346. doi: 10.1021/jp983722+.

Sutter, M. *et al.* (2016) 'Visualization of Bacterial Microcompartment Facet Assembly Using High-Speed Atomic Force Microscopy', *Nano Letters*, 16(3), pp. 1590–1595. doi: 10.1021/acs.nanolett.5b04259.

Swingley, W. D. *et al.* (2007) 'The Complete Genome Sequence of Roseobacter denitrificans Reveals a Mixotrophic Rather than Photosynthetic Metabolism', *Journal of*

*Bacteriology*, 189(3), pp. 683–690. doi: 10.1128/JB.01390-06.

Tabita, R. (2004) *Anoxygenic Photosynthetic Bacteria*. Available at: https://link.springer.com/content/pdf/10.1007%2F0-306-47954-0.pdf (Accessed: 29 August 2019).

Takaichi, S. (2000) 'Characterization of carotenes in a combination of a C18 HPLC column with isocratic elution and absorption spectra with a photodiode-array detector', *Photosynthesis Research*. Kluwer Academic Publishers, 65(1), pp. 93–99. doi: 10.1023/A:1006445503030.

Tang, K.-H., Tang, Y. J. and Blankenship, R. E. (2011) 'Carbon Metabolic Pathways in Phototrophic Bacteria and Their Broader Evolutionary Implications', *Frontiers in Microbiology*. Frontiers, 2, p. 165. doi: 10.3389/fmicb.2011.00165.

Tharia, H. A. *et al.* (1999) *Characterisation of hydrophobic peptides by RP-HPLC from different spectral forms of LH2 isolated from Rps. palustris*, *Photosynthesis Research*. Available at: https://link.springer.com/content/pdf/10.1023%2FA%3A1006281532327.pdf (Accessed: 17 July 2019).

Thornber, J. P. (1970) *Photochemical Reactions of Purple Bacteria as Revealed by Studies of Three Spectrally Different Carotenobacteriochlorophyll–Protein Complexes Isolated from Chromatium, Strain D*, *Biochemistry*. doi: 10.1021/bi00815a017.

Tiede, D. M. and Dutton, P. L. (1993) 'Electron Transfer between Bacterial Reaction Centers and Mobile c-Type Cytochromes', *Photosynthetic Reaction Center*. Academic Press, pp. 257–288. doi: 10.1016/B978-0-12-208661-8.50014-0.

Tikh, I. B., Held, M. and Schmidt-Dannert, C. (2014) 'BioBrick™ compatible vector system for protein expression in Rhodobacter sphaeroides', *Applied Microbiology and Biotechnology*, 98(7), pp. 3111–3119. doi: 10.1007/s00253-014-5527-8.

Todd, J. B. *et al.* (1998) 'In Vitro Reconstitution of the Core and Peripheral Light-Harvesting Complexes of *Rhodospirillum m olischianum* from Separately Isolated Components †', *Biochemistry*, 37(50), pp. 17458–17468. doi: 10.1021/bi981114e.

Truper, H. G. T. and Fischer, U. (1982) *Anaerobic oxidation of sulphur compounds as*

*electron donors for bacterial photosynthesis*, *Trans. R. Soc. Land. B*. Available at: https://royalsocietypublishing.org/doi/pdf/10.1098/rstb.1982.0095 (Accessed: 29 August 2019).

Tsukatani, Y. *et al.* (2004) 'Phylogenetic Distribution of Unusual Triheme to Tetraheme Cytochrome Subunit in the Reaction Center Complex of Purple Photosynthetic Bacteria', *Photosynthesis Research*. Springer, 79(1), pp. 83–91. doi: 10.1023/B:PRES.0000011922.56394.92.

Tunnicliffe, R. B. *et al.* (2006) 'The solution structure of the PufX polypeptide from Rhodobacter sphaeroides', *FEBS Letters*, 580(30), pp. 6967–6971. doi: 10.1016/j.febslet.2006.11.065.

Vasilev, C. *et al.* (2014) 'Nano-mechanical mapping of the interactions between surface-bound RC-LH1-PufX core complexes and cytochrome c 2 attached to an AFM probe', *Photosynthesis Research*. Springer Netherlands, 120(1–2), pp. 169–180. doi: 10.1007/s11120-013-9812-7.

Vick, J. E. *et al.* (2011) 'Optimized compatible set of BioBrick™ vectors for metabolic pathway engineering.', *Applied microbiology and biotechnology*. Appl Microbiol Biotechnol, 92(6), pp. 1275–86. doi: 10.1007/s00253-011-3633-4.

Vik, S. B. and Antonio, B. J. (1994) 'A mechanism of proton translocation by F1F0 ATP synthases suggested by double mutants of the a subunit.', *The Journal of biological chemistry*, 269(48), pp. 30364–9. Available at: http://www.ncbi.nlm.nih.gov/pubmed/7982950 (Accessed: 7 September 2019).

Wada, T. *et al.* (1999) 'A Novel Labeling Approach Supports the Five-transmembrane Model of Subunit *a* of the *Escherichia coli* ATP Synthase', *Journal of Biological Chemistry*, 274(24), pp. 17353–17357. doi: 10.1074/jbc.274.24.17353.

Wakao, N. *et al.* (1996) 'Discovery of Natural Photosynthesis using Zn-Containing Bacteriochlorophyll in an Aerobic Bacterium Acidiphilium rubrum', *Plant and Cell Physiology*. Narnia, 37(6), pp. 889–893. doi: 10.1093/oxfordjournals.pcp.a029029.

Walz, T. *et al.* (1998) 'Projection structures of three photosynthetic complexes from

Rhodobacter sphaeroides: LH2 at 6 Å, LH1 and RC-LH1 at 25 Å', *Journal of Molecular Biology*. Academic Press, 282(4), pp. 833–845. doi: 10.1006/JMBI.1998.2050.

Weber, J. *et al.* (1995) 'α-Aspartate 261 Is a Key Residue in Noncatalytic Sites of *Escherichia coli* $F_1$-ATPase', *Journal of Biological Chemistry*. American Society for Biochemistry and Molecular Biology, 270(36), pp. 21045–21049. doi: 10.1074/jbc.270.36.21045.

Weber, J. and Senior, A. E. (2003) 'ATP synthesis driven by proton transport in $F_1F_0$-ATP synthase', *FEBS Letters*. John Wiley & Sons, Ltd, 545(1), pp. 61–70. doi: 10.1016/S0014-5793(03)00394-6.

Weber, J., Wilke-Mounts, S. and Senior, A. E. (1994) *Cooperativity and Stoichiometry of Substrate Binding to the Catalytic Sites of Escherichia coli Fl-ATPase EFFECTS OF MAGNESIUM, INHIBITORS, AND MUTATION**, *THE JOURNAL OF BIOIQGICAL CHEMISTRY*. Available at: http://www.jbc.org/content/269/32/20462.full.pdf (Accessed: 30 August 2019).

Weyer, K. A. *et al.* (1987) 'Amino acid sequence of the cytochrome subunit of the photosynthetic reaction centre from the purple bacterium Rhodopseudomonas viridis', *The EMBO Journal*, 6(8), pp. 2197–2202. doi: 10.1002/j.1460-2075.1987.tb02490.x.

Wildling, L. *et al.* (2011) 'Probing Binding Pocket of Serotonin Transporter by Single Molecular Force Spectroscopy on Living Cells *'. JBC Papers in Press. doi: 10.1074/jbc.M111.304873.

Wöhri, A. B. *et al.* (2009) 'Lipidic sponge phase crystal structure of a photosynthetic reaction center reveals lipids on the protein surface', *Biochemistry*, 48(41), pp. 9831–9838. doi: 10.1021/bi900545e.

Wöhri, A. B. *et al.* (2010) *Light-induced structural changes in a photosynthetic reaction center caught by laue diffraction*, *Science*. doi: 10.1126/science.1186159.

X, Z., DF, B. and VT, M. (2004) 'Molecular Basis of the Dynamic Strength of the Sialyl Lewis X--selectin Interaction', *Chemphyschem : a European journal of chemical physics and physical chemistry*. Chemphyschem, 5(2). doi: 10.1002/CPHC.200300813.

Xia, D. *et al.* (1997) 'Crystal Structure of the Cytochrome bc $_1$ Complex from Bovine Heart Mitochondria', *Science*, 277(5322), pp. 60–66. doi: 10.1126/science.277.5322.60.

Xin, Y. *et al.* (2018) 'Cryo-EM structure of the RC-LH core complex from an early branching photosynthetic prokaryote', *Nature Communications*, 9(1). doi: 10.1038/s41467-018-03881-x.

Yamashita, H. *et al.* (2009) 'Dynamics of bacteriorhodopsin 2D crystal observed by high-speed atomic force microscopy', *Journal of Structural Biology*, 167(2), pp. 153–158. doi: 10.1016/j.jsb.2009.04.011.

Youvan, D. C. *et al.* (1984) *Reaction center and light-harvesting I genes from Rhodopseudomonas capsulata (photosynthesis/DNA sequence/enhanced fluorescence mutants/R-prime plasmid/genetic map)*, *Proc. Nail. Acad. Sci. USA*. Available at: https://www.ncbi.nlm.nih.gov/pmc/articles/PMC344636/pdf/pnas00602-0203.pdf (Accessed: 29 August 2019).

Yu, L.-J. *et al.* (2018) 'Structure of photosynthetic LH1-RC supercomplex at 1.9 Å resolution', *Nature*. Springer Nature, 556, pp. 209–213. doi: 10.1038/S41586-018-0002-9.

Yu, L. J. *et al.* (2018) 'Structure of photosynthetic LH1-RC supercomplex at 1.9 Å resolution', *Nature*, 556(7700), pp. 209–213. doi: 10.1038/s41586-018-0002-9.

Yurkov, V. V and Beatty, J. T. (1998) 'Aerobic anoxygenic phototrophic bacteria.', *Microbiology and molecular biology reviews : MMBR*. American Society for Microbiology (ASM), 62(3), pp. 695–724. Available at: http://www.ncbi.nlm.nih.gov/pubmed/9729607 (Accessed: 29 August 2019).

Zeng, Y. and Koblizek, M. (2017) 'Phototrophic Gemmatimonadetes: A New "Purple" Branch on the Bacterial Tree of Life', *Modern Topics in the Phototrophic Prokaryotes: Environmental and Applied Aspects*, pp. 1–492. doi: 10.1007/978-3-319-46261-5.

Zhang, X. *et al.* (2013) 'Atomic force microscopy study of the effect of HER 2 antibody on EGF mediated ErbB ligand-receptor interaction', *Nanomedicine: Nanotechnology, Biology, and Medicine*. Elsevier Inc., 9(5), pp. 627–635. doi: 10.1016/j.nano.2012.11.005.

Zhang, Z. *et al.* (1998) 'Electron transfer by domain movement in cytochrome bc1', *Nature*,

392(6677), pp. 677–684. doi: 10.1038/33612.

Zheng-Yu Wang, *,§ *et al.* (2007) 'Solution Structure of the Rhodobacter sphaeroides PufX Membrane Protein: Implications for the Quinone Exchange and Protein−Protein Interactions†,‡'. American Chemical Society . doi: 10.1021/BI0618060.

Zheng, Q. *et al.* (2011) 'Diverse Arrangement of Photosynthetic Gene Clusters in Aerobic Anoxygenic Phototrophic Bacteria', *PLoS ONE*. Edited by S. Bereswill. Public Library of Science, 6(9), p. e25050. doi: 10.1371/journal.pone.0025050.

Zinth, W. and Wachtveitl, J. (2005) 'The First Picoseconds in Bacterial Photosynthesis?Ultrafast Electron Transfer for the Efficient Conversion of Light Energy', *ChemPhysChem*. John Wiley & Sons, Ltd, 6(5), pp. 871–880. doi: 10.1002/cphc.200400458.

Zuber, H. and Cogdell, R. (2004) *Advances in Photosynthesis. Anoxygenic Photosynthetic Bacteria*. Available at: https://link.springer.com/content/pdf/10.1007%2F0-306-47954-0.pdf (Accessed: 29 August 2019).

# Appendices

## Appendix A: M22$^{+}$ Medium Recipe

### 10 x Stock:

| | | To make 4 litres |
|---|---|---|
| • Potassium dihydrogen orthophosphate | $KH_2PO_4$ | 122.4 g |
| • Dipotassium hydrogen orthophosphate | $K_2HPO_4$ | 120.0 g |
| • DL – Lactic acid (fridge) | Na lactate solution | 100.0 g |
| • Ammonium sulphate | $(NH_4)_2SO_4$ | 20 g |
| • Sodium chloride | NaCl | 20 g |
| • Sodium succinate | | 173.7 g |
| • Sodium glutamate | L – Glutamic acid | 10.8 g |
| • Aspartic acid | DL – Aspartic acid | 1.6 g |
| • **Solution C** | | 800ml |

**Solution C**

| | | Make 4 litres |
|---|---|---|
| • Nitrilotriacetic acid | | 40 g |
| • Magnesium chloride | $MgCl_2$ | 96 g |
| • Calcium chloride | $CaCl_2$ | 13.36 g |
| • EDTA | | 0.5 g |

| | | |
|---|---|---|
| • Zinc chloride | $ZnCl_2$ | 1.044 g |
| • Ferrous chloride | $FeCl_2$ | 1.0 g |
| • Manganese chloride | $MnCl_2$ | 0.36 g |
| • Ammonium heptamolybdate | $(NH_4)_6Mo_7O_{24}(H_2O)_4$ | 0.037 g |
| • Cupric chloride | $CuCl_2$ | 0.031 g |
| • Cobaltous nitrate | $Co(NO_3)_2$ | 0.0496 g |
| • Boric acid (orthoboric acid) | | 0.0228 g |

Do not autoclave, just freeze at -20°C in 400ml aliquots.

**Casamino acids (CAA):**

| | 1 litre |
|---|---|
| • Casein Hydrosylate acid | 50 g |

**1 x M22:**

| | Make up to 2 litres |
|---|---|
| • 10 x M22 stock | 200 ml |
| • CAA | 40 ml |
| • water | 1760 ml |

**Vitamins:**

| | 1 000 X | 10 000 x |
|---|---|---|
| • Nicotinic acid (poison) | 100 mg | 1 g |
| • Thiamine (poison) | 50 mg | 0.5 g |

| | | |
|---|---|---|
| • pABA (4-aminobenzoic acid) (fridge) | 10 mg | 0.1 g |
| • Biotin (d-Biotin) (fridge) | 1 mg | 10 mg |
| • water | 100 ml | 100 ml |